Australian & New Zealand Orthopaedic Research Society

# ANZORS 28th Annual Scientific Meeting

## 4-7 December 2023

## Proceedings

**General Library, Lecture Theatre 109-B15, Basement**

**University of Auckland,**

**Princes Street, Auckland CBD, Auckland 1010, New Zealand**


# ANZORS 28th Annual Scientific Meeting

# 4-7 December 2023

## CONTENTS


# President's Welcome

Kia Ora!

I am delighted to welcome you to the 28th Annual Scientific Meeting (ASM) of ANZORS. This meeting marks the first stand-alone face-to-face meeting of our society since the lifting of COVID-19 restrictions. It's wonderful to bring the ANZORS community back together, to showcase and celebrate our latest achievements in orthopaedic research. I warmly welcome old friends, new faces and international guests.

This year's meeting is hosted by The University of Auckland in the picturesque backdrop of New Zealand. As a global hub for research and innovation in healthcare, The University of Auckland produces some of the most innovative basic and translational orthopaedic research in the world.

I would like to thank the Local Organising Committee (LOC) Dr David Musson, Prof Thor Besier, Prof Ashvin Thambyah, Dr Julie Choisne, Dr Vonne van Heeswijk and Dr Geoffrey Handsfield for hosting the ASM and for their hard work organising the exciting social and networking events.

I would also like to extend my thanks to the ANZORS Program Organising Committee (Dr Martina Barzan, A/Prof Egon Perilli, Dr Dane Turner and Dr David Musson) for their tireless efforts and dedication to bring you an innovative and thought-provoking scientific program.

In the tradition of ANZORS, this year's meeting boasts a rich multidisciplinary mix of cutting-edge basic, translational and applied orthopaedic research, with broad appeal for both clinicians and basic scientists.

The program features esteemed International Plenary Speakers Professors Mary and Steven Goldring (Weill Cornell Medical College, New York), as well as several Keynote Speakers, Dr Nikki Hooper (Uni. Otago), A/Prof Paul Monk (Uni. Auckland), and Prof Haxby Abbot (Univ. Otago), showcasing some of the very best musculoskeletal and orthopaedic research from across New Zealand.

This year's program also features a dedicated Women in Science Networking Breakfast, PhD-, Early Career- and Orthopaedic Innovation Award sessions, a Young Investigator Social Event. The half-day Networking Event (at Goldie Estate) is sure to be a highlight, and where I hope that you are able to establish new and long-lasting collaborations and friendships with our ANZORS members.

A special thank you to our generous Sponsors who support the travel grants, awards and welcoming events: The University of Auckland (Auckland Bioengineering Institute, Chemmat), Maurice & Phyllis Paykel Trust, Vicon, OrbMedical and the Minghao Zheng Family Trust. Without the generosity of our sponsors these meetings would not be possible.

As well as enjoying four days of learning, networking and socialising, I encourage you to explore the harbour and natural beauty of Auckland, which has something to offer everyone, including its rich culture, fine cuisine and outdoor experiences and attractions.

Whether attending locally, 'crossing the ditch', or travelling from further abroad, I hope that you enjoy your time in Auckland and the captivating scientific and social program that lies ahead!

**Nathan Pavlos**
**President, Australian & New Zealand Orthopaedic Research Society**
**Associate Professor, School of Biomedical Sciences, The University of Western Australia**

# Thanks to our sponsors:




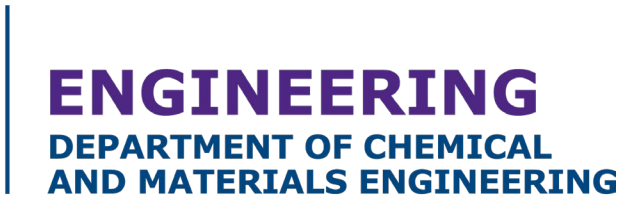





# ANZORS 28th Annual Scientific Meeting

## Committee Members

| | |
|---|---|
| **President**<br>A/Prof Nathan Pavlos | Associate Professor and Head, Bone Biology and Disease Laboratory, The University of Western Australia |
| **Secretary**<br>Dr Martina Barzan | Research Fellow, Griffith Centre of Biomedical & Rehabilitation Engineering, Griffith University |
| **Treasurer**<br>Dr Dane Turner | Senior Lecturer, Faculty of Medicine, Health and Human Sciences, Macquarie University &<br>Regional Research Manager ANZ, GE HealthCare |
| **New Zealand Representative**<br>Dr David Musson | Senior Lecturer, Department of Nutrition & Dietetics, School of Medical Sciences, The University of Auckland |
| **Immediate Past President**<br>A/Prof Egon Perilli | Associate Professor in Biomedical Engineering, The Medical Device Research Institute, College of Science & Engineering, Flinders University |
| **2023 Host Organisers** | |
| Dr David Musson | Senior Lecturer, Department of Nutrition & Dietetics, School of Medical Sciences, The University of Auckland |
| Prof Thor Besier | Professor, Auckland Bioengineering Institute, Department of Engineering Science, The University of Auckland |
| Prof Ashvin Thambyah | Professor and Head of Department, Chemical and Materials Engineering, The University of Auckland |


# Organising Committees

## Local Conference Organising Committee

Dr David Musson, University of Auckland, Chair

Prof Thor Besier, University of Auckland, Co-Chair

Prof Ashivan Thambyah, University of Auckland, Co-Chair

Dr Julie Choisne, University of Auckland

Dr Vonne van Heeswijk, University of Auckland

Dr Geoffrey Handsfield, University of Auckland

## Program Organising Committee

A/Prof Nathan Pavlos

Dr Martina Barzan

Dr Dane Turner

Dr David Musson

A/Prof Egon Perilli


# Scientific Committee

(alphabetical surname order)

| | |
|---|---|
| Dr John Abrahams | University of Adelaide |
| Prof David Ackland | University of Melbourne |
| Dr Rami Al-Dirini | Flinders University |
| Dr John Arnold | University of South Australia |
| Dr Martina Barzan | Griffith University |
| Prof Thor Besier | University of Auckland |
| Dr Stuart Callary | University of Adelaide |
| A/Prof John Costi | Flinders University |
| A/Prof Tania Crotti | University of Adelaide |
| Dr Dane Dabirrahmani- Turner | Macquarie University |
| A/Prof Justin Fernandez | University of Auckland |
| Prof David Findlay | University of Adelaide |
| Dr Jiao Jiao Li | University of Technology Sydney |
| A/Prof Rachel Li | Australian National University |
| Prof David Lloyd | Griffith University |
| Dr Joe Lynch | Australian National University |
| A/Prof Saulo Martelli | Queensland University of Technology |
| Dr David Musson | University of Auckland |
| Dr Elyse Passmore | University of Melbourne |
| A/Prof Nathan Pavlos | University of Western Australia |
| A/Prof Egon Perilli | Flinders University |
| Prof Peter Pivonka | Queensland University of Technology |
| Dr Dale Robinson | University of Melbourne |
| Dr Corey Scholes | EBM Analytics |
| A/Prof Peter Smitham | University of Adelaide |
| Prof Bogdan Solomon | University of Adelaide |
| Dr Kathryn Stok | University of Melbourne |
| A/Prof Dominic Thewlis | University of Adelaide |
| Prof Cory Xian | University of South Australia |
| Prof Yin Xiao | Griffith University |
| Prof Jiake Xu | University of Western Australia |
| Prof Minghao Zheng | University of Western Australia |
| Prof Hala Zreiqat | University of Sydney |


# ANZORS 28th Annual Scientific Meeting

## Travel Grant Recipients

(alphabetical surname order)

ANZORS is proud to support its early career researchers. This year we have awarded 33 travel grants. This represents a significant reinvestment of our funds to support the dissemination of quality orthopaedic research.

| Surname | First Name | Institution |
|---|---|---|
| Andronic | Octavian | Orthopaedic Research Foundation Western Australia, Australia |
| Boersma | Emma | University of Melbourne, Australia |
| Bruyer-Montéléone | François | Queensland University of Technology, Australia |
| Bucci | Francesca | Flinders University, Australia |
| Crowley | James | University of New South Wales, Australia |
| Dohm | Julius | Aesculap AG, Germany |
| Durongbhan | Pholpat | University of Melbourne, Australia |
| Fang | Zhou | University of Melbourne, Australia |
| Funaro | Alessia | Katholieke Universiteit Leuven, Belgium |
| Gong | Xingjian | Australian National University, Australia |
| Guo | Joyce | Otago Medical School, New Zealand |
| Huang | Yichen | University of Melbourne, Australia |
| Khuu | Stephanie | University of California, USA |
| Kok | Hui Jean | Indiana University School of Medicine, USA |
| Kumar | Anubrat | Prince of Wales Hospital, China |
| Labrune | Mélody | Macquarie University, Australia |
| Lange | Tyra | Flinders University, Australia |
| Liu | Yunxiang | Australian National University, Australia |
| Madhavan | Aswini | University of Technology, Sydney |
| Mini | Daniela | Flinders University, Australia |
| Montanari | Sara | University of Bologna, Italy |
| Nguyen | Katherine | The Australian National University, Australia |
| O'Rourke | Dermot | Queensland University of Technology, Australia |
| Roser | Megan | Queensland University of Technology, Australia |
| Shamoon | Muhammad | Australian National University, Australia |
| Stewart | Tahlia | Australian National University, Australia |
| Thompson-Bagshaw | Darcy | University of Adelaide, Australia |
| Thwaites | Simon | University of Adelaide, Australia |
| Tiew | Ryan | University of Melbourne, Australia |
| Wearne | Lauren S | Flinders University, Australia |
| Woodford | Sarah | University of Melbourne, Australia |
| Yu | Yihang | University of Melbourne, Australia |
| Zhang | Yilan | University of New South Wales, Australia |


# ANZORS 28th Annual Scientific Meeting

## Plenary Speakers

**Prof Mary Goldring**

*Past ORS President; past OARSI board of directors' member; former co-director of Tissue Engineering and Repair Program, Research Division, Hospital for Special Surgery, New York, USA. Professor of Cell and Developmental Biology, Weill Cornell Medical College.*

Mary B. Goldring, PhD, is Emeritus Senior Scientist and the former Co-Director of the Tissue Engineering Regeneration and Repair Program Hospital for Special Surgery and Professor of Cell and Developmental Biology at Weill Cornell Medical College in New York City. Her research has focused on the molecular regulation of extracellular matrix remodeling with special attention to cartilage biology and cellular mechanisms involved in the pathogenesis of osteoarthritis (OA) using in vitro and murine models of OA. Her research was continuously supported by grants from NIA, NIAMS, and the Arthritis Foundation. She was President of the Orthopaedic Research Society (ORS), serving on the ORS Board for 6 years, and was a member of the Board of Directors of the Osteoarthritis Research Society International (OARSI) for 4 years. Notable honors include the ORS Women's Leadership Forum award, the OARSI Basic Science Research award, the OARSI Lifetime Achievement award and the Alumni Achievement Award from the Robert D. Clark Honors College, University of Oregon.

**Prof Steven Goldring**

*Chief Scientific Officer Emeritus, Hospital for Special Surgery, New York, USA; Professor of Medicine, Weill Cornell Medical College.*

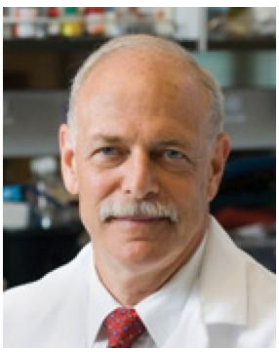

Steven R. Goldring, MD is the Chief Scientific Officer Emeritus at Hospital for Special Surgery, and a Professor of Medicine at Weill Medical College. He previously was a Professor of Medicine at Harvard Medical School and Chief of Rheumatology at the Beth Israel Deaconess Medical Center. His research interests focus on the cellular and molecular mechanisms involved in the regulation of physiological and pathological bone remodeling. He is the past President and Secretary-Treasurer of the ASBMR. He previously served as the Chairman of the Orthopaedics and Musculoskeletal Study Section at the NIH, Chairman of the Gordon Research Conference on the Molecular Biology of Bones and Teeth, and Co-Chairman of the Keystone Conference on the Pathogenesis of Rheumatoid Arthritis. He is a co-recipient of the Carol Nachman Prize in Rheumatology and has received the Arthritis Foundation's James H. Fairclough, Jr. and Marian Ropes Awards and the Paget's Disease Foundation Research Award.

# Keynote Speakers

**A/Prof Paul Monk**

*Knee and hip orthopaedic surgeon, general sports orthopaedics, trauma, arthroscopic surgery and joint replacement. Associate Professor, Auckland Bioengineering Institute, Faculty of Medical and Health Sciences, University of Auckland, NZ.*

Paul is an associate professor at the University of Auckland and a consultant orthopaedic surgeon at Auckland City Hospital. He specialises in general sports orthopaedics and takes a particular interest in all hip and knee conditions, covering the full spectrum from trauma, arthroscopic surgery and joint replacement. Paul has an international reputation for his clinical research in orthopaedics and is currently leading a team of clinical scientists undertaking biomechanical and clinical studies related to knee, hip and shoulder patients following surgery. Paul holds the rank of major in the British Army Parachute Regiment and has previously been deployed to Helmand province as a combat trauma surgeon during the Afghanistan conflict.

**Dr Nikki Hooper**

*Senior Clinical Lecturer, Orthopaedic surgeon, Paediatric orthopaedics, and trauma. University of Otago, Christchurch, NZ.*

Dr Nikki Hooper is an Orthopaedic Surgeon at Te Whatu Ora Waitaha with a sub-specialty interest in paediatric orthopaedics and adult foot and ankle surgery. She is also a senior Clinical Lecturer at the University of Otago, Canterbury School of Medicine. Nikki undertook her orthopaedic training in New Zealand, before completing a fellowship in paediatric orthopaedics at BC Children's Hospital, Vancouver. This set the foundation for multi-centre collaboration, and since returning to New Zealand Nikki has been responsible for establishing the Christchurch branch of the International Hip Dysplasia Registry, which has the goal of improving outcomes in children with hip dysplasia.

**Prof Haxby Abbott**

*Research Professor, Department of Surgical Sciences, Director of the Osteoarthritis Aotearoa New Zealand Research Network, and of the Centre for Musculoskeletal Outcomes Research, University of Otago, Dunedin, NZ.*

Professor Haxby Abbott is Director of the Osteoarthritis Aotearoa New Zealand Research Network, and of the Centre for Musculoskeletal Outcomes Research based in the University of Otago Medical School. New Zealand's highest-ranked expert in osteoarthritis, he has specialised in clinical epidemiology, clinical trials, outcome measurement, cost-effectiveness evaluation, and the implementation and evaluation of new health delivery models for people with hip and knee osteoarthritis. He has successfully competed for over $20 million of research grant funding, including a 5-year Health Research Council of New Zealand Programme Grant and a prestigious Sir Charles Hercus Health Research Fellowship. Professor Abbott is a former Editor in Chief of the international Journal of Orthopaedic & Sports Physical Therapy (JOSPT) and the New Zealand Journal of Physiotherapy.

# Venue

## General Library,
## Basement, Lecture theatre 109-B15
## University of Auckland,
## Princes Street, Auckland CBD, Auckland 1010, New Zealand

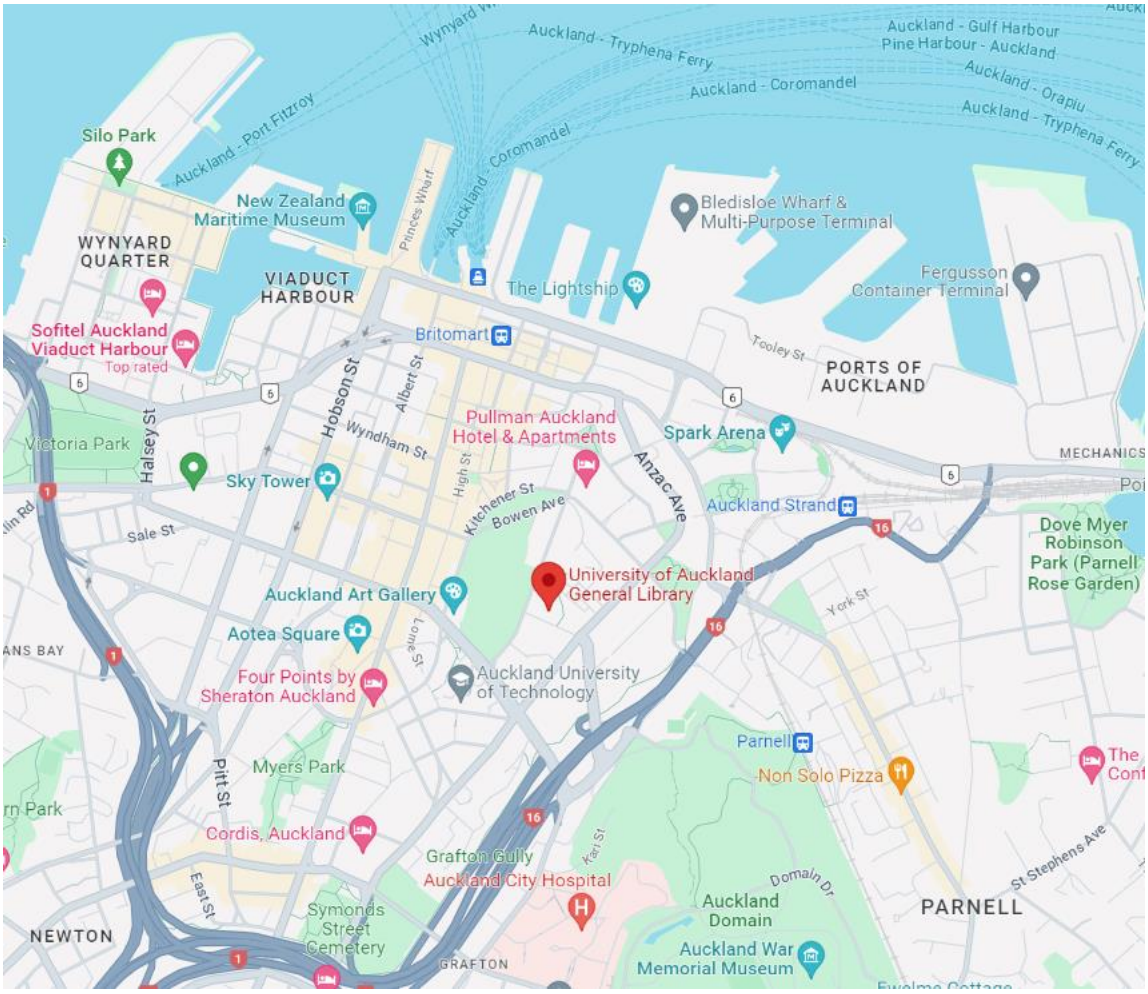


[Google maps]

**Wi-Fi Access: eduroam Wi-Fi network is active (select eduroam)**
**Username: your usual institution email address**
**Password: your usual institution email password**


# PROGRAM

# Monday, December 4

| | |
|---|---|
| **18:00** | **Welcome Reception**<br><br>at Old Government House, 24 Princes Street, Auckland CBD, Auckland 1010, New Zealand<br>4 min walk from Conference Venue<br><br>Map: Google maps |

# Tuesday, December 5 - Lecture Theatre 109-B15, Basement, General Library, University of Auckland, Princes Street, Auckland CBD, Auckland 1010, New Zealand

| | | | |
|---|---|---|---|
| **07:30-08:25** | **Women's Breakfast** at **Strata Cafe**, Level 4, Kate Edger Building, Univ. of Auckland, 1 min walk from Conf Venue Google maps | | |
| **08:00-08:30** | Coffee and registration | | |
| **08:30-08.45** | **ANZORS President's welcome: A/Prof Nathan Pavlos** | | |
| **08:45-09:15**<br>Session chair:<br>A/Prof Nathan Pavlos | **Plenary: Prof Mary Goldring, Emeritus Senior Scientist, Hospital for Special Surgery, New York, USA**<br>**"Biomarkers of Osteoarthritis and Implications for Therapy"** | | |
| **09:15-10:15** | **Name** | **Surname** | **Abstract title** |
| **Podium 1**<br>Session chairs:<br>Dr Stephanie Khuu,<br>Prof Ashvin Thambyah | Laura | Wilson | Identifying at risk morphotypes in patellofemoral osteoarthritis: a comparison of patella shape in males and females |
| | Eleonora | Olivotto | Calcium crystals detection in synovial fluid of patients with femoroacetabular impingement and correlation with clinical outcomes |
| | Dominic | Thewlis | A single intraarticular dose of a novel interleukin 10-based therapy improves knee function in people with knee osteoarthritis during walking gait |
| | Pholpat | Durongbhan | Imaging protocol for longitudinal assessment of structural changes in mouse knees |
| | Aswini | Madhavan | Spinal cord-on-a-chip: a novel microfluidic model to investigate neurological cell responses to spinal implant wear particles |
| **10:15-10:55** Morning coffee & tea; Foyer, Basement, General Library | | | |
| **10:55-11:55** | **Name** | **Surname** | **Abstract title** |
| **Podium 2**<br>Session chairs:<br>Dr Vickie Shim,<br>A/Prof Peter Smitham | Lauren S | Wearne | Assessing the initial mechanical environment of cadaveric tibiae with cementless tibial trays during stair descent and deep knee bend |
| | Julius | Dohm | Determining wear of an advanced Zrn multilayer coating total knee system manufactured out of titanium under highly demanding activities |
| | Sarah | Safavi | Optimised porous femoral stem design to reduce stress shielding |
| | Bogdan | Solomon | Hip implants with evidence of phased introduction have improved survivorship at long term follow-up |
| | Tom | Ward | Resecting tissue from the 'impingement point' improves range of motion prior to dislocation in total hip replacement surgery |
| **11:55-13:10** Lunch & poster viewing (poster viewing will take place between 12:40-13:10)<br>Foyer, Basement, General Library | | | |
| **13:10-13:40**<br>Session chair:<br>Prof David Findlay | **Plenary: Prof Steven Goldring, Research Chair, Hospital for Special Surgery, New York, USA**<br>**"Osteoarthritis, A "whole" joint disease"** | | |
| **13:40-14:28** | **Name** | **Surname** | **Abstract title** |
| **Minghao Zheng Orthopaedic Innovation Award Final**<br>Session chairs:<br>Prof Steven Goldring,<br>Dr Jiao Jiao Li | Parham | Foroutan | Development and validation of a biomechanically fidelic surgical training knee model |
| | Megan | Roser | Correlation analysis of vertebral body wedge angles and intervertebral disc wedge angles with major coronal curve angle after vertebral body tethering - a pilot study |
| | Javad | Tavakoli | An innovative technology reveals new findings: initial cell density matters for the regeneration of intervertebral disc |
| | Peter | Smitham | A cadaveric study investigating a pinless, image-free navigation system for the insertion of acetabular cups during the anterior hip approach |
| **14:28-15:20** Afternoon coffee & tea and poster viewing; (poster viewing will take place between 14:50-15:20)<br>Foyer, Basement, General Library | | | |
| **15:20-16:32** | **Name** | **Surname** | **Abstract title** |
| **Podium 4**<br>Session chairs:<br>Dr Nikki Hooper,<br>A/Prof Justin Fernandez | Anubrat | Kumar | Can post-neonatal clinical and sonographic screening parameters effectively predict hip dysplasia in children at their walking age? |
| | Sarah | Hunter | Ten year review of acute paediatric hematogenous osteomyelitis at a New Zealand tertiary referral centre |
| | Saulo | Martelli | Neuromuscular constraints of the knee contact force while walking |
| | Manuela | Zimmer | Non-invasive mechanical characterization of plantar flexor muscles using shear wave elastography |
| | Randika | Perera | Probing muscle-fascia interaction in the lower limb with advanced MRI and finite element modelling |
| | Yilan | Zhang | Anatomical information on the internal aponeurosis is needed for realistic subscapularis fascicle length measurements from diffusion tensor imaging |

| | |
|---|---|
| **18:00-** | **Young Investigators Event**<br><br>**Honours/Masters/PhD students and ECRs get free meal; must have indicated attendance during registration**<br><br>at **Superfino, Owen G Glenn Building, Univ. of Auckland (v/gf available), 2 min walk from Conference Venue**<br><br>**Map: Google maps** |

# Wednesday, December 6 - Lecture Theatre 109-B15, Basement, General Library, University of Auckland, Princes Street, Auckland CBD, Auckland 1010, New Zealand

| 08:00-08:15 | Coffee & tea | | |
|---|---|---|---|
| **08:15-09:15** | **Name** | **Surname** | **Abstract title** |
| **David Findlay ECR Award Final**<br><br>Session chairs:<br>Prof Mary Goldring,<br>Dr Javad Tavakoli | Hui Jean | Kok | Increased bone formation from isolated isometric contraction in mice |
| | Maxence | Lavaill | Benchmark and validation of state-of-the-art muscle recruitment strategies in shoulder modelling |
| | John | Abrahams | Acetabular component stability using the replace-in-situ philosophy to treat acute acetabular fractures |
| | Stephanie | Khuu | Multi-cell modelling of the skeletal muscle microenvironment to explore age-related changes in satellite cell dynamics |
| | Harnoor | Saini | Classification of glenoid wear using statistical shape modelling |
| **09:15-09:45**<br><br>Session chair:<br>Prof David Lloyd | **Keynote: A/Prof Paul Monk, Orthopaedic surgeon, University of Auckland, NZ**<br>**"Bioengineering in Orthopaedics: Innovation and Evaluation"** | | |
| **9:45-10:15** Morning coffee & tea; Foyer, Basement, General Library | | | |
| **10:15-11:15** | **Name** | **Surname** | **Abstract title** |
| **PhD Award Final**<br><br>Session chairs:<br>Prof David Ackland,<br>Ms Lauren Wearne | Reece | Joseph | Translating the in vitro anti-biofilm potential of bovine lactoferrin to applications as an in vivo anti-infective in battlefield-relevant open fractures |
| | Jo-Wai Douglas | Wang | Association of ABO blood group and rhesus factor with fracture type, comorbidities and outcomes in patients with hip fracture |
| | Tyra | Lange | Breached and non-breached screw trajectories sound and feel differently |
| | Yichen | Huang | A virtual clinical trials framework for evaluating glenoid component fixation after reverse total shoulder arthroplasty |
| | Daniela | Mini | Bone strain field prediction via graph neural network for a proximal humeral plate |
| **11:15-12:15** | **ANZORS AGM**<br><br>**All delegates welcome and encouraged to attend** | | |
| **12:30-17:00** | **Half day Networking Event**<br>**(bus transport provided; return back in Auckland by 17:00)**<br>**Pickup at 12:30 pm, in front of Conference Venue**<br><br>Goldie Estate, Waiheke Island, New Zealand | | |
| **19:00-** | **Conference Dinner in the city, including Awards Announcements**<br><br>The Maritime Room, Princes Wharf, Auckland CBD, Auckland 1010, New Zealand<br><br>Map: Google maps | | |

# Thursday, December 7 - Lecture Theatre 109-B15, Basement, General Library, University of Auckland, Princes Street, Auckland CBD, Auckland 1010, New Zealand

| 08:15-09:00 | Coffee & tea; Foyer, Basement, General Library | | |
|---|---|---|---|
| **09:00-10:00** | **Name** | **Surname** | **Abstract title** |
| **Podium 5**<br><br>Session chairs:<br>Dr Dale Robinson,<br>Dr Maxence Lavaill | Zhou | Fang | The use of inertial measurement units and computational modelling in the estimation of shoulder joint forces |
| | François | Bruyer-Montéléone | Shoulder morphologic variation: statistical shape and pose approaches |
| | David | Ackland | The influence of glenoid bone grafting using the Latarjet procedure on glenohumeral joint contact loading |
| | Dermot | O'Rourke | Failure of inlay and onlay humeral components in reverse shoulder arthroplasty: a micro-CT study |
| | Sarah | Woodford | Jaw joint loading during biting following total temporomandibular joint replacement surgery |
| **10:00-10:30**<br><br>Session chair:<br>Dr Martina Barzan | **Keynote: Dr Nikki Hooper, Paediatric orthopaedic surgeon, University of Otago, NZ**<br>**"Improving Outcomes in Hip Dysplasia"** | | |
| **10:30-11:25** Morning coffee, tea & poster viewing (poster viewing will take place between 10:55-11:25) Foyer, Basement, General Library | | | |
| **11:25-12:13** | **Name** | **Surname** | **Abstract title** |
| **Podium 6**<br><br>Session chairs:<br>Dr Julie Choisne,<br>A/Prof Dominic Thewlis | Geoffrey | Handsfield | Detecting changes to muscle architecture over time with shape and growth modelling in cerebral palsy |
| | Yidan | Xu | Development of a lower-limb statistical bone density model in children aged 4 to 18 years old |
| | Praveen | Krishna | Lower limb joint strategies used to negotiate obstacles in young and older adults |
| | Katherine | Nguyen | Shape modelling reveals age-related knee bony shape changes in asymptomatic knees |
| **12:13-13:25** Lunch & poster viewing (poster viewing will take place between 12:55-13:25) Foyer, Basement, General Library | | | |
| **13:25-13:55**<br><br>Session chair:<br>A/Prof Sue McGlashan | **Keynote: Prof Haxby Abbott, Director of Osteoarthritis Aotearoa NZ Research Network, University of Otago, NZ**<br>**"The Diagnosis and Management of Osteoarthritis in Aotearoa New Zealand"** | | |
| **13:55-14:55** | **Name** | **Surname** | **Abstract title** |
| **Podium 7**<br><br>Session chairs:<br>Prof Haxby Abbott,<br>Dr Francesca Bucci | Justin | Fernandez | IMU-augmented patient reported outcome measures for estimating post-operative patient satisfaction |
| | Simon | Thwaites | Tibial nailing patients exhibit functional deficits up to 18 months follow-up compared to healthy controls: a prospective randomised controlled pilot study |
| | Stuart | Callary | Does manufacturing method, patient age or articulation size affect the long-term wear rate of highly cross-linked polyethylene liners in total hip arthroplasty? |
| | Joe | Lynch | Kinematics are an indicator of outcome after total knee replacement |
| | Octavian | Andronic | Outcomes of secondary patella resurfacing for dissatisfaction following primary knee arthroplasty: a systematic review and meta-analysis of 604 knees |
| **14:55-15:30** Afternoon coffee & tea; Foyer, Basement, General Library | | | |
| **15:30-16:18** | **Name** | **Surname** | **Abstract title** |
| **Podium 8**<br><br>Session chairs:<br>Prof Syn Schmitt | Vonne | van Heeswijk | Modes of failure in flexed ovine lumbar motion segments subjected to impact loading |
| | Sara | Montanari | Biomechanical effect of decompressive techniques on lumbar spine |
| | Yihang | Yu | Influence of the lumbar endplate and cage related factors on cage-endplate contact: a cadaveric study |
| | Nathan | Pavlos | Characterisation of the secretory lysosome proteome reveals new regulators of osteoclast function and endolysosomal homeostasis |
| **16:18-16:30** | President's closing address | | |

# POSTERS presented on Tuesday, December 5

## Foyer, Basement, General Library, University of Auckland, Princes Street, Auckland CBD, Auckland 1010, New Zealand

| 12:40-13:10 | Lunch break | | |
|---|---|---|---|
| 14:50-15:20 | Afternoon break | | |
| **Poster #** | **First name** | **Surname** | **Abstract title** |
| **1** | Ashwini | Madhavan | Development of a 3D bioprinted model to investigate neural cell responses to wear debris from spinal instrumentation and devices |
| **2** | Yichen | Huang | The effect of rotator cuff tears and glenoid version on glenohumeral joint stability after reverse total shoulder arthroplasty |
| **3** | Lauren S | Wearne | Variation in interference fit of cementless tibial trays and its effect on post-implantation strain field: a micro-CT and digital volume correlation analysis |
| **4** | Ryan | Tiew | Experimental validation of a cadaveric femur fitted with an osseointegrated implant |
| **5** | Sara | Montanari | In vitro testing of osseointegrated transfemoral prostheses: implant stability and load transfer |
| **6** | Mohammadreza | Arjmandi | Investigating cartilage mechanics across the length scales |
| **7** | Julie | Choisne | Understanding the variation of bone mineral density in the femur and tibia in children aged 4 to 18 years old |
| **8** | Natali | Uribe | Bone shape, density distribution, and microstructural organization in adult people |
| **9** | Emma | Boersma | Towards in vivo image-guided mechanical evaluation of the murine knee joint |
| **10** | Alexander | Lee-Medland | Developing and validating a novel micro-CT based technique for measuring bone mineral density distribution |
| **11** | Sarah | Hunter | Quality of life for children up to 13 years following treatment for acute haematogenous osteomyelitis |
| **12** | James | Bilbrough | Does elastographic tendon stiffness predict return to work and sport after primary rotator cuff repair? |
| **13** | Sarah | Hunter | Early CRP trends in childhood osteomyelitis predict complicated disease |
| **14** | Joyce | Guo | Outcomes of an augmented reality paediatric supracondylar humeral fracture simulator |
| **15** | Bogdan | Solomon | Virtual biomechanical assessment of custom triflange and porous tantalum components to treat severe acetabular defects with pelvic discontinuity |
| **16** | Sarah | Hunter | Appropriate antibiotic duration in paediatric bone and joint infection: a systematic review |

**Please see next page for posters presented on Thursday.**

# POSTERS presented on Thursday, December 7

## Foyer, Basement, General Library, University of Auckland, Princes Street, Auckland CBD, Auckland 1010, New Zealand

| 10:40-11:10 | Morning break | | |
|---|---|---|---|
| 12:55-13:25 | Lunch break | | |
| **Poster #** | **First name** | **Surname** | **Abstract title** |
| **17** | Joe | Lynch | Systematic review and meta-analysis of patellar morphometric differences between males and females |
| **18** | Alessia | Funaro | Patient-specific 3D models to investigate the effect of twisted structure of the Achilles tendon on strain distribution |
| **19** | David | Musson | Incidence and economic burden of Achilles tendon injuries in Aotearoa New Zealand between 2010 and 2018 |
| **20** | Francesca | Bucci | Tibiofemoral elasticity during gait: a musculoskeletal modelling study of compliance |
| **21** | Filiz | Ates | Intraoperative force measurements to support the decision-making in muscle-tendon lengthening surgeries |
| **22** | Salindi | Herath | Effect of scaling on HKA angle in preoperative total knee replacement patients |
| **23** | Mélody | Labrune | Study of human shoulder biomechanics using computational modelling |
| **24** | Saulo | Martelli | A finite element model for evaluating graft stability in Latarjet surgery under varied fixation techniques |
| **25** | Saulo | Martelli | An efficient method to predict hip fragility fractures in statistical synthetic cohorts |
| **26** | Julie | Kim | Bone-remodelling in the foot: application to exercise during the COVID-19 lockdown |
| **27** | Octavian | Andronic | High loosening rates and inferior patient-reported outcomes of the cementless tibial base plate in a modern design of total knee arthroplasty |
| **28** | Xingjian | Gong | Potential therapeutic targets of arthrofibrosis following knee arthroplasty |
| **29** | Sarah | Nossov | Preferences and priorities for decision making in congenital femoral deficiency (CFD): a stated preference survey of patients, caregivers, and clinicians |
| **30** | Nicolo' | Malagutti | An automatic two-stage knee alignment pipeline of human lower-limb X-rays by convolutional neural network |
| **31** | Syn | Schmitt | Comparison of load-sharing and axis of rotation in generic and individualised neuro-musculoskeletal models of the spine |

**<u>All</u> posters will be displayed for the whole duration of the conference and presented on either Tuesday or Thursday by the author as indicated.**


# ABSTRACTS


# Tuesday, December 7

## PLENARY 1 – Prof Mary Goldring

"Biomarkers of Osteoarthritis and Implications for Therapy"


# Tuesday, December 7

## PODIUM 1

# IDENTIFYING AT RISK MORPHOTYPES IN PATELLOFEMORAL OSTEOARTHRITIS: A COMPARISON OF PATELLA SHAPE IN MALES AND FEMALES

[1,2]Laura A. B. Wilson, [3,4]Joseph Lynch, [1]Jo Menard, [5]Catherine R. Galvin and [3,4]Paul N. Smith

[1] School of Archaeology and Anthropology, The Australian National University, Canberra, ACT, Australia
[2]School of Biological, Earth and Environmental Sciences, UNSW Sydney, Sydney, NSW, Australia
[3]School of Medicine, The Australian National University, Canberra, Australia
[4]Trauma and Orthopaedic Research Unit, The Canberra Hospital, Canberra, Australia
[5]School of Engineering, The Australian National University, Canberra, ACT, Australia
email: laura.wilson@anu.edu.au

## INTRODUCTION

Knee osteoarthritis (OA) is a leading cause of disability in adults, with almost one in five individuals over the age of 40 suffering from the condition [1]. Patellofemoral OA, specifically, is more common in women compared to men [2], although the reasons are not fully understood. Sex differences in patellar morphology may help explain the increased prevalence of patellofemoral OA in women compared to men. In this study, we quantify differences in patella morphology between males and females in both healthy and OA populations.

## METHODS

175 age-matched adult participants, represented by 107 (52 females, 55 males) healthy individuals and 68 (41 females, 27 males) individuals with osteoarthritis were recruited as part of a larger randomised trial (PICKLeS ISRCTN75076749). All participants received a computed tomography scan of their knee. A series of 2D measurements were collected on the 3D models, comprising width and height of the patella, width and surface area of the lateral and medial facet, and facet angle. In addition, 81 landmark points were placed on the medial and lateral facet of each 3D model, to describe the shape of the articular surface. Differences between males and females, and healthy and osteoarthritic groups were assessed using Procustes ANOVA and morphological disparity. Data were ordinated using Principal Component Analysis. All analyses were undertaken in the R statistical environment using base functions and the package geomorph [3].

## RESULTS AND DISCUSSION

Our results indicated that males and females from both healthy and OA groups showed similar shape, dimensions and variance in the medial facet. In contrast, the lateral facet showed significant differences between the sexes and healthy/OA groups. OA females and OA males showed greater variance (PV=123.4-165.5) than healthy groups (PV=87.0-90.0), reflecting changes to the curvature of the lateral facet margin with OA. The lateral facet was significantly wider ($p$=0.016) and larger ($p$=0.0161) in OA males compared to healthy males. Healthy females had narrower and taller-shaped lateral facets compared to healthy males, whereas OA females and OA males had broader and shorter shaped lateral facets.

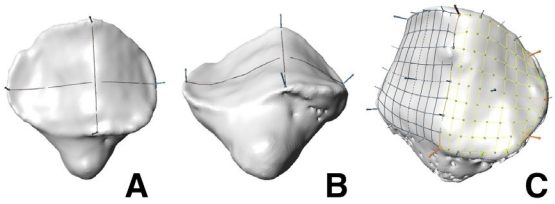


**Figure 1:** 3D model of an adult patella showing points used for 2D measurements (A, B) and landmark points used to capture the shape of the articular surface (C).

## CONCLUSIONS

Sex differences, and healthy/OA differences, in patella morphology are found to be concentrated in the lateral facet. Expansion of the lateral margin of the patella has been associated with an increased likelihood of worsening patellofemoral lesions [4], suggesting that lateral facet shape may be a candidate for inclusion in future models aimed at identifying OA risk in the patellofemoral joint and individuals who may be candidates for preventative measures.

## ACKNOWLEDGEMENTS

LABW is supported by the Australian Research Council (FT200100822).

## REFERENCES

1. Katz et al. *JAMA*. **325**: 568-578, 2021
2. Heidari. *Caspian J Intern Med.* **2(2)**: 205-212, 2011.
3. Baken et al. *Methods Ecol Evol.* **12**: 2355-2363, 2021
4. Liao et al. *J Orthop Res.* **39**: 506-515.

**Table 1:** Select patella dimensions (mm) for individuals with OA.

| Measurement | Female (mean) | Male (mean) | *P* |
|---|---|---|---|
| Patella height | 29.13 | 31.84 | 0.0002 |
| Patella width | 41.28 | 47.14 | <0.0001 |
| Medial facet width | 18.18 | 21.56 | <0.0001 |
| Lateral facet width | 25.10 | 27.55 | 0.00012 |

# CALCIUM CRYSTALS DETECTION IN SYNOVIAL FLUID OF PATIENTS WITH FEMOROACETABULAR IMPINGEMENT AND CORRELATION WITH CLINICAL OUTCOMES

[1]Eleonora Olivotto, [2]M. Favero, [3]M. Battistelli, [2]F. Oliviero, [4]A. Evangelista, [5]F. Mariotti, [5]F. Castagnini, [2]R. Ramonda, [5]F. Traina, [1]Brunella Grigolo and [5]Enrico Tassinari

[1]RAMSES Laboratory, RIT Department, IRCCS Istituto Ortopedico Rizzoli, Bologna, Italy
[2]Rheumatology Unit, Department of Medicine - DIMED, University-Hospital of Padova, Italy
[3]Department of Biomolecular Science, Urbino University "Carlo Bo", Urbino, PU, Italy
[4]General Affairs Unit, IRCCS Istituto Ortopedico Rizzoli, Bologna, Italy
[5]Orthopaedic-Traumatology and Prosthetic surgery and revisions of hip and knee implants, IRCCS Istituto Ortopedico Rizzoli, Bologna, Italy
email: eleonora.olivotto@ior.it

## INTRODUCTION

Hip Osteoarthritis (HOA) is the most common joint disorder and a major cause of disability in the adult population [1]. Thus, the early diagnosis, prevention, and treatment of the early stages of the disease and of the pre-arthritic condition, in particular in adolescents and young adults, is crucial to reducing the incidence of end-stage HOA and the need for total hip replacement (THR).

Evidence has mounted for a prominent etiologic role of femoroacetabular impingement (FAI) in the development of early HOA leading to the development of early cartilage and labral damage in the non-dysplastic hip [2].

An impaired lubrication and an increased joint friction deteriorate articular cartilage and lead to HOA [3]. As calcium crystal deposition is common in osteoarthritis, also labral calcifications are present in patients with FAI [4]. In vitro and preclinical data demonstrate that calcium crystals can activate intra-articular proinflammatory pathways and release nociceptor stimulating substances. Thus, calcium crystal deposition may be involved in generating joint pain.

The aim of the study was to investigate the potential associations among the preoperative symptoms, the outcomes after arthroscopic surgery for FAI and the presence of calcium crystal in synovial fluids (SFs).

## METHODS

Patients scheduled for hip arthroscopy for treatment of FAI and/or labral pathology were enrolled. SFs samples, when available, were obtained by aspiration just prior to surgical intervention, collected and stored as intact for microscopic crystals identification by compensated polarized light microscopy and quantitative analysis by alizarin red staining. Energy Dispersive X-ray Analysis (EDX) was also performed for the morphological and chemical analysis of SFs.

As positive controls of OA signs, SFs samples were also collected from cohort patients with HOA undergoing THR. At the baseline, OA severity was assessed with a semiquantitative radiographic scoring system (Kellgren and Lawrence). Physical examination and clinical assessment using the Hip disability & Osteoarthritis Outcome Score (HOOS) were performed at the time of surgery and at 6 months of follow up. At the time of surgery, chondral pathology using the Outerbridge score, labral and macroscopic synovial pathology based on direct arthroscopic visualization were also evaluated [4].

## RESULTS AND DISCUSSION

49 patients with FAI undergoing arthroscopy were enrolled, median age 35 years with standard deviation (SD) 9.7 and body mass index (BMI) 23.4 kg/m² with SD 3. SF samples were also collected from cohort of 15 patients with HOA undergoing THR, median age 62 years with SD 8.8 and BMI 29.8 kg/m² with SD 6.7.

SFs from FAI patients showed the presence of glycosaminoglycan released (component of the extracellular matrix), which is a sign of cartilage damage, at lower concentration compared to OA samples (FAI vs OA $p<0.001$). Although calcium crystal level was different in SFs of FAI and OA patients, in both groups it negatively correlated with glycosaminoglycan released (Spearman rho=-0.601, $p<0.001$). Interestingly, calcium crystal level in SFs from FAI patients was associated with labral lesions and OA signs. 68% of FAI patients showed radiographic labral calcification which was significantly associated with pain, worst post-operative articular function, and labral lesion.

## CONCLUSIONS

Our study showed that calcium crystals levels in SFs of FAI patients are correlated with worst post-operative outcome, and it might be used as a potential new biomarker for early diagnosis, prognosis and monitoring of therapeutic responses.

## REFERENCES

1. Fu M, et al., *Arthritis Res Ther*. **24**:8, 2022
2. Griffin DR, et al., *BrJ Sport Med.* **50**:1169-76, 2016
3. Pierannunzii L. *J Orthop Traumatol*, **20**:32, 2019
4. Oliviero F, et al., *Ann Clin Lab Sci*, **47**:253-259, 2017
5. Trisolino G, et al., *J Orthop Surg Res*. **15**(1):86, 2020

# A SINGLE INTRAARTICULAR DOSE OF A NOVEL INTERLEUKIN 10-BASED THERAPY IMPROVES KNEE FUNCTION IN PEOPLE WITH KNEE OSTEOARTHRITIS DURING WALKING GAIT

[1,2]Dominic Thewlis, [3]Stephen Collins, [3]Michael Huston, [1]Stuart Millar, [2,1]Mark Rickman

[1]Centre for Orthopaedic & Trauma Research, University of Adelaide, Adelaide, SA, Australia;
[2]Department of Orthopaedics & Trauma, Royal Adelaide Hospital, Adelaide, SA, Australia;
[3]Xalud Therapeutics Inc. New York, USA.
email: dominic.thewlis@adelaide.edu.au

## INTRODUCTION

In the absence of a cure, an effective treatment for knee OA should reduce pain and translate into improvements in physical function. XT-150, developed at the University of Colorado and licensed to Xalud Therapeutics, Inc., is a novel non-viral human IL-10 variant producing plasmid DNA in a D-mannose formulation that provides long term benefit (weeks or months) in various models of inflammatory induced pain. XT-150 IL-10v was used in this study with the goal of managing pathogenic inflammation in knee OA and its associated pain and acting to improve joint function.

The aim of this study was to investigate the effect of two different doses of intraarticular XT-150 versus a placebo control on knee biomechanics and locomotor performance during walking gait over 180 days in people with moderate to severe knee OA. A secondary aim of this study was to highlight the role functional outcomes such as gait analysis can play in the regulatory framework.

## METHODS

This study pooled data from a phase I and a phase IIb trial. Both trials were quadruple-blind, placebo-controlled clinical trials in which participants were randomised to one of two active treatment groups or a placebo treatment. Both trials were prospectively registered (NCT03282149; NCT04124042) and approved by local HREC (2018-01-105; R20191105).

Both trials used a standardised gait analysis assessment conducted at a single site in Adelaide. Participants' gait was assessed immediately prior to the administration of the intervention, and at 30, 60 and 180 days following the intervention. This study compared two doses of the active interventions of the same investigational product with an inactive placebo intervention. The active intervention (XT-150) was delivered in two doses:150-µg and 450-µg in a sterile, mannose containing, phosphate-buffered isotonic saline solution (1 mL). The placebo intervention was sterile saline solution (1 mL). All interventions were administered via an intraarticular injection into the joint space of the treated knee by one consultant orthopaedic surgeon (MR), using a handheld ultrasound machine to confirm correct placement.

The primary outcome measure used in this study was an objective measure of function from three-dimensional gait analysis of walking at a self-selected speed. We analysed walking speed by comparing the proportion of people who increased their walking speed from below 1.3 m/s at baseline to greater than 1.3 m/s at any of the follow-up assessments using Fischer's exact tests. We selected this threshold as it represents the highest speed reported required to safely cross a pedestrian crossing in the US [1]. Secondary measures explored the patterns within the time-series data for the knee joint angle over the entire gait cycle and the knee flexion moment during stance. We compared between group differences from baseline using non-parametric statistics and within group differences for time-series data using statistical parametric mapping.

## RESULTS AND DISCUSSION

Sixty-two (n=62) participants were recruited with sixty (n=60) participants receiving an intervention (Placebo n=20; 150-µg n=17; 450-µg n=21). Two participants did not receive their allocated intervention. There were no baseline differences between groups for demographics and pain scores. At day 120, both the 150-µg and 450-µg groups had a statistically significant greater proportion of participants increasing their walking speed from less than to greater than 1.3 m/s when compared to the placebo group (p=0.028 and 0.022, respectively). There were statistically significant between group main effects for the change in knee ROM from baseline at day 120 (p=0.042) and 180 (p=0.022). At day 120 and 180, post-hoc analysis showed that the change in knee ROM was statistically significant between the placebo and 450-µg group, which equated to medium-large effect sizes (Cohen's $d$ = 0.47-0.88). Importantly, from a regulatory perspective, the placebo group showed no improvement in walking gait over 180 days which contrasts with previous studies using PROMS.

## CONCLUSIONS

Pooled data from the early and middle phases of the regulatory process for XT-150 suggest that the treatment results in functional improvement for walking extending out to 180 days following a single injection. We strongly advocate for the inclusion of functional outcome measures, such as quantitative gait analysis, to become a standard part of the regulatory approval process.

## ACKNOWLEDGEMENTS

DT was supported by a NHMRC Career Development Fellowship (ID 1126229). We acknowledge Dianne Pepper and the clinical research team at CMAX, Adelaide for their support.

## REFERENCES

[1] Salbach et al. 2014. Arch Phys Med & Rehab 95:117-128. e111.

# IMAGING PROTOCOL FOR LONGITUDINAL ASSESSMENT OF STRUCTURAL CHANGES IN MOUSE KNEES

[1]Pholpat Durongbhan, [1]Han Liu, [1]Jemima E. Schadow, [1]Emma Boersma and [1]Kathryn S. Stok

[1]Department of Biomedical Engineering, The University of Melbourne, Australia
email: kstok@unimelb.edu.au

## INTRODUCTION

Recent studies have performed quantitative morphometric analysis (QMA) to assess bone, cartilage, and whole-joint changes in animal models of osteoarthritis using micro-computed tomography (microCT) [1]. Applying these techniques in longitudinal studies presents an opportunity for an efficient approach to monitor dynamic structural changes *in vivo*. However, the lack of a mechanism to maintain joint pose and alignment during image acquisition and processing presents a challenge: shifting joint pose from one scan to the other leads to inconsistent joint measurements. In this work, we propose a novel microCT imaging protocol that allows reproducible and accurate QMA of the mouse knee. The proposal consists of a positioning device to control knee pose during acquisition, and an image processing workflow to maintain consistent alignment between scans. A reproducibility study and a pilot longitudinal study were conducted to validate the proposed protocol.

## METHODS

A mouse positioning device was designed to be compatible with the *in vivo* microCT animal bed (vivaCT80, Scanco Medical AG, Switzerland) [2]. Seven healthy C57Bl/10 male mice (n = 14 knees) were sacrificed, placed in the positioning device, and scanned at 10.4 µm voxel size. Each mouse was scanned five times, with repositioning between scans.

A fully automated image processing workflow to align all scans to a common reference was developed. Removing inter-sample variation, the general shape of the tibia was represented using lower-order spherical harmonics descriptors (SPHARM), which describe objects of spherical topology as a weighted sum of spherical harmonic basis functions [2]. The joint centre of mass was measured from the aligned images, defined as a vector with length, λ (mm), and orientations, α (°); β (°); and γ (°), connecting the centres of mass of the femur and tibia [1]. Reproducibility was calculated as precision error, expressed in both absolute value (PESD) and coefficients of variation (PE%CV), as well as intraclass correlation coefficient (ICC).

The protocol was applied to a longitudinal study using four healthy C57Bl/10 mice (n = 8 knees). Each mouse was scanned *in vivo* weekly for nine weeks and processed as described. Joint centre of mass was calculated, and accuracy was expressed as relative standard deviation (RSD).

## RESULTS AND DISCUSSION

Exemplar measurements of joint centre of mass using the protocol are shown in Figure 1a. For repeated measurements, high ICC were obtained for all parameters (ICC λ: 0.832, α: 0.912, β: 0.892, γ: 0.903), indicating excellent reproducibility (ICC > 0.75). Low precision errors (PE(%CV) < 7%) for all parameters were also obtained.

Longitudinal measurement results using the protocol are shown in Figure 1b, c, d, and e for λ, α, β, and γ, respectively. Visual inspection shows low SD for each week while the mean values remain consistent. RSD for all measurements at all time points are smaller than 10%, except for β at week 8 (RSD = 11.17%), pointing to generally consistent measurements over time and demonstrating the feasibility of the proposed method.

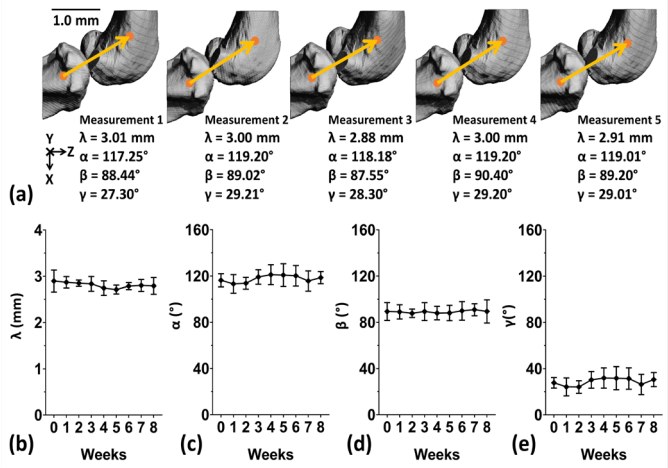


**Figure 1:** (a) Exemplar repeated measurements using the protocol showing joint centre of mass, with length, λ (mm), and orientation α (°), β (°), and γ (°) with regards to the x, y, and z axis, respectively. (b), (c), (d), and (e) Longitudinal measurement results (mean ± SD) using 8 legs from 4 animals over 9 weeks for λ (mm), α (°), β (°), and γ (°), respectively.

## CONCLUSIONS

The novel protocol, consisting of a positioning device and an image processing workflow based on spherical harmonics, enables highly reproducible and consistent QMA of the mouse knee in longitudinal studies. The protocol is now being used to reveal dynamic changes to bone and joint structures associated with musculoskeletal disease progression in animal models.

## ACKNOWLEDGEMENTS

This work was supported by the ARC (DP180101838).

## REFERENCES

1. Stok, K.S. et al., *PLOS One.* 11(1): e0147564, 2016.
2. Durongbhan, P. et al., Bone. 166:116606, 2023.

# SPINAL CORD-ON-A-CHIP: A NOVEL MICROFLUIDIC MODEL TO INVESTIGATE NEUROLOGICAL CELL RESPONSES TO SPINAL IMPLANT WEAR PARTICLES

[1]Aswini Madhavan, [1]David Wen, [1]Javad Tavakoli and [1]Joanne Tipper

[1]School of Biomedical Engineering, University of Technology Sydney, Sydney, NSW, Australia
email: aswini.madhavan@student.uts.edu.au

## INTRODUCTION

Biomaterials such as metals, polymers and ceramics are widely used in spinal implants. However, the interfaces and bearings of certain combinations of materials like metal-on-polymer can generate substantial volumes of wear particles. These particles have the potential to impact the spinal cord negatively, leading to structural damage of spinal cord meninges, inflammation, hypersensitivity, DNA abnormalities, and neurotoxicity [1]. Despite the intense research on orthopaedic implants, the impact of wear particles on neurological cells is unclear, and the possible indirect effects of implant wear are yet to be explored. Current 3D in-vitro models like hydrogel-based cell cultures are inadequate to study the indirect wear particle response and struggle to precisely control the microenvironment and mimic the spinal cord [2].

To address this, we have devised a microfluidic model optimising the analysis of neurological cell responses to wear particles, providing a cost-effective and time-efficient means to conduct relevant experiments in a controlled environment.

## METHODS

**Design and development**: The model was designed in Autodesk Inventor. Microfluidic resin moulds were fabricated using a Digital Light Processing (DLP) 3D printer, followed by casting polydimethylsiloxane (PDMS) chips. The device features two channels for cell culture and a middle channel with micropillars separating the other two channels.

**Particle Characterisation & Optimisation:** Polyether ether ketone (PEEK) particles were filtered and characterised according to their size using scanning electron microscopy (SEM) imaging. GelMA and collagen were added to the middle channel and tested for leakage between the microfluidic channels, using sterile water and media containing particles and cells.

**Experiments on biological response**: For the functionality test, rat glioma cells (C6, astrocytes) and PEEK particles (with a dose of 100 $\mu m^3$ of particles per cell ranging from 0.1 to. 10 µm in size) were added and cultured in the microfluidic device followed by viability experiments [3].

## RESULTS AND DISCUSSION

The micropillars prevented any leakage of cells or particles between the channels and enabled indirect cell connection with collagen in the middle. The PEEK particles used in the experiments had varying shapes, from round and elongated, to varying sizes. Cells were evenly distributed across the channels, and the live/ dead assay for a span of four days revealed live cells dominated. The viability experiments confirmed the compatibility of our device for neurological cell studies.

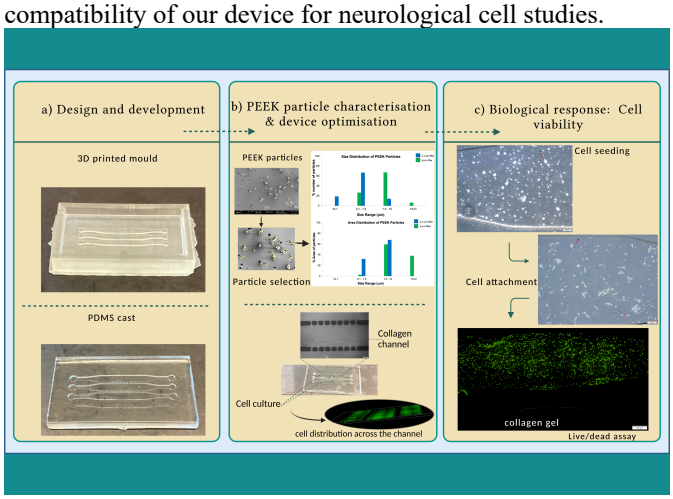


**Figure 1:** a) Developed 3D printed resin mould (top) and PDMS cast (bottom), b) Size and area distribution of PEEK particles in four ranges (<0.1 um, 0.1–1 µm, 1-10 µm and >10 µm) with 0.1 µm and 8 µm filters; uniform cell distribution across the channels with collagen in the middle, c) Cell channel displaying attached astrocytes; red arrow denotes PEEK particles; Green stained cells represent the live cells (Created with BioRender.com).

## CONCLUSIONS

Our microfluidic model facilitates neurological cell analysis to wear particles and provides a platform for indirect cell studies. This model will be an effective tool for researchers in developing longer-lasting implants with enhanced properties and may reduce the likelihood of implant failure.

## ACKNOWLEDGEMENTS

We would like to acknowledge the Australian Government for supporting with Research Training Program (RTP) Scholarship.

## REFERENCES

1. Pasko K, et al., *Front Bioeng Biotechnol*, **4,** 2016.
2. Lee H, et al.," *European Spine Journal*. **29**, 2701–2712, 2020.
3. Stratton-Powell, et al., *Clin Orthop Relat Res*. **474**, 2394 2404, 2016.


# Tuesday, December 7

## PODIUM 2

# ASSESSING THE INITIAL MECHANICAL ENVIRONMENT OF CADAVERIC TIBIAE WITH CEMENTLESS TIBIAL TRAYS DURING STAIR DESCENT AND DEEP KNEE BEND

[1]Lauren Wearne, [1]Sophie Rapagna, [2]Greg Keene, [1]Mark Taylor and [1]Egon Perilli

[1]Medical Device Research Institute, College of Science and Engineering, Flinders University, Adelaide, SA, Australia
[2]Orthopaedics Department, SportsMed, Adelaide, SA, Australia
email: lauren.wearne@flinders.edu.au

## INTRODUCTION

Primary stability, the mechanical fixation between implant and underlying bone prior to osseointegration, is crucial for the long-term success of cementless tibial trays. However, experimental studies on the initial internal strains between bone and implant are limited, due to previous experimental restrictions [1]. The aim of this study was to quantify, through micro-CT imaging and digital volume correlation (DVC), the internal strain field for seven cadaveric tibiae when subjected to two time-elapsed mechanical load sequences replicating stair descent (SD) and deep knee bend (DKB), everyday activities known to expose the tibial tray to posterior loading.

## METHODS

Seven right human cadaveric tibiae were resected and impacted with a clinically employed titanium tibial tray (Attune, DePuy Synthes) by an experienced surgeon (ethics: HREC 186.20). The tibiae were potted distally with the resected surface flat. The time-elapsed loading spanned two days, the first for SD and the second for DKB. To replicate these activities, uniaxial loads were applied to the implanted tibiae through posteriorly offset prongs, the position of which matched the average position of the femoral medial and lateral condyles on the tibial tray during each load scenario [2]. The applied loads were scaled to the body weight (BW) of each donor for sequential load steps of 0.0 (preload), 0.5, 1.0, 1.5 and 2.5BW. For DKB, the peak load was extended to 3.5BW. After 20min relaxation, a micro-CT scan was acquired at each load step at 46µm/pixel (66min scan time), resulting in 63 loaded datasets. A repeated scan of the tibia in the unloaded condition (0.0BW) was taken for zero-strain error analysis (calculated accuracy of the DVC analysis was 444µε, precision 200µε) [1,3]. Loaded scans were rigidly co-registered to the unloaded scan in each activity and DVC was performed (DaVis v8.3.1, algorithmic masking applied to remove air, 5-step progression with a final subvolume sidelength of 1.56mm (34pixels)) [1]. The minimum principal strain component ($P_{min}$) was calculated across the entire proximal tibia, before isolating subvolumes directly under the tibial tray (Fig1a), and moving radially away from that interface by 2 subvolumes (1.56 - 3.14mm from the interface) and 3 subvolumes (3.14 - 4.69mm from the interface).

## RESULTS AND DISCUSSION

With progressive loading, increased compression of trabecular bone directly under the tibial tray was observed across all load steps for the seven tibiae. The strain magnitudes varied amongst the tibiae (Fig 1b) and were high, with the 90$^{th}$ percentile ranging from -1,676µε to -73,612µε for all load steps. This exceeds the reported yield strain of tibial cancellous bone [4] and occurred as early as 1.0BW of loading. Such high strain values were predominately limited to subvolumes in direct contact with the tibial tray and in the posterior region. Strain values greater than the yield strength of bone did not extend further than 3.14mm from the bone-implant interface. No tibiae were observed to fail grossly in the experiment.

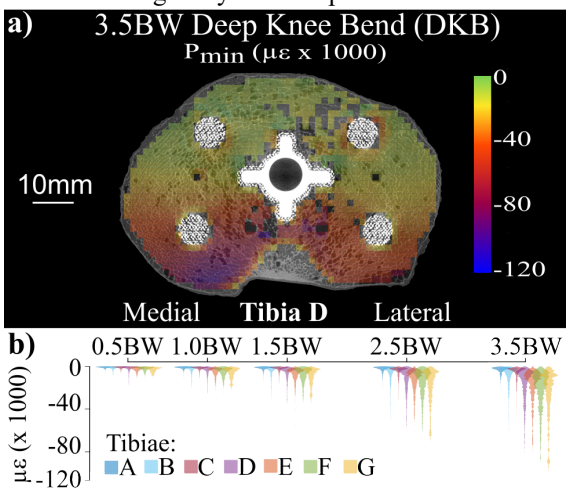


**Figure 1:** a) DKB $P_{min}$ distribution at 3.5BW via DVC; b) $P_{min}$ frequency distribution for the seven tibiae during DKB.

## CONCLUSIONS

In this time-elapsed experiment, cancellous bone strains with peak values exceeding the yield strain of bone were found, as early as at 1.0BW of loading. These predominately occurred within 1.56mm of the bone-implant interface and did not extend further than 3.14mm. Such localized and large strain values could explain the high initial migration of cementless tibial trays in the immediate post-operative period seen clinically [5].

## ACKNOWLEDGEMENTS

Australian Research Council Training Centre for Medical Implant Technologies (IC180100024).

## REFERENCES

1. Wearne LS et al, J Mech Behav Biomed Mater 134, 2022.
2. Baldwin M et al, J Biomech, 45:474-483, 2012.
3. Palanca M et al, J Biomech, 49:3882-3890, 2016.
4. Liu et al, J Biomech, 40:3515-3520, 2007
5. Koster LA et al, Bone Joint J, 105-B:148-157, 2023

# DETERMINING WEAR OF AN ADVANCED ZRN MULTILAYER COATING TOTAL KNEE SYSTEM MANUFACTURED OUT OF TITANIUM UNDER HIGHLY DEMANDING ACTIVITIES

[1,2]Julius Dohm, [1]Ana Laura Puente Reyna, [1] Berna Richter and [1,2]Thomas M. Grupp

[1]Aesculap AG, Research & Development Tuttlingen, Germany
[2]Department of Orthopeadic and Trauma Surgery, Musculoskeletal University Center Munich (MUM), Campus Grosshadern, LMU Munich, Munich, Germany
email: julius.dohm@aesculap.de

## INTRODUCTION

Generally, joint replacement materials are well tolerated and biocompatible, however CoCrMo can cause a hypersensitivity reaction in the patient due to metal ions, which include nickel, chromium, and cobalt [1].

In vitro studies of uncoated femoral and tibial component disclosed pitting and uneven wear, originating from cobalt-rich matrix material, measured using coupled plasma mass spectroscopy [2]. To reduce the risk for patients suffering from this metal hypersensitivity, titanium presents an alternative metal with good biocompatibility and a low reactivity due to its passive oxide layer. However, titanium used in implants (Ti6Al4V) is known to have a lower wear resistance compared to CoCrMo.

As a result, coatings have been introduced with the aim of reducing wear and act as allergy prevention. However, problems with monolayer physical vapor deposition (PVD) coatings have been reported in literature resulting in ablation of the monolayer due to the weak elastic modulus [3] An alternative zirconium nitrate (ZrN) multi-layer coating has been proven successful in keeping its integrity under high demanding knee wear activity (HDA) with no sign of delamination or scratches in the articulating areas [2].

The purpose of this study is thus to evaluate the wear behavior of ZrN coated total knee implants printed out of titanium with gliding surface produced out of polyethylene under High Demanding Activities Simulation [4,5]. Additionally, the degradation effect of third body particles on the gliding surface as well as the stability of the multilayer coating will be analyzed.

## METHODS

For testing, a load-controlled 3 + 1 station knee wear simulator (EndoLab GmbH, Thansau, Germany) was utilized. This simulator can replicate the HDA loads and movements over a course of 5 million cycles, which equates to an in vivo time between 15 and 30 years. The load and motion profiles used in the simulation were derived from Bergmann load profiles. Four medium size femoral and tibial components additively manufactured out of Ti6Al4V coated with ZrN in combination with medium crosslinked polyethylene with 0.1 % Vitamin E; 30 kGy gamma sterilized (MXE) 10 mm gliding surfaces were used. The gravimetric wear rate was measured after 2 million cycles of HDA testing. Afterwards, bone particles were added to the system to simulate for third body wear. Ion analysis was measured at 0.5, 1, 2, 3, 4, and 5 million HDA cycles by inductively coupled plasma mass spectrometry.

## RESULTS AND DISCUSSION

To assess if the ZrN multilayer coating system constitutes a secure barrier against the diffusion of metal ions out of TAV, a metal ion concentration measurement of zirconium (Zr), chromium (Cr) aluminum (Al), vanadium (V) and titanium (Ti) from the tested serum samples was done after each HDA interval. In addition, an analysis of the articulating surfaced (femoral components and gliding surfaces) was performed with a microscope to visualize the areas with wear patterns and asses the impact of third body particles on the wear of the TKA system.

ZrN multilayer coated implants demonstrated in previous studies up to 88% less wear as well as a significantly less immunological triggering (IL-8, IL-10) when compared to uncoated CoCr implants [6]. Furthermore, registry data of the coated implants in the AOANJRR industry report 5/2020 demonstrate a 5-year cumulative survival rate of 99 percent making it one of the best in class. In combination with additively manufactured titanium total knee implants, this encompassing solution presents a great option for patients that show allergic cutaneous reactions to metals such as nickel, chromium, or cobalt. Rigours HDA testing is thus an essential aspect to ensure full functionality and ensure that the ZrN multilayer coating shows no signs of unusual wear modes.

## REFERENCES

1. Granchi et al, *Biomaterials* **26.15: 2371-2379 (2005)**
2. Kretzer et al, *International Orthopaedics.* **38. 2: 335–340, (2014)**
3. Raimondi et al, *Biomaterials* **21.9:907-913 (2000)**
4. Schwiesau et al, *BioMed Research International* **2014 (2014)**
5. Reyna et al, *Journal of biomechanics* **79: 88-96 (2018)**
6. Thomas et al, *Orthopedics* **39(3):24-30 (2016)**

# OPTIMISED POROUS FEMORAL STEM DESIGN TO REDUCE STRESS SHIELDING

[1]Sarah Safavi, [1]Hans A Gray, [1]David C Ackland and [1]Peter VS Lee

[1] Department of Biomedical Engineering, University of Melbourne / ARC CMIT, Melbourne, Australia
email: ssafavi@student.unimelb.edu.au

## INTRODUCTION

Total hip replacement (THR) surgery is the treatment of choice for advanced hip osteoarthritis and restores joint function and improves the patient's quality of life. Despite these positive outcomes, as many as 6% of THR patients undergo revision surgery within five years [1]. Aseptic loosening is one of the most common reasons for revision and is caused by the resorption of bone surrounding the implant. Bone resorption is caused due to the shielding of bone from stress because implants are made of metal and hence are much stiffer than bone [2]. In this study, we compared a lattice structure-based porous hip implant with a solid titanium implant.

## METHODS

Finite element models (FEM) of an intact reference femur bone and an implanted bone were created. Composite bone material properties were assigned (**Table *1***). Hip loads and simplified muscle forces during walking were applied [3]. The distal end of the femur was fixed. Octahedral shear strain (OSS) was used as a mechanical stimulus to predict bone adaptation [4]. A fully porous implant with 30% porous diamond lattice structures was designed based on an optimisation algorithm. The elastic modulus of the selected additively manufactured diamond lattice structure was previously determined based on experimental results (**Table *1***).

For comparison, the mean OSS in each Gruen zone of the femur bone model was calculated for the solid titanium and the porous implant and compared to the intact reference femur model. The overall relative difference between the mean OSS in the implanted and intact bone model for the porous and solid design were reported.

**Table 1:** Material properties applied in the finite element models for the femur bone and femoral stem implant.

| Component | Elastic Modulus [MPa] |
|---|---|
| Cortical Bone | 17,000 |
| Trabecular Bone | 155 |
| Solid Titanium | 110,000 |
| 30% Porous Titanium | 9410 |

## RESULTS AND DISCUSSION

The fully porous design resulted in increased OSS and therefore reduced bone resorption in all Gruen zones compared to the solid implant (**Figure *1***). The OSS decrease for the solid implant is -10.3 % and -3.4 % for the fully porous implant.

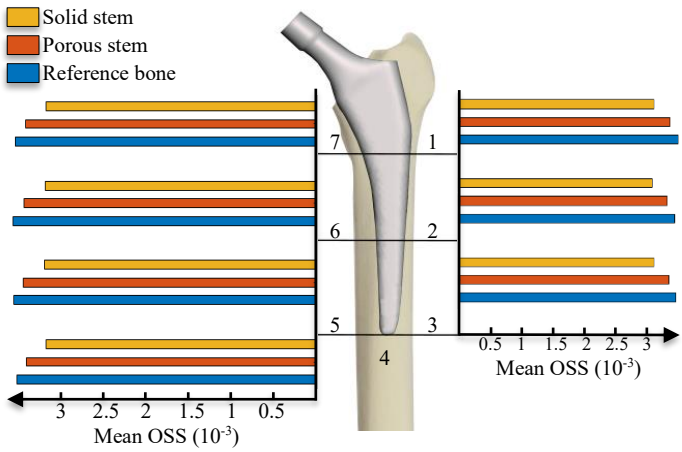


**Figure 1:** Mean OSS in Gruen zones in the reference and implanted bone models.

## CONCLUSIONS

Introducing porosity into a femoral hip stem can reduce stress shielding and thereby potentially decrease bone resorption and reduce the prevalence of aseptic loosening. Diamond lattice structures may be suitable to design porous implants with sufficient mechanical strength. Future work will include the comparison of different porous design strategies, as well as in-vitro experiments on composite femurs to evaluate the fatigue strength of the porous implant and to confirm the feasibility and effectiveness of the new designs.

## ACKNOWLEDGEMENTS

This research is funded by an Australian Research Council (ARC) Industrial Transformation Research Program (Grant No. IC180100024) and Naton Medical Group (Beijing, China).

## REFERENCES

1. G Labek *et al. J Bone Joint Surg Br* **93**, 293-297 (2011).
2. R Huiskes *et al. Clin Orthop Relat Res* **274**, 124-134 (1992).
3. https://orthoload.com/ accessed on 22 May 2023
4. M Piccinini *et al. Med Eng Phys* **38**, 1348-1359 (2016).

# HIP IMPLANTS WITH EVIDENCE OF PHASED INTRODUCTION HAVE IMPROVED SURVIVORSHIP AT LONG TERM FOLLOW-UP

[1]Chan Hee Cho, [3]Bart Pijls, [1,2]John Abrahams, [1,2]Bogdan Solomon and [1,2]Stuart Callary

[1]Centre for Orthopaedics and Trauma Research, The University of Adelaide, Adelaide, SA, Australia
[2]Department of Orthopaedics and Trauma, Royal Adelaide Hospital, Adelaide, SA, Australia
[3]Department of Orthopaedic Surgery, Leiden University Medical Centre, Leiden, Netherlands
email: chanhee.cho@adelaide.edu.au

## INTRODUCTION

Loosening of the acetabular component is a common reason for revision following a Total Hip Replacement (THR). Radiostereometric analysis (RSA) has been used to predict long-term loosening due to acetabular component loosening at two years follow-up (1). RSA is currently the most sensitive method to measure acetabular cup migration *in vivo* (2).

RSA has been previously suggested to be used as an early qualitative tool necessary for the early phased introduction of new orthopaedic hip implants internationally but not all hip implants have been studied with RSA. Despite this, it is not clear if the use of RSA in the phased introduction of acetabular components has an influence on their long-term performance. Long term survival data is best collected from national registries, rather than small cohort studies that can be limited by patient dropout.

Therefore, the aim of this study was to determine whether there was a difference in all-cause revision rate between non-RSA-tested and RSA-tested acetabular cup listed in national hip arthroplasty registries at both 5- and 10-years follow-up.

## METHODS

Survival data was collected from national orthopaedic registries that reported 10-year survivorship rates of individual acetabular cup designs. Registries were not included in the study if they did not report 10-year survivorship data of acetabular cup designs. From twenty-six national registries, seven national hip registries were included in the study. The 5- and 10-year revision rates with their corresponding 95 confidence intervals or standard errors were extracted per design. A recent meta-analysis was used to identify RSA-tested acetabular cup designs and was matched by femoral stem and cup combination (3). A random-effects model was used to calculate the pooled revision rate at 5- and 10-years follow-up for non-RSA tested and RSA-tested acetabular cups. The mean difference in revision rates at 5- and 10-years follow-up was calculated by pooling the data and using RSA as a factor in the random-effects model.

## RESULTS AND DISCUSSION

Mean all-cause revision rates at 5 years for non-RSA-tested and RSA-tested cups were 3.6% (95% CI 3.4 to 3.8) and 2.7% (95% CI 2.4 to 2.9), with a mean difference of 0.9% favoring RSA-tested implants (95% CI 0.4 to 1.3; $p < 0.001$). Mean all-cause revision rates at 10-years for non-RSA-tested and RSA-tested acetabular cups were 6.5% (95% CI 6.3 to 6.9) and 5.0% (95% CI 4.5 to 5.5), with a mean difference of 1.5% in favor of RSA-tested acetabular cups (95% CI 0.7 to 2.2; $p <0.001$). This evidence further supports the use of RSA as a surveillance tool to monitor new acetabular cup introduced in the orthopaedic market.

## CONCLUSIONS

RSA-tested acetabular cups have a significantly lower revision rates at both 5- and 10-years follow-up than non-RSA tested acetabular cups. An improvement in revision rate of approximately 1.5% at 10 years can result in a decrease of approximately 30% in revision burden during this period.

## ACKNOWLEDGEMENTS

Stuart Callary was supported by a Research Fellowship from The Hospital Research Foundation Group during this study.

## REFERENCES

1. Pijls BG, et al. Acta Orthop. 2012;83(6): 583-91.
2. Nelissen RG, et al. JBJS Am. 2011;93 Suppl 3: 62-5.
3. Cho C, et al. Acta Orthop Accepted August 2023

**Table 1:** The mean 10-years all-cause revision rates of RSA-tested and non-RSA acetabular cups from international registries

| | National Registries 10-years pooled revision rate (95% CI) | | | | | | | |
|---|---|---|---|---|---|---|---|---|
| **Acetabular Cups** | **Australia** | **Netherlands** | **Denmark** | **Finland** | **United Kingdom** | **Emiliano Romagna** | **New Zealand** | **Combined Registries** |
| **RSA-TESTED** | 5.7 (5.0-6.3) | 4.5 (3.2-5.8) | 2.0 (1.1-2.8) | 8.5 (6.7-10.4) | 3.6 (2.6 - 4.5) | 4.9 (4.2 - 5.5) | 6.4 (4.6 - 8.1) | 5.0 (4.5-5.5) |
| **Non-RSA TESTED** | 5.0 (4.5-5.4) | 4.0 (3.6-4.5) | 1.8 (1.3-2.2) | 11.7 (10.5 to 12.9) | 5.2 (4.6 - 5.9) | 5.1(4.4-5.9) | 6.3 (5.8-6.8) | 6.5 (6.3-6.9) |

# RESECTING TISSUE FROM THE 'IMPINGEMENT POINT' IMPROVES RANGE OF MOTION PRIOR TO DISLOCATION IN TOTAL HIP REPLACEMENT SURGERY.

[1]Tom Ward, [1]Tat Chow, [1]Al Burns, [1]Joe Lynch, and [1]Paul Smith

[1]Trauma and Orthopaedic Research Unit, Canberra Hospital, ACT
email: tom.ward@magdalen.oxon.org

## INTRODUCTION

Dislocation remains a major cause of morbidity after Total Hip Replacement surgery [1]. One method for reducing the risk of dislocation is to resect tissue from the anterior capsule that causes impingement and subsequent dislocation. The effect of resecting this tissue on range of motion prior to dislocation has not been widely researched. Furthermore, quantifying the location of impinging tissue has not been achieved before.

## METHODS

26 subjects undergoing total hip replacement surgery were recruited for the study. Using the Intellijoint navigation system, the range of motion to dislocation was measured as the amount of internal rotation, with the hip at approximately 90 degrees of flexion, achieved before the femoral head levered out of the acetabulum by 2 mm [Figure 1]. The was measured before and after resection of tissue around the 'impingement' point, usually anterior/superior to the acetabulum. Mass of resected tissue was measured.

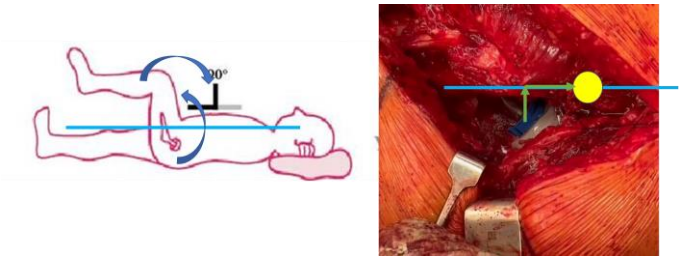

**Figure 1:** Example of impingement point location with given internal rotation and flexion.

The location of the impingement point was validated via a sawbones experiment. Known locations on the acetabulum (fixed screws) and the positions estimated by the impingement algorithm, were compared.

## RESULTS AND DISCUSSION

Five subjects were too stable to dislocate within the rotation range visible to the navigation system. Data from 21 subjects were available. Mean increase in internal rotation to dislocation was 9.3 degrees (SD 4.9 degrees). Mean mass resected was 7.1 g (SD 3.7 g).

Validation indicated errors in the impingement position were 6.2 mm (SD 5.0 mm), and 8.2 mm (SD 2.4 mm) in anterior and proximal directions, respectively.

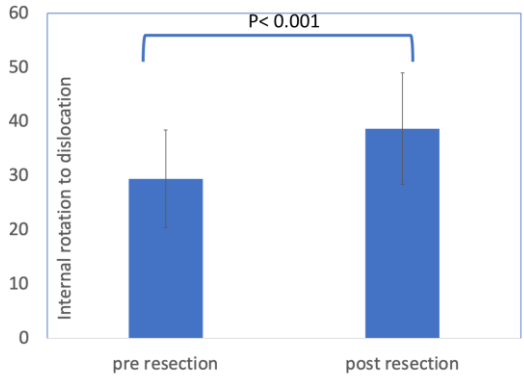


**Figure 2:** Change in Internal Rotation Angle at which dislocation occurs.

## CONCLUSIONS

Resecting anterior soft tissue from the hip increased internal rotation to dislocation by a clinically significant amount, 9.3 degrees on average. Given surgeons will often use a 10-degree lipped liner to improve stability, resecting anterior tissue is a valuable alternative.

## ACKNOWLEDGEMENTS

Andrew Strain from Intellijoint provided invaluable logistical support for this study.

## REFERENCES

1. Kunustor S, et al., *Lancet Rheum.* Oct;1(2): e111-e121., 2019.

# Tuesday, December 7

## PLENARY 2 – Prof Steven Goldring

"Osteoarthritis, a "whole" joint disease"

# Tuesday, December 7

## Minghao Zheng Orthopaedic Innovation Award

## Finalists

# DEVELOPMENT AND VALIDATION OF A BIOMECHANICALLY FIDELIC SURGICAL TRAINING KNEE MODEL

[1]Kieran J Bennett, [1]Parham Foroutan, [1]Ella Fairweather, [2]Sammuel A Sobey, [2]Nick Litchfield, [2]Mark Roe, [1]Karen J Reynolds, [1]John J Costi, [1]Mark Taylor

[1]The Medical Device Research Institute, College of Science and Engineering, Flinders University, Adelaide, SA, Australia
[2]Fusetec, Adelaide, SA, Australia
email: kieran.bennett@flinders.edu.au

## INTRODUCTION

Total knee arthroplasty (TKA) is an evolving procedure, requiring continuous learning throughout a surgeon's career. Appropriate balancing in the coronal (varus-valgus (VV) rotation) and sagittal (anterior-posterior (AP) shear and flexion) planes is a critical step contributing to successful TKA [1]. Development of this skill requires training using cadaveric specimens as current synthetic models lack biomechanical fidelity [2]. In this research, we aimed to design, manufacture, and experimentally validate a knee surgical training model which reproduces the flexion dependent VV and AP mechanics of cadaveric knees, while maintaining anatomic accuracy.

## METHODS

To design the knee model, a probabilistic finite element model (FEM) was developed based on the left knee geometry of an adult male, consisting of five ligament structures. The FEM was used to determine the range of ligament reference strains that replicate AP and VV cadaveric mechanics [3], using attachment sites from literature, and stiffnesses based on the synthetic ligaments manufactured for this study. The FEM-determined reference strain ranges were used to manufacture seven physical knee models which were experimentally tested in a six degree of freedom hexapod robot to determine agreement in VV and AP mechanics between the FEM, the manufactured models, and 20 cadaveric knees.

In both the FEM and hexapod experiments, knee kinematics were measured at extension (~15°), mid-flexion (~45°), and full flexion (~90°). At each flexion angle: 1) all off-axis shear forces and moments were minimized to determine the neutral orientation. 2) 20 N of superoinferior (SI) tensile force was applied to ensure the ligaments were taught. 3) (a) ±10 Nm VV moment was applied with all other rotation and translation axes (except SI translation) constrained; (b) ±100 N AP load was applied with all three rotations axes, and mediolateral displacement constrained.

## RESULTS AND DISCUSSION

Of the three assessed flexion angles, the manufactured models were most dissimilar to cadaveric knees in extension (Figure 1). While, in extension, all seven models showed varus rotation and anterior translation endpoints within the 95% confidence interval of the cadaveric knees, two models showed an increase of 1° in endpoint valgus rotation, and three models showed an increase of 0.3-1.7 mm in endpoint posterior translation. At full flexion, all seven models showed mechanical profiles within the 95% confidence interval of cadaveric knees.

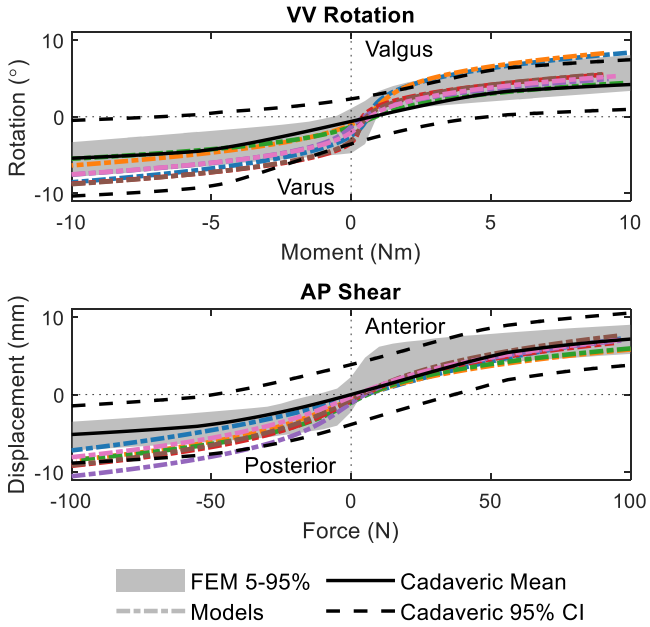


**Figure 1:** Measured VV rotation and AP shear displacement due to applied load at extension (~15°) for the seven knee models (colored lines) overlaid onto the 5-95% solution space of the FEM (shaded area), and the mean (solid line) and 95% confidence interval (dashed lines) of 20 cadaveric knees [3].

## CONCLUSIONS

The knee model developed in this work is capable of physiologically constraining AP and VV motion at multiple flexion angles, allowing for its use as a surgical training model for procedures like TKA.

## ACKNOWLEDGEMENTS

This work is funded by a Government of Australia Global Innovation Linkages Program Grant (ID: GILIII000120), with in-kind support from DePuy Synthes and Fusetec.

## REFERENCES

1. Babazadeh, S et al., *Orthopedic Review* **1**:26, 2009.
2. Clifton, W et al., *Clinical Anatomy* **33**:428-430, 2020.
3. Al-Dirini R et al., *unpublished*

# CORRELATION ANALYSIS OF VERTEBRAL BODY WEDGE ANGLES AND INTERVERTEBRAL DISC WEDGE ANGLES WITH MAJOR CORONAL CURVE ANGLE AFTER VERTEBRAL BODY TETHERING - A PILOT STUDY

[1,,2]Megan Roser, [1,2]Geoff Askin, [1,2]Robert Labrom, [1,2]Maree Izatt, , [1]Sinduja Suresh, [1]J Paige Little

[1]Biomechanics and Spine Research Group, Queensland University of Technology, Brisbane, QLD, Australia
[2]Queensland Children's Hospital, Brisbane, QLD, Australia
Email: mjnroser@gmail.com

## INTRODUCTION

Vertebral Body Tethering (VBT) is a surgical technique aiming to halt progression and correct the spinal deformity for adolescent idiopathic scoliosis (AIS). VBT is proposed to modulate vertebrae growth by applying asymmetric forces across the physes in the immature vertebrae. The aim of this study is to investigate the wedge angles of the vertebral bodies and intervertebral discs over time with a correlation analysis to the coronal major curve angles.

## METHODS

This is a retrospective study of 19 patients who underwent VBT in Brisbane, Australia. Standing PA radiographs were taken during routine clinic appointments pre-operatively and at 1-week, 2-months, 6-months, 1-year, 18-months and 2-years post-operative. ImageJ (version 1.53) was used to measure the vertebral body wedge angle and intervertebral disc wedge angle at each tethered thoracolumbar level (figure 1).

Wedge angles were correlated with major coronal curve angles using generalised estimating equations in SPSS (version 28.0.1.0). Separate models were run for each vertebral body (VB) and intervertebral disc (IVD) level with the coronal major curve angle as the dependent variable. The absolute value wedge angles were used as the predictor covariates. Patient ID were used as the subject variables and visit (appointment in months post-surgery) was used as within-subject factors. A p-value of <0.05 was accepted as statistically significant.

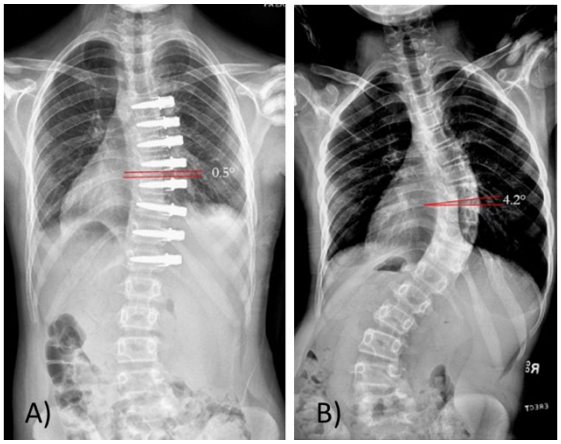


**Figure 1:** Radiographs displaying the wedge angle of the T8/9 IVD at A) pre-operative, B) 1-week postoperative.

## RESULTS AND DISCUSSION

15 patients had post-operative imaging to 2-years. The mean pre-operative major coronal curve angle was 47.3° ± 3.8° which decreased post-operatively to 20.7° ± 6.3° at 12 months, and 27° ± 7° at 2-years follow-up.

There was a statistically significant association between a number of IVD levels and major coronal curve angle. For every 1° change in the IVD wedge angle of T7/8, there was an associated 1.7° change in major coronal curve angle (p=0.001). For every 1° change in the IVD wedge angle of T8/9, there was an associated 2.5° change in major coronal curve angle (p=0.000). For every 1° change in the IVD wedge angle of T9/10, there was an associated 2.1° change in major coronal curve angle (p<0.001). For every 1° change in the IVD wedge angle of T10/11, there was an associated 2.0° change in major coronal curve angle (p<0.001).

The only statistically significant association between VB wedge angles and major coronal curve angles was at T5, in that a 1° change in the wedge angle of the T5 VB was associated with a -1.5° change of the major coronal curve angle ((p=0.018).

## CONCLUSIONS

VBT can reduce the scoliosis curve and prevent progression for a cohort of skeletally immature patients at 2-years follow up. A strong correlation was found between the wedge angles of the apical intervertebral discs and the major coronal curve angles at pre- and post-operative time points. This indicates that changes to the wedging of the apex intervertebral discs may influence the overall major coronal curve angle.

Further investigation of the vertebral body wedge and intervertebral disc angles is required to understand how VBT affects the spine at individual levels, and longitudinal follow up to skeletal maturity and beyond is essential to understand the long-term effects of this procedure.

# AN INNOVATIVE TECHNOLOGY REVEALS NEW FINDINGS: INITIAL CELL DENSITY MATTERS FOR THE REGENERATION OF INTERVERTEBRAL DISC

[1]Javad Tavakoli, [1]Joanne L. Tipper

[1]School of Biomedical Engineering, Faculty of Engineering and IT, University of Technology Sydney
email: javad.tavakoli@uts.edu.au

## INTRODUCTION

Degeneration of the intervertebral disc (IVD) is a common consequence of aging, structural defects, and injuries, yet there is currently no strategy to regenerate the IVD. Tissue engineering research seeking to address this challenge has long been hindered by the absence of a physiologically relevant in vitro IVD model to maximize the clinical relevance of experimental data [1]. We have pioneered and developed the world's first physiologically relevant IVD-on-a-chip technology which mimics the biological complexity of the native counterpart allowing precise tune of material, mechanical and biological properties in a controlled environment [2]. This technology has enabled us to readily simulate IVD health and disease conditions and perform studies with targeting of precise research questions at low cost.

To date the exact number of cells required for practical IVD regeneration is unclear and there is a strong need to identify robust cell densities to optimize the likelihood of survival post-injection and characterize how cells will function in the typical degenerative microenvironment [3]. This will determine whether cells can efficiently contribute to IVD regeneration. The delivery of large numbers of cells may intensify the degenerative microenvironment due to competing nutrient demands, which may subsequently lead to unsuccessful clinical outcomes. Therefore, this study aims to investigate the impact of the initial cell density on cell biology in degenerated IVDs.

## METHODS

5 different initial cell densities (human nucleus primary cells) ranging from 1.2 to $48\times10^3$ were perfused into the IVD-on-a-chip model under healthy and degenerated [at low oxygen (2%) and glucose concentrations (1 g/l) and under acidic condition (pH = 6.5)] conditions. The effect of different initial cell densities on cell viability was studied. Additionally, cell morphology was evaluated using fluorescent microscope and Scanning Electron Microscopy.

## RESULTS AND DISCUSSION

The overall effect of cell culture duration (day), initial cell densities, IVD status (healthy vs degenerated) and their interactions on cell viability were significant ($p < 0.001$). For all cell densities at different cell culture times, cell viability significantly decreased for degenerated compared to the healthy IVD ($p < 0.001$). After 5 days of cell culture, cell viability was significantly different between different cell densities ($p < 0.028$) for healthy IVD with an increasing trend from 1.2 toward $48\times10^3$ initial cell densities. In the simulated degenerative condition, we found significant differences between cell viability and initial cell densities ($p < 0.001$). Surprisingly, trends for cell viability increased exponentially from 1.2 toward $36\times10^3$ initial cell densities with a significant drop (≈ 77%) for $48\times10^3$ initial cell density. Our microscopic analyses revealed round cells with weak adhesion properties forming cell colonies in the degenerated condition. In contrast, cells in healthy IVD were elongated with higher adhesion properties.

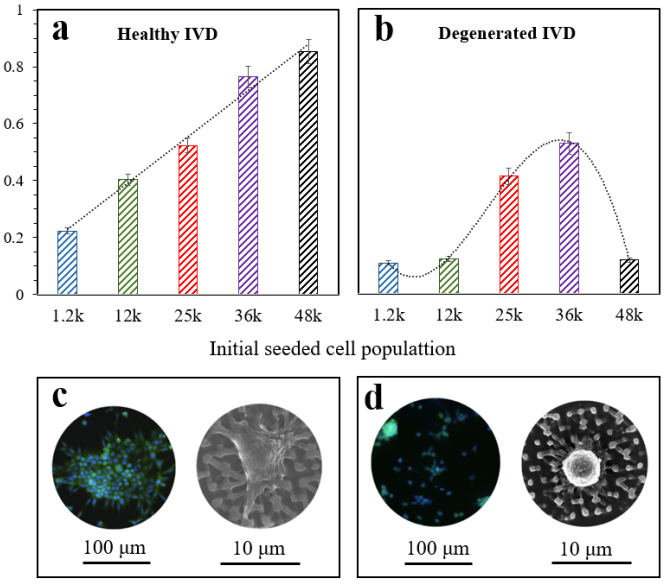


**Figure 1:** Cell viability results for (a) healthy and (b) degenerated IVDs at different initial cell densities. (c and d) fluorescent microscope and SEM images of cells in healthy and degenerated conditions, respectively. [results for day 5 cell culture]

## CONCLUSIONS

Not reported previously, initial cell density extremely affects cell viability in degenerated IVDs. The identification of proper initial cell density seems critical for proper IVD regeneration.

## ACKNOWLEDGEMENTS

This study was supported by the AO Spine and AO Foundation through the AO Spine 2022 Discovery and Innovation Award.

## REFERENCES

1. Tavakoli J, et al., *Trends in Biotechnology.* 2023.
2. Tavakoli J, et al., *Australia patent 2023901155*, 2023.
3. SakaiD, et al., *J of Orthopae Trans*, 9, 2017.

# A CADAVERIC STUDY INVESTIGATING A PINLESS, IMAGE-FREE NAVIGATION SYSTEM FOR THE INSERTION OF ACETABULAR CUPS DURING THE ANTERIOR HIP APPROACH.

[1]Peter Smitham, [1]Alexandra Bunting, [2]Tian Wang, [2]Matthew H. Pelletier, [2]Laurie Kohan, [2]William R. Walsh

[1]Discipline of Orthopaedics and Trauma, The University of Adelaide, SA, Australia
[2]Surgical & Orthopaedic Research Laboratories, Sydney, University of New South Wales, NSW, Australia

email: peter.smitham@sa.gov.au

## INTRODUCTION

In the anterior hip approach, acetabular cup alignment is particularly important as the surgical approach often involves less muscle and tissue dissection, which can make it more challenging to visualize the joint during the procedure. Accurate cup placement is essential to ensure proper joint mechanics, stability, and longevity of the implant. Furthermore, the anterior hip approach is associated with a higher risk of component malposition, particularly in the vertical and transverse planes. The use of intraoperative fluoroscopy or computer tomography (CT) navigation can aid in achieving accurate acetabular cup placement. However, these techniques are often costly, time-consuming and may result in increased radiation exposure to the patient both pre and intraoperatively.

## METHODS

This study assessed the acetabular cup position using a pin-less, image-free guidance system in a cadaver model. A total of 64 cups were inserted at various angles by 3 surgeons in 14 hips – 7 bilateral specimens. Angles ranged from 30-55 degree inclination and 0-40 degree anteversion. Angles were measured using a pin-less image-free navigation system at the time of implantation. Following cup implantation specimens underwent a computed tomography scan and cup inclination and version were measured by a blinded assessor.

Data from the CT scan measurements were tabulated and compared to the navigation measurements for statical analysis using SPSS 26. Descriptive statistics were reported for all data. The intraclass correlation coefficients (ICC) were reported for reliability and the validity was assessed using the Bland-Altman method.

## RESULTS

The mean time to use the navigation system was less than 2 minutes per case (Figure 1) with no statistical difference between surgeons. The navigation system had a 90% Confidence Interval for Implant Accuracy of ± 2.5 degrees inclination and ± 4.7 degrees anteversion.

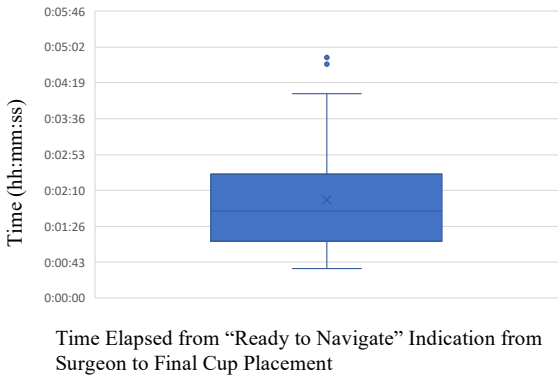


Figure 1: Mean Time for Navigated Acetabular Cup Placement using GYDER™ and 95% confidence intervals.

## DISCUSSION

The results of this analysis demonstrate the high degree of correlation between the CT scan measurements and the navigation measurements. The pin-less, image-free navigation system requires minimal additional medical waste requiring no additional pins or workflow changes along with real-time feedback & direct visibility into the surgical site.

Further cadaveric studies investigating obesity and clinical trials have been planned.

# Tuesday, December 7

## PODIUM 4

# CAN POST-NEONATAL CLINICAL AND SONOGRAPHIC SCREENING PARAMETERS EFFECTIVELY PREDICT HIP DYSPLASIA IN CHILDREN AT THEIR WALKING AGE?

Anubrat Kumar[1], Hung Lik-hang[1], Lam Tsz Ping[2], Yang Guangpu Kenneth[2]

[1]Prince of Wales Hospital (PWH), Hong Kong,

[2]Chinese University of Hong Kong, Hong Kong

email: dranubart5@gmail.com

## INTRODUCTION

Developmental dysplasia of the hip (DDH) underlies up to 9% of all primary hip replacements and up to 29% of those in people aged 60 years and younger.1 Post-neonatal secondary Screening(PNSS) for DDH aims at identifying it early enough to prevent adverse outcomes. The objectives of the study were to evaluate if the post-neonatal clinical and sonographic screening parameters can identify radiographic dysplasia at walking age?

## METHODS

The study was a retrospective case series of infants born between 1st January 2009 and 31st December 2018, screened, and managed as Post Neonatal secondary screening (PNSS) positive hips at Prince of Wales Hospital in Hong Kong. Over the study period, 2,497 infants underwent at least one USG examination at PWH. Eligible patients had their PNSS scheduled four weeks after birth. After excluding patients with teratological hip dislocation, late presentations (>6 months) and infants with no or inappropriate follow up radiographs, 155 infants were included in the study. Patient characteristics (sex and age), Clinical and sonographic screening parameters (Ortolani & Barlow manoeuvres, limited hip abduction of <70 degree, static and dynamic ultrasonography findings) and treatments adopted were extracted from clinical records. Static USG was interpreted using the modified Graf's classification.[2] Dynamic USG incorporates Barlow manoeuvre and measured percentage of Femoral Head coverage at rest and stressed positions.[3] The outcome measurement of Acetabular dysplasia was interpreted based on Acetabular Index (AI) measurements performed on walking age radiographs. Hips were then classified as 'No', 'Mildly', or 'Severely' dysplastic types if their AI values fall within one, two, or outside two standard deviations away from the mean value of the same side of the hips, adjusted for sex and age at radiographic examination.[2]

Methods for statistical analysis:

Results of PNSS tests were compared with radiographic dysplasia at walking age. The study's primary and secondary outcome were whether patients developed dysplasia and severe dysplasia, respectively. The odds ratios (OR) of screening parameters were estimated by fitting logistic regression models. A machine learning algorithm, Classification and Regression Tree (CART) were used to explore the potential optimal cut-off points of the selected parameters. The tree size was determined using a complex parameter of 0.02. The function in R (version 4.2.1, the R Foundation, Vienna, Austria), glm(), and the R-package, RPART, were used to construct the logistic regression models and the CART, respectively. A $P$ value < 0.05 were considered as statistically significant

## RESULTS AND DISCUSSION

A total of 192 hips (115 health vs 77 dysplasia) were included. Stress FHC (p=0.045) and rest FHC (p=0.050) were shown to be significant in prediction for dysplasia. According to CART analyses hips with rest FHC < 55%, near 2/3rd (62%) had dysplasia at walking age. In contrast, hips with both rest FHC and stress FHC >= 55%, none had dysplasia at 1 year. After eliminating the patients who received any Pavlik Harness management, there remained 151 hips that did not receive any treatment including 93 normal hips vs 58 dysplastic hip which allowed study of natural history of the positively screen hip. In this group better rest FRC was associated with reduced acetabular dysplasia. Hips with rest FHC < 51% were found associated with dysplasia in 86% of the hips, while in hips with rest FHC >= 60%, only 26% of them had dysplasia. In those with a rest FHC from 51% to 60%, 48% of the hips developed dysplasia.

The study identified among screening parameters only components of Dynamic USG: rest and stress FHC were significantly associated to Acetabular dysplasia at walking age. Further, we could identify cut off points in these values as potentially important clinical decision-making tools.

## CONCLUSIONS

We identified significant associations of potential cut off points in static and stress FRC with dysplasia at walking age. Multicenter study or larger data set are needed to validate the performance of the Stress and Rest FHC cut-offs.

## REFERENCES

1. Thillemann TM et al. *Acta orthopaedica*. 2008 Jan 1;**79**(6):769-76

2. Tönnis D. *Congenital dysplasia and dislocation of the hip in children and adults*. Berlin/Heidelberg: Springer-Verlag; **1987**.

3. Harcke HT et al. *American journal of roentgenology.* 1990 Oct;**155**(4):837-44.

# TEN YEAR REVIEW OF ACUTE PAEDIATRIC HEMATOGENOUS OSTEOMYELITIS AT A NEW ZEALAND TERTIARY REFERRAL CENTRE

[1]Sarah Hunter, [2]Haemish Crawford, and [3]Joseph Baker

[1]University of Auckland Faculty of Medical and Health Sciences, New Zealand
[3]Starship Children's Hospital, Orthopaedic Department, Auckland, New Zealand
[3]Waikato Hospital, Orthopaedic Department, Waikato, New Zealand.
email: shun472@aucklanduni.ac.nz

## INTRODUCTION

Acute hematogenous osteomyelitis (AHO) remains a cause of severe illness among children with the possibility of long-term consequences for growth and development. Recent research has highlighted an unusually high burden of disease in the New Zealand population compared with other Western regions. We have sought to identify trends in presentation, diagnosis, and management of AHO, with added focus on ethnicity and access to health care.

## METHODS

A 10-year retrospective review of all patients <16 years with presumed AHO presenting to a tertiary referral centre between 2008 and 2018 was performed.

## RESULTS AND DISCUSSION

One hundred fifty-one cases met inclusion criteria. The median age was 8 years with a male predominance (69.5%). Staphylococcus aureus was the most common pathogen using traditional laboratory culture method (84%). The number of cases per year decreased from 2008 to 2018. Assessment using New Zealand deprivation scores showed Māori children were most likely to experience socioeconomic hardship ($P \leq 0.01$). Median distance travelled by families to first hospital consult was 26 km (range 1 to 178 km). Delayed presentation was associated with need for pro- longed antibiotic therapy. Incidence of disease varied by ethnicity with 1:9000 cases per year for New Zealand European, 1:6500 for Pacific, and 1:4000 for Māori. Overall recurrence rate was 11%.

**TABLE 1.** Incidence of Disease by Ethnicity, Patients With AHO

| Ethnicity | Number in cohort | Population/census year | Incidence |
|---|---|---|---|
| NZE: | 68 | 61,374 | 1:9000 |
| Maori: | 70 | 28,659 | 1:4000 |
| Pacific: | 9 | 5850 | 1:6500 |
| Total | 151 | 87,483 | 1:5800 |

AHO indicates acute hematogenous osteomyelitis; NZE, New Zealand European.

**Table 1:** Incidence of Disease by Ethnicity for Patients with AHO.

**TABLE 2.** Association Between Delayed Presentation and Worse Disease for Children With AHO

| Delay to presentation and markers of worse disease | Delay > 72 h | Delay < 72 h | CHI2/ TTEST |
|---|---|---|---|
| Median deprivation index | 6.8 | 7.4 | 0.9 |
| Median distance from hospital in Km | 48 | 42 | 0.39 |
| Median antibiotic treatment in days | 42 | 36 | 0.01 |
| Median length of stay in days | 10 | 13 | 0.3 |
| Repeat surgical procedure | 14 (68) | 9 (74) | 0.17 |
| Recurrent disease | 9 | 6 | 0.32 |

AHO indicates acute hematogenous osteomyelitis.

**Table 2:** Association Between Delayed Presentation and Worse Disease for Children with AHO

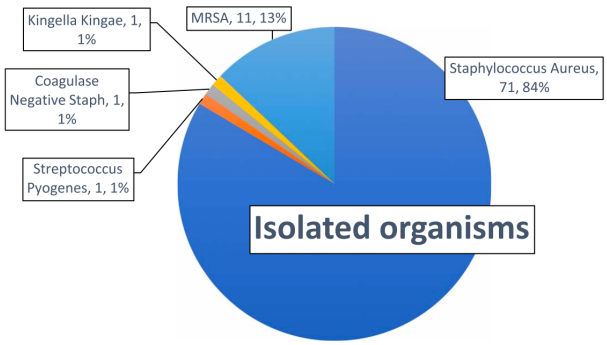


**Figure 1:** Causative Pathogens in Acute Childhood Osteomyelitis

## CONCLUSIONS

The incidence of AHO in New Zealand is concerningly high within Māori and Pacific populations. Future health interventions should consider environmental, socioeconomic, and microbiological trends in the burden of disease.

# NEUROMUSCULAR CONSTRAINTS OF THE KNEE CONTACT FORCE WHILE WALKING

[1,2]Saulo Martelli, [2]Kieran J. Bennett, [3]Dominic Thewlis, [4]Marco Viceconti

[1]School of Mech., Medical & Process Eng, Queensland University of Technology, Brisbane, Australia;
[2]Medical Device Research Institute, Flinders University, Tonsley, Australia;
[3]Centre for Orthopaedic and Trauma Research, The University of Adelaide, Adelaide, Australia;
[4]University of Bologna, Bologna, Italy
email: saulo.martelli@qut.edu.au

## INTRODUCTION

A central problem of motor control is how the redundant muscle system generates a purposeful coordinated action in a lower dimensional space (i.e., joint angles); implications are broad from men-machine interfaces to orthopedics [1,2]. During movement, the central nervous system recruits a redundant muscle system to satisfy the dynamic equilibrium defined by the task, anatomy, and physiological constraints. However, the number of independent controls can only be equal to or lower than the degrees of freedom of motion. Therefore, a reduced number of muscle controls likely determine the knee contact force while walking. Here, a preliminary analysis relevant to orthopedic research focuses on the contact force in total knee replacements and earlier data and models [2]. The aim of this study is to determine the number of muscle controls determining the knee contact force while walking.

## METHODS

The musculoskeletal model was developed earlier [20]. In summary, motion and anatomical data were obtained from the Knee Grand Challenge Competition, challenge four [1]. The musculoskeletal model available in OpenSim, gait2392, was fitted to the data. Joint angles, moments, muscle, and joint forces were calculated using the Calibrated EMG Informed Neuromusculoskeletal Toolbox (CEINMS) simulation pipeline [2]. The space of muscle forces was sampled using the Markov-Chain Monte-Carlo method implemented in METABOLICA [3], assuming normal joint torques centered in the inverse dynamic solution and 2 Nm standard deviation. The upper and lower boundaries of muscle forces were set by multiplying the peak isometric force by 5 and -1, respectively, hence focusing the analysis on anatomical and motor constraints alone. Muscle forces were obtained for the 86 frames of walking using 0.5 M samples per frame. The norm of the knee contact force was calculated for each sample by adding the contribution of the knee-spanning muscles to the inertial force component in the OpenSim simulation. Partial-least-square (MATLAB, The MathWorks Inc., Natick, USA) was used to link, via regression analysis, the hyperplanes of maximum variance in the knee and muscle force domains. The analysis was repeated frame-by-frame and for the entire walking cycle by selecting nine uniformly distributed frames, resulting in a total of 4.5 M samples. The risk of overfitting was minimized using a 100-fold cross-validation scheme. The existence of common features across the different walking phases was analyzed by determining the goodness of fit, the compactness of the model, and the relative importance of each individual muscle in the regression, both frame-by-frame and the whole gait cycle. The reduced muscle controls were then used to reconstruct the muscle forces in the OpenSim simulation.

## RESULTS AND DISCUSSION

The knee contact force in the spectrum varied from 0 to 7000 N. Three muscle coordination explained more than 99% of the knee contact force variance for each frame of the gait cycle. The whole gait model showed a similar compactness and a mean square error below 103 N using three or more muscle coordination, hence indicating the existence of a reduced set of muscle coordination independent of postural changes during gait. Muscle coordination consisted of scores for each muscle in the body whose highest importance in the regression model was found for the hamstring, the quadriceps, the triceps surae, and the gluteus maximus. The decomposition of the OpenSim muscle forces into the three corresponding muscle controls yielded a knee contact force while walking strongly associated ($R^2 = 0.96$) with corresponding OpenSim calculations (Fig. 1).

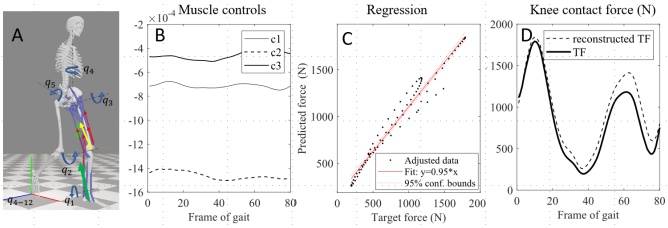


Fig. 1 – The model (A), the selected controls (B), and the comparison of reconstructed and calculated knee forces (C, D).

## CONCLUSIONS

Three muscle controls, completely determined by the anatomy of the individual, determine the knee contact force while walking. Nevertheless, the effect of posture may be more important during different motor tasks using a larger range of motion than walking. The implication of this finding can benefit studies into the mechanical environment of orthopedic devices and their causes. The possibility of determining a reduced set of controls encoded in the anatomy may benefit studying the neuromotor control system linking the central nervous system, motion, and anatomy.

## ACKNOWLEDGEMENTS

Australian Research Council (IC190100020; FT180100338).

## REFERENCES

1. Latash, *Exp Brain Res* **217**:1-5, 2012
2. Bennett et al., *IEEE Tr. Biomed. Eng* **69**:2268–75, 2022
3. Heino et al. Com. Meth. Prog. Biom. 97 :151–167, 2010

# NON-INVASIVE MECHANICAL CHARACTERIZATION OF PLANTAR FLEXOR MUSCLES USING SHEAR WAVE ELASTOGRAPHY

[1]Manuela Zimmer, [1]Filiz Ates

[1]Experimental Biomechanics Group, Institute of Structural Mechanics and Dynamics in Aerospace Engineering, University of Stuttgart, Germany,
email: manuela.zimmer@isd.uni-stuttgart.de

## INTRODUCTION

Characterizing skeletal muscles is necessary for understanding human movement and their adaptation. Direct measurement of muscle forces from its tendon would be ideal; however, such data collection is scarce due to its invasive nature [e.g. 1]. Shear wave elastography (SWE) provides a non-invasive method to assess muscles. Assuming linear elastic, transversely isotropic material characteristics, the measured shear wave velocity was shown to represent passive and active muscle mechanics [2,3]. Though relating muscle shear elastic modulus to its force is challenging. Presently, we characterized three major plantar flexors in passive and active states using SWE and hypothesized that shear elastic modulus reveals the muscles' length and activity-dependent mechanical characteristics.

## METHODS

SWE, EMG, and ankle torque were measured simultaneously on ten volunteers (24.7±1.7 years, 5 females). Gastrocnemius medialis (GM), gastrocnemius lateralis (GL), and soleus (SOL) muscles were studied at four ankle angles from 30° plantarflexion (PF) to 15° dorsiflexion (DF) during rest, maximal voluntary PF contraction (MVC), and submaximal isometric PF contractions (25%, 50%, 75% of MVC). The lengths of GM, GL, and SOL were assessed sonographically.

## RESULTS AND DISCUSSION

Muscle length ($p < 0.05$), passive shear elastic modulus ($p < 0.001$), and ankle torque ($p < 0.001$) increased from PF to DF during rest. Hence, SWE revealed the increase in passive muscle force imposed by length changes (Table 1).

MVC torque increased from 75.21 ± 25.53 Nm at 30° PF to 159.15 ± 43.88 Nm at 15° DF ($p<0.001$). Active shear elastic modulus of all muscles increased with increasing activity level during submaximal contractions ($p<0.001$) demonstrating the potential of SWE for muscle force estimation. The effect of joint position was only significant for GM ($p < 0.001$, from 30° PF to 15° DF it dropped by 7.48% (25% MVC), 46.84% (50% MVC), 59.50% (75% MVC), Figure 1).

The unchanging (for GL, SOL) and decreasing (for GM) shear elastic modulus found at longer lengths might indicate that these muscles operate at optimal to longer than optimal lengths.

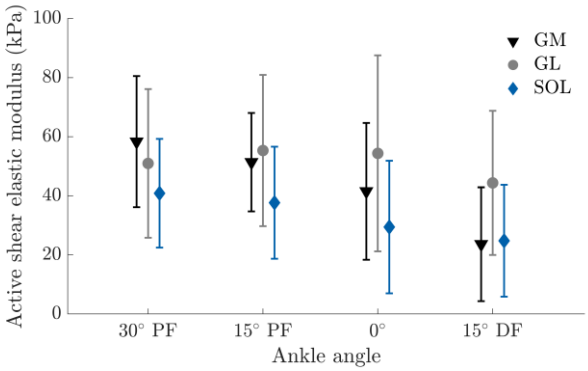


**Figure 1:** Shear elastic modulus of GM, GL, and SOL during 75% MVC at four different ankle angles from 30° PF to 15° DF.

## CONCLUSIONS

The present study supports the hypothesis posed, revealing length-dependent passive shear elastic modulus and activation-dependent active shear elastic modulus. The changes at higher length in active state might reflect force-length characteristics of the individual muscles. If validated with direct muscle force measurements, SWE has the potential to serve as an index of individual muscle force and establish a link between muscular adaptation and joint function.

## ACKNOWLEDGEMENTS

This work was supported by the German Research Foundation (GRK 2198 – 277536708) and the Federal Ministry of Education and Research through the project "3DFoot" (01EC1907B).

## REFERENCES

1. Brendecke E., et al., *Front. Physiol.* **14**:1143292, 2023.
2. Zimmer M, et al., *J. Mechanical Behavior of Biomedical Materials*. **137**:105543, 2023.
3. Ates F, et al., *Eur. J. Appl. Physiol.*, **118**:585–593, 2018.

**Table 1:** Length and passive shear elastic modulus of GM, GL, and SOL at four different ankle angles from 30° PF to 15° DF.

| | Muscle length (cm) | | | | Passive shear elastic modulus (kPa) | | | |
|---|---|---|---|---|---|---|---|---|
| | **30° PF** | **15° PF** | **0°** | **15° DF** | **30° PF** | **15° PF** | **0°** | **15° DF** |
| **GM** | 24.52 ± 1.41 | 25.50 ± 1.70 | 26.75 ± 1.80 | 27.80 ± 1.58 | 6.35 ± 1.62 | 7.36 ± 1.70 | 14.81 ± 3.96 | 31.26 ± 5.70 |
| **GL** | 22.98 ± 1.91 | 24.83 ± 1.77 | 24.83 ± 1.77 | 25.90 ± 2.32 | 4.84 ± 0.80 | 6.85 ± 0.74 | 11.68 ± 2.54 | 25.26 ± 6.48 |
| **SOL** | 31.55 ± 2.86 | 32.87 ± 2.76 | 33.96 ± 2.71 | 35.60 ± 2.29 | 6.73 ± 3.30 | 8.47 ± 1.50 | 11.08 ± 1.80 | 17.36 ± 5.01 |

# PROBING MUSCLE-FASCIA INTERACTION IN THE LOWER LIMB WITH ADVANCED MRI AND FINITE ELEMENT MODELLING

[1]M. Randika Perera, [2]Samantha Holdsworth and [1]Geoffrey Handsfield

[1]Musculoskeletal Modeling Group, Auckland Bioengineering Institute, University of Auckland, New Zealand
[2]Matai Medical Research Institute, Gisborne, New Zealand.
email: mper162@aucklanduni.ac.nz

## INTRODUCTION

Fascia is an abundant connective tissue that may be involved in force transmission in ways that are poorly understood. Prior experiments suggest that fascia may play a considerable role on musculoskeletal force distribution in animals and humans [1,2]. There is a growing interest in modelling the mechanical contribution of this tissue, which is challenging considering the thin structure of the tissue and the difficulty of obtaining details from imaging. Here, we use advanced MRI to image the fascia *in vivo* to create physics-based simulations to explore fascia mechanics and probe its role in force transmission in the musculoskeletal system.

## METHODS

We imaged the thigh and calf region of thirty adult participants on a 3T MRI scanner using a dual-echo ultrashort echo time (UTE) non-Cartesian sequence with unique vendor versions [3,4]. In plane spatial resolution was 0.7 x 0.7 $mm^2$, slice thickness was 4mm. Post-processing methods were used to increase contrast. Following image acquisition, segmentation was performed for deep fascia and lower limb muscles using ITK Snap software on axial images. To develop a finite element model of a muscle-fascia system, we created an image-based geometry of two muscle – the medial gastrocnemius & tibialis anterior – with and without a sheath of fascia enclosing the muscle. Fiber directions were incorporated using data from diffusion tensor imaging.

## RESULTS AND DISCUSSION

We found that fascia thickness varied regionally along the peripheral surface of the muscles. Fascia thickness varied between 1.5mm and 2.0mm in our population, which is consistent with literature [5]. We built a finite element model of muscle and fascia (Fig. 1) which we used to explore the mechanical contribution of fascia, finding that models containing fascia presented greater longitudinal stresses on the tendon compared to models without.

## CONCLUSIONS

Using advanced MRI, we found fascia thickness measurements *in vivo* that are consistent with the literature from dissection studies and we used our imaging results to build a finite element geometry of the tibialis anterior and its surrounding fascia. Finite element simulations show that presence of fascia may increase the forces transmitted from muscle to tendon compared to a system that lacks fascia, suggesting gains of force transmission provided by fascia. Future work should include various lower limb muscles to understand the contributions of varied muscle architecture.

## REFERENCES

1.Maas et.al. (2010), J. Biomed. Biotechnol.575672
2.Meijer et.al. (2007), J. Electromyogr.17, 698-707
3.Qian et al. (2008), Magn Reson Med.60:135-145
4.Ma et al. (2017), MR in Biomed.30: 3709.
5.Bhansing et al. (2015), Muscle Nerve,52:534-539

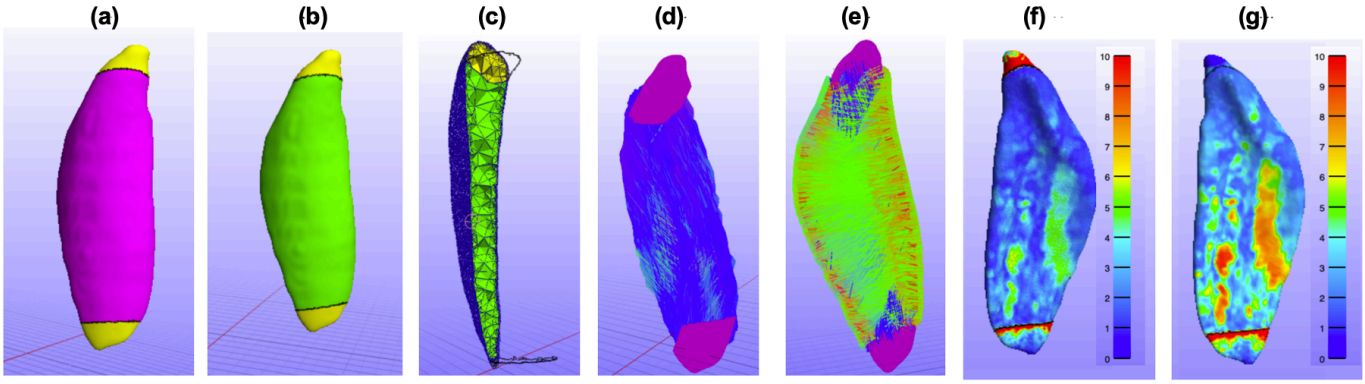


**Figure 1:** Finite element analysis of muscle and muscle-fascia system. (a) the MG muscle model with fascia, (b) MG muscle model without fascia. Images (c), (d), and (e) display cross-section of the model, fiber directions from DTI, and fascia fiber directions determined from literature . Color maps of effective stress during active contraction of model (a) & (b) are shown in in images (f) and (g) respectively.

# ANATOMICAL INFORMATION ON THE INTERNAL APONEUROSIS IS NEEDED FOR REALISTIC SUBSCAPULARIS FASCICLE LENGTH MEASUREMENTS FROM DIFFUSION TENSOR IMAGING

[1,2]Yilan Zhang, [1,2]Robert D Herbert and [1,2]Lynne E Bilston, [1,2,3]Bart Bolsterlee

[1] University of New South Wales, Randwick, NSW, Australia
[2]NeuRA, Randwick, NSW, Australia
[3]Queensland University of Technology, Brisbane, QLD, Australia
email: yilan.zhang@neura.edu.au

## INTRODUCTION

*In vivo* measurements of muscle architecture are crucial for modeling the mechanical function of skeletal muscles. Diffusion tensor imaging (DTI) fibre tractography can be used to quantify the three-dimensional (3D) muscle architecture of human muscles *in vivo*. However, when conventional DTI tractography algorithms are applied to anatomically complex muscles, fibre tracts usually do not terminate on tendons or aponeuroses, as real muscle fascicles are known to do, leading to implausible architecture measurements. This study aimed to: (1) identify the structure of the human subscapularis aponeurosis *in vivo* and (2) determine the effect of constraining DTI-based muscle fascicle length measurements with anatomical information on subscapularis aponeuroses.

## METHODS

Twenty healthy subjects (eleven males, nine females; age 28 ± 7 years; height 170 ± 8 cm; weight 63 ± 12 kg; values are mean ± SD) were included in this study. mDixon anatomical scans and DTI scans of the right shoulders were obtained with a 3T MRI scanner (Philips Ingenia CX). The subscapularis muscle and its internal aponeurosis were manually segmented on mDixon images to create 3D surface models (Figure 1A). Anatomically constrained DTI tractography [1,2] where fascicles were constrained to attach to aponeuroses, and unconstrained DTI tractography without inclusion of aponeuroses, were used to generate fibre tracts, from which mean fascicle lengths were determined. In anatomically constrained tractography, the aponeurosis mask (or segmentation) was grown by one voxel at the boundary, at which fibre tracts were seeded (initiated). Fibre tracts were propagated bidirectionally and terminated at the boundary of the aponeurosis or the muscle mask.

## RESULTS AND DISCUSSION

Reconstructed 3D surface model of the internal aponeurosis of the subscapularis showed the complex finger-shaped structure of the tissue (Figure 1A). Typically, aponeuroses appeared to have 4 or 5 “fingers”. Compared with mean muscle fascicle length measurements obtained without the application of anatomical constraints (8.9 ± 1.2 cm, values are mean ± S.D. across participants), anatomically constrained tractography provides measurements (6.3 ± 0.6 cm) in better agreement with values reported in cadaver studies (6.0 ± 1.5 cm [3]; 6.4 ± 1.3 cm [4]). Fascicle lengths measured without anatomical constraints were consistently larger (by, on average, 2.6 ± 0.8 cm) than those measured with constraints (Figure 1B), indicating the potential anatomical implausibility.

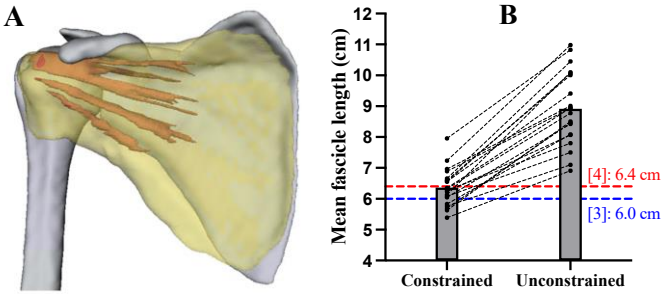


**Figure 1:** (A) Example of a 3D surface model of the muscle belly (transparent yellow) and internal aponeurosis (orange) of the subscapularis. (B) Mean fascicle lengths of the subscapularis measured in this study using anatomically constrained and unconstrained tractography. Dashed lines connect the measurements made on the same subject. Grey bars indicate the mean value over all subjects in this study. Blue and red dashed lines represent the mean fascicle length reported in [3] and [4], respectively.

## CONCLUSIONS

This study reveals the complex finger-shaped structure of the internal aponeurosis of the human subscapularis muscle, which acts as insertion sites for muscle fibres. We demonstrate that the use of anatomically constrained tractography, which constrains fibre tracts to attach to aponeuroses, results in more anatomically plausible fascicle length measurements of the complex 3D architecture of the human subscapularis muscle *in vivo*, similar to those measured from cadaver dissections [3,4]. We conclude that anatomical information on the internal aponeurosis is needed for anatomically realistic quantification of muscle architecture from DTI.

## REFERENCES

1. Smith et al., *NeuroImage* **62**: 1924-1938, 2012.
2. Bolsterlee et al., *PeerJ* **6**: e4610, 2018.
3. Ward et al., *Clin. Orthop* **449**: 157-163, 2006.
4. Mathewson et al., *J. Exp. Biol* **217**, 261-273, 2014.


# Wednesday, December 8

## David Findlay Early Career Researcher (ECR) Award Finalists

# INCREASED BONE FORMATION FROM ISOLATED ISOMETRIC CONTRACTION IN MICE

[1]Hui Jean Kok, [1]April Hoggatt, [1]Daniel Horan, [1]Joshua Huot and [1]Alexander Robling

[1]Department of Anatomy, Cell Biology & Physiology, Indiana University School of Medicine, Indianapolis, IN, USA.
email: jeankok@iu.edu

## INTRODUCTION

Skeletal muscle is a major contributor of mechanical signals for bone, where muscular contractions increase bone strains, resulting in mechanotransduction [1]. Subsequently, adaptive responses triggering bone remodeling occurs leading to increased bone accumulation and mineralization. However, the type of muscle contraction required to produce optimal bone formation has yet to be explored. The goal of this study is to determine if isometric, eccentric or a combination of both types of contraction produce optimal bone gain.

## METHODS

Nineteen male 6-month-old C57Bl/6 mice were used. Each cage houses 4 mice and were stratified to 4 groups: 1) Isometric (Iso) contraction, 2) Eccentric contraction (ECC), Isometric+Eccentric (Iso+ECC) contraction, and 4) Non-stimulated (NS) cage controls exposed to isoflurane inhalation. Mice were unilaterally stimulated using monopolar needle electrodes targeting the sciatic nerve, while the foot is taped to the foot pedal of a 300C dual-mode servomotor transducer (Aurora Scientific) and a fixed knee joint. Each stimulation was induced for 800 ms pulse duration with a frequency of 150 Hz and were repeated 4 times with 12 seconds rest in between each stimulation (1 set). Iso contraction was performed with a 90° foot angle (neutral position) throughout the stimulation and ECC with 200 ms at 90°, 300 ms at 70° and 300 ms at 110° foot angle. Each training session consisted of 4 sets of 5 stimulations with 3 minutes rest between each set. Iso+ECC animals performed 2 sets of Iso and 2 sets of ECC contractions. Animals were trained for 3 sessions a week for 4 weeks, along with dorsiflexion peak torque measurements before and after training sessions. Animals were allowed to recover for 1 week after the last training session and muscles (TA) and bones (tibia) were harvested 10 days after the last session.

## RESULTS AND DISCUSSION

There were negligible body weight changes throughout the study, indicating that most adaptation remained locally at the stimulated leg. Similar trends were observed in the muscle mass, except for the ECC group which exhibited a 13% loss in the tibialis anterior (TA) weight when compared to unstimulated contralateral leg. However, there was 25% increases in the dorsiflexion peak torque of the ECC group comparing pre- to post-training. This resulted in a 30% increase in normalized force compared to NS animals, due to increased peak torque but decreased TA mass. Next, micro-computed tomography (uCT) was used to assess changes in cortical bone properties that resulted from muscle contraction. There were significant ($p<0.01$) increases in cortical thickness (Ct.Th) and bone area (BA) at the midshaft of the tibias within the Iso and Iso+ECC groups when compared to contralateral tibias. This increase was also evident when comparing the stimulated tibias of Iso and Iso+ECC to the NS group, an indication that isometric contractions produced more bone.

## CONCLUSIONS

This study suggests that TA isometric contraction is more osteogenic than TA eccentric contraction. Conversely, eccentric contraction increases muscle strength more than isometric contraction. Thus, further assessments in the microstructure within the muscle and bone are required. For instance, the decrease in muscle mass after ECC is consistent with the effects of ECC-induced muscle damage, which likely occurred during the study. Therefore, assessments of number and size of centrally nucleated fibers are underway. Additionally, fiber-type changes within these muscles will be analyzed to determine the extent of contraction-induced fiber remodeling. In the same manner, assessments of the cancellous envelope within the tibias will be performed.

## ACKNOWLEDGEMENTS

HJK was supported by the US National Institute of Health grant K00AG068438.

## REFERENCES

1. Goodman CA, et al., *Bone.* **80**:24-36, 2015.

# BENCHMARK AND VALIDATION OF STATE-OF-THE-ART MUSCLE RECRUITMENT STRATEGIES IN SHOULDER MODELLING

[1,2]Maxence Lavaill, [3]Claudio Pizzolato, [1,4,5]Bart Bolsterlee, [1,2]Saulo Martelli and [1,2]Peter Pivonka

[1]School of Mechanical, Medical and Process Engineering, Queensland University of Technology, Brisbane, Australia;
[2]Queensland Unit for Advanced Shoulder Research, Brisbane, Australia;
[3]Griffith Centre of Biomedical & Rehabilitation Engineering, Griffith University, Brisbane, QLD, Australia;
[4]University of New South Wales, Sydney, Australia;
[5]Neuroscience Research Australia, Sydney, Australia.
email: maxence.lavaill@qut.edu.au

## INTRODUCTION

Quantifying muscle forces *in vivo* is critical for understanding shoulder biomechanics. Current state-of-the-art musculoskeletal models estimate muscle forces by solving the muscle redundancy problem either by 1) static optimisation (SO) [1], 2) computed muscle control (CMC), which optimises muscle forces using a forward dynamics approach which accounts for passive muscle stiffness, 3) EMG-assisted optimisation, which constrains the muscle excitations to electromyography recordings [2] or 4) stochastical sampling of the spectrum of possible muscle forces within admissible constraints [3]. This study aims to compare predictions of muscle and glenohumeral joint contact forces (GHJ-CF) obtained using SO, CMC, EMG-assisted and stochastic methods to electromyography and GHJ-CF measurements [4].

## METHODS

We used previously collected data from a male participant (64 years, 163 cm, 85 kg) with an instrumented shoulder hemiarthroplasty [4] who performed a shoulder abduction task holding a 2.4 kg weight in hand, while fourteen bony landmark locations (thorax, scapula, upper arm and forearm) were captured using an *Optotrack* system (Northern Digital Inc., Canada) at 50 Hz. Nine surface electrodes placed on top of surface shoulder muscles simultaneously recorded EMGs at a sampling rate of 1000 Hz. EMG envelopes were extracted. A previously developed upper-limb musculoskeletal model, consisting of 7 segments, 10 degrees-of-freedom and 91 muscle elements [1], was linearly scaled to match the anthropometry of the patient. Joint angles and moments were computed *via* inverse kinematics and dynamics using *OpenSim 4.4*.

First, muscle recruitment was estimated using SO and CMC (*OpenSim 4.4* GUI) by minimising the sum of the muscle activation squared at each frame of the motion task. Second, a calibrated EMG-assisted method was adopted. This method consisted of 2 steps. Step one was calibrating the model's muscle parameters in one (1C) [2] or two iteration(s) (2C) [5] using the CEINMS toolbox [1,5]. Step two was running CEINMS in EMG-assisted mode. This mode minimised a combination of GHJ torque errors, muscle excitation errors and muscle excitations squared. Finally, a stochastic method was used to sample 200,000 muscle recruitment solutions that satisfied the joint torques [3]. Muscle forces were bound from 0 to their maximum force. Resultant GHJ-CF were calculated using the muscle forces estimated from all four methods. The experimental total GHJ-CF was compared against the stochastic range to determine whether the solution is a part of the model solution space. Then, each method was compared against the experimental instrumented GHJ-CF.

## RESULTS AND DISCUSSION

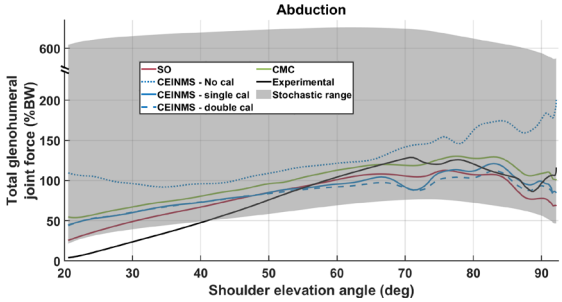


***Figure 1:*** *Glenohumeral loads from the instrumented prosthesis (black) and from the different estimated solutions, normalised against body weight (%BW)*

The GHJ-CF measurement was within the stochastic range from 40° of shoulder elevation and upwards, representing a possible solution of the model (Fig. 1). The stochastic range spanned from 20 to 660 %BW. RMSE with respect to experimental GHJ-CF were similar between the SO, CMC, CEINMS-1C, CEINMS-2C (Averaged error among all these methods: 25.4 ± 1.5 %BW). However, RMSE when the arm was above shoulder level, was lower for CMC, CEINMS-1C, and CEINMS-2C (13.9 ± 2.5 %BW) than for SO (25.0 %BW).

## CONCLUSIONS

We validated methods to solve the shoulder muscle redundancy problem for an abduction task against experimental GHJ-CF. CMC and EMG-assisted methods appear more accurate above shoulder level than SO. At low elevation angles, the model doesn't contain the experimental solution likely because of rigid-body modelling assumptions.

## ACKNOWLEDGEMENTS

Dr Nikooyan and Prof Veeger are gratefully acknowledged for making the full dataset available. The authors received support from the ARC grants IC190100020 and FT180100338.

## REFERENCES

1. Nikooyan et al., *J Biomech* **43(15)**: 3007-3014, 2010.
2. *Kian* et al., *J Biomech* **129**:109348, 2021.
3. Martelli et al., *Interface Focus* **5(2)**:1-14, 2015.
4. Bergmann et al., *J Biomech* **44(8)**: 1543-1552, 2011.
5. Silvestros et al., *J Biomech Eng* **144(3)**: 1-16, 2022.

# ACETABULAR COMPONENT STABILITY USING THE REPLACE-IN-SITU PHILOSOPHY TO TREAT ACUTE ACETABULAR FRACTURES

[1,2]John Abrahams, [1,2]Boopalan Ramasamy, [2]Alexandra Bunting, [2]Daud Chau, [2]Robyn Clothier, [2]Kerry Costi, [1,2]Stuart Callary, [1,2]Bogdan Solomon

[1]Centre for Orthopaedic and Trauma Research, The University of Adelaide, Adelaide, SA, Australia
2Department of Orthopaedics and Trauma, Royal Adelaide Hospital, Adelaide, SA, Australia
email: john.abrahams@sa.gov.au

## INTRODUCTION

Treatment of acute acetabular fractures with total hip arthroplasty (THA) is gaining popularity, but the long-term survival of these implants is not well established. The poor premorbid mobility of majority of patients with an acetabular fracture requiring an acute THA, which continues after treatment, makes it difficult to assess clinically which of these patients have failed surgical management and require revision surgery. Plain radiographs have traditionally been used to assess implant stability, but the errors of measurements are +/- 5mm. The migration of an acetabular implant in the first two-years, if measured accurately with Radiostereometric Analysis (RSA), is a surrogate for its long-term survival [1]. This study aimed to measure the migration of acetabular components of THA used to treat acute acetabular fracture through the replace-in-situ technique using RSA and plain radiographs.

## METHODS

38 consecutive patients who consented to participate and underwent primary THA for an acute acetabular fracture in our institution between Nov 2011 and Dec 2020 through a replace-in-situ technique, 29 were included in the final analysis due to: patient death within two weeks post-operatively (n=4), inability to attend follow-up due to frailty or remote location (n=4), and one patient was lost to follow-up. The mean age was 75 (range 54-91). There were 16 males and 13 females. 15 cases had an ACPHT, 12 had an ABC fracture, and there was one each with AC and TPW. Acetabular reconstruction was performed through a replace-in situ technique with pelvic distraction through an oversized trabecular metal acetabular component and, in most cases, a cup-cage technique [2]. Acetabular component migration was measured using RSA and plain radiographs, taken on day 2 post-op and then at six weeks, 3 and 6 months, 1, 2-, 3-, 5-, and 7-years post-surgery. More than 1mm of proximal component migration at 2 years was considered predictive of future loosening [1], and more than 3mm of proximal migration or 5° of sagittal rotation at any time point was deemed to be diagnostic of a loose component [3].

## RESULTS AND DISCUSSION

The mean follow-up of 29 patients was 5 years (2-10 years). All fractures healed radiologically by six months follow-up. Fifteen cases had an ACPHT, 12 had an ABC fracture, and one had AC and TPW. Acetabular component migration at 2-year follow-up exceeded the 1 mm threshold predictive of future loosening in 8/29 (28%) patients measured by RSA (Figure 1). There was disagreement between the two methods in 12 cases (41%) with respect to thresholds diagnosing loosening. Four components (14%) were diagnosed loose (>3mm at any time point) when measured with RSA. Three patients underwent revision surgery, within two-years of follow-up: one for acetabular component loosening, at 17 months, when the acetabular component was confirmed loose and revised; and one for recurrent dislocation at 4 months and one for prosthetic joint infection at 17 months.

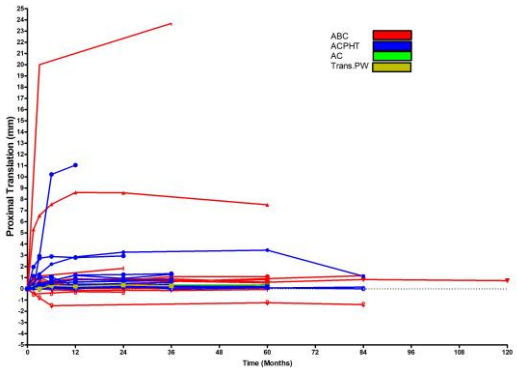


**Figure 1.** The individual proximal migration (mm) of each component by fracture type treated.

## CONCLUSIONS

This study is the first to investigate the stability of large porous tantalum trabecular metal acetabular components used to treat acute acetabular fractures using the sensitive and accurate RSA technique. With currently accepted thresholds, 14% (4/29) of cases were diagnosed as loose, and 14% (4/29) were at risk of becoming loose. Notably, measurements on plain radiographs failed to diagnose migration of the component in 1 patient (3%) and diagnosed components as loose incorrectly in 12 patients (41%). The migration pattern of the acetabular components during the fracture healing suggests that some components could gain stability after fracture healing.

## ACKNOWLEDGEMENTS

Stuart Callary was supported by a Research Fellowship from The Hospital Research Foundation Group during this study.

## REFERENCES

1. Kim YS et al 2017 BJJ, 99-B (4):465-474.
2. Solomon LB et al 2015 CORR, 473(12):3811-3819.
3. Abrahams JM et al 2017 BJJ, 99-B (4):458-464.

# MULTI-CELL MODELLING OF THE SKELETAL MUSCLE MICROENVIRONMENT TO EXPLORE AGE-RELATED CHANGES IN SATELLITE CELL DYNAMICS

[1]Stephanie Khuu and [1]Andrew McCulloch

[1]Department of Bioengineering, University of California, San Diego, La Jolla, USA
email: stkhuu@ucsd.edu

## INTRODUCTION

The regenerative potential of skeletal muscle tissue depends on cell-cell and cell-matrix interactions in the muscle microenvironment. Satellite cells (SCs) are the muscle resident stem cells that play a pivotal role in muscle fibre repair; however, the ability of the muscle milieu to adapt following damage is attributable to regulation by many cell types as well as chemical and mechanical guidance cues. Ageing muscle shows a functional decline in stem cell dynamics, with changes to polarisation and integrin density leading to increased asymmetric division relative to symmetric division [1]. Understanding the regulators of SC division in muscle fibre bundles is an important step in rescuing regenerative potential of muscle. In silico modelling offers a high throughput method to investigate chemical and mechanical regulators of cell-cell and cell-matrix interactions that is otherwise not possible. This preliminary study aims to recapitulate the effect of growth factors and cytokines, such as hepatocyte growth factor (HGF), on SC repair kinetics using multi-cell models of repair. Specifically, we evaluate the effect of increasing HGF concentration in recruiting SCs to the damage site.

## METHODS

A 3D multi-cell model of the muscle microenvironment was created using CompuCell3D (CC3D) [2]. The simulation represented four cell types: muscle fibres, satellite cell, damaged tissue, and the ECM. These cells were represented as agents, with rules governing their behaviour. Agents were implemented in a 100x10x8 lattice. Physical properties such as volume, surface area, contact and adhesion molecule density are described in Table 1. Growth factors and cytokines are diffused in the space using the following equation:

$$\frac{\partial c}{\partial t} = D\nabla\text{^}2\, c - kc + secretion$$

where k is a decay constant of concentration c and D is the diffusion constant.

**Table 1**: Initial agent properties in 3D model of skeletal muscle microenvironment.

| Agent | Volume | Surface Area |
|---|---|---|
| **Muscle fibre** | 1971 | 1664 |
| **Damaged tissue** | 24 | 52 |
| **Satellite Cell** | 4 | 18 |

Secretion of HGF from damaged tissue was varied from 0-50, and the time for SCs to reach the damage tissue location was recorded. Each time step represented one minute, and simulation end time was set to 3000 minutes. Initial SC distance from damage was set to ~20 pixels for all simulation conditions.

## RESULTS AND DISCUSSION

Satellite cells did not reach the location of damage when HGF secretion was 10 or below. SCs time to reach damage location was decreased when HGF secretion from damaged tissue was increased. With secretion set to 50 or 40, distance to damage was comparable (~800 mins). Secretion level of 30 took 1000 min to reach the damage location, while 20 took 1750 min (Figure 1).

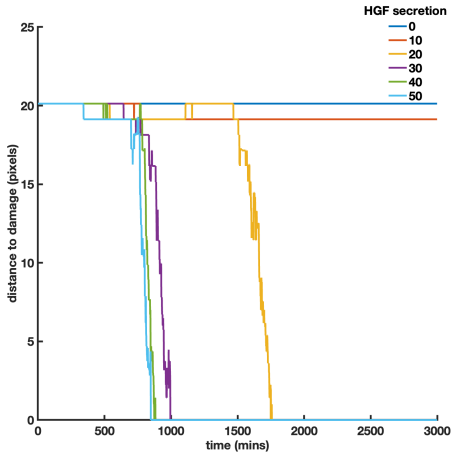


**Figure 1:** Satellite cell distance from damage over time at different HGF secretion levels. Single simulations shown only.

By changing the HGF secretion alone, this model can recapitulate the actions of known activators of SCs.

## CONCLUSIONS

In silico models of the muscle microenvironment can recapitulate its complex composition. This model can be used to explore regenerative medicine interventions and study pathways pertinent to the maintenance and rescue of the regenerative potential of skeletal muscle.

## ACKNOWLEDGEMENTS

This work is supported by the Wu Tsai Human Performance Alliance and the Schmidt AI in Science Program.

## REFERENCES

1. Feige P et al., *Cell Stem Cell*. 1;23(5):653–64. 2018
2. Swat MH et al., In: Methods in Cell Biology. 2012

# CLASSIFICATION OF GLENOID WEAR USING STATISTICAL SHAPE MODELLING

[1,*]Harnoor Saini, [2]Marc Hirner, [3]Sumit Raniga, [3]Desmond Bokor, [1]Thor Besier

[1]Auckland Bioengineering Institute, University of Auckland, Auckland, New Zealand
[2]Northland Orthopaedic Clinic, Whangarei, New Zealand
[3]Shoulder and Elbow Clinic, Macquarie University, Sydney, NSW, Australia
[*]email: h.saini@auckland.ac.nz

## INTRODUCTION

Glenoid wear classifications, such as the Walch, Sirveaux, or Burkhart, are vital for understanding joint status and treating glenohumeral osteoarthritis. These classifications help gauge bone loss and retroversion but are not without limitations. They are prone to low inter-observer reliability [1], often neglect the complex 3D surface of the glenoid, and struggle to distinguish normal anatomy from bone wear.

To address these limitations, we present a novel approach to automatically classify glenoid wear using dual statistical shape models (SSMs). This approach uses normative and pathological SSMs to classify glenoid wear according to its degree of bone loss and the uniqueness of the wear pattern.

## METHODS

Two SSMs were developed; normative (NSSM) and pathological (PSSM), using GIAS3 [2]. The NSSM was developed using n=76 healthy scapula (flipped contralateral from n=38 individuals, 31F/11M, mean 34.2±9.8years) and the PSSM using n=45 pathological scapula (flipped contralateral from n=45 individuals, 23F/22M, mean 69.1±13.3years) presenting with bone wear.

Each patient's glenoid wear was classified according to two metrics: the degree of wear (DW) and the uniqueness of wear (UW). DW was computed by predicting the pre-morbid glenoid using the NSSM, and computing distances between the prediction (pre-morbid) and the original glenoid. UW was computed by comparing the patient's glenoid wear pattern to that of the mean wear pattern from the PSSM (Figure 1a).

The pre-morbid glenoid was computed by first "masking" the worn glenoid from the patient's scapula. The NSSM was shape matched to the remaining healthy part, yielding the pre-morbid predicted glenoid. The average wear distance and centre-of-mass of wear were computed based on point-wise distances between the pre-morbid and original surfaces.

As a proof-of-concept, the glenoids of 4 patients (randomly selected from the pathological scapula set) were classified.

## RESULTS AND DISCUSSION

The NSSM was validated by predicting the pre-morbid glenoid of healthy patients (n=8, previously unseen). Over the glenoid fossa, the prediction had a mean error of 1.4±0.6mm.

The results of the classification are shown in Figure 1b. Cases 46 & 28 were classified as having low wear and a common glenoid wear pattern. Case 2 exhibited a high degree of usual wear. Lastly, case 8 was not heavily worn presented with a unique wear pattern.

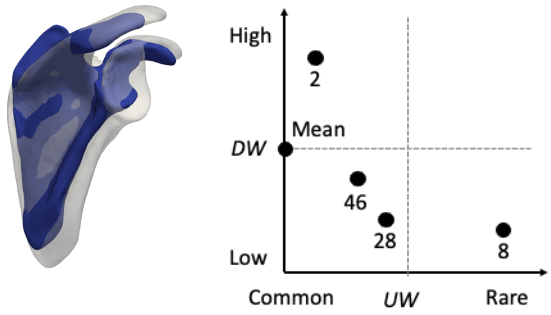


(a) (b)

**Figure 1:** (a) Comparison of a patient's scapula with the PSSM; (b) plot of 4 classifications on the degree of wear (DW) and uniqueness of wear (UW) axes

## CONCLUSIONS

In this work, we present a novel method to automatically classify glenoid bone loss in 3D using SSMs. We intend to build on these preliminary results by classifying additional patients and matching our predictions with traditional classifications performed by shoulder orthopaedic surgeons.

## REFERENCES

1. Shukla D, et al., *J Shoulder Elbow Surg.* **28**(4):625-630, 2018.
2. Zhang J et al. *Comp Meth in Biomech and Biomed Eng.* **21**(7):498-502, 2018.


# Wednesday, December 8

## KEYNOTE 1 – A/Prof Paul Monk

"Bioengineering in Orthopaedics: Innovation and Evaluation"


# Wednesday, December 8

## PhD Award Finalists

# TRANSLATING THE *IN VITRO* ANTI-BIOFILM POTENTIAL OF BOVINE LACTOFERRIN TO APPLICATIONS AS AN *IN VIVO* ANTI-INFECTIVE IN BATTLEFIELD-RELEVANT OPEN FRACTURES

[1]Reece Joseph, [1]Karen Callon, [1]Jian-ming Lin, [2]Brya Matthews, [1]Stuart Irwin, [3,4,5,6]Dustin Williams, [3]Nicholas Ashton, [1]Haemish Crawford, [7]Jingyuan Wen, [2]Simon Swift, [1]Jillian Cornish

[1]Department of Medicine, University of Auckland, Auckland, NZ
[2]Department of Molecular Medicine and Pathology, University of Auckland, Auckland, NZ
[3]Department of Orthopaedics, University of Utah, Salt Lake City, UT, USA
[4]Department of Biomedical Engineering, University of Utah, Salt Lake City, UT, USA
[5]Department of Pathology, University of Utah, Salt Lake City, UT, USA
[6]Department of Physical Medicine and Rehabilitation, Uniformed Services University of the Health Sciences, Bethesda, MD, USA
[7]School of Pharmacy, University of Auckland, Auckland, NZ
email: rjos014@aucklanduni.ac.nz

## INTRODUCTION

Up to 50% of type 3b compound fractures are complicated by biofilm infections [1]. *Staphylococcus aureus (S. aureus),* the most common cause of infection, resides within a protective biofilm. Lactoferrin (Lf), a glycoprotein with antimicrobial and immunomodulatory properties, is found naturally in human and animal milk [2]. Bovine Lf (bLf) is a potent stimulator of bone growth adding to its appeal as a treatment for compound fractures [3]. The goal of this study was to test the ability of bLf as an adjuvant to antibiotics in the context of compound fracture infections. Specifically, we aimed to: 1) *Demonstrate the in vitro anti-biofilm properties of bLf.* 2) *Translate the in vitro antibiofilm activity of bLf to an in vivo periprosthetic, biofilm infected tibia rodent model.*

## METHODS

*In vitro: S. aureus* Xen-36 biofilm was generated in a standard bioreactor on metal coupons and tested against cefazolin (CEF) and flucloxacillin (FLU) with or without bLf. Viable counts of *S. aureus* were recovered and enumerated. *In vivo:* Surgery was performed on adult male rats, where the craniomedial tibia was exposed, and a 1.5 mm defect created and inoculated with Ten µL (≈$10^7$ CFU) of *S. aureus* biofilm. A 2 mm length stainless steel pin was placed within the medullary cavity of the tibia, and the wound treated with STIMULAN® beads loaded with bLf and FLU. All rats received subcutaneous FLU 200 mg/kg immediately prior to surgery. At day 7 post infection, rats were re-anaesthetised for bioluminescent and x-ray imaging, euthanized, and tibial explant tissue/metal pins collected for bacterial colony enumeration.

## RESULTS AND DISCUSSION

*In vitro:* bLf augments the anti-biofilm activity of antibiotics such as CEF and FLU *in vitro (*Figure 1A), and in combination with FLU significantly eradicates *S. aureus* biofilm infection *in vivo* when compared against controls (Figure 2B). *In vivo* imaging confirms correct placement of metalware and inoculum (Figure 2C).

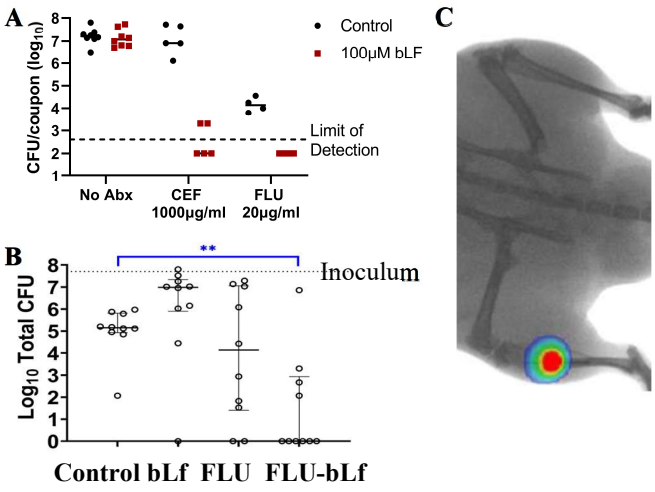


**Figure 1: A)** Viable counts (CFU) recovered from biofilm coupons treated with CEF or FLU in the presence (red) and absence (black) of bLf. One-way ANOVA with Šídák correction showed that the inclusion of bLF significantly improved the antibiofilm activity of CEF ($p<0.001$) and FLU ($p<0.0001$) **B)** One-way ANOVA with Tukey's test demonstrated that FLU-Lf beads significantly eradicated *S. aureus* compared with controls (empty bead) ($p<0.001$). **C)** Bioluminescence and x-ray imaging of a rat, periprosthetic, biofilm infected tibia.

## CONCLUSIONS

bLf holds promise as an anti-infective in battlefield relevant open fractures, supported by the anti-biofilm properties of bLF highlighted within this research. Further work is required to translate these finding into clinical practice in military conflicts.

## ACKNOWLEDGEMENTS

Funding: USA Department of Defence.

## REFERENCES

1. Gustilo R, et al., *J Trauma.* **24**:742-746, 1984.
2. Gould G, et al., *J Food Prot* **59**:82-86, 1996.
3. Cornish J, et al., *Endocrinology* **145**:4366-4374, 2004.

# ASSOCIATION OF ABO BLOOD GROUP AND RHESUS FACTOR WITH FRACTURE TYPE, COMORBIDITIES AND OUTCOMES IN PATIENTS WITH HIP FRACTURE (HF)

[1,3]Jo-Wai Douglas Wang, [1]Zehao Dominic Fong, [1]Joel Lai, [1,2,3]Alexander Fisher

[1]The Department of Geriatric Medicine, The Canberra Hospital, Canberra, ACT, Australia
[2]The Department of Orthopaedic Surgery, The Canberra Hospital, Canberra, ACT, Australia
[3]The Australian National University Medical School, Canberra, ACT Australia
email: jo-waidouglas.wang@act.gov.au

## INTRODUCTION

Osteoporosis and fractures are highly influenced by genetic factors (heritability 50% to 80%) [1-4]. However, the few studies on the potential of the ABO blood group system for identifying individuals with a risk of HF and predicting its outcome gained controversy [5-7]. We investigated in HF patients the relationship between the ABO blood system in regard to fracture type, chronic comorbidities, and hospital outcomes (mortality and length of hospital stay [LOS]).

## METHODS

The dataset comprised 3715 patients with osteoporotic (low energy non-pathological) HF aged≥65 years (mean age 82.7 ± 8.30 years [SD], 2775 [74.70%] females, 1945 [52.36%] subjects with a cervical and 1770 [47.64%] with a trochanteric fracture) treated in our institution between 1999 – 2019.
Data on fracture type, socio-demographic and lifestyle factors, ABO blood group, Rhesus factor, chronic comorbidities, laboratory parameters and hospital outcomes were prospectively recorded and analysed. ABO distribution in the general Australian population was obtained from the Australian Red Cross Lifeblood National Blood Management System [8].
Univariate and multivariate logistic regression analyses were used to determine the odds ratio (OR) and 95% confidence intervals (CI) for associations between an outcome (dependent variable) and ABO blood status, clinical and laboratory variables.

## RESULTS AND DISCUSSION

HF patients, compared to the general Australian/ACT population, have a higher prevalence of blood group O (47.8% vs. 44.8%/45.5%, p<0.005) and a lower prevalence of group B (10.4% vs. 13.3%/13.5%, p<0.001), while the prevalence of groups A (38.1% vs. 37.6%/37.0%, p=0.519/p=0.156) and AB (3.8% vs. 4.3%/4.0%, p=0.133/p=0.451) did not show statistically significant differences. The group O was slightly more prevalent among subjects with trochanteric compared to cervical HF (49.4% vs. 46.1%, p=0.047). Regarding comorbidities, patients with type 2 diabetes mellitus (T2DM) demonstrated a higher prevalence of group A (43.6% vs. 37.3%, p=0.008), Rhesus factor positive (86.4% vs. 82.5%, p=0.038) and a lower prevalence of group O (41.4% vs. 48.7%, p=0.003). Atrial fibrillation (AF) was also associated with group A (41.4% vs. 37.4%, p=0.054).
A significant link was found between the ABO blood groups and hospital outcomes. Namely, patients with group O more often had prolonged LOS (>10 days) (49.3% vs. 45.7%, p=0.029) and a lethal outcome (56.6% vs 47.2%, p=0.015).
Logistic regression analysis, after adjusting for multiple confounders (including history of coronary artery disease, chronic renal disease, chronic obstructive pulmonary disease, AF, T2DM, dementia, cerebrovascular accident, Parkinson's disease, vitamin D deficiency, hyperparathyroidism, use of walking aids, smoking and alcohol consumption status and being a permanent residential care facility resident) and controlling for age and gender revealed that group O was an independent predictor of in-hospital mortality; it increased the risk of a fatal event by 45% (OR 1.45, 1.07-1.96, p=0.016). Similar regression analysis showed that group O also independently predicted prolonged hospital stay (OR 1.20, 1.01-1.41, p=0.037). The underlying molecular mechanisms by which ABO blood system affects HF are unclear. It can be hypothesized that anti-A and anti-B IgG antibodies, which are almost unique to the O blood group [9], may contribute to increased production of multiple inflammatory cytokines, important pathophysiological factors for osteoporotic fractures.

## CONCLUSIONS

ABO blood system is significantly associated with susceptibility to HF its type, and outcome. Individuals with blood group O are more prone to a HF with a higher risk of developing a trochanteric HF, and poorer outcomes, while blood group B exhibits a protective effect. Incorporating ABO blood groups in clinical practice could help identify at-risk individuals and implement personalised preventive measures for HF.

## REFERENCES

1. Ralston SH, et al., *Endocr Rev*. **31(5)**: 629-62, 2010.
2. Trajanoska K, et al., *Bmj*. **362**: k3225, 2018.
3. Wu Q, et al., *J Transl Med*. **21(1)**: 127, 2023.
4. Ho-Le TP, et al., *J Clin Endocrinol Metab*. 2023.
5. Kuru T, et al., *Biomed Res Int*. **2020**: 1834525, 2020.
6. Toro G, et al., *Hip Int*. **28(2)**: 84-8, 2018.
7. Uzoigwe CE, et al., *Ann R Coll Surg Engl*. **96(6)**: 442-5, 2014.
8. Hirani R, et al., *Med J Aust*. **216(6)**: 291-5, 2022.
9. Stussi G, et al., *Br J Haematol*. **130(6)**: 954-63, 2005.

# BREACHED AND NON-BREACHED SCREW TRAJECTORIES SOUND AND FEEL DIFFERENTLY

Acoustic and Torsional Profiling for Breach Identification During Pedicle Screw Insertion

[1]Tyra Lange, [1]Egon Perilli, [1]John J. Costi and [1]Karen J. Reynolds

[1]Medical Device Research Institute (MDRI), College of Science and Engineering, Flinders University, Adelaide, Australia.

email: tyra.lange@flinders.edu.au

## INTRODUCTION

Freehand pedicle screw insertion is performed without intraoperative image guidance; thus, the procedure is reliant on intricate knowledge of vertebral landmarks and bone anatomy in conjunction with sense perception [1]. Auditory feedback, in the form of distinct audible vibration patterns, created during pilot hole drilling are used to deduce whether the bit has perforated cortical walls [2]. Tactile feedback during screw insertion, which is the feeling of torque in the hands, is used to determine if screws have breached cortical bone [1]. These auditory and tactile cues aid surgeons in assiduous attempts to circumvent iatrogenic cortical breach. The aim of this study was to investigate breach diagnosis using acoustic emission (AE) and insertion torque (TI) profiling.

## METHODS

*In vitro* experimental testing was conducted on 58 ovine lumbar vertebrae. Specimens were randomly allocated into three different trajectory groups: Normal Insertion, $N_I$ (n = 26), Lateral Breach, $L_B$ (n = 16) and Medial Breach, $M_B$ (n = 16). Pilot holes were drilled into bones utilising an orthopaedic drill and 2.5 mm surgical drill bit. AE was captured at a frequency of 48 kHz by a custom sound sensor module. Titanium, self-tapping pedicle screws (4.5 mm x 32 mm), having cylindrical shape and possessing singular threading, were inserted at 6.0 rpm following the predrilled trajectories, whilst TI was digitally recorded at 20 Hz. To delineate differences between breached and non-breached trajectories statistical parameters were computed. For AE signals these included: absolute maximum AE ($AE_{max}$), number of AE crossings over a 0.64 V threshold ($AE_{counts}$), total AE energy ($AE_{energy}$) calculated using Eq. (1) and total AE sound exposure ($AE_{exposure}$) from Eq. (2). For TI signals these included: maximum TI ($TI_{max}$), number of negative values in TI derivative vector ($TI_{Ncounts}$), number of approximately zero, plateaued values in TI derivative vector ($TI_{Pcounts}$) and total TI energy ($TI_{energy}$) calculated using Eq. (3).

$$AE_{energy} = \int_{t_0}^{t_1} V(t)^2 \, dt \quad (1)$$

$$AE_{exposure} = \int_{t_0}^{t_1} p(t)^2 \, dt \quad (2)$$

$$TI_{energy} = \int_{t_0}^{t_1} T(t)^2 \, dt \quad (3)$$

Where, $V$ = AE voltage, $t$ = time, $t_0$ = initial time, $t_1$ = final time, $p$ = AE wave pressure and $T$ = torque. Data were collated and stratified by trajectory group. All factors were subjected to separate, one-way ANOVA analyses, followed by Tukey-Kramer post-hoc tests, to investigate differences in AE and TI, between the breached and non-breached trajectories.

## RESULTS AND DISCUSSION

The overall effect of insertion trajectory was significant for $AE_{counts}$ and $AE_{energy}$ ($p < 0.05$), however not for $AE_{max}$ ($p = 0.85$) nor $AE_{exposure}$ ($p = 0.06$). Insertion trajectory was significant for all TI factors ($p < 0.05$), except $TI_{energy}$ ($p = 0.58$). Post-hoc tests revealed significant differences, seen in Figure 1.

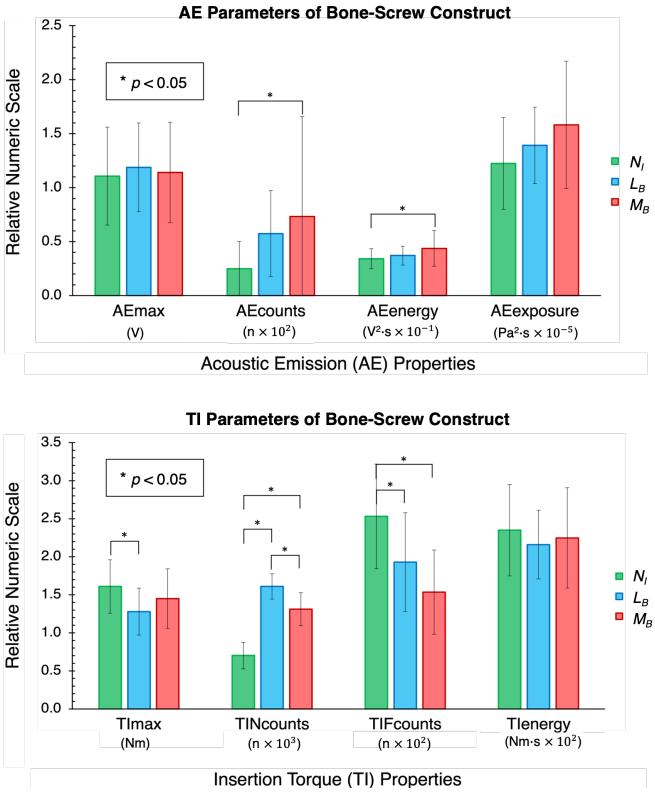


**Figure 1:** Mean (± SD) of properties from screw insertion tests.

## CONCLUSIONS

AE and TI parameters differ by trajectory, with individual insertion curves revealing valuable information about the tool path through bone. Each group had a unique insertion profile, with features describing distinctive resistance patterns experienced by surgeons when drilling or screwing in vertebrae. Changes in the AE and TI response occur during cortical wall perforation; thus, these variables could be used intraoperatively to rapidly detect and accurately diagnose breach.

## REFERENCES

1. Z. Zhang. 2020. *J Orthop surg*. DOI: 10.1111/os.12599.
2. M. Praamsma et al. 2008. *Can J Surg*. PMID: 19057732.

# A VIRTUAL CLINICAL TRIALS FRAMEWORK FOR EVALUATING GLENOID COMPONENT FIXATION AFTER REVERSE TOTAL SHOULDER ARTHROPLASTY

[1]Yichen Huang, [1]Dale L. Robinson, [1,2]Lukas Ernstbrunner, [3]Rami M. A. Al-Dirini, [3]Mark Taylor, [1]Peter Vee Sin Lee and [1]David C. Ackland

[1]Department of Biomedical Engineering, University of Melbourne, Parkville, VIC 3010, Australia

[2]Department of Orthopaedic Surgery, Royal Melbourne Hospital, Parkville, VIC 3050, Australia

[3]Medical Device Research Institute (MDRI), Flinders University, Clovelly Park, Adelaide 5043, Australia
email: yichenh2@student.unimelb.edu.au

## INTRODUCTION

Reverse total shoulder arthroplasty (RSA) is an established treatment for irreparable rotator cuff tears of the glenohumeral (GH) joint. However, complication rates of RSA remain high, with glenoid component loosening being one of the leading causes of revision surgery [1]. Glenoid component loosening after RSA is known to be related to intraoperative implant malpositioning or poor bone stock, but the interactions between these factors remain poorly understood. The aims of this study were twofold. Firstly, to develop a virtual clinical trials modelling framework for the GH joint after RSA; and second, to use this framework to quantify the effects of implant alignment (glenosphere lateralisation, baseplate tilt), and scapular bone quality on glenoid component fixation after RSA.

## METHODS

A previously published statistical shape model (SSM) was used to generate GH joint geometries of two subjects [1]. RSA was then virtually performed on each model in an automated manner using Zimmer Biomet components according to the recommended surgical technique. This was achieved using a series of Boolean operations applied to the bone geometries simulating three glenosphere lateralisation (0mm, 3mm, 5mm) and three baseplate tilt (10° inferior, neutral, 10° superior). A previously published rigid-body model was modified to match each post-operative joint model and used to calculate joint reaction forces for a high loading scenario at the glenohumeral joint, 90° arm abduction. Finite element (FE) models were then developed for the scapula of each GH joint. The material properties of the model were derived from three subjects, which had the lowest, medium, and highest average bone mineral density in the SSM training cohort. Joint reaction forces calculated from the rigid-body models were applied as joint loads in FE simulations (Figure 1 A). Bone-implant micromotion was then calculated as the relative displacements of each pair of contacting nodes at the bone-implant interface for the shoulder at 90° of arm abduction (Figure 1 B).

## RESULTS AND DISCUSSION

The peak micromotion at the bone-implant interface increased substantially in case of low bone quality when compared to the medium and high bone quality cases. For the 0mm, 3mm, and 5mm glenosphere lateralisation with superior baseplate tilt, micromotion in the case of low bone quality was 8.0µm, 15.9µm and 18.5µm larger than that in the high bone quality scapula, respectively. Superior tilt of the baseplate and increasing glenosphere lateralisation also yielded higher micromotion, especially in case of low bone quality. The highest micromotion occurred at 5mm lateralisation and superior baseplate tilt with low bone quality (59.2µm), while the lowest micromotion occurred at 0mm lateralisation and neutral baseplate tilt with high bone quality (28.1µm).

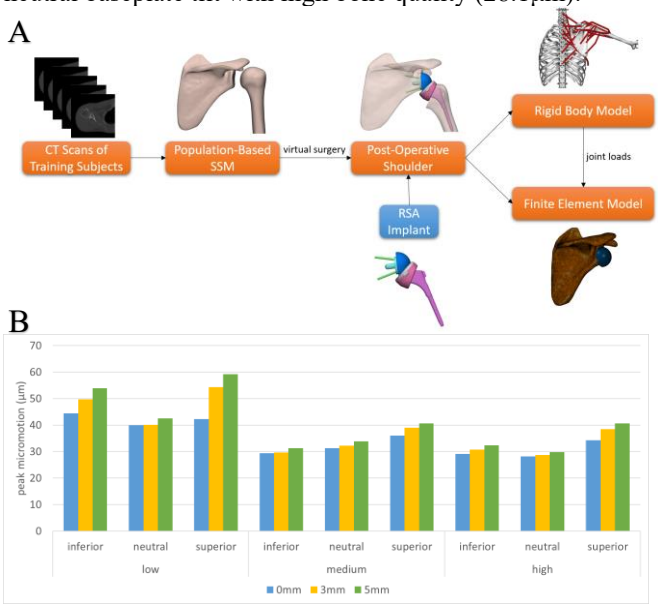


**Figure 1:** Flowchart of the virtual clinical trial musculoskeletal modelling framework (A) and peak micromotions calculated from FE simulations averaged over the two subjects (B).

## CONCLUSIONS

This study developed a virtual clinical trials modelling framework to investigate glenoid component fixation after RSA. The results showed that low bone quality, superior baseplate tilt, and glenosphere lateralisation all led to increases in micromotion at the bone-implant interface. The worst-case scenario yielded a micromotion higher than the 50µm limit, suggesting bone ingrowth may not occur and loosening may happen after repetitive loadings. This indicates that superior tilt of the baseplate should be avoided, especially in case of patients with low bone quality or when glenosphere lateralisation is employed. The findings may help to guide implant selection and intro-operative positioning of RSA to achieve optimal implant fixation and clinical outcomes.

## REFERENCES

1. Boileau P. *OTSR* **102**: S33–S43, 2016.
2. Huang Y et al. *BMMB* **21**: 249–259, 2022.
3. Wu W et al. *J Biomech* **49**: 3623-3634, 2016.

# BONE STRAIN FIELD PREDICTION VIA GRAPH NEURAL NETWORK FOR A PROXIMAL HUMERAL PLATE

[1]Daniela Mini, [2]Zhen Zhang, [2]Javen Qinfeng Shi, [1]Karen Reynolds, [1]Mark Taylor

[1]Medical Device Research Institute, College of Science & Engineering, Flinders University, Australia
[2] The Australian Institute for Machine Learning, The University of Adelaide, Australia
email: daniela.mini@flinders.edu.au

## INTRODUCTION

A high failure rate in the use of locking plates for the treatment of proximal humerus fractures has been reported with mechanical failure being a major contributing factor [1]. The number and length of screws required to stabilize a specific fracture can be chosen in a variety of ways, making it difficult to understand the mechanics of every possible combination. A standard technique for the study of fracture fixation mechanics is FE analysis, but it has limitations in terms of computational cost, making it impractical to study all possible configurations. The aim of this study is to use a combination of a Deep Learning technique and FE analysis, in order to predict the bone strain field around screws as their length varies.

## METHODS

A FE model of a proximal humerus was generated from a CT image of a cadaver from the New Mexico Decedent Image Database (NMDID)[2]. A single fracture was simulated, which was fixed using a fracture plate with seven proximal screws and three distal screws. Non-homogeneous material properties were defined, tied conditions were set between the screws and the bone and an axial bending loading condition was simulated [3]. The tip-to-joint distance (TJD) measure was introduced to vary the length of the seven proximal screws in four levels, for a total of $4^7$ possible configurations. TJD is defined as the distance between the tip of the screw and the bone surface [4], and this parameter was varied to generate training sets of a reduced number of configurations, such as 100, 200, 500 and 1000 FE data. All the models were run in Abaqus. The data from the FE models were used as input and output data to train a Graph Neural Network (GNN) model, a technique under the Deep Learning field. The information at the bone surface in contact with the screws was used as input values, such as bone elastic modulus and node positions. The minimal principal bone strain of the nodes at the same surface was used as an output parameter. Once the GNN was trained, the model was used to make a prediction of minimal principal bone strain around the screws of 100 unseen FE cases previously generated and not used for the training process. A regression analysis was performed between the GNN and FE predictions for these unseen cases.

## RESULTS AND DISCUSSION

Firstly, the size of the best training set was evaluated, showing that 200 FE data were sufficient to train the GNN. The GNN predictions of minimal principal bone strain around the proximal screws were compared with the FE results of the 100 unseen data, showing a good correlation and a low level of error ($R^2$ = 0.916, RMSE = 909.54 µstrain).
The time taken by GNN for the training process was 1.3 hours, but thereafter the time to make predictions on the 100 configurations was only 5 seconds, resulting in a powerful time-saving technique. Indeed, the generation and run of a single FE model took about 20 CPU minutes, so the GNN can be useful for exploring a large number of configurations instead of only running a FE analysis.

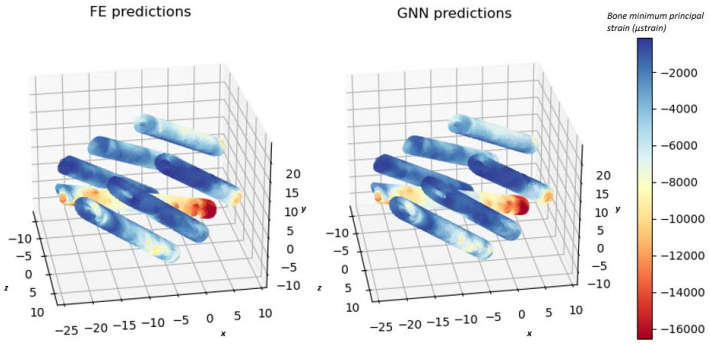


**Figure 1:** An example of FE prediction of the bone strain around the screws (left) and its corresponding GNN prediction (right). The $R^2$ was 0.965 and the RMSE was 638.25 µstrain.

## CONCLUSIONS

This study demonstrated that a Deep Learning technique can accurately and quickly predict the bone strain field when screw length is varied for a proximal humerus fracture plate. Moreover, the number of data required for the training of the GNN is relatively low compared to the total number of possible configurations.

## ACKNOWLEDGEMENTS

Funding was provided through the Australian Research Council Training Center for Medical Implant Technologies (ARC CMIT).

## REFERENCES

1. Kralinger F. *et al.*, *J. Bone Jt. Surg. - Am. Vol.*, 96(12):1026–1032, 2014
2. Edgar H. *et al.*, University of New Mexico, 2020
3. Röderer G. *et al.*, *Orthopedics*, 36(9):1134–1140, 2013.
4. Fletcher J.W.A. *et al., Arch Orthop Trauma Surg* 139, 1069–1074, 2019

# Thursday, December 9

## PODIUM 5

# THE USE OF INERTIAL MEASUREMENT UNITS AND COMPUTATIONAL MODELLING IN THE ESTIMATION OF SHOULDER JOINT FORCES

[1]Zhou Fang, [1]Damith Senanayake, [1]Peter Lee and [1]David Ackland
[1] Department of Biomedical Engineering, The University of Melbourne, Melbourne, VIC, Australia
email: mailto:zhoufl@student.unimelb.edu.au

## INTRODUCTION

Estimation of glenohumeral joint forces has played a key role in orthopedics, including evaluation of implant functional performance and longevity. The gold-standard in glenohumeral joint force measurement has been in the use of instrumented shoulder prostheses *in vivo* [1]; however, this approach is highly invasive and not practical in most research settings, and thus glenohumeral joint force is typically estimated using computational modelling and measurements of shoulder kinematics. In recent years, inertial measurement units (IMUs), which are low-cost wearable devices that measure acceleration, angular velocity, and magnetic field, have been employed to measure 3-dimentional shoulder joint motion outside of the laboratory. At present, however, their accuracy in kinematics measurement and estimation of joint force using computer modelling remains poorly understood. The aims of this study were twofold. Firstly, to develop a workflow for estimation of glenohumeral joint forces using IMU-based kinematic measurement and computational modelling; and secondly, to validate the results when using kinematics derived from an optoelectronic system.

## METHODS

Thirty healthy subjects (age: 28±4 years) were recruited. A set of 11 retro-reflective markers and an acromion marker cluster were placed on landmarks of the right upper limb of each subject so that glenohumeral joint motion was visible to an optoelectronic motion analysis system. Scapula position was registered at 21 humeral positions using an adjustable scapula locator in order to map scapula position to acromion marker cluster motion (Figure 1a). Three IMUs were also placed on the body including flat portion of the sternum, distal-lateral upper arm, and distal-dorsal forearm of the subjects. The orientations of the IMUs relative to body segments were computed using the ISB recommended coordinate systems [3] via two-stage static poses [4] and a T-pose. Subjects performed a range of activities of daily living including flexion-extension, abduction-adduction, head touching and reaching, synchronised to a metronome. Kinematics were computed using IMUs and the optoelectronic motion analysis system based on a regression model which predicts scapular protraction, external rotation and tilt in the thorax reference frame given plane of humeral elevation and humeral elevation angle. Two musculoskeletal models of each subject's upper limb were developed, comprising 10-degree-of-freedom and 26 Hill-type muscle-tendon units [5]. Kinematics derived from optoelectronic motion analysis and IMUs were used separately to drive the musculoskeletal model for calculating muscle force using static optimization. Subsequently, resultant and orthogonal components of glenohumeral joint reaction force were computed and compared between optoelectronic motion analysis and IMUs.

## RESULTS AND DISCUSSION

For the IMU-based scapular angles, the root mean square error (RMSE) in prediction of protraction, external rotation, and posterior tilt during abduction was $2.2^o$, $4.7^o$, and $1.4^o$ (Table 1). The maximum absolute error and RMSE of total glenohumeral joint reaction force predicted by IMU-based shoulder kinematics compared to the optoelectronic motion analysis was 13.8%BW and 6.8%BW, respectively. IMU-based resultant glenohumeral joint force exhibited a similar trend to that measured using an instrumented implant, with an RMSE of 11.1%BW and 14.5%BW compared to *in vivo* instrumented implant 1 and 2, respectively (Figure 1b) [1].

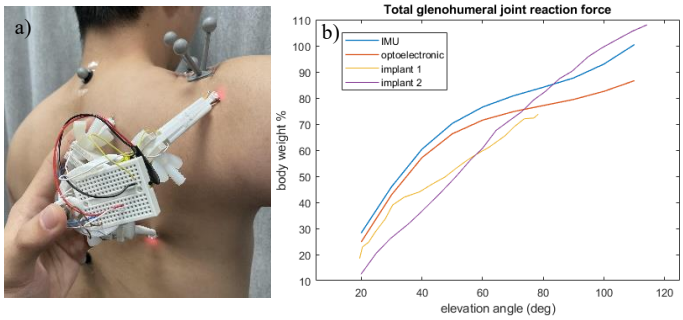


**Figure 1a:** Customized scapula locator illustrating scapular landmark digitization. **1b:** Total glenohumeral joint reaction force during abduction. Blue: IMU-based; red: optoelectronic-based; yellow: instrumented implant subject 1; purple: instrumented implant subject 2.

## CONCLUSIONS

This study presents a new method to estimate glenohumeral joint forces using IMU-based 3-dimensional scapular kinematics and musculoskeletal modelling. Scapula motion predicted using IMUs and a linear-regression model derived from healthy subjects was comparable to that obtained from an optoelectronic motion analysis (RMSE $< 5^o$). Kinematics derived from IMUs can be used with musculoskeletal modelling to predict glenohumeral joint forces with only minor deviations from predictions made using optoelectronic motion analysis. The findings underpin the utility of IMU-driven approaches in clinical orthopedics, with future applications in telemedicine and telerehabilitation.

## REFERENCES

1. Westerhoff, et al., *Med Eng & Physics.* **31**:207-213, 2009.
2. Friesen,et al., *Med Biol Eng Comput.* **61**:1521-1531,2023.
3. Wu. et al. *J Biomech*. **38**: 981-992, 2005.
4. Palermo et al. *Measurement* **52**: 145-155, 2014.
5. Wu. et al. J Biomech. 49: 3626-3634, 2016.

**Table 1:** 3D RMS error and correlation coefficient (R) of IMU-based scapulothoracic angles during an abduction-adduction task.

| Scapulothoracic angle | Pro-retraction | Ex-internal rotation | Post-anterior tilt |
|---|---|---|---|
| **RMSE (R)** | $2.2^o$ (0.95) | $4.7^o$ (0.99) | $1.4^o$ (0.98) |

# SHOULDER MORPHOLOGIC VARIATION: STATISTICAL SHAPE AND POSE APPROACHES

François Bruyer-Montéléone[1], Maxence Lavaill[1,2] Natalia Mühl Castoldi[1], Graham Kerr[1,2], Syn Schmitt[1,3], Dermot O'Rourke[1,2], Ashish Gupta[1,2,4], Saulo Martelli[1,2], Peter Pivonka[1,2]

[1]School of Mech., Medical & Process Eng, Queensland University of Technology, Brisbane, Australia;
[2]Queensland Unit for Advanced Shoulder Research, Brisbane, Australia;
[3]Institute for Modelling and Simulation of Biomechanical Systems, University of Stuttgart, Stuttgart, Germany;
[4]Orthopaedic Surgery, Sports Injury, Orthopaedics, Greenslopes Private Hospital, Brisbane, Australia
email: f2.bruyermonteleone@hdr.qut.edu.au

## INTRODUCTION

Inter-individual variability of shoulder bone morphology and posture affects joint biomechanics. However, a complete description of the upper limb anatomical and postural variation in adults is still lacking. Moreover, the intricate joint geometric constraint makes it challenging to identify bone interactions. Statistical shape models (SSM) use principal component analysis (PCA) to describe anatomical variability across a population [1]. These models have been successfully developed for individual shoulder bones to study shape properties and predict bone reconstructions [2,3]. Furthermore, bone relative neutral positions can provide additional indication of the inter-subject anatomical and functional variability, which can be assessed with statistical pose models (SPM). Yet, this analysis has only been undertaken in the lower limb with complete bones [4]. Hence, a combination of shape and pose analyses is conducted in the upper limb using partial sets of bones to investigate inter-individual variations.

## METHODS

Two sets of healthy shoulder bones were reconstructed from medical images (CT and MRI scans) using Mimics 24.0 (Materialise NV, Belgium). The two batches involved 89 humeri and scapulae (63M and 26F, age: 31.1 ± 10.0 years) and 81 clavicles and hemithoraxes (58M and 23F, age: 30.6 ± 9.1 years), respectively. Proximal humeri were medially cut along the shaft. The humeral axes were determined via the best-fitting cylinder of the shaft and tangential lines around the tubercles. The clavicular coordinate system was reproduced using the best-fitting ellipsoid of the hemithorax. Final models were smooth triangle-tessellated using Meshlab 2022.2 (ISTI, CNR). The resultant template meshes resulted in three SSMs and one SPM. Development of the SSMs consisted of three steps. Rigid registration firstly aligned the axes of the template meshes with the set of the target surface meshes. Secondly, a rigid Iterative Closest Point (ICP) algorithm performed scaling, translation and rotation of the template vertices. Then, a non-rigid registration ICP algorithm deformed the template surface mesh to locally match the target's morphology before applying PCA [6]. The SPM involved the above-mentioned methodology along with a final rigid registration step to position back the bones at their original locations. Inter-joint distances and bony orientations relative to the parent segments were accounted for. The generality, compactness and specificity of the models were assessed and compared with the literature [2][7].

## RESULTS AND DISCUSSION

The first five modes explained 95.5%, 86.7% and 92.0% of the shape variability for the humerus, scapula and clavicle, respectively (Figure 1). The first mode mostly defined scaling while version and inclination were the dominant variation described by the second scapular mode and the third humeral mode. Compactness showed similar results as evidenced in the literature (2, 8 and 4 PCs accounting for 90% of the variability for the humerus, scapula and clavicle respectively) [2][7].

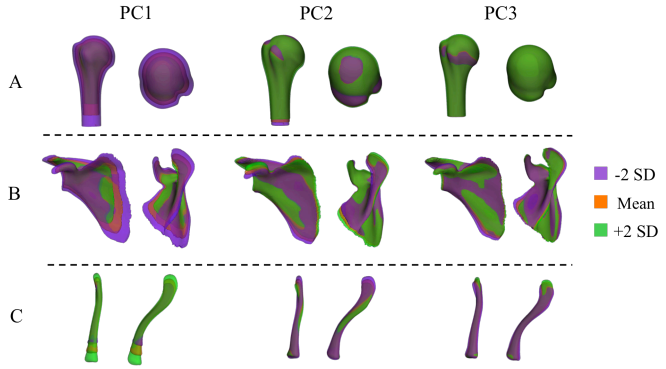


**Figure 1:** Shoulder bone mean shapes and ±2 standard deviations of the 3 main modes (PC) of variation of the humerus (A), scapula (B) and clavicle (C).

## CONCLUSIONS

In healthy shoulders, the conferred SSM and SPM have exhibited anatomical variations across individuals providing quantitative data to support surgical planning and implant design applicable to an entire population. The assessment of the model specificity and generality and the relationship between anatomy and posture are currently in progress.

## ACKNOWLEDGEMENTS

The Australian Research Council is gratefully acknowledged (IC190100020; FT180100338).

## REFERENCES

1. Pearson K, *Lond. Edinb. Dublin philos. mag. j. sci.* **2:11**:559-572, 1901
2. Abler J, et al., *JSES* **27**:1800-08, 2018
3. Huang Y, et al., *BMMB* **21**:249-259, 2022
4. Zhang J, et al., *J.* Biomech **49**:3875-81, 2016
5. Wu G, et al., *J.* Biomech **38**:981-992, 2005
6. Sarkalkan N, et al., *Bone* **60** :129-140, 2014
7. Vancleef S,et.al., *JSES* **28** : 631-638, 2019

# THE INFLUENCE OF GLENOID BONE GRAFTING USING THE LATARJET PROCEDURE ON GLENOHUMERAL JOINT CONTACT LOADING

[1]David Ackland, [1]Dale Robinson, [2]Eugene Ek and [2,3]Lukas Ernstbrunner
[1] Department of Biomedical Engineering, The University of Melbourne, Melbourne, VIC, Australia
[2] Melbourne Orthopaedic Group, Windsor, Melbourne, Australia
[3] Department of Orthopedics, Balgrist University Hospital, University of Zurich, Zurich, Switzerland Email: dackland@unimelb.edu.au

## INTRODUCTION

The Latarjet procedure is considered an effective surgical stabilisation procedure for anterior shoulder instability with glenoid bone loss, and involves augmenting the glenoid with a coracoid bone graft. Despite favourable long-term results, mediolateral mal-positioning of the graft and graft resorption remains a clinical challenge [1]. The aims of this study were twofold. Firstly, to establish the first biomechanical model of the Latarjet procedure that simulates physiological glenohumeral joint contact loading; and secondly, to assess the influence of medial-lateral graft mal-positioning on graft and glenoid cartilage loading.

## METHODS

Using the geometry of the Visible Human Male, a finite element (FE) model of one right scapula and humerus was developed comprising the scapula and humerus, and their cartilaginous articular surfaces. Bone material properties were mapped from a computed tomography (CT) scan of a healthy male, and the cartilage material properties assigned using published data [2].

Shoulder kinematics data were obtained from six healthy adult subjects for 90° of humeral abduction and full external rotation (ABER), a critical joint position in the unstable shoulder. Subject-specific muscle and joint forces calculated using a rigid-body model [3] were input into the FE model to drive simulations of glenohumeral joint contact. Glenoid bone loss was simulated by removing the anterior region of the glenoid surface area by 10% and 25%. A simulated Latarjet procedure was then performed by sectioning the distal 22 mm of the coracoid process and fixing this graft to the anterior region of the glenoid with two bicortical screws (Fig 1). Simulations of joint loading were then performed, and then repeated with the graft position perturbed by -1mm, 1mm, 2mm and 3mm in the lateral direction, which simulated intra-operative mal-positioning of the graft.

## RESULTS AND DISCUSSION

For 10% glenoid bone loss, the neutrally positioned graft did not contact the humerus; however, graft lateralisation by 2mm produced peak graft contact stresses of 36.8±1.3MPa and significantly lowered peak glenoid cartilage contact stresses (mean difference: 47.1%, $p=0.003$). A similar but more pronounced result was observed at 25% bone loss, with graft stresses increasing (mean difference: 63.7%, $p<0.001$) and glenoid cartilage stress decreasing (mean difference: 77.8%, $p<0.001$).

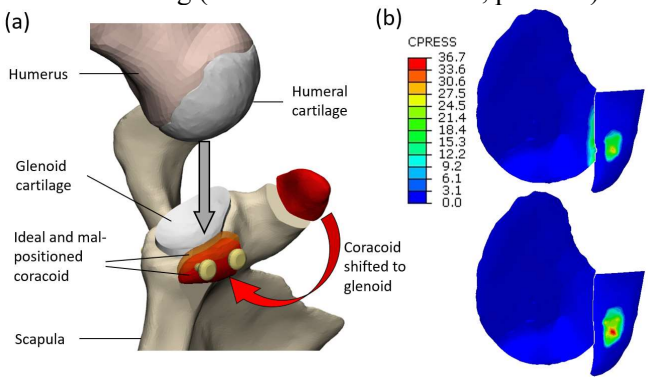


**Figure 1:** Finite element model of Latarjet procedure **(a)** and graft contact observed when positioned flush (level) with the glenoid bone face (upper image) and positioned 2mm medial to the glenoid bone face **(b)**

## CONCLUSIONS

Mal-positioning the Latarjet graft laterally by an amount corresponding to the glenoid cartilage edge thickness (2 mm) causes substantial graft load sharing. This localised, high contact pressure increases with graft lateralisation, and may ultimately result in graft failure, or reduced capacity for the graft to osseointegrate integrate. Graft positioning closer to the glenoid bone surface may enhance load sharing between the glenoid and graft, which may ultimately encourage effective bone remodelling and graft integration without graft overload. These findings provide guidance for intraoperatively graft placement in Latarjet surgery.

## REFERENCES

[1] Moroder et al. 2019, AJSM, 47(3): 688-694
[3] Büchler et al. 2002, Clinbio, 17(9-10): 630-639
[4] Wu et al. 2017, Gait and Post, 54: 87-92

# FAILURE OF INLAY AND ONLAY HUMERAL COMPONENTS IN REVERSE SHOULDER ARTHROPLASTY: A MICRO-CT STUDY

[1,2]Dermot O'Rourke, [1,2]Xiaolong Fan, [3]Egon Perilli, [3]Sophie Rapagna, [1,2]Ashish Gupta, and [1,2]Saulo Martelli

[1]ARC ITTC for Joint Biomechanics, Queensland University of Technology, Brisbane, QLD, Australia
[2]Queensland Unit for Advanced Shoulder Research, Brisbane, Australia
[3]Medical Device Research Institute, College of Science and Engineering, Flinders University, Adelaide, SA, Australia
email: dermot.orourke@qut.edu.au

## INTRODUCTION

Reverse shoulder arthroplasty (RSA) covers a broad range of indications including rotator cuff arthropathy, revision arthroplasty, and proximal humerus fractures [1]. Inlay RSA systems use an inset humeral tray which establishes bony contact [2], but the additional removal of metaphyseal bone may compromise the strength of the implant-bone construct. An RSA implant system with an Grammont-style inlay humeral stem design and minimal bone resection with autologous metaphyseal bone graft, referred to as onlay design hereafter, may maintain bony contact while increasing the strength of the bone-implant construct. However, the strength of these two implant-bone constructs and their mechanism of fracture are not fully clear. Time-elapsed, large-volume micro-CT imaging may help elucidate differences in strength of the implant-bone construct of the inlay and onlay designs [3]. The aim of this study was to investigate the failure of a humeral stem inlay design and an onlay Grammont-style humeral stem with added autologous bone graft.

## METHODS

Left and right humeral bones were obtained from a donor (M 75 yo) with no reported history of skeletal pathology. The left humerus was implanted with the **inlay** technique where the humeral head was cut with a resection guide at 155°, the proximal epiphyseal was reamed, and the implant press-fitted. The right humerus was implanted with the **onlay** technique where the humeral head was cut with a resection guide at 155°, a minimal amount of bone was manually removed in the epiphysis, and an under-sized implant was impacted with bone graft from the humeral head. Both surgeries were performed by an experienced surgeon (AG).

The implanted humerus specimen and potting cup assembly were mounted on a radio-transparent compressive stage with a screw-jack mechanism controlling the vertical displacement of the specimen. A micro-CT scan was taken of the unloaded specimen (Nikon XT H225 ST, 215kV, 209µA, 45µm/pixel [4]). The screw-jack was then actuated until the reaction force severely dropped, indicating bone-implant failure. The specimen was rescanned after failure. The reaction force was recorded throughout the experiment with a load cell.

The failed micro-CT image dataset was co-registered to the unloaded dataset (Dataviewer, Skyscan–Bruker, Kontich, Belgium), using the humerus metaphysis and potting cup as references, to analyse the implant displacement (subsidence).

## RESULTS AND DISCUSSION

The onlay construct had a greater stiffness than the inlay but a greater subsidence until fracture (Tab.1) suggesting an initial compression of the more loosely packed bone graft in the onlay before engaging trabecular support. The onlay had a greater failure load (2800 N) than the inlay (2000 N). Both techniques showed a similar failure mechanism in the micro-CT images (Fig.1) with radial expansion of the humerus when loaded, resulting in a longitudinal fracture of the cortex.

**Tab. 1:** Subsidence, stiffness, and failure loads of the implants.

| ID | Subsidence (mm) | k (N/mm) | Fracture Load (N) |
|---|---|---|---|
| Inlay | -5.985 | 309 | 2000 |
| Onlay | -7.651 | 346 | 2800 |

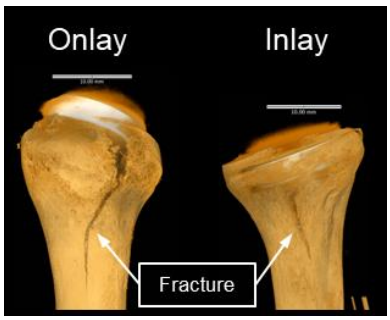


**Fig. 1:** 3D micro-CT rendering of the fracture of bone in the onlay (left) and inlay (right) implant designs under axial load.

## CONCLUSIONS

In this time-elapsed study on a cadaveric humerus, greater mechanical support was provided for the humeral component by the minimal bone resection and autologous metaphyseal bone graft in the onlay design compared to the inlay design.

## ACKNOWLEDGEMENTS

Australian Research Council (IC190100020). Flinders Microscopy and Microanalysis (FMMA).

## REFERENCES

1. Boileau P, et al., *J Shoulder Elbow Surg.* 14(1): 147-161
2. Grammont PM, et al., *Orthopedics.* 16(1):65-68, 1993.
3. Bennett K, et al., *J Biomech.* 144: 11275, 2022.
4. Wearne LS, et al., *J Mech Behav Biomed Mater*, 105336 2022.

# JAW JOINT LOADING DURING BITING FOLLOWING TOTAL TEMPOROMANDIBULAR JOINT REPLACEMENT SURGERY

[1]Sarah Woodford, [1]Dale Robinson, [2]Jaafar Abduo, [1]Peter V.S. Lee and [1]David Ackland

[1]Department of Biomedical Engineering, The University of Melbourne, Parkville, VIC, Australia [2]Melbourne Dental School, The University of Melbourne, Parkville, VIC, Australia
email: swood1@student.unimelb.edu.au

## INTRODUCTION

Unilateral total temporomandibular joint replacement (TMJR) surgery is known to reduce pain and improve quality of life in patients suffering from end-stage temporomandibular joint (TMJ) disorders. Excellent long-term outcomes are reported for reconstructed TMJs, with global revision rates of only 1.19 per 100 prosthesis-years [1]. However, unilateral TMJR patients often experience post-surgical degradation to the native contralateral joint, resulting in up to 40% of patients requiring subsequent bilateral TMJR surgery within two years [2]. There is no consensus regarding the mechanism of this damage; however, researchers speculate that it may be related to joint loading, which cannot be measured *in vivo*. The aim of this study was to evaluate subject-specific TMJ loading during maximum voluntary bite force following unilateral TMJR surgery and compare this to healthy control subjects.

### METHODS

Musculoskeletal models were created for 5 unilateral TMJR patients and 8 healthy controls. Craniofacial anatomy was captured via cone beam CT and maximum voluntary bite force recorded on the right and left first molars. A generic rigid-body musculoskeletal model of the masticatory system was anisotropically scaled to each participants mandibular length and width. The temporalis, masseter and pterygoid muscles were modelled as Hill-type muscle-tendon actuators. For unilateral TMJR patients the superior and inferior sub-regions of the lateral pterygoid muscle were removed on the operated side to reflect their intraoperative severing during condylectomy. Each participant's bite force was applied to the model and TMJ loading computed using static optimization.

## RESULTS AND DISCUSSION

Control subjects had higher net TMJ force (working (W): 86.0 ± 84.1 N, non-working (NW): 51.8 ± 44.4 N) than unilateral TMJR patients, both when biting on the contralateral (W: 14.2 ± 5.9 N, NW: 48.5 ± 10.4 N) and ipsilateral molars (W: 15.1 ± 7.9 N, NW: 25.6 ± 10.8 N); these loads were particularly low on the native contralateral joint (Figure 1). TMJR patients had significantly higher lateral joint forces when biting on the contralateral molars than when biting on the ipsilateral molars (W: median difference: 10.7 N, $p = 0.048$. NW: median difference: 7.8 N, $p = 0.048$). Furthermore, TMJR patients biting on the contralateral molars had a significantly lower ratio of TMJ force to bite force on the native working joint than healthy controls (median difference: 0.17, $p = 0.049$) (Table 1).

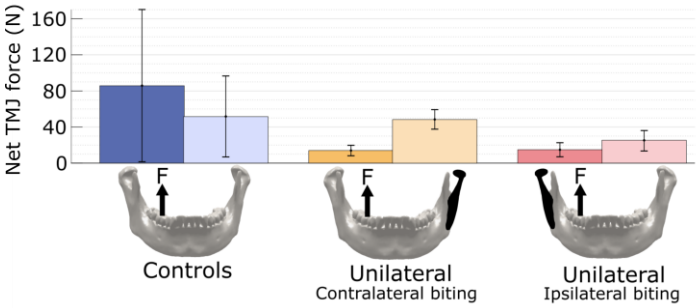


**Figure 1:** Net resultant TMJ force during maximum-force biting for healthy controls and unilateral TMJR patients biting on their contralateral and ipsilateral molars.

**Table 1:** Resultant TMJ force and ratio of TMJ force to bite force for healthy controls and unilateral TMJR patients biting on their contralateral (TMJR-C) and ipsilateral molars (TMJR-I), expressed on the working (W) and non-working (NW) joints. [a] significant difference between controls and TMJR patients; [b] significant difference between TMJR patients biting on the contralateral and ipsilateral molars.

| Subject | Joint | TMJ force (N) | | | | TMJ to BF ratio |
|---|---|---|---|---|---|---|
| | | Lateral | Anterior | Superior | Net | |
| Control (n=8) | W | 2.5 (20.9) | 3.8 (19.0) | 33.7 (116.3) | 86.0 (84.1) | 0.24 (0.12)[a] |
| | NW | -5.0 (13.0) | -10.7 (24.4) | -43.0 (43.1) | 51.8 (44.4) | 0.17 (0.12) |
| TMJR-C (n=5) | W | 12.1 (7.6)[b] | -0.1 (1.7)[b] | 6.0 (1.8) | 14.2 (5.9) | 0.06 (0.02)[a] |
| | NW | -9.4 (5.1)[b] | -16.7 (8.4)[b] | -44.3 (7.3) | 48.5 (10.4) | 0.19 (0.03) |
| TMJR-I (n=5) | W | -0.4 (1.7)[b] | -5.6 (1.4)[b] | 13.5 (8.1) | 15.1 (7.9) | 0.11 (0.07) |
| | NW | 0.0 (0.8)[b] | -4.4 (2.0)[b] | -24.9 (10.9) | 25.6 (10.8) | 0.15 (0.03) |

## CONCLUSIONS

Unilateral TMJR patients experience lower net TMJ forces than healthy controls, particularly on their native contralateral joint. This underloading may present a possible mechanism for post-operative degradation of the native joint. Results of this study may guide future implant design and evaluation and influence prescription of post-surgical physiotherapy to enhance long-term patient outcomes.

## REFERENCES

1. Back E, et al., *J Oral Maxillofac Surg.* **51**:1059-1068, 2022.
2. Franco P, et al., *J Oral Maxillofac Surg. 55-113, 1997.*


# Thursday, December 9

## KEYNOTE 2 – Dr Nikki Hooper

"Improving Outcomes in Hip Dysplasia"

# Thursday, December 9

## PODIUM 6

# DETECTING CHANGES TO MUSCLE ARCHITECTURE OVER TIME WITH SHAPE AND GROWTH MODELLING IN CEREBRAL PALSY

[1]Salim G. Bin Ghouth, [1, 2]Thor F. Besier, [1]Geoffrey G. Handsfield

[1]Auckland Bioengineering Institute, University of Auckland, Auckland, New Zealand
[2]Department of Engineering Science, University of Auckland, Auckland, New Zealand
email: g.handsfield@auckland.ac.nz

## INTRODUCTION

Cerebral palsy (CP) is neuromusculoskeletal disorder caused by a one-time brain lesion during the neonatal period [1], [2]. It is a common cause of disability in children and adolescents [1], [2]. Although the brain lesion is non-progressive in CP, the musculoskeletal movement impairments worsen progressively over time [1]. Previous research has explored structural and architectural properties of the lower limb muscles [3]. We have generated statistical shape models to explore the morphological variation of the soleus muscle in a cohort of children and adolescents with CP and a typically developing control cohort [4]. In the present study, we investigated the shape, fiber architecture, and growth of the medial gastrocnemius muscle. We created a shape and fiber tracts arrangements model and assessed the fiber architecture of the medial gastrocnemius muscle to investigate the shape progression and growth in a cohort of children and adolescents with CP and a typically developing (TD) cohort.

## METHODS

Longitudinal anatomical MRI and diffusion MRI were collected at three time points within a 15-month interval for a cohort of children and adolescents with CP as well as a TD cohort. Volumetric meshes were built based on segmented T-1 images, and fiber orientations were estimated from the diffusion MRI to represent the 3-dimensional architecture of the medial gastrocnemius muscle in both cohorts. A statistical shape and fiber tracts arrangement model was created for the TD cohort by registering each mesh to a reference mesh. Vector fields representing fiber orientations were registered accordingly and, then, interpolated using a nearest neighbor algorithm. Principal component analysis was applied to identify the dominant shape and fiber tracts arrangements (i.e., principal components) in the TD cohort. The mean and variability of the TD model outputs were analysied. Then, the mean of the TD shape and fiber tracts arrangements model was compared to the medial gastrocnemius muscle in children and adolescents with CP.

## RESULTS AND DISCUSSION

Shape and fiber tracts arrangements models of the TD cohort identified the dominant architectural characteristics and their variations at three time points over 15 months using three principal components. Size wan included in the TD model because we observed that size variations were strongly related to variations of fiber tracts arrangements. The first principal component of the TD model accounted for ~94% of total variance. The mean of TD model (shape and fiber tracts arrangements) was compared to the shape and fiber tracts arrangements of the medial gastrocnemius muscle in children and adolescents with CP. We observed similar shape and fiber tracts arrangements in the TD cohort and children and adolescents with CP with local variations at the proximal, middle and distal regions of the medial gastrocnemius muscle (see Figure 1).

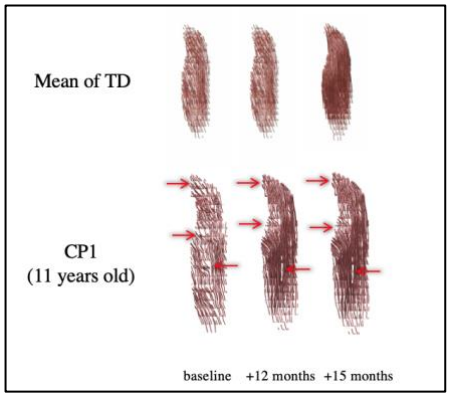


**Figure 1:** A comparison between mean of TD shape and fiber tracts arrangements model and an adolescent with CP at baseline, after 12 months and after 15 months.

## CONCLUSIONS

We introduced an approach to quantitatively describe muscle architecture progression over 15 months. The approach incorporated variation in morphology (size and shape) of muscle as well as 3D fiber architecture (estimated from Diffusion Tensor Imaging). The shape and fiber tracts arrangements models of the medial gastrocnemius muscle were built for a TD cohort and compared to children and adolescents with CP. The model enabled us to depict the progression of shape and variations in growth within the TD cohort, as well as similarity between the TD cohort and children and adolescents with CP.

## REFERENCES

1. H. K. Graham et al. *Nat. Rev. Dis. Prim.*: 2, 2016.
2. M. Oskoui et al. *Dev. Med. Child Neurol.*: 55, no. 6, 509-519, 2013.
3. S. A. Williams et al. *Dev. Med. Child Neurol.*: 2020
4. S. G. Bin Ghouth et al. *Scientific Reports*: 12, no. 1, 7711, 2022.

# DEVELOPMENT OF A LOWER-LIMB STATISTICAL BONE DENSITY MODEL IN CHILDREN AGED 4 TO 18 YEARS OLD

[1]Yidan Xu, [1]Thor Besier and [1]Julie Choisne

[1]Auckland Bioengineering institute, University of Auckland, Auckland, New Zealand

email: yxu356@aucklanduni.ac.nz

## INTRODUCTION

Recently, statistical shape models (SSM) and statistical density models (SDM) have become popular to characterize geometry [1] and bone mineral density [2] variation. A previous study has characterized shape variation of lower limbs' bones in children aged from 4 to 18 years and used the results to predict bone shape geometry in typically developing children [1]. However, no previous study has captured the bone density variation in children, although SDM has been applied on adult for years [2]. Therefore, the aim of this study was to create a SDM of the paediatric pelvis, femur and tibia from 330 CT scans and to assess the correlations between demographics in participants and principal components.

## METHODS

Template surface meshes from a previous study [1] were converted into 4-node tetrahedral volumetric meshes using TetGen (WIAS, Berlin, Germany). The volumetric template meshes were fitted into 652 tibias, 657 and 328 pelvises from 330 children aged 4 to 18 years old (136 F, Age 12 y.o. ±5, Height 148 cm ±24 and weight 49 kg ±22). Subject-specific bone mineral density (BMD) was extracted based on each volumetric mesh and the calibrated CT scans using Bonemat (IOR, Bologna, Italy). Following this process, the nodal bone mineral density in each model were used to perform a principal component analysis (PCA). PCA was performed on bone models to mathematically describe the principal components (or modes) of density variation within the tibia, femur and pelvis across the population. Correlations between demographics and first principal component were computed.

## RESULTS AND DISCUSSION

The first PC in tibia accounted for 44.8% of the variance (Fig.1 A), which primarily represented densities variability throughout the entire tibia, especially the cortical density, excluding the area around the growth plate in proximal extremity. The first PC in femur explained 26.6% of the variance (Fig. 1 B), largely capturing the variation in average density values across the femur, especially at the femur endocortical surface. In the pelvis, the first PC accounted for 37.1% of the variation (Fig. 1 C), predominantly capturing the density variation across the entire pelvis, except for the iliac fossa. The coefficient of determination ($R^2$) in the correlations between the PC1 and demographics (Table 1) showed that the pelvis had a moderate percentage variation explained by the age and height. However, no demographic factors accounted for variations in the tibia and femur BMD.

**Table 1:** Correlations between each demographic factor and the first principal component of the tibia, femur and pelvis

| $R^2$ | Sex | Age | Height | Mass |
|---|---|---|---|---|
| **Tibia** | 0.027 | 0.329 | 0.276 | 0.216 |
| **Femur** | 0.055 | 0.368 | 0.254 | 0.220 |
| **Pelvis** | 0.073 | 0.644 | 0.537 | 0.482 |

## CONCLUSIONS

We developed statistical density models for typically developing children aged 4 to 18 and found that no demographic factors strongly correlated to the bone mineral density in this study. Future study will focus on developing a combined shape and density model for the same dataset.

## ACKNOWLEDGEMENTS

The authors would like to acknowledge the Aotearoa foundation in NZ for funding this study.

## REFERENCES

1. Carman, L et al. *Sci Rep.* **12**, 3251, 2022
2. Querol, LB et al. *MICCAI* 2006
3. Fernandez JW et al. *Biomech Model Mechanobiol* **2**(3):139-155, 2004

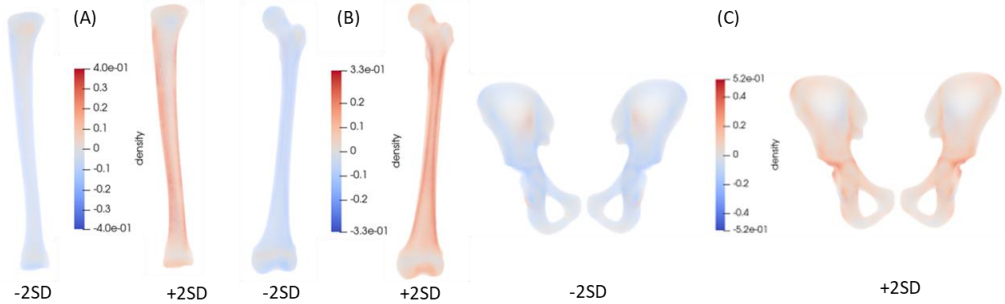


**Figure 1:** Density Variation of ±2SD in PC1 compared to average from the dataset. Densities are plot on the mean shape of the tibia (A), femur (B) and pelvis (C).

# LOWER LIMB JOINT STRATEGIES USED TO NEGOTIATE OBSTACLES IN YOUNG AND OLDER ADULTS

[1]Praveen Krishna, [1]David Ackland, [2]Rezaul Begg and [1]Peter Lee

[1]Department of Biomedical Engineering, The University of Melbourne, Melbourne, VIC, Australia
[2]Institute for Health and Sport (iHeS), Victoria University, Melbourne, VIC, Australia
email: pkkris@student.unimelb.edu.au

## INTRODUCTION

Older adults are at greater risk of falls leading to higher rates of injury and death when compared to young adults. Tripping over obstacles is a widely reported as a major cause of falls [1]. Consequently, it is of interest to determine the age effects on the ability to negotiate obstacles (cross obstacles in one's path). The aims of this study were to investigate whether kinematic and energetic joint strategies to create clearance over obstacles differ between age groups and examine whether the widely reported redistribution of joint powers with aging is robust to the task of obstacle negotiation [2]. Insights from this study may help to understand the effect of aging on biomechanics and inform exercise program development for falls prevention.

## METHODS

A preliminary cohort of 4 young adults (mean age: 27.5 ± 4 years) and 4 older adults (mean age: 71 ± 4 years) walked across level ground or negotiated obstacles at a self-selected speed. Obstacles of 4 different heights (2 cm, 4 cm, 8 cm, 16 cm) were presented in a randomized order at mid-swing of the participant's gait cycle once a steady pace had been achieved.

Motion capture data and force plate data were captured and analyzed. A generic musculoskeletal model with 23 degrees of freedom was scaled for subject-specificity and inverse kinematics and inverse dynamics procedures were performed to compute joint kinematics and joint moments respectively. Joint power was computed as the product of joint moment and angular velocity, and joint work was computed by integrating the power curve over areas of positive and negative power during the stance phase. Age and obstacle height effects on joint angles, joint moments, joint powers, and joint work were examined for the hip, knee, and ankle in the sagittal plane in the trailing leg (i.e., the leg to cross the obstacle second) while the leading limb crossed the obstacle.

## RESULTS AND DISCUSSION

Preliminary results suggest older adults exhibited an increased reliance on ankle dorsiflexion during swing as obstacle height was increased (Figure 1). Younger adults produced a larger peak ankle moment in late stance, resulting in a larger peak in positive ankle power compared to older adults -a trend that persisted across all conditions. Older adults generated more positive work at the hip through mid-stance during unobstructed walking, a result consistent with previous findings of older adults utilizing the hip instead of the ankle to generate power [2]. Obstructed conditions seem to necessitate a change in strategy in both groups resulting in a higher proportion of positive ankle work and lower proportion of positive hip work. However, older adults still produced a lower proportion of work at the ankle which may suggest that the age-related changes to gait biomechanics persist despite the presence of an obstacle.

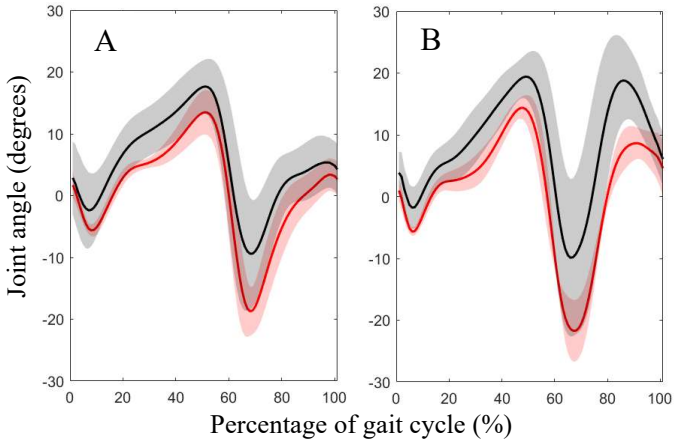


**Figure 1:** Ankle angle during unobstructed walking (A) and negotiation of the highest obstacle (B) for young adults (red) and older adults (black). Positive angle indicates dorsiflexion.

## CONCLUSIONS

Ankle dorsiflexion may play a key role in creating clearance for older adults, while ankle plantarflexor power is reduced compared to young adults. Differences in joint energetics between age groups during stance phase seem to show age related changes to mechanics persisting despite the additional challenge of an obstacle. The statistical significance of these changes will be explored as the sample size is increased.

## ACKNOWLEDGEMENTS

Funding for this study was provided by the University of Melbourne and an ARC Discovery Project grant (DP200103583).

## REFERENCES

1. Hausdorff J, et al., *Archives of Physical Medicine and Rehabilitation.* **82**:1050-1056, 2001
2. Waanders J, et al., *Medicine & Science in Sports & Exercise.* **51**:615-623, 2019.

# SHAPE MODELLING REVEALS AGE-RELATED KNEE BONY SHAPE CHANGES IN ASYMPTOMATIC KNEES

[1]Katherine Nguyen, [1,2]Diana Perriman, [3]Jennie Scarvell, [4]Mark Pickering, [5]Catherine Galvin, [2]Paul Smith and [1,2]Joseph Lynch

[1]School of Medicine and Psychology, The Australian National University, Canberra, ACT
[2]Trauma and Orthopaedic Research Unit, The Canberra Hospital, Canberra, ACT
[3]Faculty of Health, University of Canberra, Canberra, ACT
[4]School of Engineering and Information Technology, University of New South Wales at ADFA, Canberra, ACT
[5]College of Engineering, Computing and Cybernetics, The Australian National University, Canberra, ACT
email: Katherine.Nguyen@anu.edu.au

## INTRODUCTION

Osteoarthritis (OA) causes bony shape changes within the knee [1]. Furthermore, the risk of developing OA increases with age. However, age alone does not cause OA. It is therefore important to understand the healthy age-related trajectories of knee shape before attributing these changes to OA. The aim of this study was to determine the association between bony knee shape and age using statistical-shape modelling (SSM).

## METHODS

109 participants (52 females, 57 males), aged between 20 to 90, received a CT scan of their knee. Three-dimensional models were created using manual segmentation using custom software Orthovis v4 (Matlab, Mathworks, Inc., Natick, MA). Separate SSM's for the distal femur and proximal tibia were created. A template surface mesh was iteratively fit to all meshes in the dataset using radial basis functions, resulting in a training set of correspondent meshes. Meshes in the training set were rigidly aligned using a partial Procrustes analysis to account for size scaling in the model. Principal Component Analysis (PCA) was performed on the training set to create the SSM. Linear regression models were performed on the PCA weights to assess the association between age and femoral and tibial shape.

## RESULTS AND DISCUSSION

Fourteen modes of the femoral and tibial SSM's captured 67% and 73% shape variation, respectively. Femoral mode 4 and tibial modes 1, 2, 6 and 14 were associated with age. Proximal tibial and distal femoral bone size was positively correlated with aging, and we suggest that increase in femoral bone size could be part of the normal aging process and that bone increases in size to adapt to mechanical loading over time. An increase in age was also associated with an increase in the medial and lateral femoral condylar heights ($\beta = 0.398$) and an increase of the femoral trochlear depth (Figure 1). Since femoral trochlear depth is related to patellar dislocation [2], a deeper trochlear could be a protective mechanism as people age to increase patellar stability. In the tibia, aging was associated with a medial expansion of the tibial medial plateau (Figure 2); a decrease in the distance between the proximal tibio-fibular joint and the intercondylar eminence ($\beta = 0.478$). Increased tibial plateau area is known to associate with the development and progression of knee OA [3]. This suggests that the increase in tibial plateau area is part of the aging process.

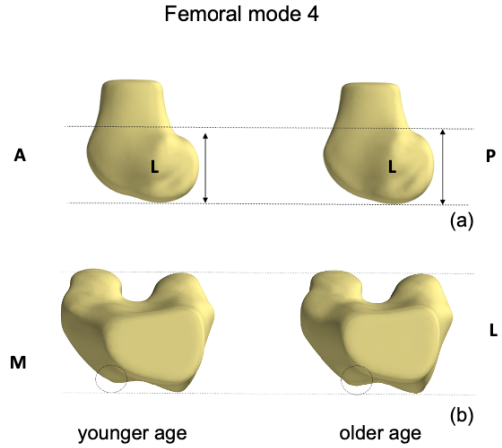


**Figure 1**. Shape variations captured in Femoral mode 4, showing increasing femoral condylar height, and a raised lateral patello-femoral apex, with older age. (M, medial; L, lateral; A, anterior; P, posterior)

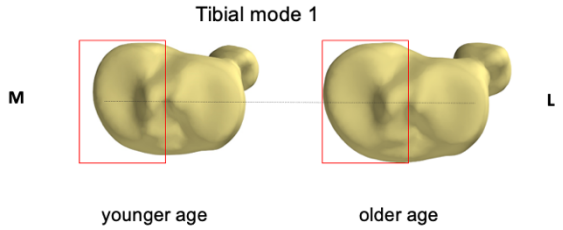


**Figure 2.** Shape variations captured in Tibial mode 1, showing decreasing and increasing size of the medial tibial plateau, with older age. (M, medial; L, lateral)

## CONCLUSIONS

Aspects of bony femoral and tibial shape were significantly associated with aging, including femoral and tibial bone size, femoral condylar heights, and medial tibial plateau area. These changes occur as a normal process of aging without osteoarthritis development. This is likely a response to mechanical loading over time. Further research investigating the effect of these changes on loading in the knee may provide valuable information for knee health in older age.

## REFERENCES

1. Wise BL, et al., *Clinical Orthopaedics and Related Research*. **478**, 2020
2. Powers CM, *Physical Therapy*. **80**:965-973, 2000
3. Ding C, et al., *Osteoarthritis Cartilage*, **15**: 479-486, 2007


# Thursday, December 9

## KEYNOTE 3 – Prof Haxby Abbott

"The Diagnosis and Management of Osteoarthritis in Aotearoa New Zealand"


# Thursday, December 9

## PODIUM 7

# IMU-AUGMENTED PATIENT REPORTED OUTCOME MEASURES FOR ESTIMATING POST-OPERATIVE PATIENT SATISFACTION

[1,4]Justin Fernandez, [1]Sabina Yang, [1]Shasha Yeung, [2]Faseeh Zaidi, [1]Sebastian Weaver, [2]Scott Bolam, [2]Megan Lovatt, [1,4]Thor Besier, [3]Jacob Munro, [5]Michael Hanlon, [1,3]Paul Monk, [1]Ted Yeung

[1]Auckland Bioengineering Institute, University of Auckland, New Zealand
[2]Faculty of Medical and Health Sciences, School of Medicine, New Zealand
[3]Faculty of Medical and Health Sciences, Surgery, New Zealand
[4]Department of Engineering Science and Biomedical Engineering, University of Auckland, New Zealand
[5]Domain Orthopaedic Surgeons, Auckland, New Zealand
email: j.fernandez@auckland.ac.nz

## INTRODUCTION

One in five patients experiences dissatisfaction following knee replacement surgery that is not explained by existing outcome assessments used in the clinic, such as patient-reported outcome measures (PROMs) [1]. Biomechanical variables such as joint kinematics and forces can be used as objective measures of outcome assessment and may explain inconsistencies in patient satisfaction when coupled with PROMs. These measurements could be collected using low-cost accessible wearable sensors such as Inertial Measurement Units (IMUs) in-clinic and out-of-clinic. IMUs remove subjectivity and the possibility of misinterpreting questionnaires. This study aimed to determine the best combination of PROMs and IMU-derived biomechanical measures for predicting postoperative patient satisfaction.

## METHODS

Synced Optical Motion Capture (OMC) and IMU data were collected from 28 patients (13 females and 15 males; 23 TKR and 5 UKR, age: 68.2 ± 6.2; height: 1.67 ± 0.11 m; body mass: 87.5 ± 19.4 kg; BMI: 31.3 ± 5.4 kg/m2, overground walking).

Knee contact forces (KCF) were calculated via biomechanical simulation in OpenSim [2] and regression models were built to predict the KCF from IMU features [3]. These features were then used to train surrogate models for predicting patient satisfaction.

Twenty-eight patient datasets (IMU + PROMs) were used to build patient satisfaction models at four time points: during physiotherapy, six weeks, six months, and one year after surgery. In addition, post-operative PROMs including the Oxford Knee Score (OKS), and EQ-5D-5L visual analogue scale, and IMU measurements during physiotherapy sessions were collected from knee arthroplasty patients.

## RESULTS AND DISCUSSION

Selected features could accurately ($R2 > 0.90$) predict the total KCF of participants across the stance phase 84% of the time. Using this result, a model to predict the EQ-5D-5L score using OKS and IMU time-series features associated with knee kinematics and KCF during the patients' recovery period was created for the four time points. The most important combinations of variables for each time point were OKS, knee kinematics with OKS, KCF with OKS, and KCF only, respectively. The chosen models were able to predict EQ-5D-5L scores within a mean difference of 0.070±4.33, 1.11±2.51, 0.29±1.85, and 0.23±1.58 units of the actual (95% confidence interval) for each time point (Figure 1).

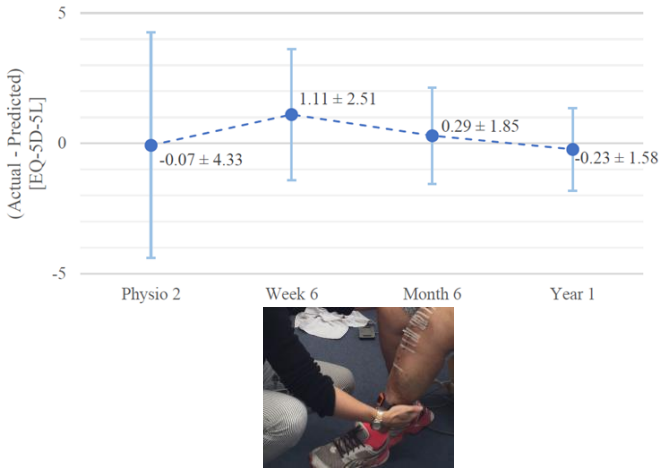


**Figure 1:** The mean difference and 95% confidence interval between the actual and predicted patient satisfaction across the four time points.

## CONCLUSIONS

We have created a clinically useful predictor of patient satisfaction corresponding to knee contact force and OKS. A further benefit of the presented approach is that we can easily predict a patient's gait parameters if their score suggests that more information is needed to assess joint function.

## ACKNOWLEDGEMENTS

We acknowledge the Science for Technological Innovation fund for supporting this study.

## REFERENCES

1. D. Beverland, *Orthopedics* **33**: 9, 2010.
2. S. L. Delp et al., *IEEE. Trans. Biomed. Eng*. **54**: 11, 2007.
3. M. Christ et al., *Neurocomputing* **307**, 2018.

# TIBIAL NAILING PATIENTS EXHIBIT FUNCTIONAL DEFICITS UP TO 18 MONTHS FOLLOW-UP COMPARED TO HEALTHY CONTROLS: A PROSPECTIVE RANDOMISED CONTROLLED PILOT STUDY

[1]Simon Thwaites, [1,2]Mark Rickman, [1,2]Dominic Thewlis

[1]Centre for Orthopaedic & Trauma Research, University of Adelaide, Adelaide, SA, Australia
[2] Department of Orthopaedics & Trauma, Royal Adelaide Hospital, Adelaide, SA, Australia
email: simon.thwaites@adelaide.edu.au

## INTRODUCTION

Intramedullary nailing (IM) is the gold standard for treating adult tibial shaft fractures. However, the optimal nail insertion technique remains inconclusive. Studies commonly describe various patient-reported outcome measures (PROMs) for pain and function, yet few studies [1] report objective, performance-based outcomes. Therefore, this prospective study aimed to investigate PROMs and performance-based outcomes following tibial nailing against a healthy reference group at 3, 6, 12, and 18 months follow-up. It was hypothesised all outcomes would be equivalent to the healthy group after 18 months follow-up.

## METHODS

Patients were recruited through an ongoing randomised controlled trial (ANZCTR: ACTRN12620000109909) comparing infrapatellar (IP) and suprapatellar (SP) nailing of extraarticular tibial shaft fractures [2]. Healthy volunteers were case-matched for age, sex, height, and body mass. PROMs included a visual analogue scale for anterior knee pain ($VAS_{AKP}{}_0^{10}$), and the Knee Injury and Osteoarthritis Outcome Score – Patellofemoral Subscale ($KOOS\text{-}PF_0^{100}$). Motion trials were captured using a marker-based approach, and included: gait, squatting, hopping, anterior reach, stair ascent, and stair descent. Variables of interest were sagittal plane joint angles, moments, and power, at the hip, knee, and ankle. Data were processed using Matlab (vR2022b), OpenSim (v4.3), and R (v4.2.2). MAPClient informed scale factors for gait [3] and deep squat [4] OpenSim models. Unpaired Student t-tests or Wilcoxen tests were used for group differences following Shapiro tests for normality. Statistical parametric mapping (SPM) [5] was used to analyse differences in time-series data.

## RESULTS AND DISCUSSION

$VAS_{AKP}{}_0^{10}$ was equivalent to the healthy reference at 6 months for both IP and SP groups whilst $KOOS\text{-}PF_0^{100}$ remained significantly different ($p<0.05$) up to 18 months (Table 1). Differences ($p<0.05$) in time-series data existed up to 18 months for squatting, hopping, anterior reach, stair ascent, and stair descent. Squatting joint angles are displayed in Figure 1, showing decreased ankle dorsiflexion during the eccentric phase at 18 months.

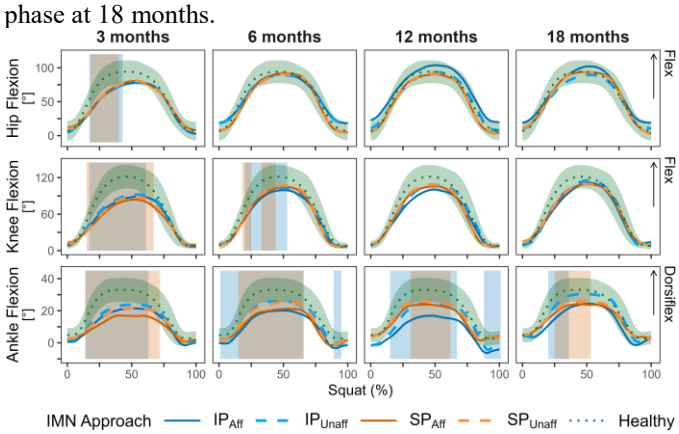


**Figure 1:** Mean squat joint angles for affected (Aff) and unaffected (Unaff) limbs for IP and SP patients. Healthy data has ± SD band. Regions of statistically significant differences between the affected limbs of IP and SP patients and the healthy group from SPM analyses are highlighted with vertical bands.

## CONCLUSIONS

Tibial nailing patients may exhibit functional deficits for up to 18 months follow-up, and perhaps longer, which is longer than the current clinical expectations of patient recovery in this cohort. As such, utilising performance-based outcomes may enhance reporting following IM nailing of tibial shaft fractures.

## ACKNOWLEDGEMENTS

The project was funded via an investigator-initiated research grant awarded by Stryker Corporation (Grant Number: N/A).

## REFERENCES

1. MacDonald D et al. *Eur J Tr Em Sur* **46**: 93-98, 2020
2. Thwaites S et al. *Pilot Feas Stud* **8**: 110-122, 2022
3. Delp, S et al. *IEEE Trans Biom Eng* **37**: 757-767, 1990
4. Catelli D et al. *CMBBE* **22**: 21-24, 2019
5. Patakay T *J Biomech* **15**, 295-301, 2012

**Table 1:** PROMS (mean ± SD) for clinical and healthy cohorts. Significant difference ($p<0.05$) from healthy indicated in bold.

| | 3 months | | 6 months | | 12 months | | 18 months | | Healthy |
|---|---|---|---|---|---|---|---|---|---|
| | IP | SP | IP | SP | IP | SP | IP | SP | |
| | (n = 9) | (n = 11) | (n = 9) | (n = 10) | (n = 5) | (n = 9) | (n = 5) | (n = 7) | (n = 18) |
| $VAS_{AKP}{}_0^{10}$ | **3.7±2.2** | 3.1±2.9 | 2.4±2.2 | 1.6±2.2 | 1.9±2.3 | 2.3±3.0 | 2.3±2.5 | 2.1±3.4 | 0.2±0.7 |
| $KOOS\text{-}PF_0^{100}$ | **41.9±16.3** | **53.5±22.9** | **60.9±18.2** | **74.8±17.5** | **65.0±18.8** | **64.9±18.2** | **70.9±27.3** | **73.4±28.1** | 94.7±12.5 |

# DOES MANUFACTURING METHOD, PATIENT AGE OR ARTICULATION SIZE AFFECT THE LONG-TERM WEAR RATE OF HIGHLY CROSS-LINKED POLYETHYLENE LINERS IN TOTAL HIP ARTHROPLASTY?

[1,2]Stuart Callary, [1,2]Deepti Sharma, [1]Taisha D'Apollonio, [1,2]Bogdan Solomon and [1,3]David Campbell

[1]Centre for Orthopaedic and Trauma Research, The University of Adelaide, Adelaide, SA, Australia
[2]Department of Orthopaedics and Trauma, Royal Adelaide Hospital, Adelaide, SA, Australia
[3]Wakefield Orthopaedic Clinic, Calvary Hospital, Adelaide, SA, Australia
email: stuart.callary@adelaide.edu.au

## INTRODUCTION

Radiostereometric analysis (RSA) is the most accurate method to measure *in-vivo* wear of highly cross-linked polyethylene (XLPE) liners [1]. Less sensitive measurement methods from plain radiographs often report higher than expected wear rates and the variation within results inhibits correct clinical interpretation. RSA studies have confirmed the very low wear rate of XLPE liners at mid-term follow-up [2] however, there is a paucity of long-term (>10 years) studies. Previously used polyethylene implants wear rate has been affected by three factors including, manufacturing method, articulation size and patient age. Hence the aim of this study was to measure the long-term wear of different designs of XLPE liners against larger articulations and in patients of varying age groups.

## METHODS

153 patients previously enrolled in six specific cohorts underwent further RSA examinations at 7-, 10-, and 14-years follow-up (Table 1). The proximal femoral head penetration (FHP) was calculated between the day 2 RSA exam and latest follow-up. The proximal wear rate was calculated as the slope of the FHP between one year and latest follow-up.

## RESULTS AND DISCUSSION

The mean proximal wear rate of one XLPE liner manufactured with a low irradiation dose (5Mrad) was significantly higher than two liners irradiated with 9- and 10-Mrad ($p<0.001$, Fig 1). Non-inferiority of XLPE wear rates against larger articulations (36/40mm) was supported when compared to standard articulations (28/32mm, Figure 2). This supports the use of larger femoral heads to reduce the risk of dislocation. Non-inferiority of XLPE wear rates in younger patients (40-64years) was supported when compared to older patients (65-74years). This supports the use of these implants in young patients who have longer life expectancy and require implant longevity.

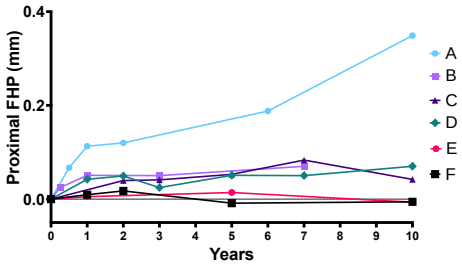


**Figure 1.** The median FHP for each cohort up to 10 years

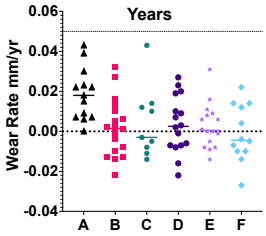


**Figure 2.** The median proximal wear rate of all cohorts. No individual was above the threshold associated with osteolysis (0.05mm/yr, dotted line)

## CONCLUSIONS

The low long-term wear rates (<0.02mm/year) are encouraging for the continued excellent survivorship of XLPE implants in their second decade of use. Companies introducing new designs of XLPE liners need to be aware that larger irradiation dose does result in a decreased long term *in vivo* wear rate.

## ACKNOWLEDGEMENTS

Stuart Callary was supported by a Research Fellowship from The Hospital Research Foundation Group during this study.

## REFERENCES

1. Callary S, et al., *J Ortho Res.* **35**:988-996, 2017.
2. Callary S, et al., *Acta Ortho.* **86**:159-168, 2015.

**Table 1:** Patient and implant details for the six cohorts

| Cohort | XLPE Type | Manufacturing Irradiation Dose | Age (yrs) | Head Size (mm) | M:F | Patients Recruited | Time Points |
|---|---|---|---|---|---|---|---|
| **A** | Marathon™ | 5 Mrad | 55-80 | 28 | 10:16 | 29* | 1, 6 & 14yrs |
| **B** | Longevity™ | 10 Mrad | 65-74 | 28 | 13:14 | 27 | 1, 2, 3, 5, 7 & 10 yrs |
| **C** | Longevity™ | 10 Mrad | 65-74 | 36 | 15:14 | 29 | 1, 2, 3, 5, 7 & 10 yrs |
| **D** | Longevity™ | 10 Mrad | 40-64 | 28 | 15:13 | 28 | 1, 2, 3, 5, 7 & 10 yrs |
| **E** | X3™ | 3 x 3 Mrad | 47-76 | 32 | 11:10 | 21 | 1, 5 & 10 yrs |
| F | X3™ | 3 x 3 MRad | 55-76 | 36/40 | 13:6 | 19 | 1, 5 & 10 yrs |

# KINEMATICS ARE AN INDICATOR OF OUTCOME AFTER TOTAL KNEE REPLACEMENT

[1,2]Joe Lynch, [1]Owen Rabak, [1]Pip Hodge, [1,2]Diana Perriman, [2,3]Jennie Scarvell, [1,2]Paul Smith

[1]Australian National University, Canberra, ACT
[2]Trauma and Orthopaedic Research Unit, Canberra; ACT
[3]Faculty of Health, University of Canberra, ACT
email: Joe.lynch@act.gov.au

## INTRODUCTION

Total knee replacement (TKR) is largely successful in reducing pain and restoring function following knee osteoarthritis. However, a proportion of patients are dissatisfied postoperatively [1] and it is unclear why. The ability to perform higher-demand activities including deep-kneeling and step-up are important for post-operative satisfaction but remain difficult for some [2,3]. Knee kinematics are complex and may influence performance of higher-demand activities which, in turn may influence outcomes after TKR. The aim of this study was to examine the relationship between step-up and deep-kneeling knee kinematics and patient-reported outcome measures (PROMS) following TKR.

## METHODS

64 patients were included at minimum 1-year follow-up. Participants performed a step-up and deep-kneeling task which was imaged via single-plane fluoroscopy. 3D prosthesis CAD models were registered to the fluoroscopy, yielding in-vivo kinematic data. At the same timepoint patients completed PROMS: Oxford Knee Score (OKS), American Knee Society Score (AKSS), Surgical Satisfaction and Pain Visual Analogue Scales. Associations between kinematics and PROMS were assessed using step-wise log-transformed linear regression models.

## RESULTS AND DISCUSSION

Kinematic factors were moderately associated with outcomes (Figure 1). For deep-kneeling, a higher total OKS was associated with more external femoral rotation and more adduction at maximal flexion. For step-up, a better total OKS was associated with more internal femoral rotation (β= -0.012; exp(β)= 0.988) and a smaller flexion angle at terminal extension rotation (β= -0.005; exp(β)= 0.995). Greater surgical satisfaction was associated with greater maximum flexion (β = -0.092; exp(β) = 0.912), more external femoral rotation at maximum flexion (β = 0.098; exp(β) = 1.103), more posterior translation at maximal flexion (β= -0.049; exp(β)= 0.953) and more adduction at maximal flexion (β= -0.151; exp(β)= 0.860) during deep-kneeling. Decreased pain VAS was associated with greater maximum flexion (β= -0.073; exp(β)= 0.930), more external femoral rotation (β= 0.088; exp(β)= 1.092), more adduction (β= -0.217, exp(β)= 0.805) and more posterior translation at maximal flexion (β= -0.060; exp(β)= 0.942) during deep-kneeling. Decreased pain VAS was also associated with more internal rotation at terminal extension during step-up.

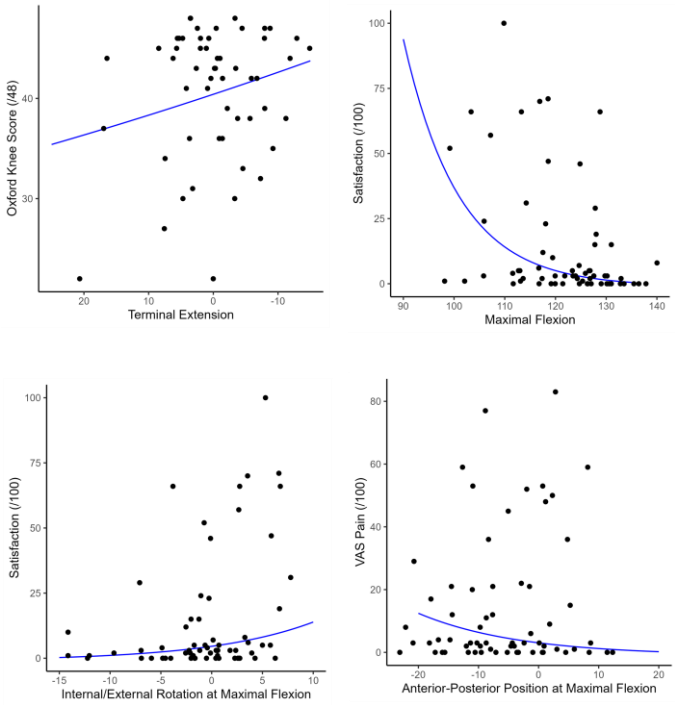


**Figure 1:** Results of log-linear models for OKS (top left); Satisfaction (top right, bottom left); and VAS Pain (bottom right)

## CONCLUSIONS

The kinematics of end of range flexion and extension during high demand tasks seem to be most associated with satisfaction and other outcome measures. Most importantly the component kinematics are individually associated with outcomes indicating that full rotation range as well as translation and even adduction for full flexion should be considered after TKR

These results have implications for the importance of rehabilitation and implant design. There needs to be a continued focus on optimising the kinematics of high-range terminal flexion and extension in total knee replacement and an expectation that these ranges are possible after TKR.

## CONCLUSIONS

[1] Bourne et al CORR, 468(1): 57 2010
[2] Dunbar et al. Bone Joint J. 96-B(10): 1285, 2014
[3] Maratt et al J Arthroplasty 30(7): 1142, 2015

# OUTCOMES OF SECONDARY PATELLA RESURFACING FOR DISSATISFACTION FOLLOWING PRIMARY KNEE ARTHROPLASTY: A SYSTEMATIC REVIEW AND META-ANALYSIS OF 604 KNEES

[1,2]Octavian Andronic, [3]Vishwa Suravaram, [4]Victor Lu, [1]Simon J. Wall, [1]Thomas A. Bucher, [1]Gareth H. Prosser, [1]Piers J. Yates and [1,5]Christopher W. Jones

[1]The Orthopaedic Research Foundation of Western Australia (ORFWA), 6150 Perth, Australia
[2]Balgrist University Hospital, University of Zurich, Forchstrasse 340, 8008, Zurich, Switzerland
[3]Faculty of Medicine, Dentistry and Health Sciences, The University of Western Australia, 6009 Perth, Australia
[4]School of Clinical Medicine, University of Cambridge, CB2 0SP, United Kingdom
[5]Curtin University, Bentley, Perth, Australia 6120
email: octavian.andronic@balgrist.ch

## INTRODUCTION

Secondary patella resurfacing (SPR) may be performed for dissatisfaction following primary total knee arthroplasty (TKA) where the native patella was retained. The purpose of this meta-analysis was to evaluate outcomes of SPR.

## METHODS

The systematic review followed the PRISMA guidelines and its protocol was prospectively registered (PROSPERO): CRD42023399062. Studies reporting on patients that underwent secondary patella resurfacing after previous primary total knee replacement with retention of the native patella were considered eligible. The risk of bias was assessed using the Methodological index for non-randomized studies (MINORs) tool. A random-effects model and the inverse-variance weighting method was used for meta-analysis.

## RESULTS AND DISCUSSION

Sixteen retrospective studies including a total of 604 knees (594 patients) with a mean follow up of 42 months (range 2 to 197 months) were included. An overall improvement in patient-reported outcomes (PROMs) was achieved in 53% of cases (Figure. 1) from pooled data available for 293 knees [95% CI (0.44, 0.62), $I^2$=68% - moderate heterogeneity]. The pooled proportion of patients satisfied with the SPR was 59% [95% CI (48, 68), $I^2$ = 70% - moderate heterogeneity] in a sample size of 415 (Figure 2). There was a minimal rate (2%) of complication incidence when performing SPR and a pooled rate of revision surgery of 10%.

## CONCLUSIONS

An improvement in pain, satisfaction and PROMs was achieved in slightly more than half of patients following SPR. Studies lacked standardized selection criteria and were based on subjective judgement for undergoing SPR. Available data was retrospective only, highly heterogenous and had significant variation and inconsistency in the methods used for reporting outcomes.

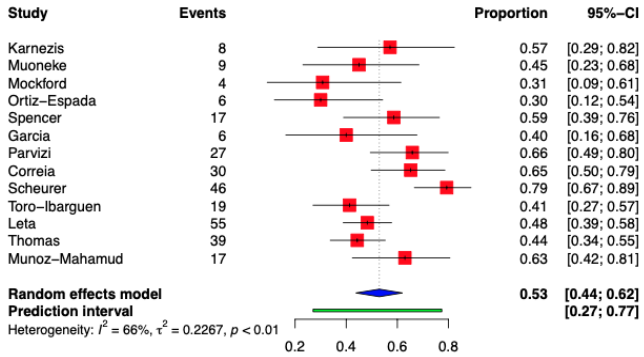


**Figure 1:** Proportion forest plot comparing patients that experienced improvement in PROMs from those who did not. Event: improvement in PROMs. The size of the square represents the weight that the corresponding study exerts. $I^2$ represents the value of calculated heterogeneity.

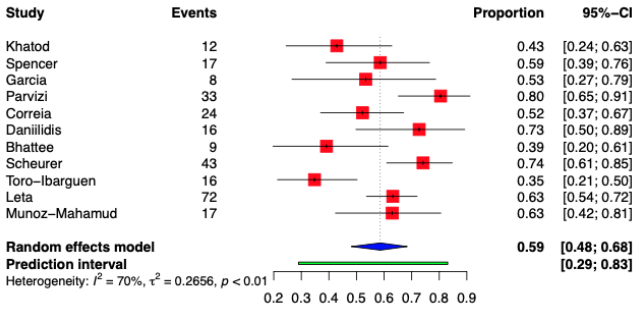


**Figure 2:** Proportion forest plot comparing patients that were satisfied following secondary patella resurfacing from those who were not. Event: postsurgical satisfaction. The size of the square represents the weight that the corresponding study exerts. $I^2$ represents the value of calculated heterogeneity.

# Thursday, December 9

## PODIUM 8

# MODES OF FAILURE IN FLEXED OVINE LUMBAR MOTION SEGMENTS SUBJECTED TO IMPACT LOADING

[1]Vonne M. van Heeswijk, [2]Peter A. Robertson, [1]Ashvin Thambyah and [1]Neil D. Broom

[1]Experimental Tissue Mechanics Laboratory, University of Auckland, Auckland, New Zealand
[2] Department of Orthopaedic Surgery, Auckland City Hospital, Auckland, New Zealand.
email: v.m.vanheeswijk@auckland.ac.nz

## INTRODUCTION

Low back pain and sciatica are commonly caused by herniation of an intervertebral disc. Previous research has shown that herniations can be successfully induced *in vitro* by compressing healthy ovine lumbar motion segments while flexed at a rate of 40 mm/min or 400 mm/min [1,2]. The higher compressive rate of 400 mm/min approximates the fastest muscle response rate when surprise loaded [2]. Interestingly, compressing flexed healthy ovine lumbar motion segments at 40 mm/min induced herniations in 58% of the tested samples [1] whereas a higher compressive rate of 400 mm/min resulted in a higher percentage of 83% of samples failing by herniation [2]. While many spine-related accidents involve impact loading, it is not known whether such loading increases even further the likelihood of herniation. Therefore, this new study aims to investigate whether impact loading might further increase the likelihood of herniation in flexed ovine lumbar motion segments.

## METHODS

Twenty-three ovine lumbar motion segments were included in this study. Each segment was fully hydrated in 0.15M saline overnight and prior to mechanical testing creep loaded at ~300 N for 1 hour to reduce their hydration to a more realistic level. Each motion segment was then mounted in an impact loading rig and flexed 7°. The flexed sample was impacted by dropping a mass of 4.3 kg from a height of 0.8 m while preventing any re-bound loading. Preliminary tests showed that a single impact with this combination of drop mass and height induces structural failure relatively close to the motion segment's limits of mechanical tolerance. After formalin fixation and formic acid decalcification, each sample was externally assessed for herniations and then cut sagittally to examine macroscopically the internal structure of the sample.

## RESULTS AND DISCUSSION

Of the 23 impacted segments, eight contained externally visible herniations (i.e. 35% of the samples) and six of these exhibited multiple herniation sites. Interestingly, out of the total of 16 herniations nine were observed in the lateral disc regions. All lateral herniations involved nuclear extrusion.

The internal structural examination by sagittal bisection revealed that one of the herniated samples also contained an obvious fractured endplate. In all remaining 15 segments (i.e. 65% of the samples), a fractured endplate was a common feature.

While the posterior and posterolateral disc regions are commonly associated with herniations via direct radial rupture of the annulus [3,4], more recent structural studies of flexed ovine lumbar motion segments compressed to failure at 40 mm/min have shown the lateral regions to be the primary site of internal disruption. From these lateral internal disruptions nuclear tissue then tracks circumferentially within the annulus towards the posterolateral aspect and can become externally visible in the well-acknowledged posterolateral and posterior herniation regions [5,6]. That most externally visible herniations in this study were observed in the lateral regions indicates that the lateral disc periphery can also be involved in the herniation mechanism under impact loading conditions. These findings support the idea that the lateral regions of the disc may have relevance to the broader study of disc herniation.

## CONCLUSIONS

This new study indicates that impact loading of flexed ovine lumbar motion segments is more likely to induce endplate fractures than herniations. Whereas lower rates of compressive loading of 400 mm/min and even as low as 40 mm/min are more likely to induce herniations [1,2].

## ACKNOWLEDGEMENTS

The authors gratefully acknowledge the Wishbone Orthopaedic Research Foundation and Medtronic Australasia for funding this study.

## REFERENCES

1. Wade KR, et al., *Spine*. **39**:1018-1028, 2014.
2. Wade KR, et al., *Spine*. **40**:891-901, 2015.
3. Maezawa S, et al., *Spine*. **17**:1309-1315, 1992.
4. Ninomiya M, et al., *Spine*. **17**:1316-1322, 1992.
5. Van Heeswijk VM, et al., *Spine*. **42**:1604-1613, 2017.
6. Van Heeswijk VM, et al., *Spine*. **43**:467-476, 2018.

# BIOMECHANICAL EFFECT OF DECOMPRESSIVE TECHNIQUES ON LUMBAR SPINE

[1]Sara Montanari, [2]Elena Serchi, [3]Giovanni Barbanti Brodano, [2]Alfredo Conti and [1]Luca Cristofolini

[1]Department od Industrial Engineering, Alma Mater Studiorum – University of Bologna, Bologna, Italy
[2]Neurosurgery Unit, IRCCS Istituto delle scienze neurologiche, Bellaria Hospital, Bologna, Italy
[3]Spine Surgery Unit, IRCCS Istituto Ortopedico Rizzoli, Bologna, Italy
email: sara.montanari22@unibo.it

## INTRODUCTION

Lumbar spinal stenosis causes the compression of neurovascular structures. Different decompression techniques remove parts of the posterior elements so as to increase the space in the spinal canal. Removal of these structures is suspected to aggravate or create spinal instability [1]. Therefore, these surgical techniques are often completed by a posterior fixation. In addition, changes in anatomy and in the load distribution could also alter the disc strains.

The aim of this study was to investigate the biomechanical effect of decompressive techniques, alone or with a posterior fixation, in the lumbar spine, in terms of mechanical stability and strains on the intervertebral discs.

## METHODS

Twelve L2-S1 spine cadaver segments were prepared preserving all the main ligaments, but removing the soft tissues around the discs and the vertebral bodies. A white random speckle pattern was sprayed to measure surface strains with Digital Image Correlation (DIC). All the specimens were mechanically tested in flexion, extension, right and left lateral bending ( 2.5 Nm). Each specimen was tested in 4 conditions:

i) in the *intact* condition;
ii) after L4-L5 *hemilaminectomy*;
iii) after full L4-L5 *laminectomy*;
iv) after L4-S1 *fixation* with pedicle screws and rods.

All the surgical procedures were performed by a surgeon; the side of the hemilaminectomy was selected randomly.

Images were acquired by a 3D-DIC system with 4 cameras (GOM Aramis 12M). Image correlation were performed using optimized parameters [2]. The Range of motion (RoM) and the tensile (Ɛ1) and compressive (Ɛ2) principal strains distribution were computed for each loading configuration.

## RESULTS AND DISCUSSION

Correlations and measurements were successfully performed for all the loading configuration and all conditions. Data were analyzed at the stage where the maximum moment of 2.5 Nm was reached. No statistically significant changes ($p>0.05$, Friedman test) were observed after the hemilaminectomy neither for the Rom nor for the strains in the L4-L5 IVD. The statistically significant ($p<0.05$, Friedman test) increase in RoM after laminectomy suggests a loss of stability in flexion and in lateral bending on the opposite side where the hemilaminectomy was performed (contralateral bending). Contralateral bending was the most challenging loading configuration also due to the statistically significant increase in maximum tensile strain on L4-L5 disc surface after laminectomy ($p<0.05$, Friedman test) (Fig. 1). Preliminary results about the effects of fixation showed a significant reduction of both RoM and tensile and compressive L4-L5 disc with respect to the intact condition.

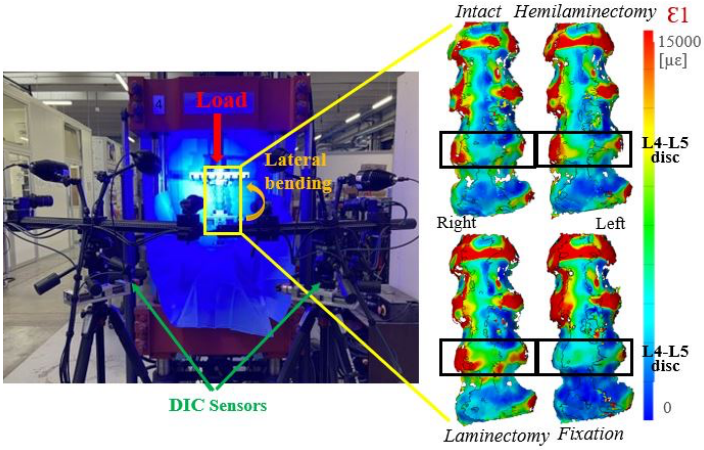


**Fig. 1:** Left: set-up for the mechanical test with the dedicated loading jig and the 4-camera DIC system. Right: distribution of DIC-measured maximum tensile strains (Ɛ1) on the vertebrae and IVD during contralateral bending the 4 conditions.

## CONCLUSIONS

This study aimed to evaluate the risk of instability and changes in the strain distribution after lumbar spinal decompression, performed by hemilaminectomy or laminectomy, and fixation. These preliminary results showed that the hemilaminectomy did not affect the biomechanics of the lumbar spine. The increased RoM in flexion, after laminectomy, did not seem to damage the L4-L5 disc. Indeed, no significant increases in strain were observed. Conversely, in the contralateral bending both the maximum tensile strain and RoM increased.

## ACKNOWLEDGEMENTS

Funded by Emilia Romagna Region (FIN-RER “Archimede”)

## ETHICS:

Bioethics Committee of UniBo (Prot. 113043 of 10 May 2021)

## REFERENCES

1. Zaina et al, *Cochrane Database Sys Rev*, Jan 29, 2016
2. Palanca et al, MEP, **52**: 76-83, 2018.

# INFLUENCE OF THE LUMBAR ENDPLATE AND CAGE RELATED FACTORS ON CAGE-ENDPLATE CONTACT: A CADAVERIC STUDY

[1]Yihang Yu, [1]Dale Robinson, [1]David Ackland, [2]Yi Yang and [1]Peter Vee Sin Lee

[1]Department of Biomedical Engineering, University of Melbourne, Melbourne, VIC, Australia
[2]Department of Orthopaedics, Royal Melbourne Hospital, Melbourne, VIC, Australia.
email: yihangy@student.unimelb.edu.au

## INTRODUCTON

Lumbar interbody fusion (LIF) using intervertebral cages is an established treatment for lumbar degenerative disc disease, however, adverse fusion outcomes occur in 19.2% of cases and are affected by risk factors such as bone mineral density (BMD) of vertebrae, endplate geometry and cage position [1,2]. These risk factors were mostly identified from observational studies comparing radiographic-based measurements to post-operative outcomes; however, this approach does not allow direct measurement of endplate-cage contact variables that affect LIF. The aim of this study was to use cadaveric experiments, which allow precise control and measurement of volumetric BMD (vBMD) of vertebrae, cage type, position, orientation, endplate geometry and cage-endplate contact variables, to better understand the dependency between endplate/cage related factors and contact variables.

## METHODS

Five vertebral body specimens were respectively harvested from five male donors, of which there was one specimen from each of the five lumbar spine positions. The lower half of each vertebra was potted and placed in a material testing machine (Instron 8874). A spinal cage was clamped to the machine then lowered to bring it into contact against the superior endplate. A lockable ball-joint was used to rotate the cage such that its inferior surface was congruent with the local endplate surface. A pressure sensor (Tekscan) was placed between the cage and endplate to record contact area, peak and average contact stress. Axial compression of 400 N was performed for five positions using a straight cage, and in one anterior position using a curved cage (Figure 1A). Two linear mixed model analyses were performed: a) contact variables against vBMD, $A_{pred}$ and cage positions, and b) predicted contact area ($A_{pred}$, Figure 1B) against cage type, orientation and endplate concavity depths.

## RESULTS AND DISCUSSION

The linear mixed model results (Table 1) indicated that peak contact stress correlated significantly with vBMD ($p=0.041$), while average contact stress correlated with lateral cage position ($p=0.051$), while trends were observed between contact area and vBMD & $A_{pred}$ ($p=0.081$ and $p=0.057$, respectively). Also, $A_{pred}$ was significantly correlated with cage orientation ($p<0.001$). These results indicate that higher vBMD and centrally positioned cage led to higher contact stress, while lower vBMD and transverse cage position led to higher contact area.

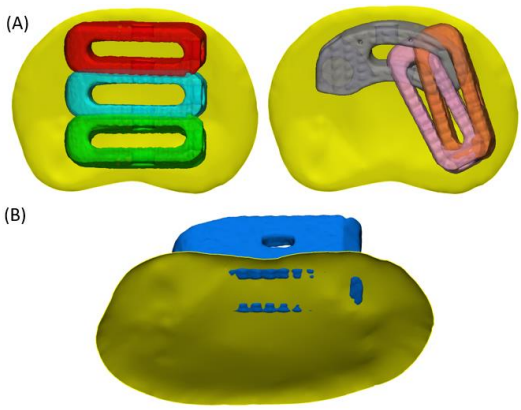


**Figure 1:** Five positions considered for spinal cage and measurement of $A_{pred}$: (A) straight cage: anterior (red), middle (blue), posterior (green), lateral (brown) and second lateral (pink); curved cage: anterior (grey); (B) the overlapped area (blue region underneath endplate) between cage and endplate (yellow) was measured as $A_{pred}$ when cage was compressed with 10% of experimental displacement.

**Table 1:** Linear mixed model results which contain trends and significant correlations.

| Dependent variable | Standardized covariates | B | p value |
|---|---|---|---|
| **Peak contact stress** | vBMD | 2.985 | 0.041 |
| **Average contact stress** | Lateral cage position | -0.216 | 0.051 |
| **Contact area** | vBMD | -26.760 | 0.081 |
| | $A_{pred}$ | 13.434 | 0.057 |
| **$A_{pred}$** | Cage orientation | -7.377 | <0.001 |

Note: B, B-coefficient representing regression slope between predictor and dependent variable

## CONCLUSIONS

In conclusion, the study identified significant correlations between vBMD, cage position and orientation on cage-endplate contact. These findings facilitate cage selection and customisation for LIF. In future work, the established correlations will be used to guide patient-specific cage design.

## REFERENCES

1. Joseph et al., *Neurosurgical focus*, **39(4)**: E4, 2015.
2. Park MK et al., *Spine J.* **19(3)**:437-47, 2019.

# CHARACTERISATION OF THE SECRETORY LYSOSOME PROTEOME REVEALS NEW REGULATORS OF OSTEOCLAST FUNCTION AND ENDOLYSOSOMAL HOMEOSTASIS

Amy B.P. Ribet[1], Yixiao Zou[1], Jamie Tan[1], Pei Ying Ng[1] and Nathan J. Pavlos[1]

[1]Bone Biology & Disease Laboratory, School of Biomedical Sciences, The University of Western Australia, Perth, WA, 6009
email: nathan.pavlos@.uwa.edu.au

## INTRODUCTION

Osteoclasts are bone-digesting cells that play a central role in the homeostatic regulation of skeletal bone mass. These multinucleated giants harbour specialized endo-lysosome-related organelles termed 'secretory lysosomes' that give rise to the ruffled border, the osteoclasts' bone-resorbing apparatus [1]. Fusion of secretory lysosomes with the ruffled border equips its membrane folds with molecular machinery required to dissolve bone mineral and excavate the underlying organic matrix [2]. Understanding the nature and contribution of secretory lysosome proteins therefore holds potential to discover new regulators of osteoclast function and thus anti-resorptive drug targets for the treatment bone-wasting diseases like osteoporosis. Using a proteomic approach, we recently resolved the molecular landscape of osteoclast secretory lysosomes and identified the sugar transporter Slc37a2 as a new and physiologically important regulator of osteoclast function and skeletal bone mass [3]. Here to further validate the utility of osteoclast secretory lysosome proteome, we interrogated the potential functional contribution(s) of a number of endo-lysosomal proteins predicted to participate in secretory lysosome membrane transport or trafficking in osteoclasts using a short-interfering RNA (siRNA)-based approach.

## METHODS

Of the 218 proteins identified on osteoclast secretory lysosomes, we selected a number of high-confidence membrane proteins from the transporter or trafficking protein families that were significantly enriched on secretory lysosome membranes (LogFC > 1.5 and $p<0.05$). siRNAs specific to each target gene were delivered into primary mouse bone-marrow macrophage (BMM)-derived osteoclasts. Knockdown efficiency was monitored by assessing the mRNA and protein levels by quantitative PCR and immunoblotting, respectively. Optical, reflective and high-resolution confocal microscopy was used to assess the impact of targeted gene suppression on key osteoclast parameters including: (i) differentiation into tartrate-resistant acid phosphatase (TRAP) positive multinucleated cells (> 3 nuclei); (ii) polarization/F-actin ring formation (iii) extracellular acidification; (iv) bone resorption on devitalized bone discs and; (v) endo-lysosomal morphology by immunofluorescence and electron microscopy.

## RESULTS AND DISCUSSION

The knockdown efficacy of our siRNA-based protocol in osteoclasts was validated by comparing the osteoclast and bone resorption phenotypes of two well-established components of osteoclast secretory lysosomes: (i) *Tcirg1,* which encodes the osteoclast-specific α3 subunit of the V-ATPase proton pump; and (ii) Sorting Nexin 10 (SNX10) an endo-lysosomal trafficking protein essential for bone digestion. The optimised protocol was then used to functionally characterize several candidate secretory lysosome genes in osteoclasts using a high-throughput screen.

Remarkably, despite all being constituents of secretory lysosome membranes, knockdown of individual target genes resulted in differential and unexpected changes in (i) osteoclast morphology, (ii) polarisation and (iii) their capacity to acidify and digest bone. In addition, knockdown of several genes lead to striking morphological disturbances in the size and positioning of osteoclast endo-lysosomes (**Figure 1**).

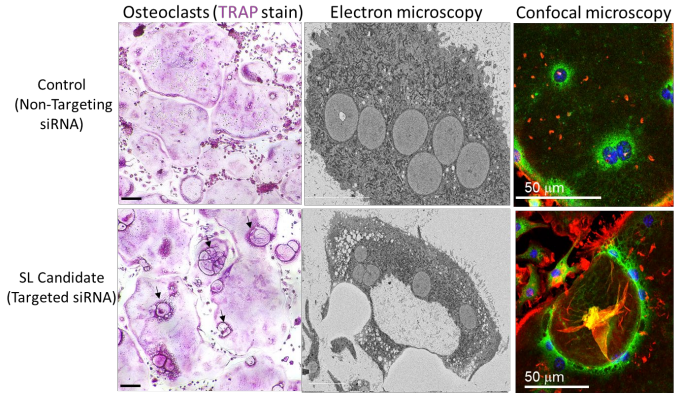


**Figure 1:** Osteoclast and endo-lysosomal phenotype following siRNA-mediated knockdown of a candidate secretory lysosome (SL) gene.

## CONCLUSIONS

Together, this work unveils several new regulators of bone resorption and endo-lysosomal homeostasis and highlights the value of coupling 'omic' based datasets with *in vitro* studies in physiologically relevant cells to validate potential regulators of osteoclast function, paving the way for future *in vivo* investigations using genetically modified organisms.

## ACKNOWLEDGEMENTS

This work is supported by NHMRC funding (APP2020097)

## REFERENCES

1. Ng et al., *Biochem Soc Trans.* **47(2)**:639-650, 2019.
2. Ribet et al., *Front Cell Dev Biol.* **9:**644986, 2021.
3. Ng, Ribet, Guo et al., *Nature Commun.*, **14(1)**:906. 2023.


# Tuesday, December 7

## POSTERS

# DEVELOPMENT OF A 3D BIOPRINTED MODEL TO INVESTIGATE NEURAL CELL RESPONSES TO WEAR DEBRIS FROM SPINAL INSTRUMENTATION AND DEVICES

David Wen, Aswini Madhavan, Javad Tavakoli, Joanne L Tipper

School of Biomedical Engineering, University of Technology Sydney, Sydney, NSW, Australia
email: davidjiawei.wen@student.uts.edu.au

## INTRODUCTION

Common biomaterials used in spinal instrumentation and devices consist of metals, polymers, and ceramics. The interfaces of spinal implants, including bearing surfaces, and endplate/bone interface may generate wear debris, which potentially induce adverse biological responses [1]. Although there has been extensive research on hip and knee replacements, information on the biological effects of wear debris produced from spinal implants on neural cells is very limited.

Recent 3D models of cast collagen hydrogels with encapsulated cells demonstrated challenges of batch-to-batch variability and inadequate long-term stability [2]. To overcome these issues, 3D bioprinting of hydrogels can provide greater precision in spatial control. Gelatin methacryloyl (GelMA) is a hydrogel that provides tailorable physical properties, and the transparent nature allows efficient examination of cellular activity inside the hydrogel. Thus, our study developed a 3D bioprinted model as a "proof of concept" to investigate neural cell responses to wear debris from spinal implants.

## METHODS

**Preparation of GelMA:** Preparation of the GelMA hydrogel solution was conducted using the GelMA Kit (CELLINK), which consisted of GelMA powder and a photoinitiator (LAP). The photoinitiator was dissolved in phosphate-buffered saline (PBS) and mixed at 60°C for 20 minutes to make a solution with 0.25% (w/v) concentration. The solution was then added to the GelMA powder and mixed at 50°C for 20 minutes to make a GelMA solution with a 5% (w/v) concentration.

**3D bioprinting of GelMA with cells and particles:** C6 astrocyte-like cells were seeded into GelMA hydrogels with appropriate volumes of Zirconia Toughened Alumina (ZTA) particles. BIO X/BIO X6 printers (CELLINK) were used to bio-print GelMA droplets into well plates, using a nozzle with gauge and inner diameter of 25G and 0.25 nm, respectively. The GelMA was printed at a pressure and speed of 10-12 kPa and 8-10 mm/s, respectively. The droplets were photo-crosslinked at 365 nm for 90 seconds. The droplets were cultured in Ham's F-12 nutrient medium, containing 15 % (v/v) horse serum, 10% (v/v) Fetal Bovine Serum (FBS) and 100 $U.ml^{-1}$ penicillin/100 $\mu g.ml^{-1}$ streptomycin, and incubated at 37°C, 5% (v/v) $CO_2$.

**Cell viability of the 3D bioprinted cell culture model:** Quantitative analysis of cell viability was conducted using luminescent ATP assay (3D CellTiter-Glo). Measurements of luminescence were obtained using the microplate reader. Qualitative analysis was performed using a live/dead assay kit, with Calcien AM (green stain) representing live cells.

## RESULTS AND DISCUSSION

The results demonstrated that C6-astrocyte like cells embedded in GelMA were viable over the duration of 5 days, when exposed to ZTA particles. The proliferation of cells was similar in both control group (GelMA and cells) and experimental group (GelMA embedded with cells and ZTA particles). These results showed that the implementation of 3D bioprinting particles with cells was feasible.

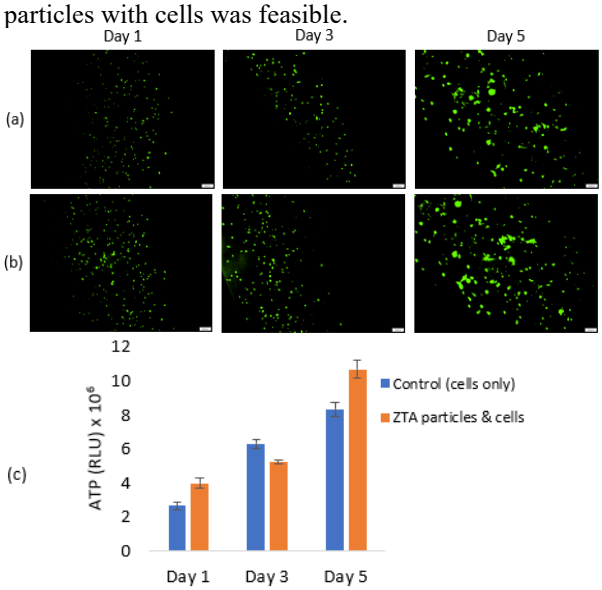


**Figure 1:** Cell viability of C6 astrocyte-like cells with ZTA particles, embedded in GelMA at days 1, 3 and 5. (a) GelMA and cells (b) GelMA embedded with cells and ZTA particles stained with Calcien AM (live cells). (c) Measurement of luminescence using ATP cell viability assay.

## CONCLUSIONS

This study showed that the "proof of concept" of bioprinting hydrogels with particles can be implemented for future studies investigating cellular responses to particles. Additionally, C6 astrocyte-like cells were viable when exposed to ZTA particles conducted in our 3D bioprinted model.

## REFERENCES

1. Punt I.M, et al., *Biomaterials.* **30**:2079-2084, 2009.
2. Lee H, et al., *European Spine Journal*. **29**:2701–2712, 2020.

# THE EFFECT OF ROTATOR CUFF TEARS AND GLENOID VERSION ON GLENOHUMERAL JOINT STABILITY AFTER REVERSE TOTAL SHOULDER ARTHROPLASTY

[1]Yichen Huang, [1]Dale L. Robinson, [1,2]Lukas Ernstbrunner, [3]Rami M. A. Al-Dirini, [3]Mark Taylor, [1]Peter Vee Sin Lee and [1]David C. Ackland

[1]Department of Biomedical Engineering, University of Melbourne, Parkville, VIC 3010, Australia

[2]Department of Orthopaedic Surgery, Royal Melbourne Hospital, Parkville, VIC 3050, Australia

[3]Medical Device Research Institute (MDRI), Flinders University, Clovelly Park, Adelaide 5043, Australia

email: yichenh2@student.unimelb.edu.au

## INTRODUCTION

Reverse total shoulder arthroplasty (RSA) is now the most widely performed shoulder replacement surgery. However, anterior instability after RSA remains the most prevalent complication, occurring at a rate of up to 9.0% [1], and is the leading cause of revision arthroplasty. Glenoid version and rotator cuff tears are known to affect the stability of the native glenohumeral (GH) joint, but little is known about the influence after RSA. The aims of this study were to develop a multi-body musculoskeletal modelling framework and to employ this framework to quantify the effects of glenoid version and rotator cuff tear on GH joint anterior stability after RSA.

## METHODS

A previously published statistical shape model (SSM) was used to generate scapular and humeral geometries of 2nd percentile (small), 50th percentile (medium) and 98th percentile (large) [1]. This was achieved by applying the mode of variation for size to the mean geometry. Similarly, four glenoid versions (6° anteversion, neutral, 6° retroversion and 16° retroversion) were generated for each scapula size.

For each GH joint geometry, RSA was virtually performed in an automated manner using Zimmer Biomet components according to the recommended surgical technique. This was achieved via a series of pre-defined rules linked to bony landmarks and implant geometries. A previously published rigid-body model matching each post-operative shoulder model was used to calculate joint reaction forces for 45° arm abduction with (i) an intact rotator cuff, (ii) an isolated tear to supraspinatus, (iii) a combined tear to supraspinatus and infraspinatus and (iv) a combined tear to supraspinatus and subscapularis (Figure 1 A) [2]. Finite element (FE) models were then developed for each post-operative shoulder. Joint force calculated from the rigid-body model was applied to the FE model, and then the joint was anteriorly dislocated in the FE simulation (Figure 1 B). Dislocation force, the force required to dislocate the joint anteriorly, was calculated for each GH joint model and used as a proxy for joint stability (Figure 1 C).

## RESULTS AND DISCUSSION

The dislocation force of the GH joint decreased substantially in the case of a rotator cuff tear, especially when a combined tear to supraspinatus and infraspinatus or to supraspinatus and subscapularis was involved. The smallest dislocation force, indicating the most inherently unstable shoulder, occurred at a combined tear to supraspinatus and infraspinatus at neutral version for the 2nd percentile shoulder (10.6% BW), at 16° retroversion for the 50th percentile shoulder (9.3% BW) and at neutral version for the 98th percentile shoulder (12.3% BW). Increasing glenoid retroversion yielded higher dislocation forces for the intact or supraspinatus deficient shoulder, suggesting the shoulder has higher capacity to sustain anterior dislocation. The intact rotator cuff combined with 16° retroversion yielded the highest dislocation force for each scapula size.

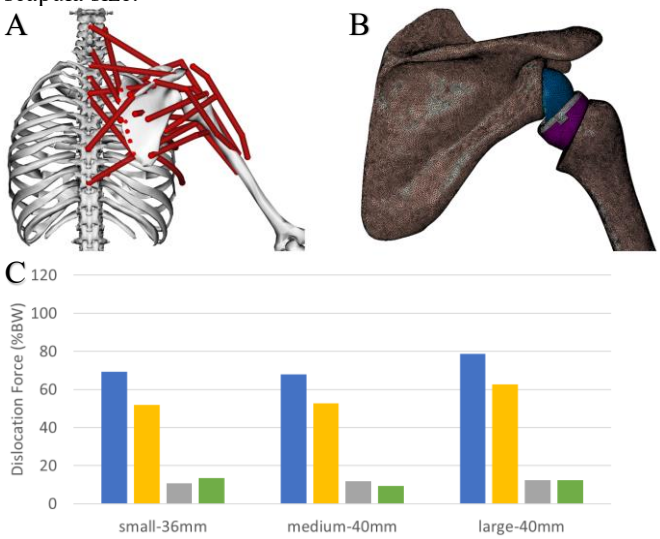


**Figure 1:** Joint force from rigid-body model (A) was used in FE model (B) to calculate anterior dislocation force for shoulder after RSA with neutral version (C).

## CONCLUSIONS

This study developed a multi-body musculoskeletal modelling framework to investigate shoulder joint anterior instability after RSA. The results show that a combined tear to supraspinatus and infraspinatus (or subscapularis) substantially reduced shoulder joint dislocation force after RSA thus increased the risk of early joint instability, while glenoid retroversion yielded a more stable joint. The findings will help to guide surgical planning, intro-operative implant positioning, and rehabilitation to RSA patients to avoid early joint dislocation.

## REFERENCES

1. Markes A.R., Cheung E. & Ma C.B. *Curr Rev Musculoskelet Med* **13**: 1–10, 2020.
2. Huang Y et al. *BMMB* **21**: 249–259, 2022.
3. Wu W et al. *J Biomech* **49**: 3623-3634, 2016.

# VARIATION IN INTERFERENCE FIT OF CEMENTLESS TIBIAL TRAYS AND ITS EFFECT ON POST-IMPLANTATION STRAIN FIELD: A MICRO-CT AND DIGITAL VOLUME CORRELATION ANALYSIS

[1]Lauren Wearne, [1]Sophie Rapagna, [2]Greg Keene, [1]Mark Taylor and [1]Egon Perilli

[1]Medical Device Research Institution, College of Science and Engineering, Flinders University, Adelaide, SA, Australia
[2]Orthopaedics Department, SportsMed, Adelaide, SA, Australia
email: lauren.wearne@flinders.edu.au

## INTRODUCTION

In order to achieve sufficient primary stability of cementless tibial trays an interference between the implant and underlying bone is established during surgery, whereby the bone is under-resected relative to the implant's geometry.

Little is known of the achieved interference (termed the actual interference), which differs from the nominal interference due to surgical variation and induced bone damage [1]. Furthermore, the resulting mechanical response of cancellous bone due to the impaction process has not been previously quantified for cementless tibial trays. The aim of this study was to quantify the actual interference and the resulting internal cancellous strain field after implantation of seven cadaveric tibiae with a commercially available cementless tibial tray.

## METHODS

Seven right human cadaveric tibiae, striped of all soft tissue, were resected and impacted with a commercially available titanium tibial tray (Attune, DePuy Synthes) by an experienced surgeon (ethics HREC 186.20). Micro-CT scans of the tibiae were procured prior to surgery (intact, at 23µm/pix) once resected (resected, 46µm/pix) and after implantation (implanted, 46µm/pix) [2]. Intact and resected micro-CT datasets were rigidly co-registered to the implanted dataset for each tibiae.

The actual interference was defined as the distance between the resected cut to the impacted position of the tibial tray, with a positive value (blue, Fig 1a) denoting an interference and a negative value (red, Fig 1a) a gap. Digital volume correlation (DVC) was performed between the resected to implanted micro-CT datasets to quantify the mechanical response of cancellous bone to implantation by extracting the internal strain field (DaVis v8.3.1, 5-step progression with a final subvolume sidelength of 1.56mm (34pix)). Algorithmic masking was applied to remove the presence of the implant (greylevels > 170) and air (greylevels < 20). The minimum principal strain component ($P_{min}$) was calculated across the entire proximal tibia, Fig 1b, with negative values representing compression, before isolating subvolumes directly under the tibial tray (within 0-1.56mm from the bone-implant interface).

Eleven volumes of interest (VOIs) were established: across each of the four pegs, across the Keel, and six across the surface of the tray. For each VOI, the median actual interference, median $P_{min}$ and bone volume fraction (BV/TV, intact dataset) were calculated. Linear regression analysis was undertaken, with actual interference and BV/TV as predictor variables and $P_{min}$ as the response variable.

## RESULTS AND DISCUSSION

An inhomogeneous actual interference was quantified across each of the seven tibial trays, with a median interference of 0.70±0.25mm across the peg VOIs (nominal 1.00mm) and 0.95±0.50mm across the Keel (nominal 1.20mm) [3]. Little interference was found in the tray VOIs (0.02±0.12mm), with 54.4±8.2% of the tray in contact with bone after impaction.

Compressive strains in the cancellous bone were quantified between the resected to implanted datasets, concentrated under the pegs and keel (-9,529±2,949µε). A statistically significant relationship was quantified between the actual interference and post-implantation strain ($R^2 = 0.450$, $p < 0.01$). No statistically significant relationship was found between BV/TV and post-implantation strain ($p = 0.885$).

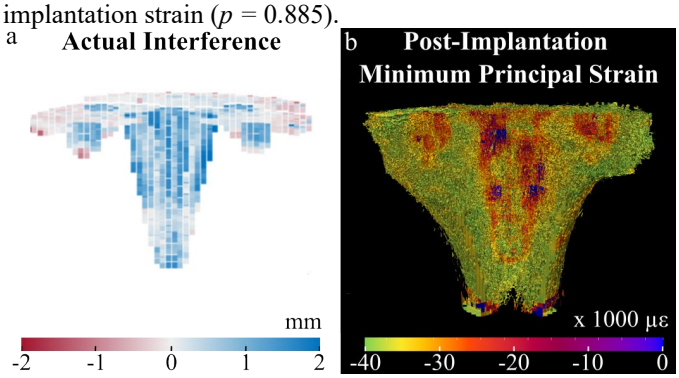


**Figure 1:** a) Actual interference and b) post-implantation $P_{min}$ across the tibial tray and tibia, respectively.

## CONCLUSIONS

An inhomogeneous actual interference was found across the pegs and keel that was lower than the nominal interference. Little interference was quantified across the tray, with bone-implant contact limited to 54.4±8.2% of the tray surface. Compressive strains were quantified for cancellous bone in contact with the implant. The extent of compressive strains post-implantation could not be fully explained by neither the actual interference nor by BV/TV, highlighting the complexity of this interaction.

## ACKNOWLEDGEMENTS

Australian Research Council Training Centre for Medical Implant Technologies (IC180100024).

## REFERENCES

1. Berahmani S et al., *Clin Biomech.* **51**:1-9, 2018.
2. Wearne LS et al, J Mech Behav Biomed Mater 134, 2022
3. DePuy Synthes, Attune Surgical Technique, 2016.

# EXPERIMENTAL VALIDATION OF A CADAVERIC FEMUR FITTED WITH AN OSSEOINTEGRATED IMPLANT

[1]Ryan Tiew, [1]Hans Gray, [1]Dale Robinson, [1]David Ackland and [1]Peter Lee

[1]Department of Biomedical Engineering, University of Melbourne, Melbourne, VIC, Australia
email: etiew@student.unimelb.edu.au

## INTRODUCTION

Bone-anchored-prostheses have been gaining popularity amongst lower limb amputees over the past few decades due to increased mobility and reduction in challenges from socket prostheses. Finite element (FE) modelling is commonly used to study the loading conditions of these implanted bones [1]. However, before such a model can be used to inform any design/clinical decisions, credibility of said model must first be validated. Hence, the purpose of this study was to develop a validated FE model that can be used to investigate these implanted bones under a multitude of loading conditions.

## METHODS

A left cadaveric femur (68, M) was surgically fixed with an Osseointegrated Prosthetic Limb (OPL) implant by a trained surgeon following manufacturer's guidelines. The implanted bone was oriented to represent loading conditions during six activities of daily living [2], clamped rigidly at the distal end, and load was applied to the femoral head. To collect surface strain data, eight sets of triaxial strain rosettes (SR) were bonded to the implanted bone at regions of interest – the trochanteric region (anterior, medial, posterior, and lateral), femoral neck (anterior and posterior), and distal femoral shaft (anterior and posterior). For cross-validation purposes, 3D-digital image correlation (DIC) was also used to capture surface strains on the anterior-trochanteric region. Each loading configuration was performed twice, and measured strains were averaged across the two trials.

The FE model of the bone-implant construct was generated from a set of QCT images, and the locations of the bonded SRs were registered using post-op QCT scans. Loading and boundary conditions in the experiment were replicated in the FE model, and the respective principal surface strains calculated. Linear regression was performed for the FE-SR and FE-DIC dataset pairs separately. DIC-SR regression was also performed to cross-validate the measured SR and DIC data.

## RESULTS AND DISCUSSION

Principal strains for the FE-SR and FE-DIC linear regressions had $R^2 = 0.89$ and $R^2 = 0.87$ (Figure 1) with a slope (m) of 1.33 and 1.85, respectively (Table 1). Results indicate that the current FE model is less stiff compared to the implanted bone. Further investigation of the material property assignment algorithm is required to stiffen the FE model.

Comparing DIC to SR measured strains, the regression fitted the measured datasets with $R^2 = 0.87$ and m = 0.84. Cross-validation of the DIC-SR measured strain datasets gives us confidence that the measured strains are valid and were not affected by SR-related localisation issues [1].

**Table 1: Linear regression coefficients of regression models.**

| Regression Model | $R^2$ | Slope, m | y-intercept, c |
|---|---|---|---|
| **FE-SR** | 0.89 | 1.33 | 10.1 |
| **FE-DIC** | 0.87 | 1.85 | -13.2 |
| **DIC-SR** | 0.87 | 0.84 | -6.5 |

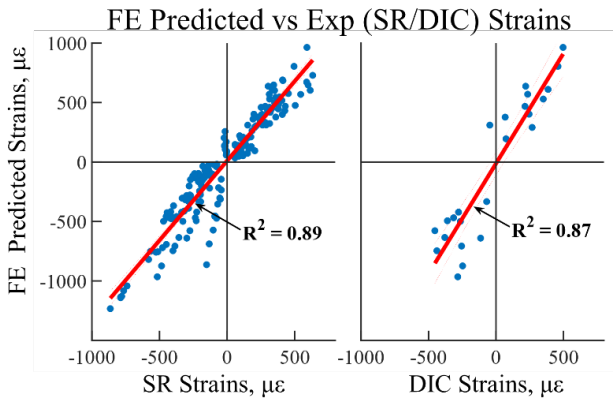


**Figure 1: Linear regressions based on strain rosette (left) and digital image correlation (right) strains.**

## CONCLUSIONS

The current computational model is in fair agreement with experimental results. Future work will focus on improving the model and incorporating more specimens for testing to avoid overfitting the FE model to this specimen.

## ACKNOWLEDGEMENTS

This research is funded by the Australian Research Council (ARC) and Blatchford Inc. (UK). Implants and implant models were provided by Osseointegration Group Australia.

## REFERENCES

1. Rankin K., et al., *Exp Methods in Ortho Biomech. 65-83* (2017).
2. rossard L., et al., *J of Rehab R&D.* **50:** 619-634 (2013).

# *IN VITRO* TESTING OF OSSEOINTEGRATED TRANSFEMORAL PROSTHESES: IMPLANT STABILITY AND LOAD TRANSFER

Giulia Galteri, [1]Marco Palanca, [1]Valentina Betti, [2]Kavin Morellato, [2]Emanuele Gruppioni, [1]Luca Cristofolini

[1] Department of Industrial Engineering, Alma Mater Studiorum - University of Bologna, Bologna, Italy
[2]Centro Protesi INAIL, Vigorso di Budrio, Italy
email: luca.cristofolini@unibo.it

## INTRODUCTION

Osseointegration provides direct connection between the external prosthesis and the remaining bone of amputees, granting several advantages over socket prostheses. However, like any other uncemented prosthesis, it exposes the patient to the risk of aseptic implant loosening and stress-shielding. The influence of implant stiffness on the bone strain has been assessed experimentally at selected locations of the femur for some straight-stemmed implants [1,2]. The OTN device has a curved stem, intended to match the anatomical shape of the femoral canal. However, the implant stability and load transfer of the OTN has not been investigated. The aim of this study was to test the stability and load transfer of the OTN prosthesis.

## METHODS

Five pairs of human cadaveric femurs were CT-scanned (slice thickness 0.6 mm, in plane resolution 0.5 mm) and randomly assigned to an OTN implant or to a prototype (not part of this paper). The proximal femur was embedded with resin in a metal pot. A OTN uncemented stem (Badal Xtm, OTN) was implanted on each femur following the manufacturer's instructions for pre-op planning, reaming and broaching.

The implanted femurs were loaded cyclically (100 cycles, 850N peak, corresponding to 30Nm at the osteotomy level). The force was delivered through a dedicated loading jig in the direction corresponding to heel strike during gait (Fig. 1) [3]. The full-field displacements and strains were measured throughout the test by a 4-camera 3D-DIC system (Aramis Adjustable 12M, GOM, 15 fps). A high-contrast speckle pattern was prepared on the femur. To track stem-bone micromotions, markers were placed on the distal end of the prosthesis. Implant stability was quantified as elastic micromotion (inducible stem displacement within each cycle) and permanent migration (accumulated throughout the test). Strains were investigated in the bone just above the osteotomy and near the stem tip.

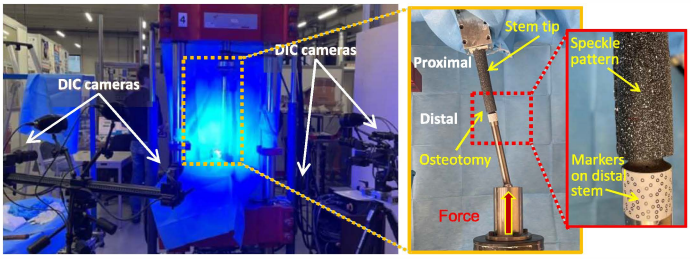


**Fig. 1:** Experimental setup: testing machine and DIC system (left); implanted femur constrained proximally and loaded distally (centre); detail of the speckle pattern and markers for DIC acquisition (left).

## RESULTS AND DISCUSSION

The inducible micromotions were 21±43 micron (average ± SD, 5 specimens). The permanent migrations were 6±1 micron. While on average implant motions were small, it must be noted that one implant out of 5 had inducible motions of 97 micron. This magnitude exceeds the threshold for bone ingrowth and possibly leads to fibrous tissue formation [4].

The DIC full-field strain measurements showed how the OTN implant leads to a significant strain shielding at the distal region (femur osteotomy) and a mild strain concentration proximally (stem tip). The measured strains were similar to those reported in a previous study of straight-stemmed implants [1], and comparable to the *in vivo* measured physiological strains [5].

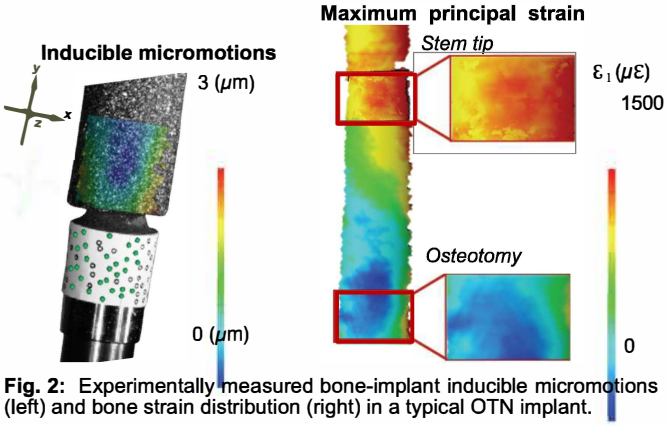


**Fig. 2:** Experimentally measured bone-implant inducible micromotions (left) and bone strain distribution (right) in a typical OTN implant.

## CONCLUSIONS

An experiment was designed that allowed to reliably measure implant inducible and permanent micromotions, as well as bone strains in femurs implanted with osseointegrated stems. While on average micromotions were safely small, in 1 implant out of 5 they exceeded the threshold for osseointegration. Stress shielding was observed near the osteotomy, while a mild strain concentration occurred near the stem tip. Future work will include testing an innovative stem design for implant stability and load transfer.

## ACKNOWLEDGEMENTS

INAIL is acknowledged for the research funds and the support (grant PR19-CR-P5-OsteoCustom).

## REFERENCES

[1] Tomaszewski *et al* (2013) JMBBM [2] Ahmed *et al* (2020) Ann. Biom. Eng. [3] Lee *et al* (2008) Med.Eng.Phys. [4] Pilliar *et al* (1986) Clin Orthop [5] Lanyon (1975) Acta Orth Scand

# INVESTIGATING CARTILAGE MECHANICS ACROSS THE LENGTH SCALES

[1]Mohammadreza Arjmandi, [2]Morgan Berton, and [1]Ashvin Thambyah

[1]Department of Chemical and Materials Engineering, University of Auckland, Auckland, New Zealand
[2] Polytech Montpellier, Universite De Montpellier, Montpellier, France
email: r.arjmandi@auckland.ac.nz

## INTRODUCTION

Osteoarthritis (OA) is a mechanically driven degenerative joint disease whose initiation remains unclear. It has been proposed that there exists a 'pre-OA' state of the tissue where cartilage is vulnerable to the onset of the disease process [1]. We have shown that the pre-OA state of the joint involves subtle 'destructuring' of the collagen network which results in a *loss of fibrillar interconnectivity* [2]. The aim of this study is to investigate how changes at the submicron length-scale of the collagen network is associated with macro-scale tissue mechanics.

## METHODS

To achieve our objective, we have adopted the analogy of cartilage weight bearing as demonstrated by a 'balloon-string' model [3]. These two components provide the load bearing function, analogous to that shown in Figure 1A. Cartilage is composed of an extracellular matrix comprising a network of collagen fibrils (stings) entrapped in which are the hydrophilic proteoglycan molecules (balloons). We then developed an FE model geometry of the balloon-string construct (Figure 1A and 1B), composed of hollow deformable spheres with an internal hydrostatic pressure magnitude, embedded in a network of strings.

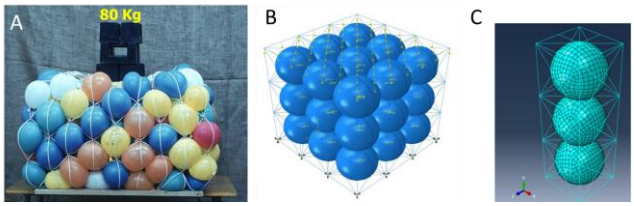


**Figure 1:** (A) The balloon-and-string model [1], demonstrates the interplay, or coupling, between the tension-resistant collagen network (string) and compression-resistant water-rich proteoglycans (balloon). (B and C) Composite FE models allow for the studying of stresses and their distribution at the elemental level, which include that of the 'fibril' and intra-network spaces.

From our extensive work on cartilage microstructure, we have shown that with early cartilage degeneration there is an unravelling of the network, which would be akin to the string network losing its interconnected structure. Effectively three groups of tissue states were modelled: healthy tissue G0 with the strong network fully intact, mildly degenerated G1 with < 15% removal of linkages, and moderately degenerated G1+ with greater but <20% removal. In conjunction to the model, experimental tests were conducted on cartilage-on-bone samples obtained from bovine patella, from G0, G1, and G1+ cohorts, these grades and their availability have been described in an earlier study [4]. A 40N load was applied at 0.5N/s through a cylindrical indenter 5mm in diameter on a relatively flat region of the tissue submerged in 0.15M saline solution. The Young`s modulus was obtained and used as an input for the FE model. The individual E values of the string linkages for the G0 computer model were manually adjusted until a similar stress-strain curve was obtained compared to that of the experiment. Various permutations of '*string-interconnectivity*' were then tested in the model to match the G1 and G1+ experimental data.

## RESULTS AND DISCUSSION

From the experiments, there was a significant decrease in the Young`s modulus (E, MPa) with increasing degeneration**:** 9.50 ± 1.02 (G0), 7.10 ± 0.14 (G1), and 5.66 ± 0.17 (G1+).
In the G1 and G1+ models, adjusting the stiffnesses of the diagonal linkages (as opposed to the purely horizontal) were the most influential to yield a mechanical response that best matched the experimentally derived E. The diagonal linkages, represent the *summative effect of sub-micron transverse interconnectivity* or 'lateral entwinning' in the collagen networks. Previous work using scanning electron microscopy imaging has indeed revealed that such loss of transverse interconnectivity occurs in cartilage degeneration [2, 5], which in turn has been proposed as the pre-OA tissue state [4].

## CONCLUSIONS

This study provides a mechanical rationale on how the loss of transverse interconnectivity in the collagen fibrillar network, occurring at the sub-micron length scale, can cause a corresponding loss in macro-scale tissue stiffness.

## REFERENCES

1. Ryd L, et al., *Cartilage*. **6(3)**: 156-165, 2015.
2. Thambyah A, et al., *J Mech Behav Biomed Mater.* **5(1)**: 206-15, 2012.
3. Broom N.D., *Connect. Tissue Res.* **14(1)**: 1-8, 1985.
4. Hargrave-Thomas EJ., *Journal of anatomy* **223 (6)**, 651-664, 2013.
5. Nickien M, et al., *J Mech Behav Biomed Mater.* **7**: 390-98, 2017.

# UNDERSTANDING THE VARIATION OF BONE MINERAL DENSITY IN THE FEMUR AND TIBIA IN CHILDREN AGED 4 TO 18 YEARS OLD

[1]Julie Choisne, [2]Jannes Brüling, [1]Yidan Xu and [1]Thor Besier

[1]Auckland Bioengineering Institute, The University of Auckland, Auckland, New Zealand
[2]Biomedical Engineering, University of Luebeck, Luebeck, Germany
email: j.choisne@auckland.ac.nz

## INTRODUCTION

Bone Mineral Density (BMD) is a widely used measure to determine mechanical properties and fracture risk prediction in the femur [1]. Childhood and adolescence are a crucial time for bone mineral accumulation with 25% of BMD being laid during puberty [2]. Poor BMD development during growth is also correlated with the development of osteoporosis later in life [3]. Mapping the variation of BMD in a paediatric population is important to understand how BMD change with age and sex. Therefore, the aim of this study was to evaluate the variation of BMD in the long bones for a paediatric population.

## METHODS

CT-scans of 278 children and adolescents (F: 111, age: 11 ± 4 years, height: 147 ± 24 cm, mass: 47 ±23kg) were obtained from the Victorian Institute of Forensic Medicine (VIFM, Melbourne, Australia). A Mindways calibration phantom was present in scans, allowing us to convert Hounsfield Units (HU) to BMD. Femora and tibiae were segmented using Mimics (Materialise, BE). A template volumetric mesh was created and morphed to a total of 556 femora and 550 tibiae ensuring nodal correspondence using registration and host mesh fitting. Material mapping to the mesh elements was performed in Bonemat (v3.2, Instituto Ortopedico Rizzoli, Italy) using the relationship between HU and BMD obtained from the phantom CT-calibration. Volumetric BMD was calculated for each femur and tibia and analysed by regions of interest; femur and tibia proximal and distal epiphysis, shaft, femoral head, neck and greater trochanter. A two-way ANOVA was conducted to examine the effect of age and sex in BMD.

## RESULTS AND DISCUSSION

Volumetric BMD increased with age for the tibia (from 0.38 g/cm3 ±0.05 at 4 y.o. to 0.46 g/cm3 ±0.02 at 18 y.o,, r=0.56) and femur (0.36±0.03 at 4 y.o. to 0.39±0.03 at 18 y.o., r=0.39). Simple main effects analysis showed that BMD significantly increased with age ($p<0.05$, figure 1). An interaction was found between age and sex on all average BMD regions at the femur and tibia except for tibial shaft ($p<0.05$). No sex simple main effect was found. This finding contrasts with another study, which found lower BMD in females than males aged 17-21 in the proximal femur and distal tibia using DXA [4].

## CONCLUSIONS

From our paediatric population, we found that the regional BMD increases with age in the tibia and femur but sex did not have an effect on BMD. Future work will include the cortical thickness in the femur and tibia to estimate the structural stiffness of the cohort.

## ACKNOWLEDGEMENTS

The authors would like to thank the Aotearoa Foundation and Friedlander Foundation for funding this study and the VIFM for the CT scans.

## REFERENCES

1. Bedbrenner T et al. *JBMR* **29**: 2090-2100, 2014.
2. Bailey D et al. *JBMR* **15**: 2245-2250, 2000,
3. Faulkner R et al. *Med and Sport Sc* **51**: 1-12, 2007.
4. Nieves J W et al. J of *Bone and Miner Res* **20**: 529–535, 2005

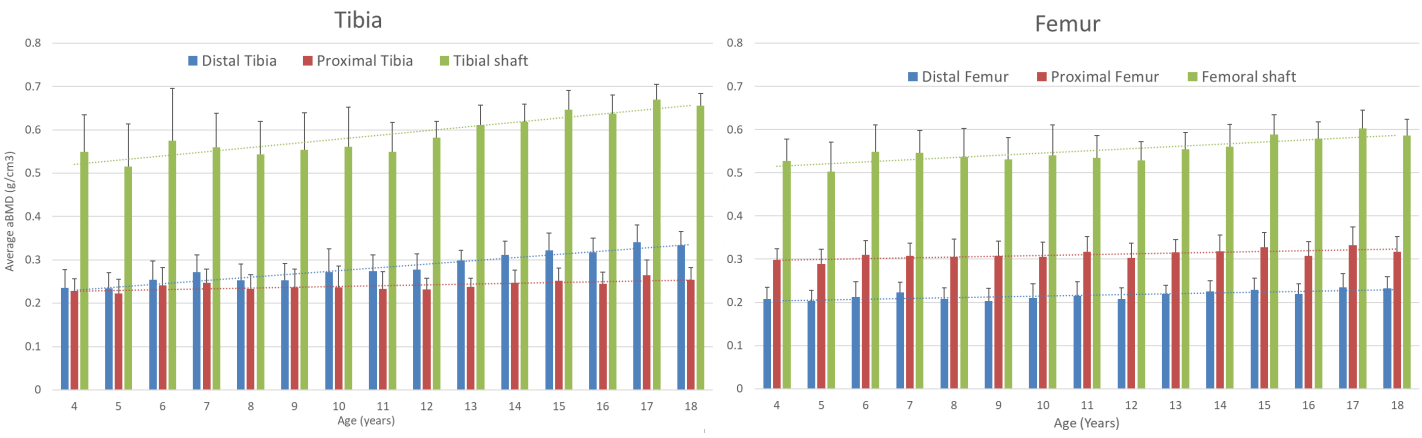


Figure 1: Distal (blue), proximal (red) and shaft (green) average Bone Mineral Density across age for the tibia (left) and femur (right).

# BONE SHAPE, DENSITY DISTRIBUTION, AND MICROSTRUCTURAL ORGANIZATION IN ADULT PEOPLE

[t1]Natali Uribe, [1]Peter Pivonka and [1]Dermot O'Rourke, [1,2]Saulo Martelli

[1]School of Mechanical, Medical and Process Engineering, Queensland University of Technology, Brisbane, Australia
[2]Medical Device Research Institute, College of Science and Engineering, Flinders University, Adelaide, Australia
email: natali.uribeacosta@hdr.qut.edu.au

## INTRODUCTION

Age-related factors exert a substantial influence on the susceptibility to hip fractures and the daily bone mechanical performance [1]. To study this prevalence, statistical models have been used. However, most 3D models are either based on people in advanced age or do not incorporate microstructural changes [2,3]. This study details the development of a statistical model using geometry, bone density distribution and microstructural morphometry in High-Resolution peripheral Quantitative Computed Tomography images (HR-ρQCT) in people spanning the entire age range of adulthood.

## METHODS

HR-ρQCT images (SCANCO Medical, 82 µm/pixel Switzerland) of the proximal femur in 92 patients aged between 20-92 years old were obtained from a public database comprising equal numbers of men and women [4]. **A**utomatic segmentation was performed using MATLAB (The MathWorks Inc., MA, USA). Then, bones were trimmed distally at the same level. The surface of the mask was meshed using triangulated mesh smoothed using 9 iterations of the Laplacian Smooth implemented in MeshLab. A template solid mesh of the proximal femur was taken from a previous study [3]. The template was morphed to all the specimens. Firstly, the template surface was rigidly registered to the target surface using an ICP algorithm. Secondly, an ICP-based non-rigid registration algorithm was applied to perform locally deform of the baseline model to match the shape of each target using 4 – 10 iterations by providing the displacement of superficial nodes. Third, the template volume was elastically registered to the target by applying to the superficial nodes the calculated displacements. An in-house MATLAB code was used for mapping the material properties to each morphed mesh from the original CT scans. The grey levels in the images were calibrated to equivalent bone mineral density levels using an interpolation where marrow was equivalent to water (0 g/cm$^3$) and the maximum grey level was assumed to be compact cortical bone (1.3g/cm$^3$). An empirical relationship was used to convert the ash density (g/cm$^3$) to elastic modulus $E = 14644\, x\, \rho^{1.49}$ [5]. For microstructural analysis, the entire femur was subdivided in cubes of 5x5x5 mm³ in size, resulting in average in 164.029 cubes per specimen. The morphometric analysis of the cubes was completed using CT analyzer software (Skyscan, Kontich, Belgium) automatically run in batch for all the cubes. A single threshold value was used to segment all the cubes matching morphometric variations expected in the population [6]. Preliminary results focus on the statistical description of geometry, bone density distribution and young modulus, as mapping the morphometric analysis on the isotopological meshes is still in progress. The model was obtained using a principal component decomposition of the entire dataset. The compactness of the models was analyzed and compared to current documented models for older adults in terms of variance explained and modes of variation [6]. The generalization of model analyzed using leave one out cross-validation scheme.

## RESULTS AND DISCUSION

The first mode of variation explains 22.39% of the variance in appearance. To account the 90% of the variance 60 bones were used. The model displayed variations in the intertrochanteric distance, complete length, and angles for its first three modes, as also reported in the work conducted by Bryan, et al. [3] in older adults. The first three modes of density variation displayed noticeable changes. In PC1, a +2SD variation increases the modulus in both the medullary cavity and cortical bone, while a -2SD variation decreases in both areas. PC2 and PC3 show the opposite effect compared to PC1, with variations of 47.9% between +/-2SD for PC1 and PC2, and 17.93% for PC1 and PC3, showing that overall, the distributions in material properties seemed realistic (Fig. 1a).

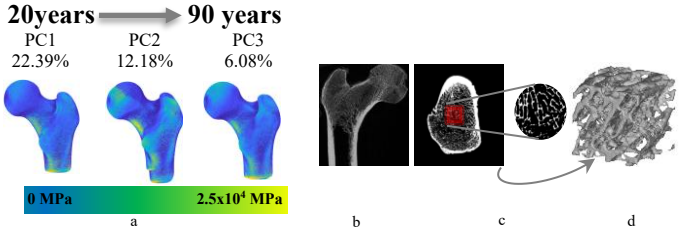


**Fig. 1**. *Statistical model (left) 5mm cube (right).* a, the statistical model. b, cross- section of the complete proximal femur. c, cross-section of one of the slices, the red square details the region of interest where cubes were extracted, ROI contains trabecular bone. d, representative 5mm cube after segmentation.

A generalization mean error of 1.8mm in terms of geometry and 3.6x10$^3$Mpa in terms of appearance was found when using the first 10 modes of variation. For the microstructural analysis, a single threshold value of 50 was used to segment all the samples, this value allows for the precise distinction of trabecular bone from surrounding structures avoiding over-segmentation, the value was confirmed by obtained results of microstructural parameters and compared it with the literature [6].

## CONCLUSIONS

The model displays significant differences in the modes and the variance explained by each PCA like earlier reports [3] in the upper range of age variation analyzed here. The completion of the morphometric analysis may reveal further age-related changes at a deeper level of detail, enabling studies of the relationship between motor demand, bone shape and density distribution, and age.

## ACKNOWLEDGEMENTS

Australian Research Council (IC190100020; FT180100338).

## REFERENCES

1. S, Martelli et al. *Curr osteoporos rep* ***18****:301-311, 2020*
2. O' Rourke et al. *J Biomech* **119:**1-13, 2021.
3. Bryan, et al., *Med Eng Phys* **32**:57-65, 2010.
4. Clement J. Melbourne Femur Collection, 2016
5. Morgan, et al., *J Biomech* **36**:897-904, 2003.
6. Shen Q. *Hip and pelvis*. **33**:190-199, 2021

# TOWARDS *IN VIVO* IMAGE-GUIDED MECHANICAL EVALUATION OF THE MURINE KNEE JOINT

[1]Emma C. Boersma, [1]R.Y. Nigel Kour, [2]Eric Schoof, [1]Kathryn S. Stok
[1]Department of Biomedical Engineering, The University of Melbourne, Australia
[2]Department of Electrical Engineering, The University of Melbourne, Australia
email: kstok@unimelb.edu.au

## INTRODUCTION

The osteochondral interface is a dynamic system with a robust connection between different material types. For this reason, it can serve as an inspiration for engineered soft-hard interfaces. The mechanical and structural properties of the osteochondral connection are challenging to identify due to the small scale and limited techniques. Numerous mechanical tests and structural observations have been done *ex vivo, in situ,* and *in vitro*; however, only limited to no information is available when it comes to *in vivo* knowledge of the osteochondral tissues on a microscale [1, 2]. A better understanding of the behaviour of this interface *in vivo* could lead to new insights in the field of structural and biological engineering. In this work, we are creating a novel measuring method to analyse the mechanical properties of the osteochondral connection in the murine knee joint *in vivo.*

## METHODS

The device for image-guided mechanical evaluation was designed in-house with the aim to observe the mechanical and structural properties of the osteochondral interface in murine knees (Figure 1). It was designed according to the following design objectives, animal welfare, accurate mechanical measurements of force, displacement, and strain, and microCT compatibility. The device contains two 5N load cells (resolution of ±10 mN), connected to displacement actuators (10 µm step size) to move the load cells toward the point of compression. The system is driven by Arduino and MATLAB. Several design improvements have been tested *in situ*, within the microCT scanner (VivaCT80, Scanco Medical, Bruttisellen, Switzerland), on excess mice obtained from the Medical Animal Facility at the University of Melbourne. For the validation of the mechanical data acquisition, stress-relaxation tests were performed on a viscoelastic solid material (Agilus30), using a compression machine (Zwick, Ulm, Germany) with a load cell of 5 kN. Similar tests were performed on the new device. Three-step tests with a strain increase of 1% were executed. The holding time between each step was 5 minutes. The data analysis of both machines is performed through a custom in-house app.

**Figure 1:** The device for image-guided mechanical evaluation of the murine knee.

## RESULTS AND DISCUSSION

Several features of the design have been updated; a system has been designed to achieve optimal microCT scans of the knee joints. In addition, the application to control the device has been updated in such a way that it can perform stress-relaxation tests (Figure 2). This also demonstrates that it can capture the viscoelasticity of a material. For accurate measurements of the mechanical properties of tissues, it is of great importance that can it observe viscoelasticity. A lower force was measured with the novel device, compared to the compression machine, this might be due to the difference in loading direction and the use of different load cells. To use this device for an *in vivo* study, more mechanical data should be obtained to improve joint positioning and the data analysis app. Thereafter, to complete the protocol for this device, an imaging registration method should be designed.

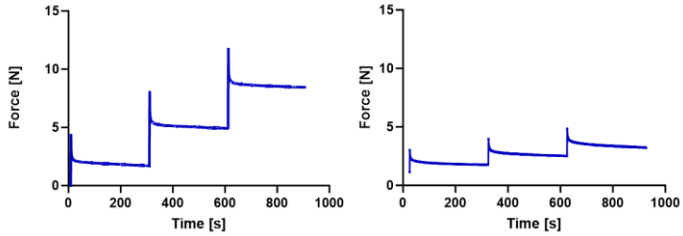


**Figure 2**: Stress-relaxation tests with the compression machine (left) and the in-house built device (right).

## CONCLUSIONS

The novel device for image-guided mechanical evaluation can be used to evaluate the mechanical properties of materials. Future research is required to validate the joint positioning of the murine knee during microCT scanning and define a specific loading profile. This will lead to a protocol for observing the mechanical and structural properties of the osteochondral interface in the murine knee *in vivo.*

## REFERENCES

[1] Hargrave-Thomas, E., et al. *Osteoarthritis and Cartilage,* **23**: 1755-1762, 2015.
[2] Fleischhauer, L., et al. *Applied Sciences,* **12**, 2022.

# DEVELOPING AND VALIDATING A NOVEL MICRO-CT BASED TECHNIQUE FOR MEASURING BONE MINERAL DENSITY DISTRIBUTION

[1]Alexander Lee-Medland,[1]Edmund Pickering, [2]Andrew Kingston, [2]Levi Beeching, [2]Qiheng Yang and [1]Peter Pivonka

[1]Queensland Unit for Advanced Shoulder Research, Queensland University of Technology, Brisbane, QLD, Australia
[2]X-Ray Tomography and Application Group, Australian National University, Canberra, ACT, Australia
email: alexander.leemedland@hdr.qut.edu.au

## INTRODUCTION

Bone mineral density (BMD), typically measured at several mm length scale, is a tissue level measure of bone density and mineralisation. On the other hand, bone mineral density distribution (BMDD), typically measured at a micron length scale, is a micro level measure which allows the assessment of the heterogeneity of mineralisation (i.e. calcium content) in the bone matrix. BMDD is linked with mechanical properties of the bone matrix and is an important bone quality parameter that provides insights into the effects of bone disease and drug treatments. BMDD has previously been used to characterize "bone health". Quantitative backscattered electron imagining (qBEI) is a technique used for the assessment of BMDD. This technique is valuable for scanning small specimens but only collects a 2D representation of the bone. Computed micro-tomography (micro-CT) has the potential to be used for 3D assessment of BMDD. Micro-CT offers the potential to explore BMDD in 3D but suffers three major challenges (1) beam hardening, (2) the development of the theoretical framework, (3) the validation of the system. This works aims to develop a technique to interrogate BMDD using specialized micro-CT.

## METHODS

The methodology involved two stages (1) collection of qBEI data to be used for validation, and (2) development of a calibration method for determining bone mineral density. For the first stage ovine samples were prepared matching the recommendation of Roschger et al. [1]. The samples were scanned using the qBEI at QUT with the Tescan TIMA technique at a resolution of 1 µm, using the calibration standards of carbon and $SiO_2$. Following this the samples were given to our colleagues at ANU for micro-CT scanning. The samples were then scanned at 60 kV with 2 mm of Al filtering. For the calibration of the micro-CT a specifically made phantom was used to link mineral content with grey level. The qBEI results will act as validation for the accuracy of the micro-CT calibration and scan data.

## RESULTS AND DISCUSSION

Preliminary results found the mean BMDD for the micro-CT to match the trend observed in the qBEI results as shown in Figure 1. The mean calcium concentration for the qBEI results was 25.8, 23.8 and 24.4% for the three samples compared to the micro-CT results of 23.8, 23.3 and 23.6%. However, the biggest point of difference between the different scan methods is the peak widths as shown below in Figure 1.

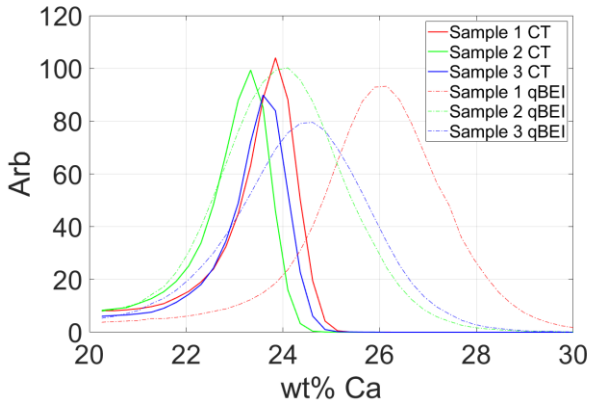


**Figure 1:** Mean weight percentage calcium results for the three ovine samples scanned with micro-CT and qBEI.

While these preliminary results do not directly match the qBEI results it offers promise to the effectiveness of the technique. With further development and reproducibility testing this offers a valuable method for BMDD assessment. However, the ultimate application for this technique will be the examination of human bone. One of the greatest challenges with micro-CT is beam hardening which acts as a high-pass filter 'hardening' the results. To explore the effects of beam hardening on the scan results this study will be expanded to examine larger samples. As this work aims to expand into examining human bone, the selected larger samples were obtained from the Melbourne Femur Research Collection. These samples will be examined at 60 kV, 80 kV and 100 kV with the 100 kV scan having two different levels of filtering with 0.5 mm and 1 mm stainless steel.

## CONCLUSIONS

The results show promise and demonstrate the potential for micro-CT to be used for the assessment of BMDD. With further development of the technique, it provides a powerful tool for the examination of BMDD and bone quality. Further exploration on the accuracy of the technique will be pursued with the use of synchrotron micro-CT scanning to compare high resolution scans with conventional micro-CT scans.

## REFERENCES

1. Roschger, P, et al., B*one*, **23**(4), 1998

# QUALITY OF LIFE FOR CHILDREN UP TO 13 YEARS FOLLOWING TREATMENT FOR ACUTE HAEMATOGENOUS OSTEOMYELITIS

[1]Sarah Hunter, [2]Joseph Baker

[1]Waikato Hospital Department of Orthopaedic Surgery, Hamilton, New Zealand
[3]Faculty of Medical and Health Sciences, University of Auckland, New Zealand
email: shun472@aucklanduni.ac.nz

## INTRODUCTION

Acute Haematogenous Osteomyelitis (AHO) remains a cause of severe illness among children with the possibility of long-term consequences for growth and development. Previous research on sequelae from AHO rarely considers outcomes more than two years following treatment. This study aims to establish the quality of life of patients diagnosed with AHO in childhood up to 13 years after diagnosis, evaluating the impact on social, emotional, physical, and school function.

## METHODS

Children treated for AHO between 2008-2018 at a tertiary referral centre in New Zealand were identified. PedsQL™ questionnaires were conducted via phone with either the child or primary caregiver and responses analysed.

## RESULTS AND DISCUSSION

40 patients met inclusion criteria, were contactable by phone, and consented to participate. The mean age was 7 years (range 0-15) and most were female (60%). Health related quality of life (HRQOL) was scored as a percentage with most participants scoring >80% (n=27). Those who do experience reduced quality of life following treatment for AHO were likely to complain of pain, stiffness, or anxiety. The impact of significant childhood illness on mental health was not adequately captured by the PedsQL™ but was highlighted qualitative feedback.

**Figure 1:** Most Commonly Reported Issues Up to 13 Years Following Treatment

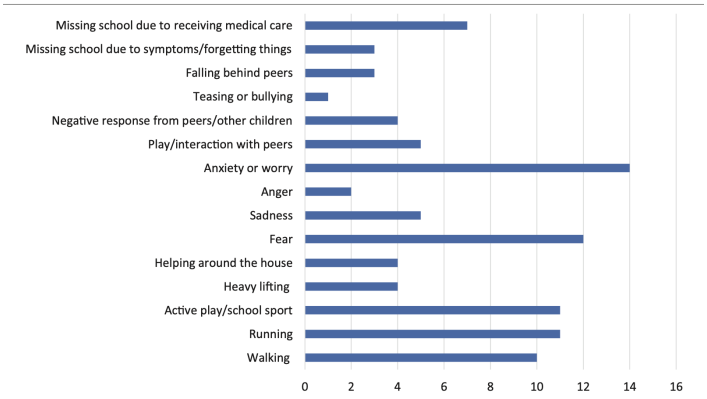


## CONCLUSIONS

The majority of children treated for AHO reported excellent health-related quality of life up to 13 years following treatment although an negative impact on mental health was reported using qualitative analysis. A refined scoring system is needed to assess the long-term impact of musculoskeletal infection.

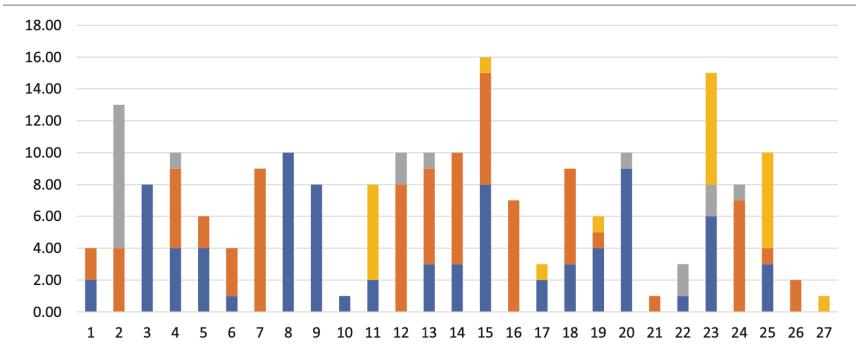


**Figure 1:** PedsQL™ Scores by Functional Domain, Blue = Physical Function, Orange = Emotional Function, Yellow = School Function, Grey = Social Function

# DOES ELASTOGRAPHIC TENDON STIFFNESS PREDICT RETURN TO WORK AND SPORT AFTER PRIMARY ROTATOR CUFF REPAIR?

[1]Alexander G Maloof, [1]Christyon Hayek, [1]James Bilbrough, [1]Lisa Hackett and [1]George Murrell

[1]Orthopaedic Research Institute, St George Hospital, Kogarah, Sydney, NSW, Australia

email: alexandergmaloof@gmail.com

## INTRODUCTION

Over a third of all patients are unable to return to their pre-operative levels of work and sport following primary rotator cuff repair at 8 months [1]. Most studies to date have focused on the association of preoperative demographic factors with return to work and sport post-rotator cuff repair, with few studies investigating the association between post-operative imaging modalities and return to work and sport. Shear wave elastography ultrasound (SWEUS) is a recent technology which can quantify tendon stiffness post-rotator cuff repair to investigate the healing of supraspinatus tendons. The elastographic stiffness of a repaired supraspinatus tendon has been found to improve as tendons heal. We wondered if the elastographic stiffness of a repaired supraspinatus tendon would be associated with improved return to work and sport post-cuff repair. The aim of this study was to determine whether there was an association between repaired supraspinatus tendon stiffness and patient return to work and sport.

## METHODS

This was a prospective cohort study of 50 patients undergoing primary arthroscopic rotator cuff repair. Pre-operatively, all patients completed a questionnaire ranking their level of sport and work activity on a four-point Likert scale. Postoperatively, at 8 days, 6 weeks, 12 weeks, 6 months, and 1 year, patients reported their current levels of sport and work on the same Likert-scale and had SWEUS measurements taken at three points of their repaired supraspinatus tendons. Each patient's scores for level of work and sport activity were compared to the SWEUS stiffness measurements of the supraspinatus tendon post-repair using spearman's correlation coefficients, with one-way ANOVAs for parametric data.

## RESULTS AND DISCUSSION

The SWEUS determined stiffness of supraspinatus tendons at their repaired insertion sites increased at all three locations by an average of 22% from 8-days to 12 months (p=0.0001). Elevated supraspinatus tendon stiffness at 12 weeks and 6 months were strongly associated with return to sport at 12 months. Supraspinatus tendon stiffness at 6 weeks and 12 weeks were strongly associated with return to work at 12 months. Patient return to both sport (r = 0.46) and work (r=0.49) and was most strongly associated with SWEUS stiffness at 12-weeks post rotator cuff repair.

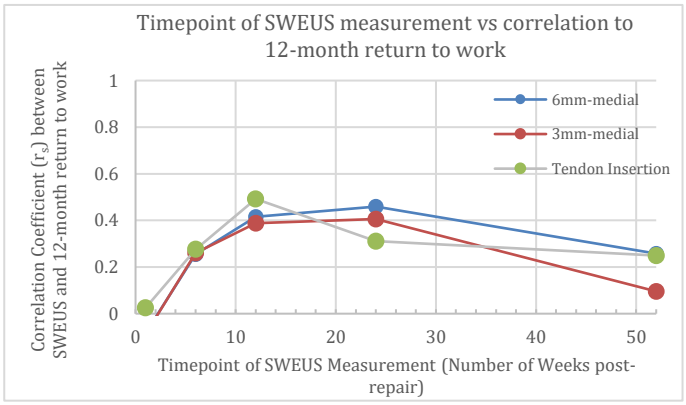


**Figure 1:** Timepoint of SWEUS-measured tendon stiffness vs its correlation to return to work 12-months post-cuff repair.

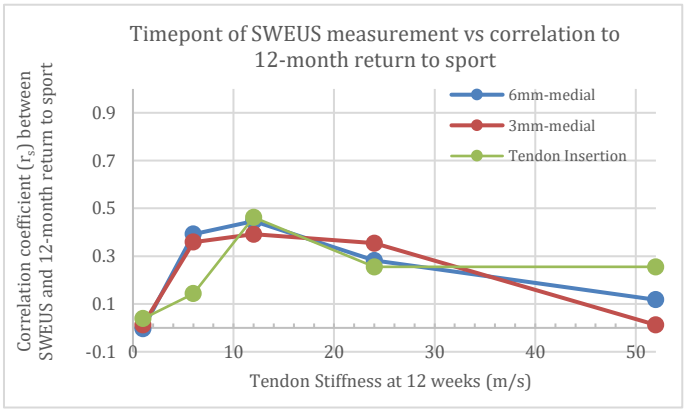


**Figure 2:** Timepoint of SWEUS-measured tendon stiffness vs its correlation to return to sport 12-months post-cuff repair.

## CONCLUSIONS

This data supports the hypothesis that the stiffness of a repaired supraspinatus tendon (measured by shear wave elastography) is associated with improved return to work and sport after primary rotator cuff repair. Tendon stiffness at 12-weeks post rotator cuff repair was best at predicting both return to work and sport after 12-months.

## REFERENCES

1. Haunschild ED, et al., Return to work after primary rotator cuff repair: a systematic review and meta-analysis. *Am J Sports Med.* **49(8)**:2238-47, 2021.

# EARLY CRP TRENDS IN CHILDHOOD OSTEOMYELITIS PREDICT COMPLICATED DISEASE

[1]Sarah Hunter, [2]Joseph Baker

[1]Waikato Hospital Department of Orthopaedic Surgery, Hamilton, New Zealand
[3]Faculty of Medical and Health Sciences, University of Auckland, New Zealand
email: shun472@aucklanduni.ac.nz

## INTRODUCTION

Acute hematogenous osteomyelitis (AHO) remains a cause of severe illness among children. Contemporary research aims to identify predictors of acute and chronic complications. Trends in C-reactive protein (CRP) after treatment initiation may predict disease course. We have sought to identify factors associated with acute and chronic complications in the New Zealand population.

## METHODS

A retrospective review of all patients younger than16 years with presumed AHO presenting to a tertiary referral centre between 2008 and 2018 was performed. Multivariate was analysis used to identify factors associated with an acute or chronic complication. An "acute" complication was defined as the need for 2 or more surgical procedures, a hospital stays longer than 14 days, or recurrence despite intravenous antibiotics. A "chronic" complication was defined as growth or limb length discrepancy, avascular necrosis, chronic osteomyelitis, pathologic fracture, frozen joint, or dislocation.

## RESULTS AND DISCUSSION

One hundred and fifty-one cases met the inclusion criteria. The median age was 8 years (69.5% male). Within this cohort, 53 (34%) experienced an acute complication and 18 (12%) a chronic complication. CRP trends over 96 hours differentiated patients with AHO likely to experience severe disease. From the point of admission, children admitted with the uncomplicated disease had a much lower median CRP which resolved in response to treatment. This difference is most striking at the 96-hour time point, where the median CRP for the uncomplicated disease is only 20 mg/L and those with acute or chronic complications have median CRP of 73 mg/L and 111 mg/L respectively (Figure 1).

Regression analysis showed that contiguous disease, delayed presentation, and failure to reduce CRP by 50% at day 4/5 predicted an acutely complicated disease course. Chronic complication was predicted by the need for surgical management and failed CRP reduction by 50% at day 4/5.

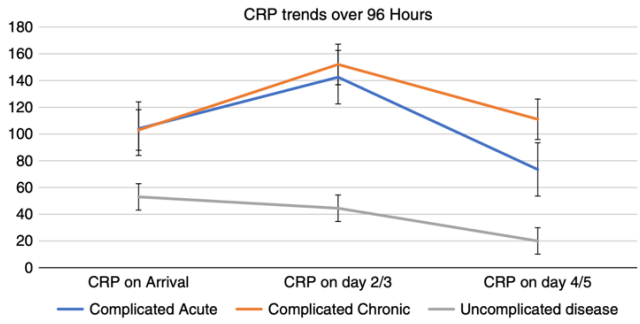


**Figure 1:** CRP trends over 96 hours in acute haematogenous osteomyelitis demonstrating that children with severe and complicated illness have markedly different CRP trajectory.

## CONCLUSIONS

CRP trends over 96 hours after the commencement of treatment differentiate patients with AHO likely to experience severe These findings encourage close follow-up for children who demonstrate either sustained CRP elevation or a need for surgical intervention.

| Backwards Stepwise Regression Analysis-Predictors of Acute Complication | | | | | |
|---|---|---|---|---|---|
| ***R*** | ***R²*** | **Adjusted *R²*** | ***S*** | ***F*** | ***P*** |
| **0.55572** | **0.30883** | **0.27427** | **0.41295** | **8.93637** | **< 0.001** |
| **VAR** | **Coefficients** | **Standard Error** | **β** | ***t*** | ***P > t*** |
| Duration of symptoms (d) | 0.01801 | 0.00682 | 0.20192 | 2.64216 | 0.00934 |
| Contiguous disease | 0.14644 | 0.08327 | 0.14914 | 1.75853 | 0.08121 |
| White cell count | 0.01706 | 0.008 | 0.16926 | 2.13269 | 0.03499 |
| Failed CRP reduction 50% | 0.14567 | 0.08597 | 0.14687 | 1.6945 | 0.09276 |
| Multifocal sepsis | 0.33196 | 0.13485 | 0.20841 | 2.46163 | 0.01525 |
| Bone drilling | 0.27747 | 0.11576 | 0.20043 | 2.39688 | 0.01808 |
| Intercept | −0.12378 | | | | |

CRP indicates C-reactive protein; S, standard error; TOL, Tolerance; VAR, variable; VIF, Variance Inflation Factor. .

**Table 1**: Regression Analysis for Predictors of Acutely Complicated Illness

# OUTCOMES OF AN AUGMENTED REALITY PAEDIATRIC SUPRACONDYLAR HUMERAL FRACTURE SIMULATOR

[1]Joyce Guo, [1]Phil Blyth, [2]Kari Clifford, [3]Nikki Hooper, and [4]Haemish Crawford

[1]Department of the Dean, Otago Medical School, University of Otago, Dunedin, New Zealand
[2]Surgical Outcomes Research Centre Otago, Otago Medical School, University of Otago, Dunedin, New Zealand
[3]Department of Orthopaedic Surgery, Otago Medical School, University of Otago, Christchurch, New Zealand
[4]Department of Orthopaedics, Starship Children's Hospital, Auckland, New Zealand
email: phil.blyth@otago.ac.nz

## INTRODUCTION

Supracondylar humeral fractures (SCHF) of the elbow are one of the most common orthopaedic causes of morbidity in childhood. The gold standard for management of operative cases is closed reduction and percutaneous pinning (CRPP). By nature, traditional apprenticeship style orthopaedic training allows for repetition of individual case types but not deliberate practice of certain aspects of the skills, such as only percutaneous pinning in CRPP. Numerous studies on learning and teaching for adults have shown that independent, deliberate, and repeated practice is most effective for skill acquisition [1-3]. Our team has developed an augmented reality simulator - BoneDoc SCHF, for the percutaneous pinning component of CRPP in paediatric SCHF. Using this technology, skill acquisition may take place before entering the operating room, thereby reducing risk to patients and improving efficiency of theatre time use.

## METHODS

Fourteen SET1 orthopaedic trainees undertook first simulator contact and testing under controlled environments. Participants were instructed to perform a lateral percutaneous pinning procedure on a simulated model of a Gartland Type II SCHF. The simulator assessed accuracy of entry and exit points relative to fracture X-ray given, number of fluoroscopy shots taken, and number of air shots.


**Figure 1** BoneDoc SCHF simulator in

Trainees were then given simulation sets and instructed to perform monthly practices at their home centre. Their performance on the simulator was reassessed using the simulator at the subsequent training weekend seven months later. Differences in the variables of interest were summarised according to pre and post simulator use. The simulator is seen in use in Figure 1.

## RESULTS AND DISCUSSION

Means and standard deviations lowered for trainee performance across all simulator operation outcomes after exposure to simulator (Table 1). The researchers note varying engagement in usage of the simulator, with 8/14 participants reporting less than monthly use. Trainees who were unable to attend the initial training weekend and instead received individual initial testing, reported more frequent use of the simulator. We are conducting further qualitative studies to determine participant and simulator factors associated with usage.

## CONCLUSIONS

Results suggest improvement in simulator outcomes following use. Trainee engagement in self-regulated simulator use was lower than expected. Further studies are needed to explore associations between simulator use and outcomes, as well as barriers and facilitators to usage.

## ACKNOWLEDGEMENTS

The authors thank Prue Elwood and Tim Gregg (New Zealand Orthopaedic Association) for organising and allowing this project to be introduced in training weekends. This project is supported financially by The Wishbone Orthopaedic Research foundation of New Zealand and the Dunedin School of Medicine Research Student Support Committee.

## REFERENCES

1. Bae DS, *J Pediatr Orthop*. **35** (5 Suppl 1), 2015
2. Duvivier RJ, *BMC Med Educ.* **11**:101, 2011
3. Ericsson K, et al., *Psychol Rev*. **100**:363-406, 1993.

**Table 1:** Simulator outcomes at first simulator contact (pre-simulator) and after seven months (post-simulator), Mean (±SD).

| Time point | X-rays taken | Total length of mistakes (mm) | Total number of air shots | First wire time (sec) | Second wire time (sec) |
|---|---|---|---|---|---|
| ***Pre-simulator*** | 94 ± 76 | 24.97 ± 31.2 | 29 ± 44 | 213.4 ±138.6 | 212.3 ± 179.5 |
| ***Post-simulator*** | 60 ± 40 | 15.91 ± 11.37 | 12 ± 10 | 171.8 ± 116.9 | 137.2 ± 118.9 |

# VIRTUAL BIOMECHANICAL ASSESSMENT OF CUSTOM TRIFLANGE AND POROUS TANTALUM COMPONENTS TO TREAT SEVERE ACETABULAR DEFECTS WITH PELVIC DISCONTINUITY

Stuart Callary[1,2], Demien Broekuis[3], Jessica Barends[3], Boopalan Ramasamy[1,2], Rob Nelissen[3], Bart Kaptein[3], Bogdan Solomon[1,2]

[1]Centre for Orthopaedic and Trauma Research, The University of Adelaide, Adelaide, SA, Australia
[2]Department of Orthopaedics and Trauma, Royal Adelaide Hospital, Adelaide, SA, Australia
[3]Leiden University Medical Center and Leiden University, Leiden, The Netherlands
email: bogdan.solomon@sa.gov.au

## INTRODUCTION

The incidence of revision total hip arthroplasty (THA) has increased over time [1], and this upward trajectory is projected to continue. Excluding re-revision for infection, acetabular components' survival in first-time revision THA is only 64% at 10 years [2]. The risk of failure due to loosening also increases with each subsequent re-revision [3]. Reconstruction options for treating large acetabular defects at revision THA include antiprotrusio cages, porous tantalum metal acetabular revision system (TMARS) with augments and shells, bone impaction grafting with metal meshes, hemispherical implants with hook and flanges, cup-cage reconstructions and custom triflange acetabular components (CTAC).

While TMARS and CTAC components have the most promising reported re-revision rates for aseptic loosening in these cases, the re-revision rates are still high. It would be advantageous to investigate biomechanical factors known to influence initial implant stability, a surrogate for longer-term success. To the best of the authors' knowledge, no study exists that analyses these different revision systems used to treat the exact same large acetabular defects with pelvic discontinuity, and directly compare implant-related modifiable factors that influence the outcomes. This study aimed to compare 1) the amount of hip bone removed for reconstruction; 2) the location and amount of IBA achieved; and 3) the restoration of the hip joint COR between actual TMARS reconstructions and a virtual CTAC implant designed for the same cases.

## METHODS

Pre- and post-operative CT scans from 10 patients who underwent revision THA with a TMARS construct for a Paprosky IIIB defect with pelvic discontinuity were prospectively collected. Computer models of the CTAC implant were generated from preoperative CT scans for each case. Computer models of the TMARS construct were segmented from postoperative CT scans using a semi-automated method. The amount of hip bone removed; the implant-bone apposition (IBA) achieved; and the restoration of the hip centre of rotation (COR) were calculated for each for CTAC and TMARS reconstructions.

## RESULTS AND DISCUSSION

The median amount of bone removed for CTAC implants was significantly less than TMARS reconstructions (1.16cm$^3$, range 0.05-10.1 versus 9.07cm$^3$, 2.27-67.3, p=0.007). There was no significant difference between the median overall IBA between CTAC and TMARS reconstructions (56.6cm$^2$, 13.6-84.3 versus 54.8cm$^2$, 24.2-107.7, p=0.683). However, there was significantly less IBA within the residual acetabulum (25.5cm$^2$, 4.7-64.9, versus 45.2cm$^2$, 24.2-90.25, p=0.001), and conversely, significantly more IBA with the outer cortex of the hip bone for CTAC compared to TMARS reconstructions (23.2cm$^2$, 7.1-63.3, versus 0cm$^2$, 0-38.8, p=0.009). The mean hip joint COR of TMARS reconstructions differed a mean 11.1mm (range 3-28) compared to CTAC implants.

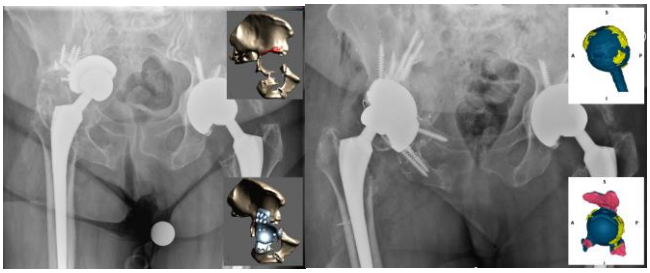

**Figure 1:** (A) Preoperative AP pelvis radiograph of Case 1. The top inset image illustrates the pelvic bone planned to be removed (in red) to reconstruct this defect with a CTAC implant, and the bottom inset image of the CTAC implant modelled. (B) Immediate postoperative AP pelvis radiograph after reconstruction with a TMARS construct. The top inset image illustrates the IBA achieved (yellow) with the TMARS construct, and the bottom inset image demonstrates the IBA with the planned CTAC implant (yellow).

## CONCLUSIONS

In using TMARS more bone is removed, thus achieving more IBA within the residual acetabular bone. In CTAC, the amount of bone removed is minimal, while the IBA is more evenly distributed between the residual acetabulum and the outer cortex of the hip bone. These differences suggest that these implants used to treat pelvic discontinuity might achieve short and long term stability through different mechanisms.

## ACKNOWLEDGEMENTS

Stuart Callary was supported by a Research Fellowship from The Hospital Research Foundation Group during this study.

## REFERENCES

1. Schwartz AM, et al. *J Arthroplasty.* 2020;35(6S):S79-S85
2. AOA. Australian Orthopaedics Association National Joint Replacement Registry. Adelaide; 2018
3. Espehaug B, et al., *CORR 1998(351):135-48.*

# APPROPRIATE ANTIBIOTIC DURATION IN PAEDIATRIC BONE AND JOINT INFECTION: A SYSTEMATIC REVIEW

[1]Sarah Hunter, [2]Heidi Chan, [3]Haemish Crawford, and [4]Joseph Baker

[1]University of Auckland Faculty of Medical and Health Sciences, New Zealand
[2]Auckland City Hospital, Orthopaedic Department, Auckland, New Zealand
[3]Starship Childrenôs Hospital, Orthopaedic Department, Auckland, New Zealand
[3]Waikato Hospital, Orthopaedic Department, Waikato, New Zealand.
email: shun472@aucklanduni.ac.nz

## INTRODUCTION

Optimal duration of antibiotic therapy for childhood bone and joint infection (BJI) remains controversial, despite recent literature in support of shorter courses and early oral switch. We have reviewed the literature to summarize current evidence for reduced duration of antibiotic therapy with particular attention to regional variation in pathogen type and treatment success.

## METHODS

Systematic review was undertaken over the period Jan 1980 - Dec 2022 for children aged up to 18 years. Cohort studies, systematic reviews, randomized controlled trials, and prospective studies were analysed for data on treatment success rates and time of therapy.

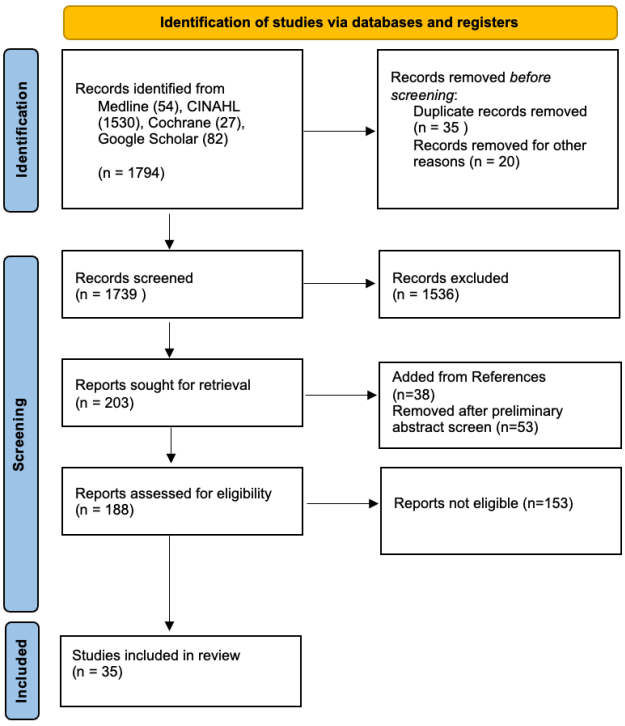


**Figure 1: Flow Chart of Studies Included in Systematic Review**

## RESULTS AND DISCUSSION

A total of 34 studies met inclusion criteria reporting treatment duration for 8337 cases of BJI. There were five prospective studies, 21 cohort studies, six randomized controlled trials, and three systematic reviews. The shortest duration of treatment trialed was a combined oral and intravenous course of fifteen days for children with either AHO or SA. In the populations tested by this review, there were no increased rates of treatment failure as a consequence of shortened antibiotic therapy. Comparisons between studies limited by heterogenous inclusion criteria; children with complex disease or comorbidity are usually excluded from analysis. Randomized controlled trials could be classed as moderate grade of evidence due to issues with blinding, follow-up, and prolonged recruitment.

## CONCLUSIONS

There is moderate evidence for shortened duration of therapy with early switch to oral antibiotics in select patients. Studies reporting good success for reduced therapy included healthy patients with uncomplicated disease. Regional disease variation and study protocol heterogeneity limits widespread adoption of short-course treatment. The experience of BJI is diverse. Although the majority of children respond well to treatment there is subset who demonstrate acute or chronically complicated disease. Pathogen virulence and host genetic vulnerability likely impact recovery. Further research is needed to define patient and disease factors that contribute to treatment failure.

# Thursday, December 9

## POSTERS

# SYSTEMATIC REVIEW AND META-ANALYSIS OF PATELLAR MORPHOMETRIC DIFFERENCES BETWEEN MALES AND FEMALES

[1,2]Tahlia J Stewart*, [2]Jo Menard, [1,3]Joe Lynch and [2]Laura AB Wilson

[1]Trauma & Orthopaedic Research Unit, Canberra Health Services, Canberra, ACT, Australia
[2]School of Archaeology & Anthropology, Australian National University, Canberra, ACT, Australia
[3]Medical School, Australian National University, Canberra, ACT, Australia
email: tahlia.stewart@act.gov.au

## INTRODUCTION

Estimating sex differences in patellar morphology is of considerable interest in understanding the etiology of knee joint pathologies [1]. Studies on sex differences in patellar morphology report mixed results on local populations, using measurements obtained via CT, MRI, Xray, or calipers on fresh or dry bone [2-6]. Here we assess sex differences of patellar morphometrics in healthy individuals and investigate how these vary with measurement and imaging methodologies.

## METHODS

A literature search identified 2,256 articles. Following duplicate removal, title, and abstract screening, 20 articles were included in the systematic review and meta-analyses. These 20 papers were assessed for methodologic quality using MINORS [7]. Data extracted comprised patella height, width, thickness, articular facet height, patella facet thickness, lateral and medial facet widths, patella tilt angle, volume, and mass. Quality effects meta-analyses were performed to determine differences in the pooled means. Heterogeneity scores ($I^2$) and weighted mean differences (WMD) were reported. Sensitivity analyses were performed to assess the effect of dry or fresh patellae, and imaging modality on outcomes.

## RESULTS AND DISCUSSION

2,788 participants were included. Male patellae were consistently larger in all measurements, however there was high heterogeneity, and broad ranges in many measures [Table 1]. Further investigation of sex differences could inform sex-specific etiology of knee pathologies identified elsewhere [8].

**Table 1:** Quality effects analysis, $p$ <0.05.

| Measurement | $I^2$ (%) | WMD | 95% CI |
|---|---|---|---|
| **Height** | 65 | 5.56mm | 5.15-5.97 |
| **Width** | 77 | 5.38mm | 4.88-5.89 |
| **Thickness** | 86 | 2.45mm | 2.05-2.85 |
| **Articular Facet Height** | 80 | 3.45mm | 2.68-4.21 |
| **Mass** | 97 | 4.65g | 2.95-6.36 |
| **Facet Thickness** | 95 | 1.52mm | 0.40-2.64 |

Modality subgroup heterogeneity was inconsistent, with MRI and CT scoring 0% for PH and PW respectively, but all other heterogeneity scores were >25% [Figure 1], which makes quantifying sex differences challenging.

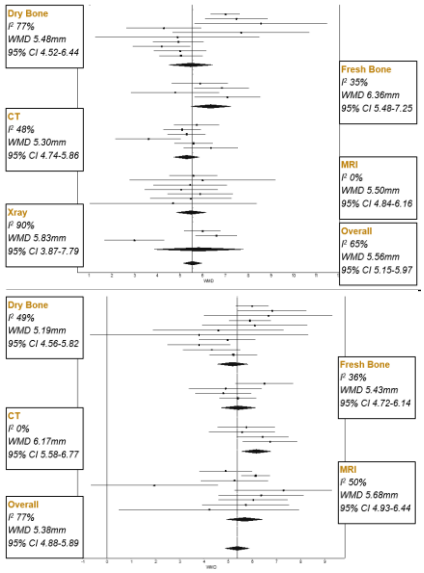


**Figure 1:** Patella height quality effects [top], and patella width [bottom] by measurement and imaging subgroup.

## CONCLUSIONS

Differences in measurements between image modality have been identified [9], but our results indicate that even within sub-groups, high heterogeneity persists, implying that variance cannot be wholly attributed to this. This variance could be due to non-uniform patella measurements, or wide human variation.

## REFERENCES

1. Fox AJ, et al., *The Journal of Knee Surgery.* **25**:127-142, 2012.
2. Li M, et al., *Orthopaedic Surgery*. **13**:458-465, 2021.
3. Muhamed R, et al., *Anatomy & Cell Biology*. **50**:99-103, 2017.
4. Singla K, et al., *Journal of Punjab Academy of Forensic Medicine & Toxicology*. **21**:58-68, 2021.
5. Abdel Moneim WM, et al., *American Journal of Forensic Medicine & Pathology*. **29**:136-140, 2008.
6. Akhlaghi M, et al., *Journal of Forensic & Legal Medicine.* **17**:150-155, 2010.
7. Slim K, et al., *ANZ Journal of Surgery*. **73**:712-716, 2003.
8. Boling M, et al., *Scandinavian Journal of Medicine & Science in Sports*. **20**:725-730, 2010.
9. Carew RM, et al., *Journal of Forensic Radiology & Imaging.* **19**:100348, 2019.

# PATIENT-SPECIFIC 3D MODELS TO INVESTIGATE THE EFFECT OF TWISTED STRUCTURE OF THE ACHILLES TENDON ON STRAIN DISTRIBUTION

[1]Alessia Funaro, [2]Vickie Shim, [1]Ine Mylle and [1]Benedicte Vanwanseele

[1] Human Movement Biomechanics Research Group, KU Leuven, Leuven, Belgium
[2]Auckland Bioengineering Institute, University of Auckland, Auckland, New Zealand
email: alessia.funaro@kuleuven.be

## INTRODUCTION

The Achilles tendon (AT) is a complex structure, consisting of three twisting sub-tendons [1], which influence the AT strain [2]. In Achilles tendinopathy, the tendon material properties and geometry are altered, in particular decreased Young's modulus and tendon thickening [3]. The unilateral heel drop and heel rise exercises are commonly included in the rehabilitation protocols, but it remains unknown if these exercises provide an optimal strain [4] in Achilles tendinopathy patients. Finite element (FE) models of the AT facilitate the investigation of the effects of tendinopathic changes on local tendon strain [5]. The main aim of this study was to investigate the impact of two types of rehabilitation exercises on AT strain in patients with Achilles tendinopathy, including the effect of twist of the Achilles sub-tendons.

## METHODS

Ten participants with mid-portion Achilles tendinopathy (7 males, 3 females; age = 46 ± 16 years; weight = 75 ± 16 kg; height = 178 ± 10 cm; VISA-A score: 76 ± 17) participated in the study. The subject-specific geometries of the free AT were developed using 3D freehand ultrasound. Free form deformation method was used to develop subject-specific FE models of the AT for each type of twist, as in our previous study [6]. As a result, each subject had three different meshes, leading to total 30 subject-specific FE models used in our study. Material properties were defined as an incompressible, transversely isotropic hyperelastic material [7]. The subject-specific Young's modulus was calculated as the slope of the line fitted to the stress-strain data between 30% and 60% of the peak force for each patient (Young's modulus: 484.9 ± 125.7 MPa). Muscles forces of each patient were obtained by a combination of 3D motion capture and musculoskeletal modelling during a unilateral heel drop and a unilateral heel rise. The average of the muscle forces among patients was used as force boundary conditions for running subject-specific FE analysis. The average strain in the mid-portion and the location of the peak of the maximum principal strain were calculated to compare the strain patterns between different exercises and twist types.

## RESULTS AND DISCUSSION

Average strain in the mid-portion of the AT is larger during unilateral heel drop compared to heel rise ($p < 0.05$), for all the types of twist (Type I: 0.097 ± 0.028 and 0.084 ± 0.014, Type II: 0.097 ± 0.015 and 0.088 ± 0.013, Type III: 0.1 ± 0.017 and 0.09 ± 0.014, average ± standard deviation, for heel drop and heel rise, respectively). There was no significant effect of the twist for unilateral heel drop ($p=0.846$) nor for the heel rise ($p=0.067$). The peak strain is located in the mid-portion, where the thickened area is for the majority of the patients (n=6).

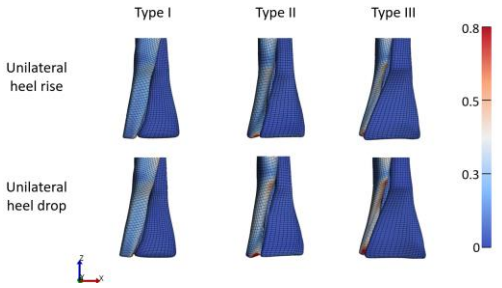


**Figure 1:** A representative example of the distribution of the maximum principal strain for the three types of twist and the two exercises.

## CONCLUSIONS

The eccentric unilateral heel drop exercise resulted in significantly higher average strain compared to concentric unilateral heel rise, for all the three types of twist. The twist didn't influence the average strain. However, it influenced the location and magnitude of the peak strain. None of the exercises induce an optimal strain [4]. The location of the peak strain showed large variation across patients but it didn't change between exercises. The location of the peak strain is more related to the individual material properties and geometry rather than the muscle forces. Using these models, we will be able to further investigate the large variability in geometry and material properties amongst Achilles tendinopathy patients. This could allow to explore the potential of patient-specific rehabilitation programs, by including patient-specific material properties, geometry and muscle forces.

## REFERENCES

1. Pękala et al, *Scand J Med Sci Sports*, **27**:1705-1715, 2017.
2. Knaus et al, *Front. Bioeng. Biotechnol*, **9**:1-10, 2021.
3. Arya and Kulig, *J Appl Physiol*, **108**:670–675, 2010.
4. Pizzolato et al, *Br. J. Sports Med*, **53**:11-12, 2019.
5. Shim et al, *J. Biomech*, **82** :142-148, 2019.
6. Funaro et al, *Front. Bioeng. Biotechnol*, **10**:1207, 2022.
7. Weiss et al, *Comput. Methods Appl. Mech. Eng*, **135**:107–128, 1996.

# INCIDENCE AND ECONOMIC BURDEN OF ACHILLES TENDON INJURIES IN AOTEAROA NEW ZEALAND BETWEEN 2010 AND 2018

[1]Scott Bolam, [1]Dorit Naot, [1]Ha Seong You, [1]Subhajit Konar, [1]Gregory Gamble, [1]Sarah-Jane Paine, [1]Nicola Dalbeth, [1]Jillian Cornish, [1]David Musson

[1]School of Medical Sciences, University of Auckland, Auckland, New Zealand
email: s.bolam@auckland.ac.nz

## INTRODUCTION

Achilles tendon injuries are prevalent and require lengthy and costly management. This study aimed to determine the relationship between demographic variables and the incidence and economic burden of Achilles tendon injuries in the Aotearoa New Zealand population.

## METHODS

This retrospective cohort study used data collected from 2010 to 2018 by the New Zealand Accident Compensation Corporation (ACC), which covers every individual injured in an accident. Achilles injury data were categorised by sex, ethnicity, age, and socioeconomic deprivation index. Age-ethnicity-specific population estimates from the 2018 census were sourced from Statistics New Zealand.

## RESULTS AND DISCUSSION

Over the study period, 130,339 claims related to Achilles injuries had been accepted by ACC, with an associated cost of over NZ$180 million. The average cost per claim increased by 37.48% (95% CI 34.83%, 40.2%) during that time, and in 2018 was 83.11% (95% CI 80.87%, 85.13%) higher for males than females. The number of claims was higher for people living in areas of less economic deprivation, but the average cost per claim was higher for those in more deprived areas. Analysis of the 2018 standardised claim number for the four main ethnicities in Aotearoa New Zealand—Asian, European, Māori, and Pacific Peoples—found that number of claims/ 100,000 people was highest for people of European ethnicity (307 claims) and lowest for people of Asian ethnicity (82). The total cost of claims/ 100,000 people was lowest for people of Asian ethnicity (NZ$250,000) and highest for Māori (NZ$820,000). Analysis of age-standardised cost found the highest claim cost for Māori aged 40–59 years.in single column format.

## CONCLUSIONS

The incidence and economic burden of Achilles tendon injuries increased over the nine-year study period. The socioeconomic disparities and the differential representation of ethnic groups identified here should be addressed to achieve equity in health outcomes and reduce the burden of Achilles tendon injuries.

# TIBIOFEMORAL ELASTICITY DURING GAIT: A MUSCULOSKELETAL MODELLING STUDY OF COMPLIANCE

[1]Francesca Bucci, [1]Mark Taylor, [1]Rami Al-Dirini and [2]Saulo Martelli

1. Medical Device Research Institute, College of Science and Engineering, Flinders University, Adelaide, SA, Australia
2. School of Mechanical Medical & Process Engineering, QUT, Brisbane, Australia
email: francescabucci@flinders.edu.au

## INTRODUCTION

Personalized musculoskeletal models enable studying individual features of tibiofemoral motion. Understanding the separate effects of tibiofemoral (TF) geometry [1] and elasticity [2] during normal activity is crucial for researchers and clinicians. However, complex geometry-based musculoskeletal models are computationally expensive and challenging to identify in vivo [3]. We propose using fast rigid-body models [4] for tibiofemoral geometry and a lumped-parameters compliance matrix for the elastic response [5]. This work aims to demonstrate studying tibiofemoral motion during normal activity using the compliance matrices.

## METHODS

A healthy female subject (23 years old, height=1.65m, mass=61kg) [5] was modeled with a 25-segment, 52-degree-of-freedom system, incorporating tibiofemoral contact surfaces and 14 non-linear ligament springs. OpenSim Joint and Articular Mechanics - JAM framework [5] were used for calculating active and passive TF kinematics, inverse dynamics, muscle activation, forces, and tibiofemoral contact forces. TF forces were provided by elastic foundation contact [5]. Active TF motion was replicated from Lenhart gait simulation [5]. To simulate passive TF motion, knee-spanning muscles were removed, external forces were scaled down to 1%, gravity was set to zero, and ligament stiffness was reduced by 50% to reduce the average ligament reaction force to less than 50N. The 6x6 compliance matrices (CMs) were defined as follows:

$$[CM] \cdot \{F_a - F_p\} = \{X_a - X_p\},$$
$$where\ \{X_a - X_p\} = (\Delta t_{AP}, \Delta t_{SI}, \Delta t_{ML}, \Delta\theta_{AA}, \Delta\theta_{IE}, \Delta\theta_{FE})$$
$$and\ \{F_a - F_p\} = (\Delta F_{AP}, \Delta F_{SI}, \Delta F_{ML}, \Delta M_{AA}, \Delta M_{IE}, \Delta M_{FE})$$

where (a) are active and (p) passive relative variations of TF linear (t) and angular (θ) displacements, forces (F), and moments (M) in the knee joint coordinate system in Anterior-Posterior (AP), Superior-Inferior (SI), Medial-Lateral (ML), Adduction-Abduction (AA), Internal-External (IE), Flexion-Extension (FE). CMs were calculated for each frame of the gait cycle and analyzed along with the compliance of each axis.

## RESULTS AND DISCUSSION

The tibiofemoral compliance results during walking were as follows (mean ± standard deviation): AP, 2262 N/mm (± 3757 N/mm); SI, 4.9e+04 N/mm (± 4.7e+05 N/mm); ML, -146 N/deg (± 191 N/deg); AA, 14 N/deg (± 203 N/deg); IE, 549 N/deg (± 7296 N/deg). All values were scaled down by a factor of 10^5. The AP case study was used to illustrate elasticity, as translation and forces along the AP axes showed the highest variability across the gait cycle (Fig.1). Passive and active differences in AP translation, contact force, and compliance were reported for each frame (Fig.1); a 3D representation of the CMs is shown for knee representative flexion angles.

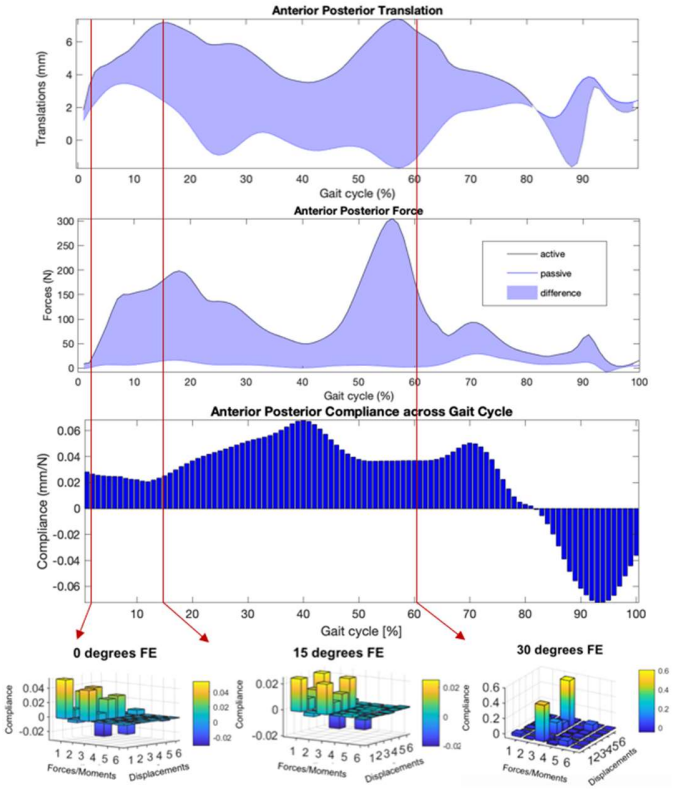


**Figure 1:** TF differences in AP translation, contact forces (passive vs. active), and compliance during walking. 3D representation of in vivo CMs at 0°, 15°, and 30° knee flexion.

## CONCLUSIONS

This study's method offers a viable alternative to characterize the in-vivo TF elasticity and load-dependent behaviour of the knee during physical activity, while reducing the computational time. Future work will provide better understanding of knee elasticity and its inclusion into musculoskeletal models.

## REFERENCES

1. Smoger et al., J.Orthop.Res., **33(11)**:1620-1630,2015
2. Myers et al., Am. J. Sports Med., **40(1)**:170-178,2012
3. Lenhart et al., Annu.Rev. Biomed. Eng., **43(11)**: 2675-2685, 2015.
4. Martelli et al, Gait Posture, **80**: 374-382, 2020
5. Lamberto et al, Med. Eng. Phys, **64**: 80-85,2019

# INTRAOPERATIVE FORCE MEASUREMENTS TO SUPPORT THE DECISION-MAKING IN MUSCLE-TENDON LENGTHENING SURGERIES

[1]Filiz Ates, [2]Stefanos Tsitlakidis, [2]Marco Götze, [2]Sébastien Hagmann, and [2]Sebastian I. Wolf

[1]Experimental Biomechanics Group, ISD, Aerospace Engineering, University of Stuttgart, Stuttgart, Germany.
[2]Universitätsklinikum Heidelberg, Klinik für Orthopädie, Heidelberg, Germany.
email: filiz.ates@isd.uni-stuttgart.de

## INTRODUCTION

Joint deformities, whether congenital or caused by neurological diseases, significantly impede human movement. Patients often undergo surgical interventions in order to correct the deformities and improve their gait. Achilles tendon lengthening (ATL) is a commonly employed surgical technique to expand the restricted ankle range of motion (ROM). To date, there is no objective means to quantitatively determine the required extent of lengthening that can alleviate joint stiffness without resulting in critical muscle weakening. This study aims to implement an intraoperative approach [e.g. 1, 2] to assess the effects of ATL surgery on the triceps surae muscle group and ankle joint. The research questions addressed are the extent to which ankle ROM is increased and the potential decrease in muscle forces post-ATL, and whether forces measured in patients with a neurological disease exhibit different characteristics compared to those with idiopathic foot deformities.

## METHODS

The isometric forces generated by the triceps surae muscle were measured from ten patients (11.3 ± 3.0 years old) undergoing ATL surgery. Among the patients, five had idiopathic foot deformity, four had cerebral palsy, and one had a hereditary motor and sensory neuropathy. To measure the forces, a buckle force transducer was directly attached to the Achilles tendon. Data on muscle-tendon forces were collected at various ankle positions both before and after the ATL procedure. In six patients, additional data on active forces were collected by stimulating the muscle group to its maximum capacity. The values of passive and active forces were analyzed in relation to the ankle angle.

## RESULTS AND DISCUSSION

Ankle ROM increased (pre-ATL: 33.0°±9.0° vs post-ATL: 62.5°±9.6°; $p<0.0001$), while passive forces decreased (on average, 42.5N; $p<0.0001$) after the ATL intervention [3]. These findings support the anticipated effect of ATL on ankle movement, which includes reducing passive resistance and enhancing the joint range.

Consistent with previous reports [1,2], we observed substantial inter-subject variability for both passive and active forces.

Importantly, patients with neurologic involvement showed higher passive muscle forces than patients with idiopathic foot deformities (43.0N on average, $p=0.0016$) (Fig. 1). This indicates a different muscular adaptation mechanism between neurologic and non-neurologic conditions.

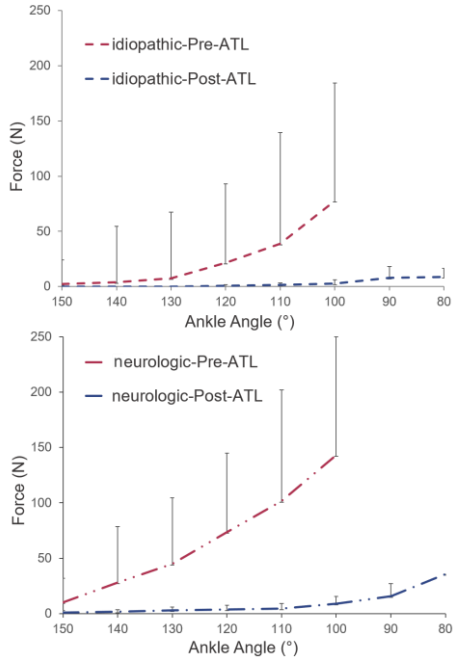


**Figure 1** Passive muscle force-ankle angle characteristics of patients with (upper panel) idiopathic food deformities and (lower panel) neurologic diseases pre- and post-ATL.

## CONCLUSIONS

Our study proposes a novel approach that offers immediate and objective muscle force data during surgery, challenging the reliance on surgeons' intuition when determining the appropriate lengthening "dose." Our findings indicate that this approach can assist in the intraoperative decision-making process by aiding in the determination of optimal muscle-tendon length and joint position. To gain a comprehensive understanding of the underlying mechanisms in muscular adaptation between neurological and non-neurological conditions, further investigation involving intraoperative data collection and histological examinations is warranted.

## ACKNOWLEDGEMENTS

This work was supported by the Federal Ministry of Education and Research through the project ”3DFoot” (01EC1907B).

## REFERENCES

1. Ates F, et al., *Clinical Biomechanics* **28** (1), 48-54, 2013.
2. Ates F, et al., *J Electromyogr Kinesiol* **28**, 130-6, 2016.
3. Brendecke E, et al., *Frontiers in Physiol* **14**, 366, 2023.

# EFFECT OF SCALING ON HKA ANGLE IN PREOPERATIVE TOTAL KNEE REPLACEMENT PATIENTS

[1]Salindi P. Herath, [1]David Hobbs, [2]Dominic Thewlis, [3]Christopher Wilson, [1]Mark Taylor

[1]Medical Device Research Institute, Flinders University, Adelaide, SA, Australia [2]Faculty of Health and Medical Sciences, University of Adelaide, Adelaide, SA, Australia [3]College of Medicine and Public Health, Flinders University, Adelaide, SA, Australia

email: salindi.herath@flinders.edu.au

## INTRODUCTION

The accuracy of musculoskeletal models, used to simulate joint motion and dynamics, is limited by the ability to capture the differences between individuals. Body segments are commonly scaled linearly using markers placed on surface anatomical landmarks. However, atlas based statistical shape modelling can also be used to scale and may create models that are more physiologically accurate [1].

Inclusion of lower limb alignment in musculoskeletal models can produce changes in knee joint kinematics, kinetics, and more accurately estimated knee joint loading [2]. People with no knee pathology tend to have a hip-knee-ankle angle within 3° of 180°. However, people with knee joint pathologies such as osteoarthritis can have varus or valgus malalignments. The aim of this study was to investigate the reproducibility of frontal plane knee joint alignment across different scaling methods.

## METHODS

This study examined HKA angle from four scaling methods on 11 people (6 male and 5 female) awaiting total knee replacement surgery for osteoarthritis. All consented participants underwent gait analysis, had supine lower limb computed tomography (CT) scans and long leg X-rays taken pre-operatively. X-rays were used to measure the HKA angle of each participant.

A musculoskeletal model available on OpenSim (Modified gait2392 model) [3] was used in this study with knee adduction/abduction motion limited to 0° as this rotation cannot be accurately captured using external markers. For each person, the following four scaling methods were implemented using OpenSim 3.3.

1. Linear scaling based on external markers
2. Atlas based statistical shape modelling using marker positions captured during a static trial using MAPClient
3. Atlas based statistical shape modelling using marker positions placed on anatomical landmarks of surface models from segmented supine, non-weight bearing CT scans using MAPClient
4. Method 3 with the addition of the femoral and tibial mechanical axes from weight bearing X-rays

The HKA angle was calculated from a static trial after scaling using each method and compared to the HKA angle obtained from a weightbearing X-ray for each participant. Coronal plane knee joint moments from inverse dynamics (OpenSim) were compared across all four models.

## RESULTS AND DISCUSSION

HKA angle varied between 166° and 202°. Most participants (n=9/11) were varus aligned, one was mechanically aligned (178°), and one was valgus aligned. For all varus and valgus participants, scaling method 4 led to an HKA angle closest to that obtained from weightbearing X-rays (Table 1). Method 3 was just as accurate as Method 4 for the participant who was mechanically aligned (179° vs 177°).

*Table 1. Median and ranges of HKA angles from X-ray and each method.*

| | X-RAY | 1 | 2 | 3 | 4 |
|---|---|---|---|---|---|
| MEDIAN | 171 | 181 | 179 | 179 | 171 |
| MIN | 166 | 177 | 176 | 176 | 165 |
| MAX | 202 | 214 | 209 | 206 | 205 |

For most participants (n=7/11), Method 3 led to the lowest magnitude of internal abductor/adductor moments and Method 4 led to the largest abductor/adductor moment (n=9/11). During stance phase, knee abductor moment increased in all varus aligned participants by 0.012 Nm/kg*ht (minimum increase) to 0.227 Nm/kg*ht (maximum increase) from Method 3 to 4. In the participant who was mechanically aligned, knee abductor moment increased by 0.121 Nm/kg*ht and in the participant with valgus alignment, there was an increase in internal knee adductor moment of 0.424 Nm/kg*ht.

## CONCLUSIONS

Changes in alignment affect joint motion and dynamic predictions from musculoskeletal modelling and standard scaling methods do not accurately capture the HKA angle of people with knee joint malalignments. Including the HKA angle obtained from weightbearing X-rays during scaling generated models that more accurately captured varying alignments.

## ACKNOWLEDGEMENTS

We acknowledge ARC-CMIT for providing funding for this study.

## REFERENCES

1. Bakke D, et al., *J of Biomech.* **107**. 2020
2. Lerner Z, et al. *J of Biomech.* 48**(4)**. 2015.
3. Saxby D, et al., *Gait and Posture*. **49**. 2016.

# STUDY OF HUMAN SHOULDER BIOMECHANICS USING COMPUTATIONAL MODELLING

[1]Mélody C Labrune, [2]S.H. Hosseini Nasab, [1,3] David T Axford, [1]Robert Potra, [1]Joseph Cadman, [1]Danè Dabirrahmani, [2]William R. Taylor, [1,3]Louis M Ferreira, [1] Sumit Raniga, [1]Richard Appleyard

[1]Faculty of Medicine, Health and Human Sciences, Macquarie University, Sydney, NSW, Australia
[2]ETH Zürich, Institute for Biomechanics, Zürich, Switzerland
[3]Dept of Mechanical and Materials Engineering, Western University, London, Canada
email: melody.labrune@hdr.mq.edu.au

## INTRODUCTION

Computational modelling, considered as non-invasive tool, is often used to study human joint biomechanics. One of the most unconstrained joints of the human body is the shoulder joint, often associated with multiple clinical challenges. Several *in-silico* studies have been previously performed; however, their validations were generally insufficient. The aim of this study is to develop *in-silico* models including musculoskeletal and finite element models to investigate the impact of the different shoulder clinical challenges on its biomechanics. The focus of this abstract is to introduce one part of the model's validation.

## METHODS

A subject-specific musculoskeletal model (MM) and finite element model (FEM) were developed using OpenSim [1] and Abaqus (Dassault Systemes, 2021), respectively. Based on previous published models [2] the six degree of freedom (DoF) MM (Fig. 1), is actuated by eight Millard 2012 Equilibrium type muscles {Anterior, Lateral and Posterior Deltoids (AD, LD, PD respectively), Subscapularis Superior (SBS) and Inferior (SBI), Supraspinatus (SSP), Infraspinatus (ISP), Teres Minor (TM)}. The FEM was developed using the subject's CT scans and bone properties were mapped from CT scans using an Abaqus plug-in, Bonemappy (https://github.com/mhogg/bonemapy.git).
Muscle and joint reaction forces were predicted for the MM using Concurrent Optimization of Muscles Activation and Kinematics (COMAK) algorithm [3]. Healthy shoulders were tested under different ranges of motion (RoM) {Abduction (ABD) and Forward Flexion (FF)}. The validation of the model was performed by comparing the kinematics and muscle forces from the MM to our in-house world leading cadaveric shoulder simulator. These validated MM muscle and joint reaction forces were then used as inputs for the FEM. FEM bone strain was also validated by comparing with localised strain gage readings generated by the cadaveric shoulder simulator.
In this abstract, first results for the MM are presented during FF. Muscle forces from the MM and the cadaveric shoulder simulator forces were compared using Pearson correlation coefficients, allowing an assessment of the validity of the MM.

## RESULTS AND DISCUSSION

During FF, both specimens showed a high correlation (Pearson's r>0.5) for dominant muscles (Specimen 1: AD, SBS, SBI, SSP, Specimen 2: AD, LD, PD, SBS, SSP, ISP and TM) and a low correlation (Pearson's r<0.5) for the others.

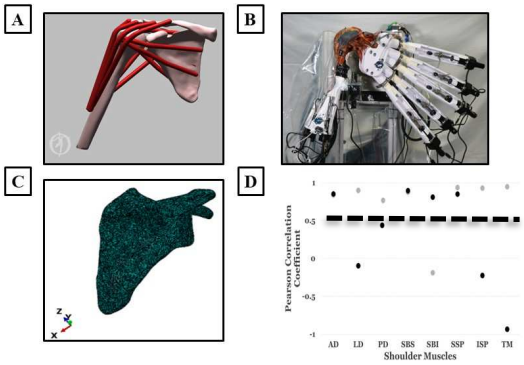


**Figure 1:** (A) MM, (B) In-house world leading cadaveric shoulder simulator, (C) FEM, (D) Shoulder muscle forces during FF. Black dotted line: Pearson's r= 0.5, Black dots= Specimen 1, Grey dots= Specimen 2.

Therefore, the results showed an agreement for dominant muscles for FF between the MM and the cadaveric shoulder simulator. The results for the non-dominant muscles can be explained by the use of different strategies between the two methods to solve the muscle redundancy problem.

## CONCLUSIONS

Only results for FF were introduced in this abstract showing close agreement between the cadaveric shoulder simulator and the MM for dominant muscles for forward flexion. The forces predicted were then input in the FEM and compared to the cadaveric shoulder simulator for validation. This double computational modelling approach allows non-invasive tools to be developed to study the shoulder biomechanics and the impact of shoulder clinical challenges.

## ACKNOWLEDGEMENTS

We would like to thank Macquarie University for the scholarship funding this research, and Dr. Sara Sadat Farshidfar and Michael Hogg for their technical support.

## REFERENCES

1. Delp SL, et al. *IEEE Trans Biomed Eng*. 2007;**54**(11):1940-50.
2. Saul KR, et al. *Comput Methods Biomech Biomed Engin*. 2015;**18**(13):1445-58.
3. Wu G, at al. *J Biomech*. 2005;**38**(5):981-92.
4. Smith, C. R., et al. *Journal of biomechanics*, **82**, 124-1

# A FINITE ELEMENT MODEL FOR EVALUATING GRAFT STABILITY IN LATARJET SURGERY UNDER VARIED FIXATION TECHNIQUES

[1]Hamid Reza Jarrah, [2,3] Deniz Erbulut, [1]Peter Pivonka, [2]Nicholas R Green and [3]Ashish Gupta, [1]Saulo Martelli

[1] School of Mechanical, Medical and Process Engineering, Queensland University of Technology, Brisbane, QLD, Australia

[2] Herston Bio fabrication Institute, Metro North Hospital and Health Service, Brisbane, QLD, Australia

[3] Queensland Unit for Advanced Shoulder Research (QUASR), Queensland University of Technology, Brisbane, QLD, Australia

email: hamid.jarrah@qut.edu.au

## INTRODUCTION

The Latarjet procedure is a surgical intervention that is commonly used to treat recurrent shoulder dislocations or instability. There is an open debate on the stability and strength of different types of fixations of the graft in this surgery. In the previous studies[1-2] that only investigated graft stress with one type of fixation, we have created a Finite Element(FE) model that can compare the effects of different fixations on graft stability. This model has been validated against a biomechanical study conducted on cadavers [3]. Using this FE model, researchers can study the impact of fixation on graft stability without having to conduct time-consuming and expensive experiments in the lab.

## METHODS

In this study, a CT scan of an intact scapula of a 68-year-old male cadaver with a Body Mass Index (BMI) of 20.24 kg/$m^2$ was chosen. The Screw-Screw fixation method was used for his scapula. A virtual Latarjet procedure surgery was performed with 3D printed jigs for costuming the coracoid transfer procedure. A reproducible 20% glenoid defect was done by aiding the 3D printed tool. The graft then underwent a hundred cycles of loading, ranging from 50 to 160N at a frequency of 1Hz, with the load applied using an indenter[4]. The segmentation process enabled the extraction of the 3D geometry of the scapula, which was then imported into 3-Matic-16 software. The cortical and cancellous bones were modeled independently, and appropriate Elastic modulus (Cortical:10GPa[1], Cancellous:180MPa[4]) were applied separately to these bones. For the analysis of the process, the software ABAQUS/CAE 2022 was selected. A homogeneous, isotropic, and linear elastic model was adopted to the model. To ensure accuracy and reliability, a convergence study was conducted, the size of 0.4mm was chosen as an outcome. Consequently, the model was constructed with a total of 377,183 elements. The load was applied to the graft using an indenter. The constraint in the load direction was free, while in other directions were fixed. The touch point between the graft and the indenter was positioned equidistantly between the screws. To model the interaction between the screws and the graft, a tie (bonded) contact was applied, while the contact between the screws and the glenoid was modeled as a frictional contact(μ=0.3[1]). Additionally, the cortical and cancellous bone were tied (bonded) together. The cannulated screws were represented by a hollow cylindrical shape. A sensitivity study was conducted to examine the impact of Young's modulus(4GPa <Cortical<17GPa[1],60MPa <Cancellous<470MPa[4]) on graft displacement.

## RESULTS AND DISCUSSION

The FE model presented in this research follows the experimental graft stiffness (Figure 1). The model can somewhat encompass the effects of dissipation arising from the friction. In the sensitivity study, the range of the peak displacement values was set between 0.1 and 0.5 mm.

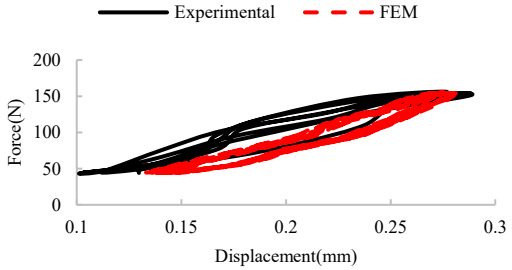


**Figure 1:** Comparison of FE and experimental results

## CONCLUSIONS

The FE model provides an opportunity to assess graft displacement and stiffness, enabling the investigation of fixations' effects on the graft.

## ACKNOWLEDGEMENTS

QUASR, the Herston Bio-fabrication Institute, and the Australian Research Council (IC190100020; FT180100338) are gratefully acknowledged.

## REFERENCES

1. Sano H, et al., Shoulder and Elbow Surgery, **29**: 2632-2639, 2020.
2. Sano H, et al., Shoulder and Elbow Surgery, **30**: 2260-2269, 2021.
3. Ziegenfuss B, Shoulder and Elbow Surgery, **32**: 1370-1379, 2023.
4. Kalouche I, et al., Clinical Biomechanics, **25**: 292-298, 2010.

# AN EFFICIENT METHOD TO PREDICT HIP FRAGILITY FRACTURES IN STATISTICAL SYNTHETIC COHORTS

[1,2,3]Andrea Sgarzi, [1,2]Antonino A. La Mattina and [3]Saulo Martelli

[1]Department of Industrial Engineering, Alma Mater Studiorum - University of Bologna, Italy
[2]Medical Technology Lab, IRCCS Istituto Ortopedico Rizzoli, Via di Barbiano 1/10, 40136 Bologna, Italy
[3]School of Mechanical, Medical and Process Engineering, Queensland University of Technology, Brisbane, Australia

## INTRODUCTION

Testing new osteoporosis drugs requires observing thousands of patients for several years, resulting in extremely high clinical trial costs [1,2]. An emerging option to reduce the number of enrolled subjects is the use of synthetic cohorts for the simulation of clinical trials (the so-called *In Silico* Trials). Yet, running in silico trials is computationally demanding. Recently, a method was proposed, namely the Superposition Principle Method Squared (SPM$^2$), for efficient and accurate calculation of bone strain during activity in statistical populations [3]. The aim of the present work was to implement SPM$^2$ for predicting the risk of fracture in a published synthetic cohort for the prediction of fragility [1]. The SPM$^2$ performance was assessed in terms of efficiency and accuracy relative to corresponding finite-element (FE) solutions.

## METHODS

The statistical cohort was taken from a previous study showing AUC = 0.82 in classifying clinical fracture and non-fracture cases [2]. In summary, the synthetic cohort consisted of 1080 proximal femur models drawn from an Active Shape and Appearance Modelling (ASAM) including 93 principal components (PCs). Femur strength was calculated using 28 finite-element FE simulations representing a range of impact directions during sideways fall. The boundary conditions included the distal hinge, the contact between the ground and the greater trochanter and the hip contact force applied to the femoral head center [3]. The contact model was linearized by replacing the contact with the reaction forces applied, for simplicity, on the first geometric contact node, ensuring the global equilibrium. The SPM$^2$ was constructed by generating 5 instances ranging from -2 SD to +2 SD (1 SD steps) along each of the $m$ PCs in the ASAM model. Strain variations $\Delta\bar{\bar{\varepsilon}}$ were then calculated using the mean ASAM instance strain $\overline{\overline{\varepsilon}}_M$ as reference and plotted against the same 5 scores $w_p$. Cubic functions were fitted to the data thereby providing a link $\overline{\Delta\overline{\varepsilon}_{j,k}}(w_p)$ between changes in geometry, density, and strain. The process was repeated for each of the $n$ forces applied to the model and 49 of the 93 PCs. The strain tensor $\bar{\bar{\varepsilon}}_i$ was then calculated as the superposition of the strain generated by each nominal, arbitrarily chosen, unitary force $f_{unit}$, applied along each $k$ force component in the model and stress changes caused by changes in geometry and bone density for each loading case $i$, according to the equation:

$$\bar{\bar{\varepsilon}}_i = \sum_{j=1}^{n}\sum_{k=1}^{3}\left\{\left[\overline{\overline{\varepsilon}}_M(j,k) + \sum_{p=1}^{m}\overline{\Delta\overline{\varepsilon}_{j,k}}(w_p)\right] \times \frac{f_{i,j,k}}{f_{unit}}\right\} \qquad (1)$$

The SPM$^2$ model was assessed by 1) quantifying the effect of a reduced number of PCs; 2) quantifying the effect of strain interpolation for a 5-PCs ASAM instance with 3 randomly chosen forces, 3) comparing SPM$^2$ and FE solutions for 50 ASAM instances and all the 28 load directions, and 4) quantifying the effect of the simplification of the contact at the greater trochanter and of the hip contact force. All elements were considered, apart from case 3), where the region of interest was the neck surface. The models were compared using RMSE, linear regression and the absolute percentage error. The SPM$^2$ generation, prediction and post-processing time were compared to corresponding FE solution. The SPM$^2$ absolute percentage error was calculated using the FE solution as reference.

## RESULTS AND DISCUSSION

Preliminary results showed that using 49 of the 93 PCs caused a strain error lower than 1.3%. The interpolation of the strain coefficients showed an almost perfect correlation with the corresponding FE solutions ($R^2$ = 1.00, slope = 1.01). The RMSE was 58 με and the maximum median fitting error was equal to 0.44%. The RMSE for the simplified contact at the greater trochanter was < 0.79% in all cases. The simplification of the hip contact force caused the highest errors in the inner head and medial neck reaching RMSE = 1180 με ($R^2$ = 0.4, Slope = 0.79) and decreasing to RMSE = 46 με on the bone surface, or 0.03% of the peak strain. Overall, the strain error in the SPM$^2$ model was 93 – 99% (SD = 38 – 41%). Generating the model took about a week, while a single instance strain was predicted in 5s on a standard laptop computer, which represents a 100x speed up over corresponding FE simulations.

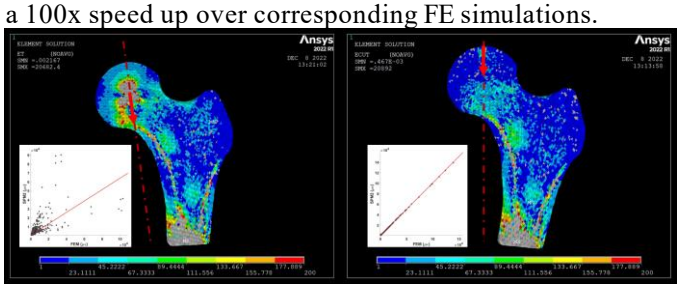

Fig. 1: transversal sections of the element-wise absolute error of SPM$^2$ on the 5-PCs ASAM instance for the single stance (left) center force and (right) surface force.

## CONCLUSIONS

The SPM$^2$ considerably speed up calculation of the fracture risk in a virtual population. The error in both the methods is mostly due to the simplification of the hip contact force and can be moderated by moving the point of application to the head surface. Further research is necessary to complete the quantification of model simplification and verify its capacity to classify fracture and non-fracture cases.

## ACKNOWLEDGEMENTS

Australian Research Council (FT180100338)

## REFERENCES

1. La Mattina et al. *Annals of Biom. Eng.* **51**: 117-124, 2023.
2. Altai et al. *Clinical biomechanics* **68**: 137-143, 2019.
3. Ziaeipoor et al. *Annals of Biom. Eng.* **48** 1694-1701, 2020

# BONE-REMODELLING IN THE FOOT: APPLICATION TO EXERCISE DURING THE COVID-19 LOCKDOWN

[1]Julie Kim, [1]Liangliang Xiang, [2]Piaras Kelly, [1,3,4]Qichang Mei, [5,6]Silmara Gusso, [1,2]Thor Besier and [1,2,4]Justin Fernandez

[1]Auckland Bioengineering Institute, University of Auckland, Auckland, New Zealand
[2]Department of Engineering Science, University of Auckland, Auckland, New Zealand
[3]Faculty of Sports Science, Ningbo University, Ningbo, China
[4]Research Academy of Grand Health, Ningbo University, Ningbo, China
[5]Department of Exercise Sciences, University of Auckland, Auckland, New Zealand
[6]Liggins Institute, University of Auckland, Auckland, New Zealand.
email: hkim375@aucklanduni.ac.nz

## INTRODUCTION

Inspired by Wolff's law, many bone remodelling algorithms have been developed and evaluated, but their application has not been explored in the foot. This study aims to extend the application further, evaluating numerically predicted osteogenic responses at the foot against experimental hopping data collected during the COVID-19 lockdown in New Zealand. Firstly, a subject-specific finite element (FE) model was developed to study morphogenesis at the calcaneus using the bone remodelling algorithm (Model A). Secondly, a FE foot model of the participant from the hopping experiment was built to explore if the algorithm can predict temporal density changes from mechanical loading environmental changes (Model B).

## METHODS

Following ethical approval, participants attended scanning sessions on a SIEMENS scanner (Model A) and a 1.5T Avanto Fit scanner (Model B). Their feet were segmented in Mimics and meshed in HyperMesh to provide a finite element geometry that was solved in Abaqus. A lumped soft tissue model was assigned with Young's modulus of 1.15 MPa, and Poisson's ratio of 0.49. Plantar fascia was represented by linearly elastic connectors with stiffness of 200N/mm. Plantar pressure measured during gait, and Achilles tendon force were applied to load the foot. Model A included walking to reproduce morphogenesis induced by the most dominant daily activity. Model B followed an experiment [1] where a subject performed a hopping exercise on the allocated exercise leg while the other leg served as a control. The exercise lasted one year, with the COVID-19 pandemic lockdown affecting the subject's activity level during the first eight months. Computed tomography (CT) and dual X-ray absorptiometry (DEXA) were collected for Model A and Model B, respectively. A continuum damage mechanics based anisotropic bone remodelling model [2] with evolving setpoint according to the cellular accommodation theory [3] was employed to predict the osteogenic responses.

## RESULTS AND DISCUSSION

A cortical bone layer of similar thickness as the measurement was predicted in Model A by the bone remodelling algorithm around the outer edges of the calcaneus (Figure 1A). Density changes predicted in Model B also shared a similar trend with the measured data (Figure 1B); both legs showed subtle density changes during the lockdown interval, but they gained densities after the lockdown, with more increase happening at the exercise leg.

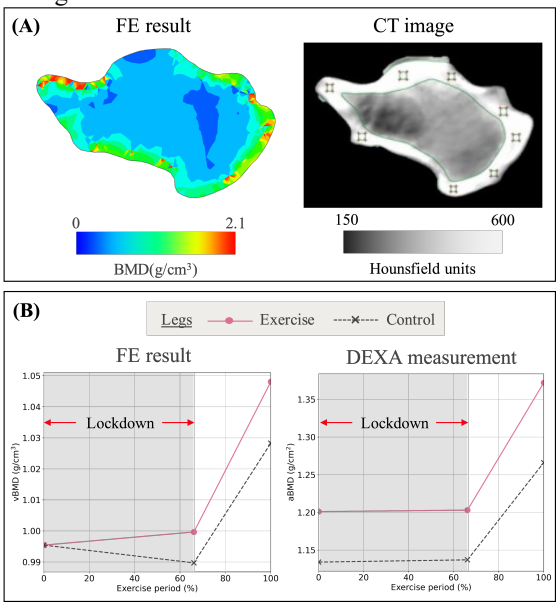


**Figure 1:** (A) Density distribution predicted by the bone remodelling algorithm in Model A, and CT showing relative Hounsfield units at the calcaneus. (B) Predicted and measured density changes during the hopping exercise.

## CONCLUSIONS

This study showed that a widely used bone remodelling algorithm can be successfully extended to the foot and reproduce subject-specific morphological features and how the frequency and the intensity of daily loading influence density changes.

## REFERENCES

1. Allison S J et al., *Bone*. **53**:321–328, 2013.
2. Doblaré M and García J M, *J. Biomech*., **35**:1–17, 2002.
3. Turner C H, *Calcif. Tissue Int.*, **65**:466–471, 1999.

# HIGH LOOSENING RATES AND INFERIOR PATIENT-REPORTED OUTCOMES OF THE CEMENTLESS TIBIAL BASE PLATE IN A MODERN DESIGN OF TOTAL KNEE ARTHROPLASTY

[1,2,3]Octavian Andronic, [1,2]Yue Hao Yang, [1,2,4]Christopher W. Jones and [1,2,5]Piers J. Yates

[1] Department of Orthopaedics, Fiona Stanley and Fremantle Hospitals Group, Murdoch, Western Australia, Australia
[2] Orthopaedic Research Foundation Western Australia (ORFWA), Perth, Western Australia
[3]Balgrist University Hospital, University of Zurich, Forchstrasse 340, 8008, Zurich, Switzerland
[4]Curtin University, Bentley, Perth, Australia 6120
[5]Department of Orthopaedics, St. John of God Hospital Murdoch, Murdoch, Western Australia
email: octavian.andronic@balgrist.ch

## INTRODUCTION

This study reports the short-term outcomes of a modern mobile-bearing TKA design with a cementless tibial base plate with the full-cemented version of the implant.

## METHODS

Patients receiving cementless tibial base plates were compared to those who received a cemented tibial component from the same manufacturer (DePuy Synthes, ATTUNE). Outcome endpoints included: revision rates and reason for revision, complications, patient-reported outcomes (PROMs) using oxford knee score (OKS). The unpaired two-tailed Student's t-test (numerical variables) and the Chi-square test (binary variables) were used to evaluate differences.

## RESULTS AND DISCUSSION

A total of 131 knees with uncemented tibial base plates were compared to a fully-cemented cohort with a minimum follow-up of 12 months. Eleven (8.3%) knees with cementless tibial baseplates were revised (Figure 1), compared to none in the cemented cohort ($p<0.001$). The most common cause of failure was aseptic loosening (91%). The majority of the patients were females (91%), active (Table 1) and heavy (average BMI was 34 kg/m$^2$). The average OKS score difference from preoperative to 12 months was worse in the cementless tibial baseplate group (15.37 ± 12.76 vs 19.61 ± 9.46, p=0.013).

**Figure 1:** Retrieved tibial base plated covered or with traces of fibrous tissue with insufficient osseointegration

## CONCLUSIONS

We have observed higher early failure rates with most revisions for aseptic loosening, as well as worse patient-reported outcomes for the uncemented tibial base plate within one year following TKA.

**Table 1:** Findings in revised uncemented tibial base plates

| Sagittal Stability | Time in situ [years] | Age [years] | Weight [Kg] | Height [cms] | BMI | Gender | Activity Level |
|---|---|---|---|---|---|---|---|
| PS | 0.2 | 72 | 115 | 168 | 40.75 | Female | Moderate |
| PS | 0.5 | 72 | - | - | - | Female | High |
| PS | 0.3 | 76 | 78 | 152 | 33.76 | Female | High |
| PS | 0.5 | 73 | 95 | 172 | 32.11 | Female | High |
| PS | 1 | 67 | 70 | 157 | 28.4 | Female | High |
| PS | 0.7 | 75 | - | - | - | Female | Low |
| PS | 0.5 | 68 | 110 | 158 | 44.06 | Female | High |
| PS | 1 | 81 | 100 | 165 | 36.73 | Female | High |
| CR | 0.1 | 64 | 93 | 182 | 28 | Male | Low |
| PS | 1 | 59 | 90 | 163 | 33.87 | Female | High |
| PS | 1.3 | 72 | 60 | 152 | 25.97 | Female | Moderate |
| *Average* | 0.6 | 70.8 | 90.1 | 163.2 | 33.7 | | |
| *St Dev* | 0.4 | 6.0 | 18 | 9.8 | 6.0 | | |

PS – posterior stabilized; CR – cruciate retaining; BMI – body mass index; St Dev – Standard Deviation

# POTENTIAL THERAPEUTIC TARGETS OF ARTHROFIBROSIS FOLLOWING KNEE ARTHROPLASTY

[1,2]Xingjian Gong, [1,2]Paul N. Smith, [1]Joe Lynch, [1]Tahlia Stewart, [1]Tom Ward, [1,2]Rachel W. Li

[1]Trauma and Orthopaedic Research Unit, ACT Health, Canberra, ACT, Australia
[2]College of Health & Medicine, Australian National University, Canberra, ACT, Australia
email: Xingjian.gong@anu.edu.au

## INTRODUCTION

Total knee arthroplasty (TKA) is an effective surgical procedure to reduce knee pain and restore function in patients suffering from end-stage arthritis. While generally a successful procedure, 3–10% of the patients go on to develop fibrosis in the form of arthrofibrosis post-surgery [1]. Severe arthrofibrosis can lead to excruciating pain and a significant reduction of the knee's range of movement. Some patients have to go through manipulation under anaesthesia (MUA) or revision surgery. Knee arthrofibrosis is a histopathologic response that is influenced by factors like implant materials, surgical techniques, and the patient's individual response. In this study, we use RNA sequencing to screen for potential epigenetic biomarkers and potential pharmaceutical targets.

## METHODS

We have collected blood, soft tissue, and hard tissue from patients undergoing primary TKA for osteoarthritis (age, 18-70 years old) and from patients undergoing MUA due to arthrofibrosis in post TKA. Trizol and Qiagen RNeasy Mini Kit was provided from Qiagen, Australia). MicroRNA isolation and RNA Sequencing were conducted.

## RESULTS AND DISCUSSION

While this project is still ongoing, we are aiming to collect and process samples from 300 patients who underwent primary TKA and MUA. From our pilot study, we have found significant genetic responses in pathways involved in the coordination of inflammatory cytokine release and growth factors. We have identified up or down regulated circulating miRNA from the blood samples, which might be the regulatory factors responsible for abnormally expressed mRNAs and proteins in the knee or skin tissues. One example is shown in Figure 1.

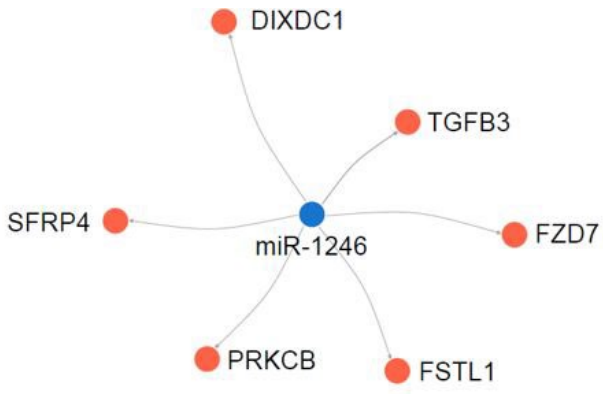


**Figure 1:** Network visualization plot of miR-1246 and its target tissue genes. miR-1246 is one of the differentially expressed miRNAs we have identified in our patient samples.

## CONCLUSIONS

This preliminary investigation is part of a large prospective study. We aim to better understand the pathophysiology of knee arthrofibrosis by studying the influences of TKA on various genetic factors and these factors' profibrotic actions. The results lay the groundwork for further study using techniques like CRISPR to understand the mechanism of action and identify potential pharmaceutical targets.

## ACKNOWLEDGEMENTS

We thank NHMRC Project Grant APP1106411 (to RWL and PNS) and Canberra Orthopaedic Research and Education Foundation (to RWL and PNS) for support.

## REFERENCES

1. Schiavone Panni, A., *J Orthop Traumatol*. **10**(3): p. 111-8, 2009.

# PREFERENCES AND PRIORITIES FOR DECISION MAKING IN CONGENITAL FEMORAL DEFICIENCY (CFD): A STATED PREFERENCE SURVEY OF PATIENTS, CAREGIVERS, AND CLINICIANS

[1]Sarah Nossov, [2]Ilene L. Hollin, [1]Henrike Schmalfuss, and [3]Corinna Franklin

[1]Shriners Hospital for Children, Philadelphia, PA, Unites States of America (USA)
[2]Temple University College of Public Health, Philadelphia, PA, USA, [3]Yale University School of Medicine, New Haven, CT, USA
email: snossov@shrinenet.org

## INTRODUCTION

Congenital femoral deficiency (CFD) is a rare disease that is a spectrum of longitudinal deficiency and lower extremity deformity. There are many alternatives to treatment that range from amputation and accommodation to highly complex reconstruction and limb lengthening[1]. The decision between treatment pathways can be controversial and is subject to preferences. To understand preferences for treatment decision making in CFD and sources of decisional conflict, we asked: 1) What is the importance of various treatment features when making this decision? 2) What are the most/least difficult aspects of making a treatment decision?

## METHODS

52 children (>=14 years old), 135 parents, and 55 clinicians were surveyed. Patients and caregivers were identified using an administrative database from a multicenter, pediatric orthopedic hospital system. Surveys included a discrete choice experiment to measure treatment features that influence decision making to calculate weight of importance[2]. A best worst scaling experiment measured the greatest sources of decisional conflict via preference shares[3].

## RESULTS AND DISCUSSION

Children and parents ranked importance of treatment features similarly. The highest weighted treatment feature was mobility outcome, followed by similarly weighted features (Table 1). The least weighted treatment feature was number of follow-up appointments - weighted more heavily by parents than children (11.3% vs. 4.8%). Clinicians also placed the greatest weight on mobility outcome (47.2%) - more than double the weight of the next most important feature (chance of serious complications; 19.3%). For clinicians, less weight was assigned to avoiding amputation (10.2%) than for children (23.3%) and parents (21.7%).

Table 1. Treatment feature importance.

| Weight of Importance (%) | Treatment Feature Importance | | |
|---|---|---|---|
| | Child | Parent | Clinician |
| **Mobility** | 38.9 | 30 | 47.2 |
| **Avoid Amputation** | 23.3 | 21.7 | 10.2 |
| **Number of surgeries** | 18.5 | 19.8 | 16.7 |
| **Chances of serious complications** | 14.6 | 17.1 | 19.3 |
| **Number of follow-up appointments** | 4.8 | 11.3 | 6.5 |

The preference share for decisional conflict sources varied across groups (Table 2). For children, lack of information about conditions and treatments was the most difficult aspect of decision making, for parents it was permanency of the decision. The least difficult aspect for children was worry that their parent would disagree with their choice, for parents it was the timing of the decision. Clinicians believed that the most difficult aspect for their patients and families would be weighing the pros and cons of treatment options and the least difficult aspect of decision making would be the lack of information about conditions and treatments.

Table 2. Contribution to difficulty in decision making.

| Preference Share (%) | Contribution to Difficulty of Decision Making | | |
|---|---|---|---|
| | Child | Parent | Clinician |
| **Lack of information** | 24 | 11 | 3 |
| **Uncertainty of outcomes** | 19 | 11 | 8 |
| **Uncertainty of psych/social impact** | 13 | 16 | 6 |
| **Timing of decision** | 12 | 8 | 4 |
| **Permanency of decision** | 11 | 22 | 24 |
| **Weighing pros and cons of treatments** | 9 | 9 | 39 |
| **Worry parent/child will disagree w/choice** | 3 | 15 | 12 |

## CONCLUSIONS

Preference-sensitive decisions (i.e., those in which an efficacy advantage is unclear) are difficult for decision makers as there is no obvious best choice. The results of this study improve our understanding of the priorities of decision makers, as well as these sources of decisional conflict. This is foundational to developing decision tools and aids that can help selection of treatment strategies that are concordant with decision maker's values, and in turn reduce decisional conflict and regret. Differences between preferences and clinician perceptions of preferences highlights the need for a patient-centered approach to shared decision-making.

## ACKNOWLEDGEMENTS

Shriners Hospitals for Children Development Grant

## REFERENCES

1. Nossov SB, et al. PFFD/CFD: Evaluation & Management. *J Am Acad Orthop Surg* **30**(13):e899-e910, 2022.
2. Soekhai V, et al. Discrete Choice Experiments in Health Economics: Past, Present and Future. *PharmacoEconomics* **37**:201–226 2019.
3. Hollin IL, et al. Best–Worst Scaling and the Prioritization of Objects in Health: A Systematic Review. *PharmacoEconomics* **40** :883–899, 2022.

# AN AUTOMATIC TWO-STAGE KNEE ALIGNMENT PIPELINE OF HUMAN LOWER-LIMB X-RAYS BY CONVOLUTIONAL NEURAL NETWORK

[1]Yunxiang Liu, [1]Nicolo Malagutti, [2]Joseph Lynch

[1]College of Engineering, Computing & Cybernetics, Australian National University, Canberra, ACT, Australia
[2]Trauma and Orthopaedic Research Unit, Australian National University, Canberra, ACT, Australia
email: Yunxiang.Liu1@anu.edu.au

## INTRODUCTION

Understanding native knee alignment is fundamental for the pre-operative planning in Total Knee Arthroplasty [1]. Traditionally, clinicians manually analyse knee alignment from long-leg X-rays by identifying anatomical landmarks and measuring key angles, such as the hip-knee-ankle angle, lateral distal femoral axis and medial proximal tibial axis. However, with the rapid development of deep learning algorithms in medical image analytics, fully automatic pipelines for analysing knee alignment from radiographs using Deep Neural Networks (DNNs) [2] are now possible.

We propose here a two-stage approach which employs a Convolutional Neural Network (CNN) to segment femoral and tibial contours, followed by a rule-based postprocessing algorithm to detect mechanical axes and compute the Hip-Knee-Ankle Angle (HKAA).

## METHODS

Data was sourced from the Osteoarthritis Initiative Project 60 [3] dataset, which includes a large collection of long-leg X-rays and associated manual HKAA measurements. We selected 145 X-rays for model training and manually segmented femurs and tibias. Additionally, we computed a distance transform to obtain implicit bone shape annotations. The CNN model, based on a U-net structure [4], was then trained using this information. The segmentation masks help the CNN identify the regions of interest (femur and tibia), while implicit shape labels assist with more effective recognition of bone shapes. Following CNN-based segmentation, we implemented a post-processing algorithm which would analyse dimensions and curvatures of the bone contours to locate the femoral head centre, femoral notch, centre of tibial spines and centre of the tibial plafond. From these landmarks, we derived femoral and tibial mechanical axes and computed HKAA.

The algorithm was tested on n=1231 unseen images. We evaluated performance using Mean Absolute Error (MAE), Rate of Failure (HKAA computation failed), intraclass correlation (ICC-2) metrics and Bland-Altman plots.

## RESULTS AND DISCUSSION

The algorithm achieved good accuracy across the OAI dataset (Table 1). MAE was of comparable magnitude to other published (semi)-automated methods [5], and a high ICC-2 score showed strong consistency with the reference manual measurements. We observed a considerable number (453, for a rate of 18.39%) of computation failures, which were likely a result of poor image quality and presence of implants for several patients, as well as an unbalanced representation of digital and analogue X-ray images in the training set, these aspects will be controlled in future work. Bland-Altman plots (Figure 1, left) revealed, on average, a slight underestimation of HKAA by -0.5°. Furthermore, there were errors up to ±4° in some samples. However, linearity was excellent throughout a wide range of HKAA angles with an $R^2$ of 0.917 (Figure 1, right).

| Number of knees | MAE ± std (°) | Rate of Failure (%) | ICC-2 score |
|---|---|---|---|
| 2462 | 0.713±0.592 | 18.392 | 0.958 |

**Table 1:** Quantitative evaluation on HKAA as computed by our pipeline, compared against expert measured results.

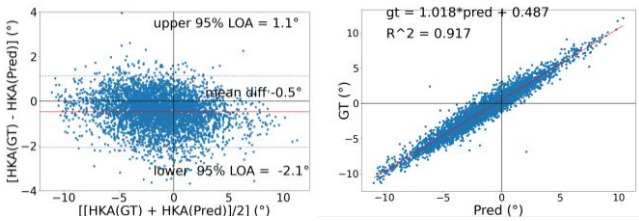


**Figure 1:** (left) Bland-Altman and (right) linear correlation showing agreement between automatically computed (Pred) and manually determined (GT) HKAA results for the test dataset.

## CONCLUSIONS

We have proposed an automatic two-stage image processing pipeline for the analysis of long-leg X-rays through a combination of CNN-based segmentation and bone shape analysis. Experimental results have shown good accuracy in HKAA results, demonstrating the potential for our methodology to deliver time-efficient, repeatable assessments of knee alignment. However, residual issues of failed detections and outlier results limit the potential for immediate clinical use of our tool. Re-training of the algorithm on a more exhaustive and diverse dataset will be required before the pipeline can be dependably implemented in clinical practice.

## REFERENCES

1. Insall J. N., et al. T. *Clin. Orthop. Relat. Res.*, 192 (1985).
2. Zhang, Y. Z., et al. . *Int. j. comput. assist. radiol. surg.*, 11 (2016).
3. National Institutes of Health (2023). The Osteoarthritis Initiative. URL: https://nda.nih.gov/oai/. Accessed 01/08/2023.
4. Ronneberger, O., et al. . *Medical Image Computing and Computer-Assisted Intervention (MICCAI)*, Springer (2015)
5. Sled, E. A., et al. . *Rheumatol. Int.*, 31 (2011

# COMPARISON OF LOAD-SHARING AND AXIS OF ROTATION IN GENERIC AND INDIVIDUALISED NEURO-MUSCULOSKELETAL MODELS OF THE SPINE

[1]Maria Hammer, [3]Robert Rockenfeller, [1]Julia M. Riede, [1,4]Laura Meszaros-Beller, [4]Paige Little, [4]Peter Pivonka and [1,2,4]Syn Schmitt

[1]Institute for Modelling and Simulation of Biomechanical Systems, University of Stuttgart, Stuttgart, BW, Germany
[2]Stuttgart Center for Simulation Science, University of Stuttgart, Stuttgart, BW, Germany
[3]Mathematical Institute, University of Koblenz, Koblenz, RP, Germany
[4]School of Mechanical, Medical and Process Engineering, Queensland University of Technology, Brisbane, QLD, Australia.
email: schmitt@simtech.uni-stuttgart.de

## INTRODUCTION

Individualisation of spine models will benefit the subject-specific treatment of spinal injuries and diseases but poses a major challenge to state-of-the-art biomechanics simulation studies. Here, we compare the kinematics and internal forces of generic population-based and subject-specific individualised spine models. More precisely, we present the differences in load sharing between ligaments, muscles and intervertebral discs (IVDs) as well as finite helical axis (FHA) trajectories.

## METHODS

We investigated the differences in the lumbar kinematics and load sharing between a generic and a subject-specific neuro-musculoskeletal spine model during purely muscle-driven flexion-extension movements. Both models are fully articulated with six degree of freedom joints in the entire thoracolumbar spine. The generic model is based on a validated passive lumbar spine model [1], whereas the subject-specific model was derived from it by geometric individualisation [2]. We applied the FHA analysis from [3] to predict the trajectory of the axis of rotation in both models. All forward-dynamic simulations were performed in the biophysics simulator for muscle-driven systems demoa (http://get-demoa.com)..

## RESULTS AND DISCUSSION

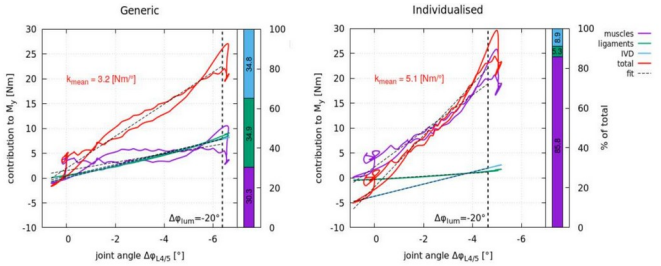


**Figure 1:** Comparison of load sharing between muscles, ligaments and IVD during flexion-extension movement (up to Δphi lum = 20°) in generic and individualised model. Mean stiffness (kmean) was analysed for both models. [2]

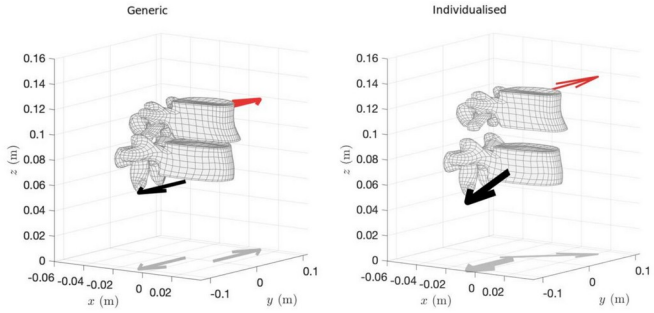


**Figure 2:** Comparison of mean FHA of L4|5 in generic and individualised spine model during flexion (black) and extension (red) movement (graphic primitives not true to scale).

In upright stance, compressive as well as rotational loading was higher in the individualised model. During flexion, the contribution of passive structures to the net joint torque was markedly lower in the individualised model than in the generic model with a predominant muscle contribution (Figure 1). Mean FHA visualises differences between flexion and extension and both models (Figure 2).

## CONCLUSIONS

While generic models remain valuable for general population-oriented research questions, subject-specific modelling seems key to individualised treatment of spine injuries and diseases. We show how to individualise the geometry and the resulting differences in the dynamics, i.e., load sharing and FHA. Nevertheless, both simulation results lie within an acceptable corridor of reported literature data.

## REFERENCES

1. Mörl et al., *Biomech Model Mechanobiol* **19**:2015-2047, 2020.
2. Meszaros-Beller et al., *Biomech Model Mechanobiol* **22**:669–694, 2023.
3. Rockenfeller et al. *Comput Biol Med* **135**:104528, 2021.


# ANZORS 28th Annual Scientific Meeting

## List of Registered Delegates

(at the time of printing, surname ordered alphabetically)

| Title | First name | Last name | Institution | email |
|---|---|---|---|---|
| Dr | John | Abrahams | University of Adelaide | John.abrahams@sa.gov.au |
| A/Prof | Dave | Ackland | University of Melbourne | dackland@unimelb.edu.au |
| Dr | Hadi | Alimadadi | Azad University of Tehran | hadialimadadi49@gmail.com |
| Dr. | Octavian | Andronic | Orthopaedic Research Foundation Western Australia | and_octavian@gmx.ch |
| Dr | Reza | Arjmandi | University of Auckland | r.arjmandi@auckland.ac.nz |
| Dr | Filiz | Ates | University of Stuttgart | filiz.ates@isd.uni-stuttgart.de |
| Dr | Martina | Barzan | Griffith University | m.barzan@griffith.edu.au |
| Prof | Thor | Besier | University of Auckland | t.besier@auckland.ac.nz |
| Mr | James | Bilbrough | Orthopaedic Research Institute, St. George Hospital, University of New South Wales | jpbilbrough@outlook.com |
| Ms | Emma | Boersma | University of Melbourne | eboersma@student.unimelb.edu.au |
| Mr | Francois | Bruyer-Monteleone | Queensland University of Technology | f2.bruyermonteleone@hdr.qut.edu.au |
| Dr | Francesca | Bucci | Flinders University | francesca.bucci@flinders.edu.au |
| Mr | Stuart | Callary | University of Adelaide | stuart.callary@adelaide.edu.au |
| Dr | Sornrith | Chanvichka | JAYAVARMAN 7 Hospital | Viichz55@gmail.com |
| Dr | Julie | Choisne | University of Auckland | j.choisne@auckland.ac.nz |
| Prof | Jillian | Cornish | University of Auckland | j.cornish@auckland.ac.nz |
| Dr | Chris | Dawe | Grace Orthopaedic Centre | cldawe@xtra.co.nz |
| Mr | Julius | Dohm | Aesculap AG | julius.dohm@aesculap.de |
| Mrs | Claire | Dunham | University of Auckland | c.dunham@auckland.ac.nz |
| Mr | Pholpat | Durongbhan | University of Melbourne | pdurongbhan@student.unimelb.edu.au |
| Mr | Daniel | Everett | University of Auckland | deve718@aucklanduni.ac.nz |
| Mr | Zhou | Fang | University of Melbourne | zhouf1@student.unimelb.edu.au |
| A/Prof | Justin | Fernandez | University of Auckland | j.fernandez@auckland.ac.nz |
| Prof | David | Findlay | University of Adelaide | david.finday@adelaide.edu.au |
| Mr | Parham | Foroutan | Flinders University | parham.foroutan@flinders.edu.au |
| Miss | Alessia | Furnaro | Katholieke Universiteit Leuven | alessia.funaro@kuleuven.be |
| Mr | Xingjian | Gong | Australian National University | xingjian.gong@anu.edu.au |
| Miss | Joyce | Guo | University of Otago | Guojo892@student.Otago.can.nz |
| Dr | Geoffrey | Handsfield | Auckland Bioengineering Institute | g.handsfield@auckland.ac.nz |
| Mr | Christyon | Hayek | Orthopaedic Research Institute | z5320156@ad.unsw.edu.au |
| Ms | Salindi | Herath | Flinders University | salindi.herath@flinders.edu.au |
| Mr | Yichen | Huang | University of Melbourne | yichenh2@student.unimelb.edu.au |
| Dr | Sarah | Hunter | Wellington Hospital | 5arahhntr@gmail.com |
| Prof | Reece | Joseph | University of Auckland | rjos014@aucklanduni.ac.nz |

| | | | | |
|---|---|---|---|---|
| Miss | Shannon | Kaefer | Queensland University of Technology | shannonkaefer@gmail.com |
| Dr | Stephanie | Khuu | UC San Diego | stkhuu@ucsd.edu |
| Ms | Julie | Kim | University of Auckland | hkim375@aucklanduni.ac.nz |
| Dr | Jean | Kok | Indiana University School of Medicine | jeankok@iu.edu |
| Mr | Praveen | Krishna | University of Melbourne | pkkris@student.unimelb.edu.au |
| Miss | Matilda | Krywanio | University of Adelaide | matilda.krywanio@adelaide.edu.au |
| Dr | Anubrat | Kumar | Prince Of Wales Hospital | dranubrat5@gmail.com |
| Mrs | Melody | Labrune | Macquarie University | melody.labrune@hdr.mq.edu.au |
| Ms | Tyra | Lange | Flinders University | tyralange@me.com |
| Dr | Maxence | Lavaill | Queensland University of Technology | maxence.lavaill@qut.edu.au |
| Prof | Peter | Lee | University of Melbourne | pvlee@unimelb.edu.au |
| Mr | Alexander | Lee-Medland | Queensland University of Technology | alexander.leemedland@qut.edu.au |
| Dr | Jiao Jiao | Li | University of Technology Sydney | jiaojiao.li@uts.edu.au |
| Prof | David | Lloyd | Griffith University | david.lloyd@griffith.edu.au |
| Dr | Joe | Lynch | Trauma and Orthopaedic Research Unit | joe.lynch@act.gov.au |
| Mrs | Aswini | Madhavan | University of Technology Sydney | aswini.madhavan@student.uts.edu.au |
| Dr | Nicolo | Malagutti | Australian National University | nicolo.malagutti@anu.edu.au |
| A/Prof | Saulo | Martelli | Queensland University of Technology | saulo.martelli@qut.edu.au |
| A/Prof | Sue | McGlashan | University of Auckland | s.mcglashan@auckland.ac.nz |
| Ms | Daniela | Mini | Flinders University | mini0017@flinders.edu.au |
| Ms | Sara | Montanari | Alma Mater Studiorum - University of Bologna | sara.montanari22@unibo.it |
| Ms | Katherine | Nguyen | Australian National University | katherine.nguyen@anu.edu.au |
| Dr | Sarah | Nossov | Shriners Hospital for Children - Philadelphia | snossov@gmail.com |
| Dr | Eleonora | Olivotto | IRCCS Istituto Ortopedico Rizzoli, Bologna, Italy | eolivotto@gmail.com |
| Dr | Dermot | O'Rourke | Queensland University of Technology | dermot.orourke@qut.edu.au |
| A/Prof | Nathan | Pavlos | University of Western Australia | nathan.pavlos@uwa.edu.au |
| Mr | Randika | Perera | Auckland Bioengineering Institute | randikaperera.m@gmail.com |
| A/Prof | Egon | Perilli | Flinders University | egon.perilli@flinders.edu.au |
| Ms | Roshni | Raghvani | University of Auckland | rrag962@aucklanduni.ac.nz |
| Dr | Mohammadreza | Rajabi | Shiraz University of Medical Sciences | M.rezarajabi92@gmail.com |
| Dr | Dale | Robinson | University of Melbourne | drobinson@unimelb.edu.au |
| Dr | Megan | Roser | Queensland University of Technology | mjnroser@gmail.com |
| Ms | Sarah | Safavi | University of Melbourne | ssafavi@student.unimelb.edu.au |
| Dr | Harnoor | Saini | University of Auckland | h.saini@auckland.ac.nz |
| Prof | Syn | Schmitt | University of Stuttgart | schmitt@simtech.uni-stuttgart.de |
| Dr | Vickie | Shim | University of Auckland | v.shim@auckland.ac.nz |
| A/Prof | Peter | Smitham | University of Adelaide | peter.smitham@adelaide.edu.au |
| Prof | Lucian Bogdan | Solomon | Royal Adelaide Hospital | Bogdan.Solomon@sa.gov.au |
| Dr | Javad | Tavakoli | University of Technology Sydney | javad.tavakoli@uts.edu.au |
| Prof | Mark | Taylor | Flinders University | mark.taylor@flinders.edu.au |
| Prof | Ashvin | Thambyah | University of Auckland | ashvin.thambyah@auckland.ac.nz |
| A/Prof | Dominic | Thewlis | University of Adelaide | dominic.thewlis@adelaide.edu.au |
| Mr | Simon | Thwaites | University of Adelaide | simon.thwaites@adelaide.edu.au |
| Mr | Ryan | Tiew | University of Melbourne | etiew@student.unimelb.edu.au |
| Dr | Dane | Turner | Macquarie University | Daneh.Turner@mq.edu.au |
| Ms | Natali | Uribe | Queensland University of Technology (QUT) | natali.uribeacosta@hdr.qut.edu.au |

| | | | | |
|---|---|---|---|---|
| Dr | Vonne | van Heeswijk | University Of Auckland | v.m.vanheeswijk@auckland.ac.nz |
| Dr | Timo | van Leeuwen | Katholieke Universiteit Leuven | timo.vanleeuwen@kuleuven.be |
| Dr | Jo-Wai Douglas | Wang | Australian National University/Canberra Health Services | jowaidwang@gmail.com |
| Dr | Tom | Ward | Australian National University/Canberra Hospital | tom.ward@magdalen.oxon.org |
| Ms | Lauren | Wearne | Flinders University | lauren.wearne@flinders.edu.au |
| A/Prof | Laura | Wilson | Australian National University | Laura.Wilson@anu.edu.au |
| Dr | Stephen | Wood | Ferntree Gully Chiropractic and Acupuncture Centre | stephen@stephenwood.com.au |
| Ms | Sarah | Woodford | University of Melbourne | swood1@student.unimelb.edu.au |
| Miss | Yidan | Xu | Auckland Bioengineering Institute | yxu356@aucklanduni.ac.nz |
| Mr | Yihang | Yu | University of Melbourne | yihangy@student.unimelb.edu.au |
| Miss | Yilan | Zhang | University of New South Wales/NeuRA | yilan.zhang@neura.edu.au |
| Ms | Manuela | Zimmer | University of Stuttgart | manuela.zimmer@isd.uni-stuttgart.de |